UNIVERSITY OF PARMA

Department of Life Sciences

Ph.D. in Biotechnologies

XXVIII COURSE

S. cerevisiae as a model for studying mutations in the human gene *OPA1* associated with dominant optic atrophy and for drug discovery

Coordinator of the Ph.D. Program:
Prof. Nelson Marmiroli

Mentor:
Prof. Tiziana Lodi

Tutors:
Dott. Enrico Baruffini
Prof. Paola Goffrini

Ph.D. student:
Cecilia Nolli

Table of Contents

Introduction

1. Mitochondria

1.1. Mitochondrial structure

Mitochondria are eukaryotic organelles originated, according to the endosymbiontic theory, to an ancestral symbiotic event (Margulis, 1975; Margulis and Bermudes, 1985). They are commonly referred as the "powerhouse" of the cell, because of their main function to generate chemical energy in form of ATP, through the processes of aerobic respiration and oxidative phosphorylation. In addition to their essential role in ATP production, other several processes occurs in mitochondria such as heme and Fe/S cluster biogenesis, calcium homeostasis, pyruvate oxidation, reactions of the tri-carboxyilic acid cycle (Krebs cycle) and of fatty acids, amino acids and nucleotides metabolism (Scheffler, 2008). Mitochondria take also part in the transduction of the intracellular signal, apoptosis, aging and they are the main sites of oxygen reactive species (ROS) production. The multitude of different mitochondrial functions reflects into the complexity of their structure. Mitochondria are elliptic organelles of variable size, ranging from 3-4 µm of length and 0.2-1 µm of diameter. They are surrounded by a double membrane, the outer mitochondrial membrane (OMM) and the inner mitochondrial membrane (IMM), which creates different compartments carrying out specialized functions (McBride et al., 2006). The OMM is a lipid rich layer containing a large number of integrated proteins (porins) which forms channel, through which, molecules smaller than 10kDa freely diffuse across the membrane in both directions. Larger molecules are moved across the membrane thanks to a multi-subunit protein called translocase of the outer membrane (TOM) which recognizes the mitochondrial import sequence at the N-terminus of the proteins (Herrmann and Neupert, 2000). The IMM shows the highest ratio protein-phospholipid among the biological membranes and is enriched with the cardiolipin phospholipid (Herrmann, 2011). This particular composition makes the IMM highly impermeable. However, the metabolites exchange is allowed by specific carriers, among which it is worth to mention the translocase of the inner mitochondrial membrane (TIM). This protein is also responsible for the formation of an ionic gradient across IMM (Guérin, 1991).

The space between the OMM and the IMM is called inter-membrane space (IMS), while the space enclosed by the IMM is the mitochondrial matrix. The IMM is folded into numerous invaginations, called *cristae*, where all the respiratory complexes are located. This particular organization of the IMM expands the surface area of the membrane enhancing its ability to produce ATP.

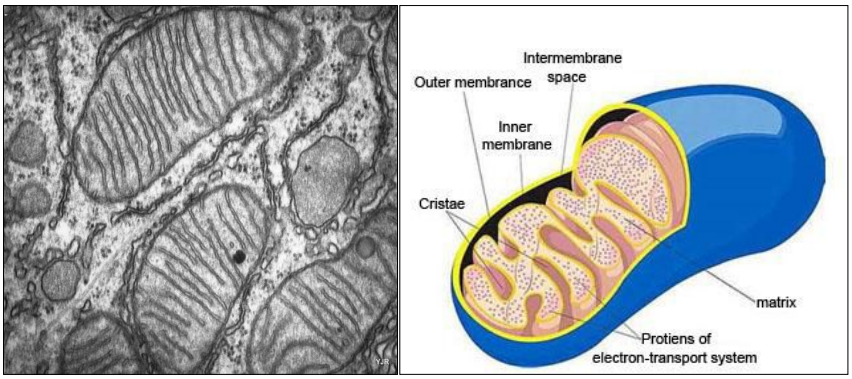

Figure 1.1. Left panel: an electron microscopy image of mitochondria. Right panel: graphic representation of a mitochondrion. From http://www.opencurriculum.org/.

The number and morphology of the *cristae* reflect the response of mitochondria to the cell energy demand. Highly folded *cristae*, with a large surface area, are typically found in tissues with high energy demand such as brain, muscle and heart (Scheffler et al., 2008). The number of mitochondria varies depending on cell type, and their distribution inside the cell depends on the site where mitochondria output is required (Bereiter-Hahn and Vöth, 1994; Warren and Wickner, 1996). Inside the cell mitochondria are organized in a highly ranched network due to the ongoing fusion and fission events (Nunnari et al., 1997, Dimmer, 2002). Mitochondrial dynamics will be further discussed in Section 2. A peculiar aspect that characterizes mitochondria is that they retain their own genome (mtDNA) and the machinery for protein synthesis. Damage, and subsequent mitochondrial dysfunctions, can lead to various human diseases. Mitochondrial disorders include a wide range of clinical phenotypes and often present themselves as neurological disorders, but can also manifest as myopathy, diabetes or multiple endocrinopathy (Wallace, 2001; Zeviani and Di Donato, 2004).

1.2. Mitochondrial DNA structure and organization

Mitochondrial DNA is present into mitochondria in multiple copies whose number varies depending on growth conditions, environmental factors and, in metazoans, on the tissue we consider. In the majority of studied organisms mtDNA is a circular molecule whose extension varies considerably between metazoans, plants and fungi. Human mtDNA is a double-stranded circular molecule of 16.5 Kb (Fig.1.2) whose complete sequence has been characterized. Usually 100-10.000 copies of mtDNA per cell are present (Anderson et al., 1981). The nucleotide content of the two strands of mtDNA is different: the guanine rich strand is referred as the heavy strand and the cytosine rich strand is referred as the light strand.

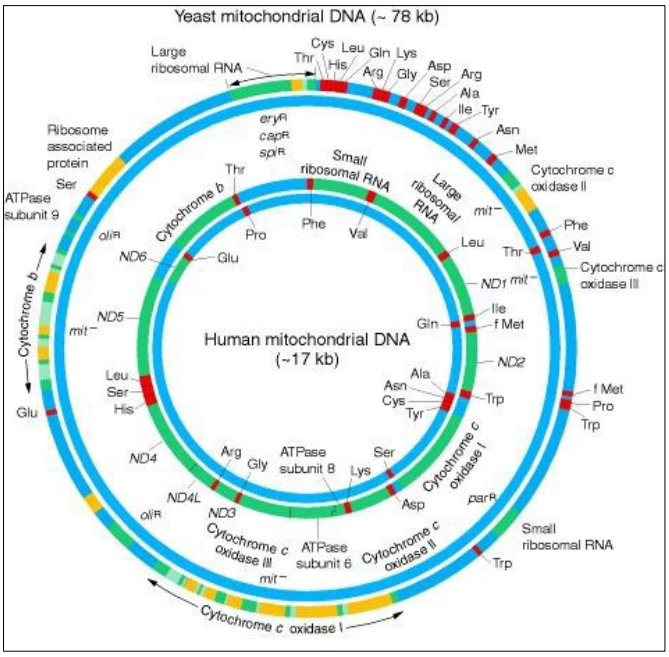

Figure 1.2. Maps of yeast and human mtDNAs. Each map is shown as two concentric circles corresponding to the two strands of the DNA helix. Green: exons and uninterrupted genes, red: tRNA genes shown by their amino acid abbreviations, yellow: URFs (unassigned reading frames). ND: genes code for NADH dehydrogenase subunits. From: Inheritance of Organelle Genes, 1999, Freeman and Company.

Most of the original mitochondrial genes have been transferred to the nuclear genome which now harbors the vast majority of the genes encoding for the ca. 1500 proteins localized to mitochondria. Among the 37 genes contained in human mtDNA, 28 genes are encoded by the heavy strand and 9 by the light strand: 13 genes encode for proteins of respiratory complexes, 22 encode for mitochondrial tRNAs and 2 for mitochondrial rRNAs (12S and 18S) essential for mitochondrial translation. Yeast mtDNA is organized both in linear and circular molecules and has a size ranging from 68Kb (short strains) to 86 Kb (long strains) whose difference is imputable to non-coding and intronic sequences (Bendich, 1996; Nosek and Tomàska, 2003). In particular the complete sequence of the *Saccharomyces cerevisiae* mitochondrial genome of 86 Kb was first published in 1998 (Foury et al., 1998). The yeast mtDNA contains genes for cytochrome c oxidase (COX) subunits (*COX1, COX2* and *COX3*), ATP synthase subunits (*ATP6, ATP8, ATP9*), cytochrome b of the Complex III, a single ribosome protein Var1 and several intron related ORFs. It is worth to mention that unlike human mtDNA, in yeast there are no genes for Complex I that consists of only one protein encoded by nuclear genome. In addition yeast mtDNA encodes for 21S and 15S ribosomal RNAs, 24 tRNAs that recognize all codons, 9S RNA component of RNAse P and seven to eight replication origin-like region. Unlike nuclear DNA, mtDNA is not associated with histones and organized in nucleosomes. Several proteins interact with mtDNA, packing it in a structure called nucleoid, which was found to be associated with the IMM (Miyakawa et al., 1987; Chen and Butow, 2005; Malka et al., 2006; Kucej and Butow, 2007). Haploid cells of the yeast *Saccharomyces cerevisiae* contain 40 nucleoids per cell, each one holding more than one copy of mtDNA, and representing an inheritable unit (Williamson and Fennel, 1979; Jacobs et al., 2000). Nucleoid is a dynamic structure whose organization changes according to metabolic cues and whose proper distribution requires frequent events of mitochondria fusion and fission (MacAlpine et al., 2000; Kucej et al., 2008). The packing of mtDNA requires both proteins directly involved in mtDNA maintenance and proteins with apparently unrelated functions (Chen et al., 2005).

In the yeast *S. cerevisiae* 22 proteins involved in the nucleoid formation have been identified and they can be divided in two groups: proteins associated to mtDNA and involved in mtDNA replication, transcription, repair, recombination and proteins involved in cytoskeletal organization, import and mitochondrial biogenesis, metabolism or protein responsible of protein quality control. Abf2 is a protein that belongs to the first functional category and is able to bend mtDNA inducing supercoiling in the presence of a topoisomerase. Abf2 has been shown to be involved in the recruitment of other mitochondrial protein to nucleoids (Newman et al., 1996; Friddle et al., 2004). Other proteins have been shown to bend mtDNA such as Rim1 (protein that binds ssDNA), Mgm101 (enzyme involved in mtDNA repair) and Sls1 (involved in mtDNA transcription). In the other functional class we find many bi-functional proteins as mtHsp60, mtHsp70, mtHsp10 which are involved both in mitochondrial protein import and nucleoid organization. Many proteins involved in Krebs cycle, glycolysis or amino acid metabolism are involved also in mtDNA stabilization. Among these there are Aco1 (aconitase), required for the tri-carboxylic acid cycle, and Ilv5, a protein involved in leucine, isoleucine and valine biosynthesis. It has been hypothesized that bi-functional proteins act as sensors for metabolic changes that can be transmitted by nucleoids to regulate mtDNA maintenance (Kucej and Butow, 2007). Mitochondrial DNA accumulates mutations at a significantly higher rate compared to nuclear genome for several reasons: the lack of protective histones, the high replication rate and the proximity to IMM and electron chain transport which is the major source of ROS. For all these reasons the nucleoid has a pivotal role in protecting mtDNA from oxidative damage and genome instability.

1.3. Mitochondrial functions

As pointed out before, mitochondria are involved in many processes, although their main role is to produce the majority of ATP for cellular functions via the oxidative phosphorylation. The most important energy sources for the cell are sugars, fatty acids and proteins whose oxidative degradation takes place in cytosol. In aerobic organisms these substrates are oxidized to CO_2 and H_2O coupled to ATP production through a series of reaction, known as cellular respiration, inside mitochondria.

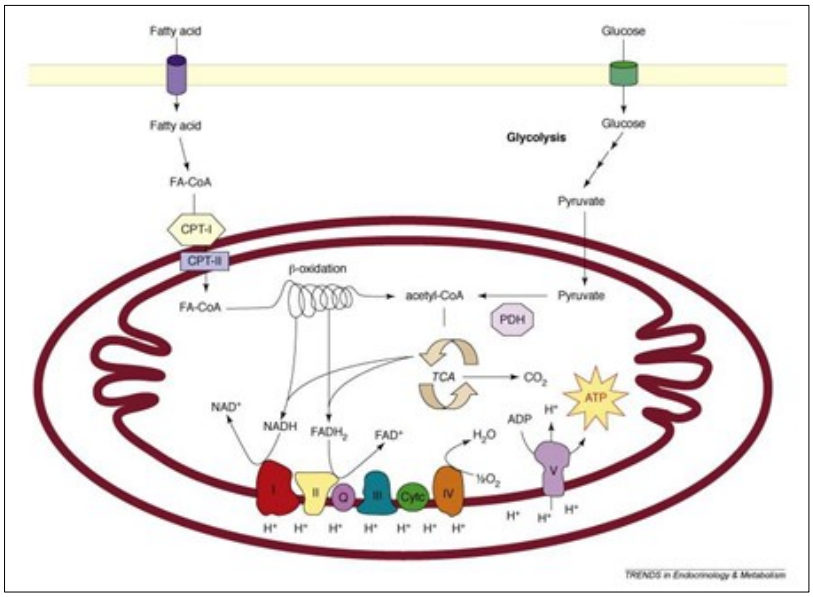

Figure 1.3. Some metabolic pathways that take place inside mitochondria for energy supply. From Turner and Heilbronn, 2008.

1.3.1. Sugar and fatty acids oxidation

Different catabolic pathways are involved in the oxidation of sugars and fatty acids: cytosolic glycolysis is a central pathway that allows the conversion of glucose in two molecules of pyruvate, 2 ATP and 2 NADH for each molecule of glucose processed. In aerobiosis glycolysis represents only the first step of glucose degradation: each pyruvate molecule produced is actively transported inside mitochondria, where it undergoes further oxidation by pyruvate dehydrogenase to acetyl-CoA that enters in Krebs cycle with a net gain in ATP production (Perham, 2000). In anaerobiosis pyruvate

is converted to ethanol by alcoholic fermentation in yeast. Fatty acids are highly negative charged molecules which need to be activated and converted to acyl-CoA in the cytosol. Once activated, fatty acids are imported into mitochondria, through an acetyl-carnitine carrier and oxidized to acetyl-CoA by a four steps reaction, commonly known as β-oxidation. Acetyl-CoA is a key component of metabolism and represents the conversion point of different degradation pathways. The acetyl-CoA units obtained both from glycolysis, fatty acids oxidation and from catabolism of some amino acids (glutamate, lysine) enter the Krebs cycle and are oxidized to CO_2.

1.3.2. Krebs cycle

Krebs cycle, also known as tricarboxylic acid cycle (TCA), consists of eight reactions conserved in all aerobic organisms and plays a key role in energetic metabolism. The Krebs cycle is an amphibolic pathway: many catabolic processes converge on it and many intermediates produced by the cycle are precursors used in anabolic reactions (e.g. α-ketoglutarate is precursor for amino acids and nucleotides, succinil-CoA is used for heme biosynthesis) (Scheffler, 2008). In eukaryotic cells the TCA cycle occurs in mitochondrial matrix, where acetyl-CoA is oxidized to CO_2 with the reduction of NAD+, FAD+ and ubiquinone. Stoichiometrically 1 molecule of acetyl-CoA is converted in 2 CO_2 with production of 3 NADH, 1 $FADH_2$ and one high energy GTP molecule. All the enzymes of the citric acid cycle are soluble enzymes in mitochondrial matrix, with the only exception of succinate dehydrogenase. This enzyme is the only one, in Krebs cycle, directly linked to the electron transfer chain (Complex II) and represents the connection between TCA cycle and oxidative phosphorylation. The cycle is useful to increase the cell ATP production by generating reduced carriers whose electrons are passed through the respiratory chain.

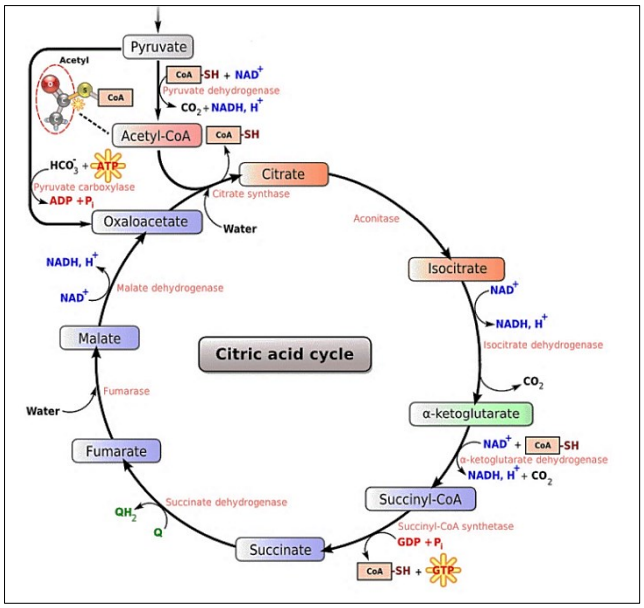

Figure 1.4. Schematic representation of all reactions and intermediates involved in Krebs cycle.

1.3.3. Oxidative phosphorylation

Catabolic pathways involved in the oxidation of carbohydrates, proteins and fatty acids flow together into the final step of cellular respiration: the ATP synthesis. During oxidative phosphorylation the electrons derived from NADH or $FADH_2$ are passed across the electron transport chain (ETC) consisting of carriers of increasing reduction potential, the respiratory complexes, ultimately being deposited on molecular oxygen with formation of water. The free energy derived from the electron flow is used to actively pump out protons from the mitochondrial matrix to the intermembrane space (DiMauro and Schon, 2003). This generates an electrochemical potential across the membrane, which is used to drive ATP synthesis, by allowing protons to flow back across the IMM. NADH electrons are sufficient to produce three ATP molecules, while two ATP molecules are obtained from $FADH_2$ electrons.

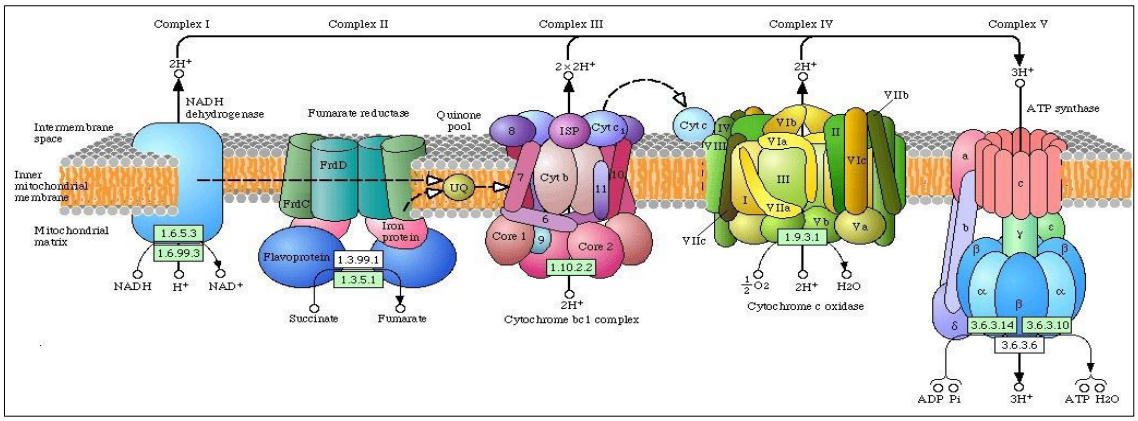

Figure 1.5. Mitochondria electron transport chain complexes and soluble carriers. Image taken from KEGG pathway.

1.3.3.1. Complex I: structure and function

Complex I (NADH dehydrogenase) is normally considered as the "entry point" of electrons to the respiratory chain. It catalyzes the transfer of electrons from NADH to ubiquinone using flavin mononucleotide (FMN) as a cofactor, eight redox groups and an iron-sulfur group. Complex I is the biggest complex of the ETC, formed by 45 subunits encoded by both mtDNA and nuclear DNA. Until now, its crystal structure has not been obtained. Electron microscopy showed that it has an "L" shape, with one arm dispersed into the IMM and the other one facing mitochondrial matrix (McKenzie and Ryan, 2010). Unlike mammals, common fission and budding yeasts lack of Complex I and use instead a completely different enzyme for electron transfer from NADH to ubiquinone which does not pump protons out of the matrix.

1.3.3.2. Complex II: structure and function

Complex II (succinate dehydrogenase) consists of four subunits: two integral membrane proteins anchor the complex to the inner mitochondrial membrane while the two largest peptides organize the enzyme catalytic core. The latter transfers the electrons from succinate to a flavin adenine dinucleotide cofactor (FAD), and then to three Fe/S clusters with subsequent reduction of coenzyme Q (CoQ). Complex II does not pump electrons from matrix to IMS, because the amount of free energy originated from electron transfer from $FADH_2$ to CoQ is too low.

This is the reason why the electrons flowed in ETC by $FADH_2$ produce only 2 ATP molecules instead of the three obtained from Complex I NADH oxidation. Complex II has two functions: during the Krebs cycle it catalyzes the oxidation of succinate into fumarate and during the electron transport chain it transfers electrons from $FADH_2$ to ubiquinone. The mechanism of Complex II assembly is still unknown.

1.3.3.3. Complex III: structure and function

The Complex III of the respiratory chain (ubiquinol-cytochrome *c* oxidoreductase or simply cytochrome bc_1) catalyzes the transfer of electrons from ubiquinol to cytochrome *c* coupling this reaction with the pumping of two protons from the mitochondrial matrix to the intermembrane space. This complex is a multi-subunits protein, whose components are quite similar in different species such as yeasts, animals and plants. Only the cytochrome *b* subunit is codified by the mtDNA, while the others (8 in yeast and 10 in mammals) are encoded by nuclear DNA and imported for assembly in the IMM. Functionally the most important subunits of cytochrome bc_1 are the cytochromes b (b562 and b566) and c_1, and the Rieske iron-sulfur protein. These are the only proteins participating in the reaction. Anyway, yeast mutants for each subunit of Complex III are respiratory deficient, indicating that even the subunits lacking the prosthetic groups have a relevant role, perhaps in the assembly and stabilization of the complex (Scheffler, 2008).

1.3.3.4. Complex IV: structure and function

Complex IV, or cytochrome *c* oxidase, is the last complex of the electron transport chain. It catalyzes the oxidation of cytochrome c, donating the electrons to O_2, to generate 2 molecules of H_2O. This reaction involves two steps: two electrons are transferred on the IMS side, while four protons are taken up from the matrix side, resulting in the transfer of four positive charges across the membrane. Complex IV in mammals is composed by 13 proteins while in yeast there are only 9 subunits.

In all organisms the three biggest subunits are encoded by mtDNA and synthesized in the matrix. The complex is a large integral membrane protein which includes two cytochromes (a and a3) and copper centers involved in the electron transfer.

1.3.3.5. Complex V/ATP synthase: structure and function

ATP synthase (also called Complex V) catalyzes the synthesis of ATP from ADP + P_i using the energy of the electrochemical proton gradient generated by the electron transport chain. The complex is composed by 16 proteins that form two functional domains: F_1 and F_0 (Futai et al., 1989). The F_1 region is localized in the mitochondrial matrix and it is composed by 5 subunits containing the catalytic domain of the protein. The F_0 fraction is integral to the membrane and acts as a proton pore transferring protons to the F_1 by a rotatory movement (Stock et al., 1999). Once produced, ATP is exported into the cytosol by an ATP/ADP carrier that, at the same time, imports ADP inside the matrix to be recycled. ATP synthase components are encoded both by mitochondrial and nuclear genes; in yeast the nuclear genes appear to be constitutively expressed, regardless of the carbon source, in contrast to nuclear genes for ETC (Ackerman and Tzagaloff, 2005).

2. Mitochondrial dynamic

Mitochondria are high dynamic organelles. They frequently move inside the cell, fuse with each another and then split apart again. The morphological plasticity of this organelle results from its ability to undergo two dynamical opposed processes called fusion and fission. Fusion allows the exchange of contents, DNA, and metabolites between neighboring mitochondria, including damaged or senescent mitochondria, promoting their survival (Yoneda et al., 1994, Nakada et al., 2001). Mitochondria cannot be created *de novo* and therefore mitochondrial growth and division are essential for proliferation, and ensure that a full complement of mitochondria is inherited by daughter cells following mitosis (Yaffe, 1999, Boldogh et al., 2001).

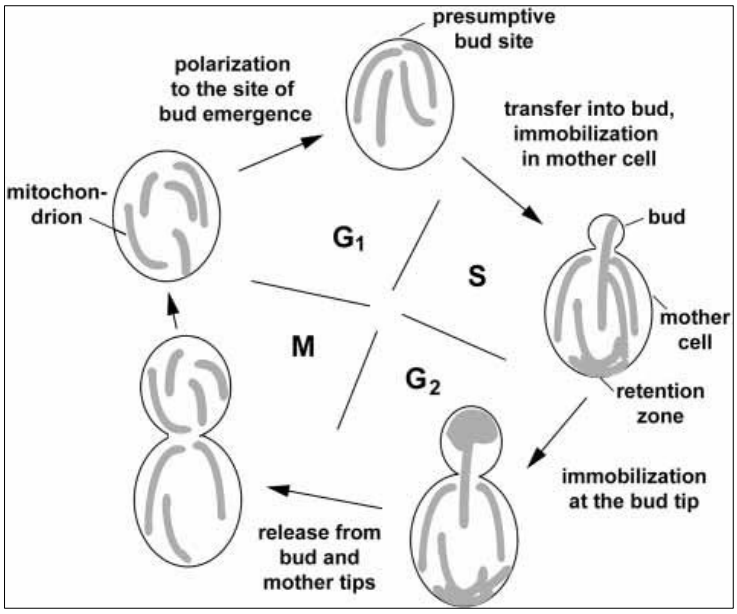

Figure 2.1. The mitochondrial inheritance cycle (Boldogh et al., 2001).

Mitochondrial fission is also required to help clear old or damaged mitochondria from the cell through an autophagic process referred to as mitophagy (Kim et al., 2007). The importance of keeping the right balance of mitochondrial fusion and fission is also evident from the fact that several diseases are associated with defects in the fusion and fission machineries.

Importantly most of the proteins mediating mitochondrial fusion and fission are conserved in yeast, flies, worms, plants, mice and human indicating that the fundamental mechanism has been maintained during evolution (Okamoto and Shaw, 2005). Thanks to this high level of conservation, much of our knowledge about the molecular components and cellular roles of mitochondrial fusion and fission has been gained from research with yeasts, worms and flies (Westermann, 2010).

2.1. The fusion pathway

2.1.1. Fzo1/MFN1-MFN2

Mitochondrial fusion requires the evolutionarily conserved GTPase called Fzo1 (fuzzy onions 1) in budding yeast (Hermann et al., 1998; Rapaport et al., 1998) and fruit flies (Hales and Fuller, 1997), and MFN (mitofusin) in mammals (Eura et al., 2003; Rojo et al., 2002; Santel et al., 2001, 2003). Yeast Fzo1 is an integral outer mitochondrial membrane protein with its N-terminal GTPase domain facing the cytosol. The two transmembrane regions span the outer membrane twice, placing the N- and C-terminal portions in the cytosol, where they are in position to mediate important steps during fusion (Fritz et al., 2001, Hermann et al., 1998). In mammals two homologs of Fzo1 were found, called mitofusin 1 (MFN1) and mitofusin 2 (MFN2) widely expressed in many tissues. MFN1 (741 residues) and MFN2 (757 residues) are two large nuclear-encoded dynamin-like GTPases that have both their N-terminus and C-terminus exposed to the cytosol. MFN1 and MFN2 display high identity (81%), similar topology and both reside in the outer mitochondrial membrane. (Santel and Fuller, 2001; Legros et al., 2002; Rojo et al., 2002; Chen et al., 2003; Santel et al., 2003). Mitofusins have been suggested to facilitate membrane tethering similar to the action of SNAREs, with both homo and hetero-oligomeric complexes of MFN1 and MFN2 formed via the interaction of coiled-coil domains in a GTP dependent manner (Chen et al., 2005; Ishihara et al., 2006; Detmer et al., 2007). While both MFN1 and MFN2 are capable of facilitating mitochondrial outer membrane fusion, a growing body of evidence suggests that they share both complementary and disparate roles in mitochondrial

fusion. Mutations in the gene encoding MFN2 have been shown to cause Charcot-Marie-Tooth disease type 2A (CMT2A), an autosomal dominant neuropathy (Zuchner et al., 2004). In contrast, no MFN1 deficient patient has been reported to date. Interestingly mitochondrial fragmentation observed following loss of either MFN1 or MFN2 is morphologically distinct (Chen et al., 2003). These results suggest differing roles for these proteins in mitochondrial fusion. Indeed, MFN1 and MFN2 have different tethering capabilities, with MFN1 exhibiting higher GTP dependent tethering activity than MFN2 (Ishihara et al., 2004). Furthermore MFN2 is enriched at the endoplasmic reticulum (ER)-mitochondrial interface, and silencing of MFN2 affects both mitochondrial and ER morphologies (de Brito and Scorrano, 2008; Merkwirth and Langer, 2008). Recently several proteins have been identified to bind to MFN2. Among these, two pro-apoptotic Bcl-2 family members called Bax and Bak seem to bind specifically to MFN2, but not to MFN1 (Suen et al., 2008). These results suggest that MFN1 and MFN2 seem to play different roles in mitochondrial dynamics with MFN1 that (in cooperation with OPA1) exquisitely regulates mitochondrial fusion and MFN2 that plays a role not also in fusion, but also in the apoptotic pathway.

2.1.2. Mgm1/OPA1

2.1.2.1. Mgm1

Mgm1 protein is a dynamin family member that was first discovered in *S. cerevisiae* in a genetic screening for nuclear genes required for the maintenance of mtDNA (Jones and Fangman, 1992). Dynamin protein superfamily includes classical dynamin and dynamin-related proteins (DRPs), large GTPases that undergo GTP cycling and that act as mechanoenzymes to mediate intracellular membrane-remodeling events, such as vesicle budding and organelle fusion and fission. Members of the dynamin superfamily are composed of three specific domains: a GTPase domain, a middle domain, and a GTP effector domain (GED). Orthologues of Mgm1 have been identified in others eukaryotes including *Schizosaccharomyces pombe* (Msp1) and mammals (OPA1). Although the sequence identity is approximately 20%, they display a high conserved secondary structure.

As shown in Fig.2.2, Mgm1 structure consists of a MTS (mitochondrial target signal) at the N-terminus, followed by an hydrophobic segment (TM), a Rhomboid cleavage region (RCR), a GTPase domain, a middle domain and a putative GED domain (GTPase effector domain).

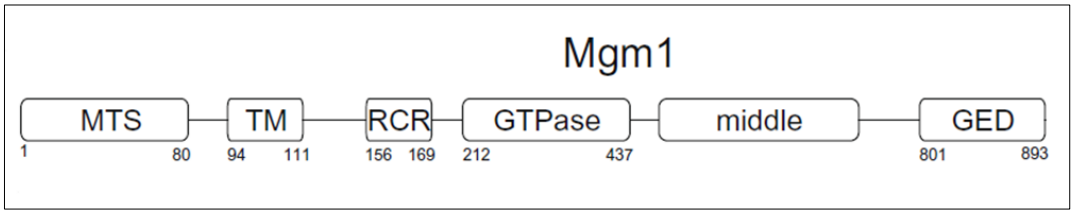

Figure 2.2. Schematic representation of Mgm1. From Zick et al., 2009.

Studies in yeast revealed that the MTS of Mgm1 is cleaved by the MPP (mitochondrial processing peptidase) as soon as the protein enters the organelle. Herlan and collaborators demonstrated that Mgm1 is processed in two isoforms, a long one, called long-Mgm1 (l-Mgm1) and a short one, s-Mgm1, which are present in roughly equal amount under steady-state conditions (Herlan et al., 2003). Long isoform starts from residue 81 and is generated immediately after the MTS removal by MPP cleavage. Mgm1 long isoform is anchored in the inner mitochondrial membrane (IMM) via its N-terminal transmembrane domain (Zick et al., 2009). s-Mgm1, which lacks the transmembrane domain, resides in the intermembrane space and is generated by the proteolytic cleavage by Pcp1 protein at the rhomboid cleavage region (RCR). Yeast Pcp1 is homolog of Rhomboid serine protease, known to be involved in intercellular signaling in *D. melanogaster,* and it is known to reside in the inner mitochondrial membrane. Herlan and collaborators proposed a model, called alternative topogenesis, in order to explain the processing of Mgm1 in long and short isoforms (Fig.2.3). According to this model, Mgm1 is imported into the mitochondria and this import is driven by the mitochondrial membrane potential. The immediately following first hydrophobic segment after MPS can act as a stop-transfer sequence. Processing by the mitochondrial processing peptidase (MPP) and insertion into the inner membrane leads to l-Mgm1. At high levels of matrix ATP the mitochondrial import

motor “pulls in” part of the pre-protein further, and the second hydrophobic segment reaches the inner membrane. Pcp1 cleavage within this segment generates s-Mgm1. In this way, insertion of the first hydrophobic segment into the inner membrane, yielding l-Mgm1, and further ATP driven import with subsequent Mgm1 processing, yielding s-Mgm1, are competing processes. This novel pathway of alternative topogenesis of Mgm1 during import into mitochondria is a key regulatory mechanism, which is crucial for the balanced formation of both isoforms (Herlan et al., 2004).

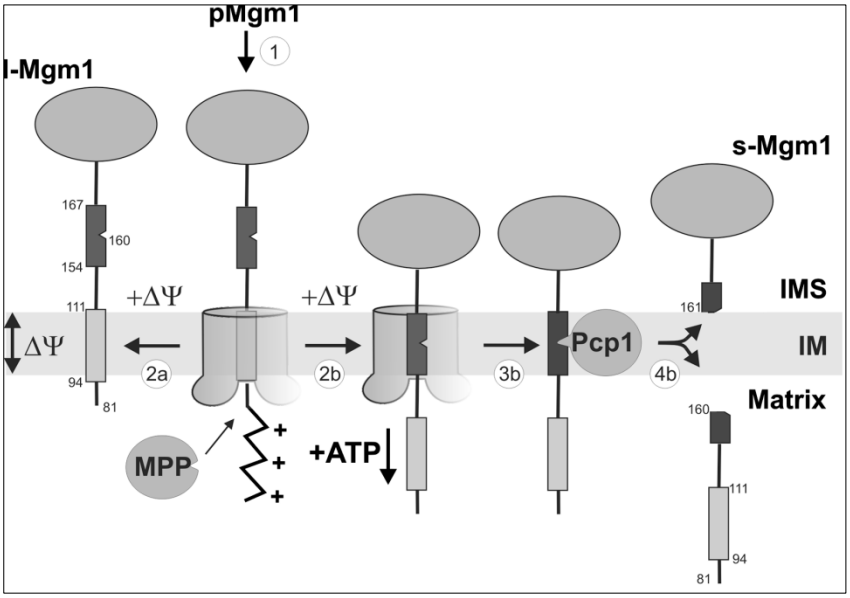

Figure 2.3. Model of alternative topogenesis of Mgm1. The TIM23 translocase is shown in transparent gray color. The first and second hydrophobic segments in Mgm1 are indicated by gray and dark gray boxes, respectively. Numbers describe the order of the topogenesis pathway for the generation of l-Mgm1 (1 and 2a) and s-Mgm1 (1, 2b, 3b, and 4b). IMS, intermembrane space; IM, inner membrane; ΔΨ, membrane potential; MPP, mitochondrial processing peptidase; pMgm1, precursor protein of Mgm1. From Herlan et al., 2004.

Mutants lacking Mgm1 contain highly fragmented mitochondria, because of the absence of the fusion machinery. They are also unable to segregate mtDNA because of defective fusion. After few generations, cells are devoid of mtDNA and become respiratory deficient (RD) due to the absence of mitochondrial encoded respiratory enzymes subunits (Rapaport et al., 1998; Hermann et al., 1998; Jones and Fangman, 1992; Sesaki et al., 2001).

As pointed out before, the ratio between the two Mgm1 isoforms appears tightly regulated. Despite this fact, the two isoforms seem to have distinct roles. Zick and colleagues demonstrated that a shift of Mgm1 isoforms ratio towards the long form has a strong dominant negative effect on mitochondrial fusion, whereas a shift toward the shorter form has no detectable effects. In addition, they demonstrated that a GTPase functional domain is not indispensable in the l-form but it is fundamental in s-Mgm1 for mtDNA maintenance. Taking together, the presence of an N-terminal transmembrane segment, and the dispensability of a functional GTPase domain in l-Mgm1, suggest a primary role of l-Mgm1 in anchoring the fusion machinery to the inner membrane. l-Mgm1 may act as a docking receptor for s-Mgm1, eventually involving also other fusion factors (Zick et al., 2009). A number of studies indicated an additional role for Mgm1 in *cristae* structure maintenance. Meeusen and collaborators postulated that *trans* Mgm1/Mgm1 interactions, generated from opposing inner membranes, function to promote inner membrane fusion and to form and maintain *cristae* structures (Meeusen et al., 2006). These observations are consistent with findings indicating that OPA1, the human orthologue of Mgm1, also functions in *cristae* structure via intermolecular interactions (Frezza et al., 2006).

2.1.2.2. OPA1

OPA1 was first identified, in an "*in silico*" analysis, as the human homolog of Mgm1 in *S. cerevisiae* and Msp1 in *S. pombe*. Human OPA1 ORF is composed of 30 exons distributed across more than 90Kb of genomic DNA on chromosome 3q28-q29. OPA1 is ubiquitously expressed with the highest levels in retina, brain, testis, heart and muscle (Alexander et al., 2000). Alternative splicing of exons 4, 4b and 5b leads to 8 differentially expressed isoforms (Delettre et al., 2001). While exon 4 is evolutionarily conserved, both exons 4b and 5b are specific to vertebrates (Olichon et al., 2007). The *OPA1* gene encodes for a protein that belongs to the dynamin family, with which it shares 3 conserved domains: a GTPase domain, a middle domain and a GED domain (GTPase effector domain). As shown in Fig.2.4 OPA1 is composed of a N-terminal mitochondrial import sequence (MIS) followed by a predicted transmembrane helix

(TM1) which is conserved in all OPA1 homologs. Two additional hydrophobic domains, TM2a and TM2b, are present, and they are encoded by alternatively spliced 4b or 5b exons.

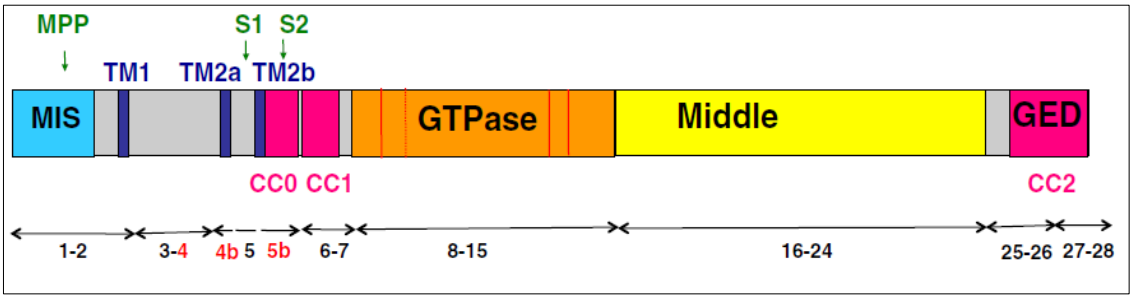

Figure 2.4. Schematic representation of OPA1. From Belenguer et al., 2013.

Translated precursors of the 8 *OPA1* mRNA are targeted to mitochondria via their MIS which is removed by mitochondrial processing peptidase (MPP) to give rise to long isoforms of the GTPase, collectively called long-OPA1 (l-OPA1). Each long isoform can then be subjected to a proteolytic process to generate a short isoform called s-OPA1 (Olichon et al., 2002; Satoh et al., 2003). Different l-OPA1 isoforms can be processed in two different short isoforms depending on the exon present. Numerous studies on the generation of s-OPA1 have been conducted, leading to the identification of 3 different mitochondrial peptidases, recognizing two different cleavage sites (S1 and S2), in each long isoform. A low abundant s-form of OPA1 can be originated by the cleavage of PARL (protease PRESENILIN associated rhomboid-like) (Cipolat et al., 2006). A mAAA protease called PARAPLEGIN cleaves l-OPA1 at S1 site generating a short isoform as shown in Fig.2.5 (Ishihara et al., 2006). However both these proteases cannot wholly explain the processing of OPA1 since their knock-out does not affect the ratio between the l-form and the s-form of the dynamin (Duvezin-Caubet et al., 2007; Griparich et al., 2007; Guillery et al., 2008). Furthermore contribution in OPA1 processing of two subunits of mAAA protease AFG3L1 and AFG3L2 was revealed by experiments conducted in yeast (Duvezin-Caubet et al., 2007) and the iAAA protease YME1L was shown to be responsible to the cleavage at S2 site (Fig. 2.5) (Song et al., 2007).

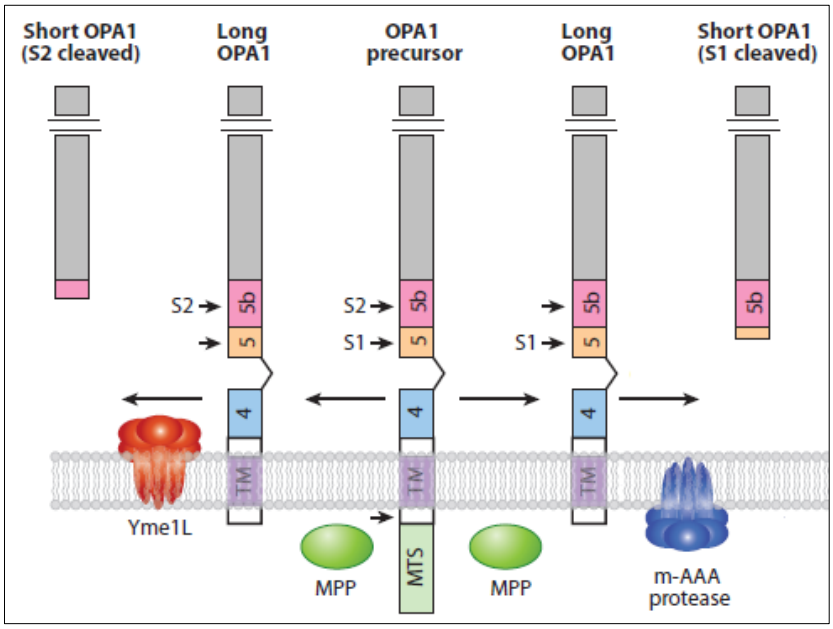

Figure 2.5. Protease processing of OPA1. In the center, the precursor polypeptide is shown. After import of the amino terminus into the matrix, the mitochondrial targeting sequence is cleaved by the MPP to yield the membrane-anchored, long isoform of OPA1. Further processing by the Yme1L protease at the S2 cleavage site yields a short isoform of OPA1 (left side). Cleavage at the S1 site also yields a short isoform. The m-AAA protease is activated to cleave at the S1 site (right side). From Chan, 2012.

Loss of OPA1 function, by RNAi or gene knock-out, causes fragmentation of the tubular mitochondrial reticulum (Griparich et al., 2004; Wong et al., 2000; Olichon et al., 2003; Song et al., 2009). The pro-fusion activity of OPA1 was further confirmed by experiments showing that following OPA1 depletion, or in OPA1$^{-/-}$ cells, mitochondrial fusion is impaired (Cipolat et al., 2004; Chen et al., 2005). Consistent with its localization in the organelle, fusion of the inner membrane is the primary role of OPA1. Interestingly fusion of the OM is not abolished by OPA1 knock-out, as seen in OPA1$^{-/-}$ cells (Song et al., 2009). Fusion of IM and OM seems not to be as tightly coupled in mammals as it is in yeast, where Mgm1 depleted mitochondria can fuse their OM *in vitro* but not *in vivo*. Furthermore OPA1 is needed only on one mitochondrion to promote fusion of two adjacent mitochondria *ex vivo*, while in yeast Mgm1 is required on both mitochondria for an efficient fusion (Meeusen et al., 2006).

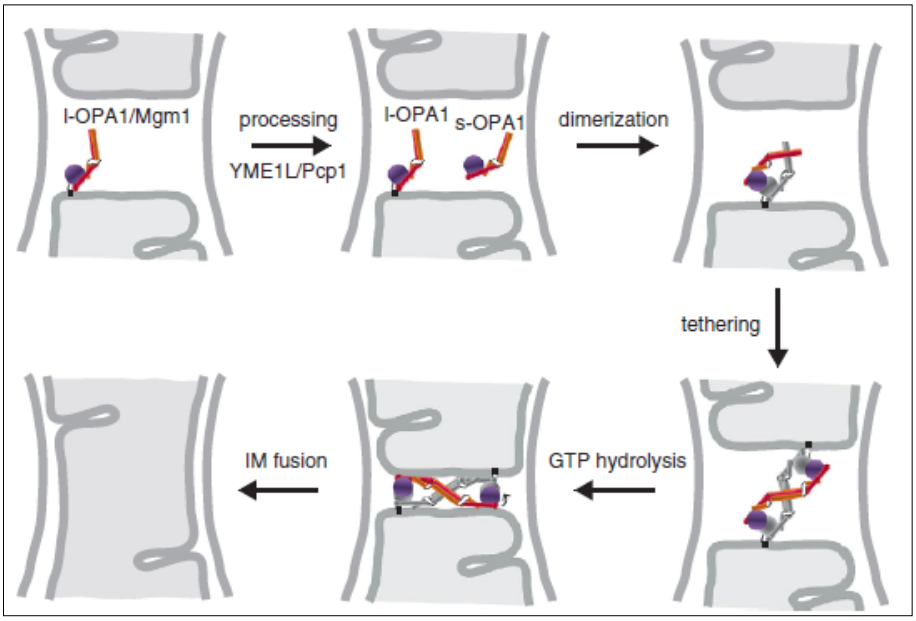

Figure 2.6. Model for mitochondrial IM fusion. l-OPA1 is anchored to the IM by an N-terminal transmembrane domain, the rest of the protein resides in the IMS. l-OPA1/Mgm1 is partially cleaved by YME1L/Pcp1, generating an equilibrium between the two isoforms, which dimerize on one membrane. IM tethering involves *trans* interactions between OPA1/ Mgm1. GTP hydrolysis probably induces a conformational change possibly triggering convergence of the opposing membranes before IM fusion. The arrow indicates the conformational change at the hinge region upon GTP hydrolysis based on dynamin. From Escobar-Henriques and Anton, 2012.

The role of OPA1 is not limited to mitochondrial fusion. Loss of mtDNA and mitochondrial nucleoids was reported in OPA1$^{-/-}$ cells (Chen et al., 2007; Chen et al., 2010) in agreement with studies demonstrating that, in yeast, Mgm1 inactivation leads to mtDNA depletion (Jones et al., 1992; Pelloquin et al., 1998). Elachouri and colleagues proposed a model in which OPA1 contributes to nucleoid attachment to IM and supports mtDNA replication and distribution (Elachouri et al., 2011). It has been hypothesized that the mechanism involved in mtDNA maintenance is different in human and in yeast, and it may be linked to the absence of the sequence encoded by exon 4b of OPA1 in Mgm1. The mechanisms linking mtDNA maintenance and mitochondrial dynamics are poorly understood and constitute a future challenge. Interestingly many studies revealed an association between OPA1 and *cristae* structure, linking OPA1 with energetic defects. Zanna and collaborators demonstrated a physical interaction between OPA1 and respiratory complexes I, II and III, suggesting that OPA1 regulates oxidative phosphorylation by stabilizing the mitochondrial

respiratory chain complexes (Zanna et al., 2008). In addition to mitochondrial fragmentation, loss of mtDNA and impairment in respiratory activity, a down-regulation of OPA1 promotes cell death through spontaneous and induced apoptosis (Olichon et al., 2003; Lee at al., 2004; Olichon et al., 2007; Frezza et al., 2006). OPA1 overexpression protects cells from apoptosis by preventing cytochrome c release. Anti-apoptotic function of OPA1 was attributed to the formation of OPA1-containing complexes that maintain the structure of the *cristae* junction, thus sequestering cytochrome c (Frezza et al., 2006; Landes et al., 2010). Olichon and colleagues showed that it is possible to uncouple fusion activity from anti-apoptotic activity knocking-down particular OPA1 isoforms. Isoforms containing exon 4 seem to be important for fusion, whereas isoforms including exon 4b or 5b regulate apoptosis (Olichon et al., 2007). While different OPA1 isoforms are involved in either pro-fusion or anti-apoptotic activities of the GTPase, little is known about the molecular mechanisms that controls the alternative splicing of its mRNA. Until now all the effects of OPA1 were attributed to its role within the mitochondrion but we are still far from having examined this protein from all angles.

2.1.3. Ugo1

The *UGO1* gene (ugo is Japanese for fusion) was identified in a genetic screen for components acting antagonistically to the mitochondrial division machinery in the yeast *Saccharomyces cerevisiae* (Sesaki et al., 2001). Ugo1 protein shares limited sequence similarity with members of the mitochondrial carrier family, a group of proteins that transport small molecules across the inner membrane (Sesaki and Jensen, 2001). Clear homologues outside the fungal kingdom have not been found, suggesting that its role in mitochondrial fusion is not conserved. Ugo1 is a 58 kDa protein embedded in the mitochondrial outer membrane, with the N-terminal region facing the cytosol and the C-terminal region facing the inter-membrane space (Sesaki and Jensen, 2001). Ugo1, Fzo1 and Mgm1 assemble into a fusion complex. The N-terminal cytoplasmic domain of Ugo1 binds Fzo1 near its transmembrane region and the C-terminal half of Ugo1 binds Mgm1 in the inter-membrane space.

Indeed, Ugo1 is required for the formation of a Fzo1-Mgm1 complex (Sesaki and Jensen, 2004; Wong et al., 2003). Based on these data, Ugo1 may provide a scaffold for the assembly of a fusion complex that spans the outer and inner membranes and could provide a link that coordinates Fzo1 and Mgm1 fusion.

2.2. The fission pathway

2.2.1. Dnm1/DRP1

Yeast Dnm1 is a dynamin related protein with a GTPase activity. It is located in the cytoplasm and it is recruited to the mitochondrial outer membrane (OM) to regulate mitochondrial fission. Dnm1 has an N-terminal GTPase domain, a dynamin-like middle domain and a GTPase effector domain (GED) located in its C-terminal (Okamoto and Shaw, 2005; Otera et al., 2013). During mitochondrial fission Dnm1 is recruited as small oligomers to the mitochondrial OM, at mitochondrial fission sites. Binding of Dnm1 to OM-anchored receptors, and subsequent formation of the functional fission complex, are essential for the initial step of mitochondrial fission (Otera et al., 2011; Zhao et al., 2012).

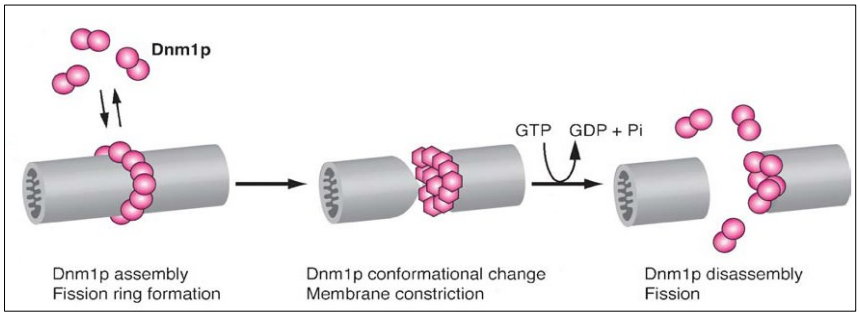

Figure 2.7. Model for Dnm1 mediated mitochondrial fission. From Okamoto and Shawn, 2005.

The mechanisms by which Dnm1 is recruited and activated on mitochondrial fission sites is well-known in yeast, but remains unclear in mammals where DRP1 is the homologue of yeast Dnm1. As in *S. cerevisiae* cytosolic DRP1 is recruited on mitochondrial outer membrane and assembles as oligomers to fission sites. Although several proteins have been identified as DRP1 candidate receptors in mammals their role in mitochondrial fission remains unclear (Elgass et al., 2013; Otera et al., 2011).

2.2.2. Fis1/hFIS1

Fis1 is an outer mitochondrial membrane protein both in yeast and in mammals. In yeast it transiently interacts with Dnm1, indicating that Fis1 acts as the mitochondrial Dnm1 receptor. Dnm1 recruitment in yeast requires two cytosolic adaptors named Mdv1 and Caf4. These adaptors contain a N-terminal domain that dimerizes and binds to Fis1 and a C-terminal domain containing WD40 repeats that binds to Dnm1 (Cerveny and Jensen, 2003; Griffin et al., 2005). In this way Mdv1 and Caf4 bridge the interaction of Fis1 with Dnm1 (Fig. 2.8).

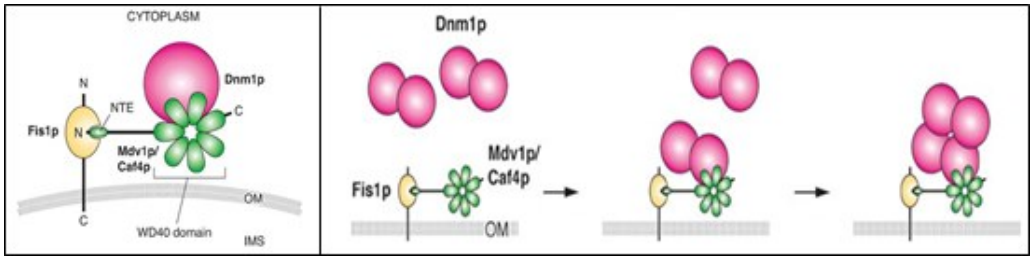

Figure 2.8. Left panel: topology of proteins acting in the mitochondrial fission pathway. Mdv1 and Caf4 interact with Fis1 and Dnm1 via their N-terminal extensions (NTE) and WD40 domains, respectively. Right panel: assembly of Fis1-Mdv1/Caf4-Dnm1 complex on OM. Abbreviations: OM, outer membrane; IMS, intermembrane space. From Okamoto and Shaw, 2005.

The role of Fis1 in mitochondrial fission is supported by the observation that yeast *fis1Δ* mutant displays elongated mitochondria due to impairment of the fission process (Okamoto and Shaw, 2005). The function of hFIS1 in mammalian cells remains unclear because Mdv1 and Caf4-like adaptors homologues have not been found in mammals (Yoon et al., 2003). hFIS1 is thought to recruit DRP1 via indirect or direct interactions as in yeast. However, it is supposed that hFIS1 and yeast Fis1 are structurally divergent or act through different mechanisms, since hFIS1 cannot rescue the *fis1Δ* mutant phenotype in yeast (Stojanowski et al., 2004). Recently, an additional protein involved in the mitochondrial fission machinery was identified in mammals and it was called MFF (mitochondrial fission factor). MFF is anchored to the outer mitochondrial membrane via its C-terminal tail and can transiently recruit Drp1, via its cytosolic N-terminal domain independently of Fis1 (Otera, 2013). MFF localizes in discrete sites on mitochondria, and its overexpression causes recruitment of Drp1 to mitochondria and

mitochondrial fragmentation. Conversely, MFF deficiency leads to reduced Drp1 at the mitochondrial fission sites and to mitochondrial elongation (Otera et al., 2010).

3. Physiological function of mitochondrial dynamic

At first, when proteins essential for mitochondrial fusion and fission were discovered, many observers asked why mitochondria are dynamic. It soon became clear that the balance between fusion and fission plays a role in maintaining the characteristic mitochondrial morphology in a given cell type (Bleazard et al., 1999; Chen et al., 2003; Sesaki et al., 1999). However, over the past decades, it has become clear that the function of fusion and fission goes beyond the regulation of mitochondria shape and size, and that both these processes have important physiological consequences. Perhaps the most important consequence of mitochondrial fusion is content mixing between two mitochondria. Of the approximately 1000 proteins present in the mitochondrion, only 13 are encoded by mtDNA. The remaining proteins are encoded by the nuclear genome and must be imported from the cytosol. During mitochondrial biogenesis the levels of these two sets of proteins must be coordinately regulated. Supposing that mitochondrial fusion does not exist, each of the several hundreds of mitochondria in each cell would act autonomously, both biochemically and functionally, leading to increased heterogeneity within the mitochondrial population in each cell. By mitochondrial fusion the organelle contents are homogenized, and therefore mitochondria could act as a coherent population. Cells with loss of fusion show a dramatic reduction of mtDNA level. Because mitochondrial genome encodes for 13 essential respiratory chain complexes proteins, cells lacking mtDNA are respiratory deficient. Yeast cells without Fzo1 and Mgm1 proteins are devoid of mitochondrial DNA and respiratory deficient. The same phenotype could be observed in mammalian cells lacking MFN1/MFN2 and OPA1 (Chen et al., 2010; Hermann et al., 1998; Rapaport et al., 1998; Wong et al., 2000). Fusion and fission processes are strictly connected with the apoptotic pathway. Apoptosis depends on the release of cytochrome c from the inner membrane space to the cytosol. Once released in the cytosol, cytochrome c binds to apoptotic protease-activating factor 1, leading to the

apoptotic pathway activation, which results in degradation of many substrates and cell death. In cellular models of apoptosis mitochondria undergo increased fission and fragmentation near the time of cytochrome c release (Frezza et al., 2006). So, while fission seems to play an important pro-apoptotic role, fusion seems to protect mitochondria, and then the cell, against some apoptotic stimuli (Sugioka et al., 2004). During cell life mitochondria undergo a quality control process, called mitophagy, that selectively leads to degradation of dysfunctional mitochondria by autophagy (Kim et al., 2007). Numerous studies demonstrated that during mitophagy among the most degraded proteins are MFN1 and MFN2. It is thought that degradation of these proteins inhibits fusion, thus promoting the segregation of dysfunctional mitochondria from the rest of mitochondrial population (Chan et al., 2011; Gegg et al., 2010; Poole et al., 2010). In addition, during mitophagy, DRP1 is actively recruited to mitochondria. An enhanced mitochondrial fission could reflect the need to reduce mitochondrial size, for the engulfment by the autophagosome (Tanaka et al., 2010). Taken together these results underline the importance of mitochondrial dynamic, in particular in cells and tissues that have a special dependence on mitochondrial function. Defects in mitochondrial dynamic can affect mammalian development, apoptosis and disease. As our knowledge of mitochondrial dynamic increases, we can expect to learn more about its involvement in other processes.

4. Mitochondrial dynamic and neurodegeneration

The importance of mitochondrial dynamic has been demonstrated in neuronal cells, where mitochondrial dysfunction seems to be a key factor in neurodegenerative disorders. The preferential degeneration of neurons, especially neurons with long axons such as peripheral sensory neurons and motor neurons, when mitochondrial dynamic is compromised, reflects several aspects of neuronal physiology that have particular demand for mitochondrial function. First, synaptic transmission, a key feature of neuronal function, requires plasma membrane potential maintenance, synaptic neurotransmitter release and reuptake, and build-up of vesicles reserve pool for prolonged or high-frequency firing. All these processes are energy demanding and require a sufficient number of active mitochondria to be present at synaptic sites. In addition, the extremely polarized morphology of neurons and the considerable distance separating the nerve terminal from the cell body make it necessary to place the site of adenosine triphosphate production near the site of demand. This is especially true for peripheral sensory and motor neurons, which have disproportionately long axons and are the most polarized cells in the body. For these neurons, mitochondrial transport must act cooperatively with mitochondrial fission/fusion to ensure that sufficient mitochondria reach the synapses. Genetic studies in *Drosophila* have identified Milton and Miro as key proteins that regulate the anterograde mitochondrial transport in axons. Both proteins can be considered as cargo adaptor proteins which link mitochondria to kinesin-1 motors in neurons. Miro attaches the outer mitochondrial membrane, with the help of the mitochondria specific adaptor protein Milton, which is directly linked to the kinesin-1 heavy chain (Guo et al., 2005; Glater et al., 2006). Mitochondria are also retrograde transported to the neuronal soma, with the use of dynein moto proteins, via the adaptor protein dynactin (Pilling et al., 2006).

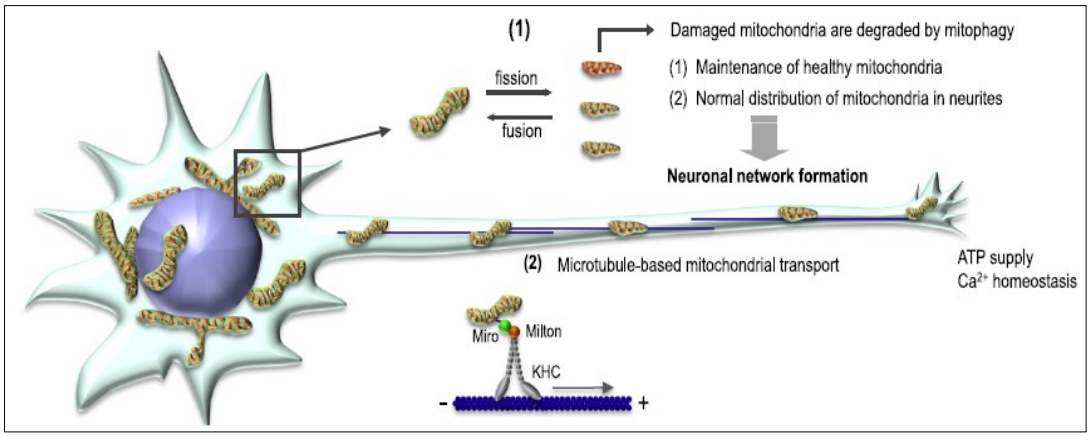

Figure 4.1. Physiologic function of mitochondrial fusion and fission in neuronal cells. Mitochondria are usually distributed throughout the soma and neurites of normal neuronal cells by microtubule-based mitochondrial transport and cargo adaptors proteins Miro and Milton. Abbreviations: KHC, kinesin 1 heavy chain. From Otera et al., 2013.

Initially, mitochondrial dynamic changes were associated with few rare inherited neurodegenerative disorders; however, expanding evidence suggests that mitochondrial dynamic dysfunction is involved in some common diseases affecting almost all organs. In this section five neurodegenerative disorders linked to alterations in mitochondrial dynamic will be described.

4.1. Charcot-Marie-Tooth type 2A (CMT2A)

CMT is the most inherited neuromuscular disorder with a prevalence estimated at 1/2500. It affects both motor and sensory neurons (Vance, 2000). Three main forms of CMT diseases are classified according to genetic inheritance: dominant CMT type 2A, recessive CMT type 4 and recessive X-linked CMT, named CMTX. Typical clinical symptoms of CMT2A include progressive distal limb muscle weakness and atrophy, stepping gait with foot drop and distal sensory loss. Almost 60 mutations on the *MFN2* gene have been reported in CMT2A patients. Most of these are missense mutations in the GTPase domain (>50%), but mutations have been detected also in the N-terminal region, in the first transmembrane region and in the C-terminus, specifically in the region facing the cytoplasmic site. Mutations of MFN2 responsible for CMT2A show autosomal dominant inheritance; consequently they may lead to haploinsufficiency or dominant gain of function.

Interestingly it was reported that defective mitochondrial fusion observed in CMT2A cells models is rescued by overexpression of MFN1, which is consistent with the observation that MFN1 physically associate with both wild-type MFN2 and MFN2 CMT2A mutant to promote mitochondrial fusion (Amiott et al., 2008; Detmer and Chan, 2008). Recently transgenic mice expressing a mutant form of MFN2, with a presumed gain of function specifically in motor neurons, have been generated. These mice show a phenotype consistent with the clinical symptoms detected in CMT2A and provide a useful system to determine the function of mitochondria in the axons of motor neurons (Detmer and Chan, 2008).

4.2. Parkinson Disease (PD)

Parkinson disease is characterized by progressive loss of the nigrostriatal dopaminergic neurons in the midbrain region. An individual suffering from PD usually presents postural instability, tremors at rest and slow movements (Abou-Sleiman et al., 2006; Hughes et al., 1992). Emerging evidence suggests that the mitochondrial dysfunction is an essential component of PD pathogenesis and this is supported by genetic PD models characterized by abnormal mitochondrial dynamic. Juvenile Parkinsonism is characterized by mutations in two genes *PARKIN* and *PINK1*. The serine/threonine kinase PINK1 (Pten-induced kinase 1) is constitutively repressed in healthy mitochondria by import into the inner mitochondrial membrane and degradation by the rhomboid protease PARL. When a mitochondrion is damaged, protein import to the inner mitochondrial membrane is prevented, so PINK1 is diverted from PARL and accumulates on the outer mitochondrial membrane. On the damaged mitochondrion PINK1 recruits the ubiquitin E3 ligase PARKIN from the cytosol. Once there, PARKIN ubiquitinates outer mitochondrial membrane proteins, including mitofusins, and induces autophagic elimination of the damaged mitochondrion. Therefore this PINK1/PARKIN pathway can be considered as a quality control mechanism to eliminate damaged mitochondria (Fig.4.2).

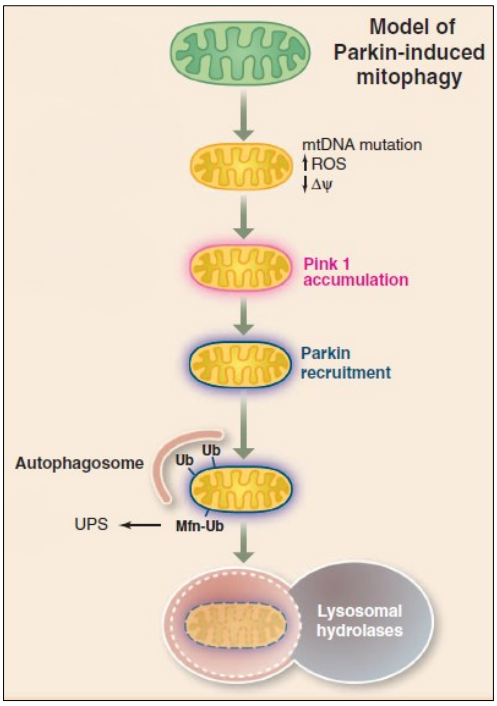

Figure 4.2. Schematic representation of PINK1/PARKIN induced mitophagy. Abbreviations: Ub, ubiquitin; UPS, ubiquitin proteasome system. From Youle and van der Blick, 2012.

Furthermore it has been shown that the PINK1/PARKIN pathway is involved in mitochondrial dynamic regulation, supporting mitochondrial fission in PD models. It promotes a downregulation of MFN1, MFN2 (via PARKIN mediated ubiquitination) and OPA1, and an upregulation of DRP1, thus resulting in an increase of DRP1 recruitment on the mitochondrial outer membrane and consequent mitochondrial fragmentation (Deng et al., 2008; Wang et al., 2011). Recent genetic studies in flies demonstrated that overexpression of DRP1 or downregulation of MARF (a fly homologue of mammalian MFNs) or OPA1 can dramatically ameliorate the phenotypes of PINK1 or PARKIN mutant flies. These striking observations indicate a genetic interaction between the PINK1/ PARKIN pathway and mitochondrial dynamic.

4.3. Alzheimer's Disease (AD)

Alzheimer's disease is the most common form of dementia worldwide and is clinically characterized by deterioration in memory, language skills and visual acuity (Castellani et al., 2010). Afflicted brains carry intracellular neurofibrillary tangles and extracellular amyloid plaques composed of amyloid beta (Aβ) derived from amyloid precursor protein (APP). Although the pathological mechanism for AD is still unknown, the predominant hypothesis is that excess Aβ production results in cellular toxicity. In addition, mitochondrial dysfunction, altered Ca^{2+} homeostasis and elevated ROS are all features of AD affected neurons, clearly linking mitochondria to the pathogenesis of this type of neurodegeneration (Beal, 2005). Impaired mitochondrial morphology has been described in AD neurons which have fewer and larger mitochondria than wild-type neurons, suggesting a potential incidence of abnormal mitochondrial dynamic in the AD brain (Hirai et al., 2001). Many studies reveal significant changes in protein levels such as decrease of MFN1, MFN2 and OPA1 affecting mitochondrial fusion. In addition an increase in FIS1 level has been observed, leading to a high rate of mitochondrial fission in AD brains. (Wang et al., 2009; Manczak et al., 2011, 2012). Furthermore the interaction of DRP1 with the amyloid beta (Aβ) leads to an abnormal mitochondrial dynamic and damage to the synapses, resulting in AD disease progression (Chen and Chan, 2009). Together these results suggest that the increased mitochondrial fragmentation in AD likely contributes to mitochondrial dysfunctions and, ultimately, to disease progression.

4.4. Huntington Disease (HD)

HD is a late onset autosomal dominant neurodegenerative disorder caused by the abnormal CAG triplet expansion in the exon 1 of the *HUNTINGTIN* gene. HD patients suffer from cognitive, psychiatric and motor abnormalities resulting from the loss and dysfunction of neurons in the striatum and deep layers of the cortex. Mutant huntingtin (HTT) causes widespread cellular dysfunction, among which mitochondrial dynamic seems to play an important role.

Studies on cellular models of HD, as well as HD postmortem brain tissues, have reported increased expression of DRP1 and FIS1 and depressed expression of mitofusins and OPA1 (Kim et al., 2010; Shirendeb et al., 2011; Song et al., 2011; Wang et al., 2009). Although the mechanism linking HD and mitochondrial dynamic dysfunction remains to be cleared, it is supposed that mutant HTT and DRP1 directly interact. This interaction may stimulate the GTPase activity of the pro-fission factor leading to an increase in mitochondrial fragmentation. As a consequence the balance between fusion and fission is impaired and neuronal cell death increases. These evidences support a role for impaired mitochondrial dynamic in Huntington disease.

4.5. Autosomal Dominant Optic Atrophy (ADOA or DOA)

Dominant Optic Atrophy (OMIM #165500), initially called Kjer's optic atrophy, has first been described by the Danish ophthalmologist Dr. Poul Kjer (Kjer, 1959). DOA is caused by mutations in *OPA1* gene (Optic atrophy 1) and is characterized by degeneration of retinal ganglion cells (RGCs), whose axons form the optic nerve. This disease is characterized by an insidious onset of visual impairment in early childhood with moderate to severe loss of visual acuity and abnormalities of color vision. ADOA shows variable expression, both between and within families, ranging from an asymptomatic state to a legal blindness (Votruba et al., 1998; Thiselton et al., 2002; Yu-Wai-Man et al., 2010). DOA associated OPA1 mutations cluster mostly in the GTPase domain (Exons 8-15) and dynamin central region (Exons 16-23), with single base-pair substitutions representing the most common mutational subtype, followed by deletions, and insertions (Olichon et al., 2006; Ferre et al., 2009) as shown in Fig.4.3.

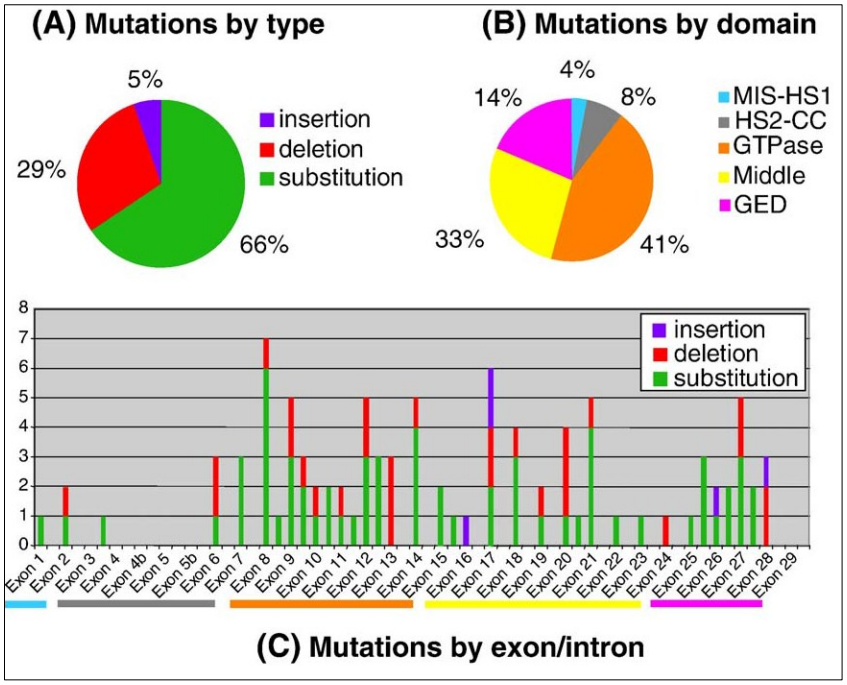

Figure 4.3. Mutation spectrum of OPA1. Distribution of the 96 mutations of OPA1 according to their type (A), domain (B) and location (C). In C colored bars under exons indicate their belonging to OPA1 domains. From Olichon et al., 2006.

The majority of OPA1 mutations results in premature termination codons, with production of truncated mRNAs which are unstable and mostly degraded by protective cellular mechanisms, such as nonsense mediated mRNA decay (Pesch et al., 2001; Schimpf et al., 2008; Zanna et al., 2008). The reduction in OPA1 protein level, leading to haploinsufficiency, is the major disease mechanism in DOA. However, about 30% of patients with DOA harbor missense OPA1 mutations, and those located within the catalytic GTPase domain, are more likely to exert a dominant negative effect. A dominant negative mechanism is well documented for dynamins with deficient GTPase activity (Marks et al., 2001). This is related to the ability of the mutated dynamin to form oligomers with the wild-type protein and thus interfering with the GTPase activity. The patients carrying these mutations display a syndromic form of DOA, named DOA plus (DOA+). DOA plus is characterized by extra ocular signs as sensorineural hearing loss, myopathy associated with mtDNA deletions and peripheral neuropathy. Amati-Bonneau and colleagues were the first to identify, in 2003, a mutation in OPA1 causing DOA+.

Patients bearing the R445H substitution, which affects the GTPase domain of OPA1, displayed sensorineural hearing loss. In addition to this, fibroblasts from these patients were shown to contain highly fragmented mitochondria (Amati-Bonneau et al., 2003, 2005). The major problem in studying DOA pathophysiology concerns the question why RCGs are most specifically affected by this disease, while the *OPA1* gene is expressed in all cells of the body. Histochemical studies revealed a peculiar distribution of mitochondria in retinal ganglion cells; they are accumulated in the cell bodies and in the intra-retinal unmyelinated axons and are conversely scarce in the myelinated part of axons after the lamina cribrosa (Andrews et al., 1999). These observations emphasize the importance of mitochondrial network dynamic, in order to maintain the appropriate mitochondrial intracellular distribution that is critical for axonal and synaptic functions, and point to a possible pathophysiological mechanism associated to OPA1.

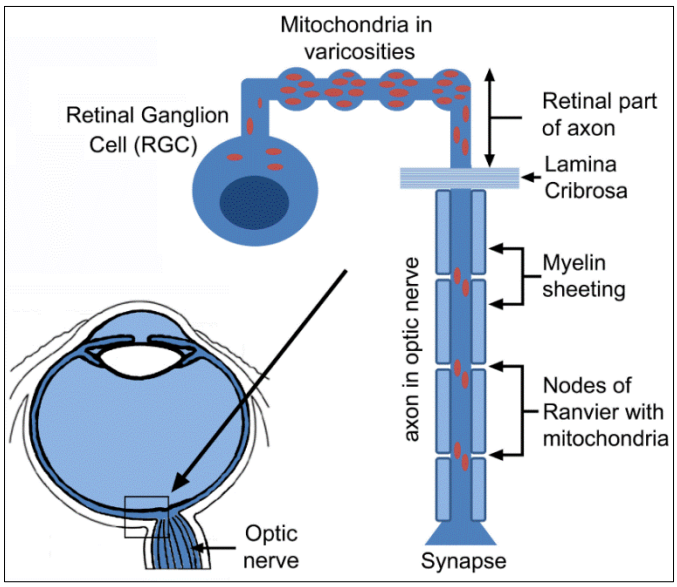

Figure 4.4. Mitochondrial distribution in the optic nerve.

Alternatively, RGCs are the only neurons that are exposed to the day long stress of light, which generates oxidative species favoring the apoptotic process (Osborne et al., 2008). Therefore, the mitochondrial fragility conferred by OPA1 mutations, together with the photo-oxidative stress, could lead RGCs to premature cell death.

A third pathophysiological hypothesis involves the tremendous energetic requirements of RGCs, as these neurons permanently fire action potentials, in addition through axons that are not myelinated in the eye globe. One can hypothesize that due to the uncoupling of mitochondrial respiration in OPA1 mutant cells, the ATP synthesis in RGCs is limited, and cannot fulfill the physiological energetic requirements for long term cell survival. Which of these hypotheses represents the *princeps* mechanism responsible for the RGCs degeneration remains unknown. In DOA and DOA plus study two major challenges are still unanswered: the first is the *princeps* mechanism that is affected in DOA and the second is deciphering why mainly RCGs are degenerating in this disease. Answering these questions should allow both to gain more insight into the disease mechanism and to facilitate the future design of treatments. Nowadays the current absence of treatment for this disease is raising a tremendous challenge in testing therapeutic strategies on different available models, from cell lines to animals. As described in this section, mitochondrial dynamic plays a vital role in maintaining health through the regulation of mitochondrial function. Unbalanced mitochondrial fusion and fission has been identified in many mitochondrial related genetic diseases. The growing investigation of the mitochondrial dynamic pathways will provide new insights both into the mechanisms involved in these disorders and into therapeutic approaches to these genetic diseases.

5. *Saccharomyces cerevisiae* as a model organism for the study of mitochondrial diseases

The yeast *Saccharomyces cerevisiae* is one of the most intensively studied model organisms to investigate the molecular and genetic basis of human diseases. Despite its simplicity, yeast shares many cellular activities and metabolic pathways with humans and for this reason *S. cerevisiae* has been defined "honorary mammal" (Resnick and Cox, 2000). *S. cerevisiae* was the first eukaryote organism to have its genome fully sequenced and published (Goffeau et al., 1996). Remarkably about 46% of human known proteins have homologs in yeast: among these, proteins involved in DNA replication, recombination, transcription and translation, cellular trafficking and mitochondrial biogenesis were found (Venter et al., 2001). Moreover about 40% of human genes, whose mutations lead to diseases, have an orthologue in yeast (Bassett et al., 1996). For this reason yeast has been widely used to decipher molecular mechanisms underlying diseases in general. However, the study of mitochondrial functions and dysfunctions is of a special interest in yeast, because it is in this organism that mitochondrial genetics and recombination have been discovered (Bolotin et al., 1971). Specific reasons led to choose *S. cerevisiae* for mitochondrial studies. First yeast metabolism is regulated in accordance to carbon sources and oxygen availability. When grown in presence of glucose yeast uses glycolysis to produce ATP, while the respiration is almost completely suppressed. When glucose is exhausted there is a rapid metabolic shift from fermentation towards respiration, with the consequent induction of all genes responsible for coding respiratory enzymes subunits. Although glucose is the preferred source, yeast is able to use also glycerol, ethanol, acetate and lactate as non-fermentable carbon sources. Utilization of these metabolites requires a proper mitochondrial function. *S. cerevisiae* possesses the peculiar characteristic to be a facultative aerobe organism. Moreover, yeast is the only eukaryote able to survive in the absence of both mitochondrial function and mtDNA, so long as a fermentable carbon source is available. Yeast mutants impaired in OXPHOS functions are known as respiratory deficient (RD) mutants, and are not able to grow on oxidative carbon sources, strictly depending on fermentable carbon sources.

RD mutants are distinguishable from respiratory competent strains both for their morphology and physiology. Actually they give rise to small colonies, if grown on non-fermentable carbon sources, and for this reason they are known as *petite* mutants. The small size of these peculiar mutants depends on their inability to metabolize the ethanol produced by glucose fermentation, and this consequently results in a stopped growth. *Petite* colonies arise from mutations on genes for OXPHOS components encoded both by nuclear and mitochondrial genome. In the latter case it is possible to distinguish rho^- mutants, with large deletion on mtDNA, and rho^0 mutants, with a complete loss of mitochondrial genome (Dujon, 1981; Tzagaloff and Dieckmann, 1990). Thanks to its ability to survive in absence of its mitochondrial genome yeast is defined as *petite*-positive. This feature makes it possible to study all mutations of the mitochondrial genome without cell lethality. As previously said, both mitochondrial genes and functions are conserved between yeast and humans. Thanks to the numerous genetic tools available to detect phenotypes related to mitochondrial dysfunction, *S. cerevisiae* has been largely used as a model organism for the study of mitochondria related pathologies. Mutations affecting mitochondrial function in yeast usually result in an impaired or reduced oxidative growth, decrease or absence of respiratory activity and/or a rearrangement of the respiratory cytochromes structure (Rinaldi et al., 2010). Different approaches have been used in the study of human diseases in yeast. When a homolog of the gene involved in the disease is present in the yeast genome, the mutation can be introduced in the yeast gene and its effects can be evaluated both at a physiological and molecular level. Furthermore the possibility to duplicate as haploid or diploid makes this organism a flexible tool for assessing the dominant or recessive nature of a mutation. On the other hand, when the disease-associated gene does not have the counterpart in yeast the transgene can be heterologously expressed in yeast and the resulting strain, named “humanized yeast”, can be subjected to functional analysis. A large number of mitochondrial diseases are associated with mtDNA defects, which are caused by point mutations, rearrangements, and/or deletions. The utility of using yeast to model these diseases is exemplified by the unique ability to directly transform yeast mtDNA.

In yeast, biolistic transformation (shooting at high velocity micro-projectiles layered with manipulated DNA), was initially shown by Johnston et al., and Fox et al., and now it has been improved enough to be used as a routine technique (Johnston et al., 1988; Fox et al., 1988). This procedure allows a defined mutation, identified in human patients, to be studied in the context of one host nuclear genetic background. Of course, this capability additionally allows distinct mtDNA mutations, in the same gene or different genes, to be studied, compared and contrasted in the same genetic background. During the last decades yeast models have enabled us to gain important insight into the underlying molecular basis of pathology of disease-associated mutations. Importantly, once validated, yeast models of human diseases are a very useful platform for high-throughput screenings as a first-line approach in the discovery of new genes that might have potential as therapeutic targets, as well as in the identification of new drugs with therapeutic value as described in the next section.

6. *S. cerevisiae* as a model organism for drug discovery

Drug discovery is a highly complex and multidisciplinary process whose goal is to identify compounds with therapeutic effects, i.e. molecules able to modulate the function of both a protein or a cellular pathway involved in a human disease. The current paradigm for *de novo* drug discovery begins with the identification of a potential target (usually a protein), and proceeds through the validation of the target in animal and/or cell culture models. Once the target is validated, the process first goes on with the development and execution of a screening system to obtain small molecules that modulate the activity of the target, and after, with the characterization and optimization of these small molecules. Active compounds are subsequently tested for their efficacy, toxicity, and side effects in animals and/or cell culture models, and finally a series of FDA-supervised clinical trials are performed to evaluate safety, pharmacology, and efficacy in comparison to existing treatments for the same indications (Hughes, 2002). The entire progression typically lasts a decade and costs millions of dollars for every molecule reaching the market. Improvement and acceleration of the drug discovery and development process at virtually any step is therefore of interest from commercial, economic and medical viewpoints.

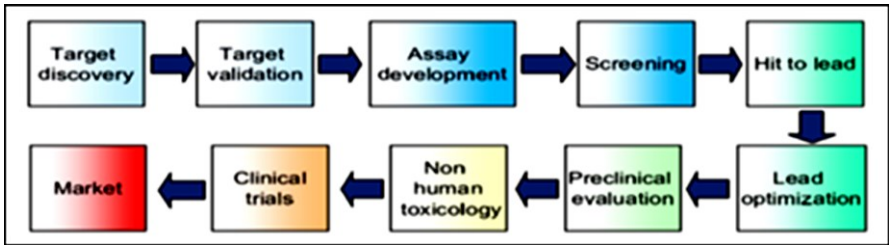

Figure 5.1. Diagram of the *de novo* drug discovery process. From Carnero, 2006.

For this reason current approaches to drug discovery require an assay that can test simultaneously hundreds of thousands of compounds, hence high throughput screenings (HTS) have become the major tools in this emerging field. HTS allow the isolation of dozen to thousands of molecules to be further tested and ranked for development priority.

On such a scale it is fundamental that HTS assays can be performed in small volumes, high density (i.e. 384- and 1536-well microplates) and with the help of robotic processing. In general HTS assay formats can be classified into two types; *in vitro* target-based biochemical assays and cell-based assays. *In vitro* target-based biochemical screening is an effective approach with a well-defined pathology and highly validated target. Its biggest advantage is that the exact target and mechanism of action are known. However, many of the most commonly used drugs function through unknown mechanisms and target-based approaches have a few drawbacks. First, the success of target-centric approaches hinges on correctly predicting the link between the chosen target and disease pathogenesis. Second, this biased approach may not actually target the best or most "druggable" protein to provide optimal rescue. Third, it is not always possible to accurately predict the activity of compounds *in vivo*. Finally, the small molecules obtained *in vitro* may have chemical liabilities that preclude efficacy *in vivo*, including entry into cells, solubility, metabolism, distribution, excretion, and off-target effects (Tardiff and Lindquist, 2013). These potential pitfalls can hinder validation of a compound within the context of a cellular or animal model. In contrast, cell-based assays do not require purified target proteins and can be engineered to produce a simple, measurable readout of cellular processes for HTS (Barberis et al. 2005). Furthermore, in these formats the activity of any compound against a specific target is analyzed in a cellular context that more closely resembles the *in vivo* scenario. Finally, a cell-based HTS can identify those compounds that are generically cytotoxic or may exhibit problems with stability or solubility *in vivo*. As such, and compared with *in vitro* biochemical assay platforms, cell-based assays have the potential to identify compounds with drug-like properties which are ready for further development. The most significant barrier in cell-based screens is determining a compound mechanism of action and protein target. However, the genetic tractability of model organisms offers new approaches for target discovery, although this is often difficult. Of course, a limiting factor for cell-based screening is that a compound potential is only as valid as the model from which it was derived. Cellular screens should ideally be performed with cells of human origin, which evidently provide the

most physiologically relevant model system. However, human cells are expensive to culture and sometimes difficult to propagate in automated systems used for HTS. Moreover, the genetic manipulation of mammalian cells is generally problematic and time-consuming. The high degree of conservation of basic molecular and cellular mechanisms between yeast and human cells underscores the value of *S. cerevisiae* as a tool for drug discovery. In yeast cells the function of human proteins can often be reconstituted and aspects of some human physiological processes can be recapitulated. Thus, yeast represents an inexpensive and simple alternative system to mammalian culture cells for the analysis of drug targets and for the screening of compounds in a heterologous, yet cellular, eukaryotic environment. One major advantage of yeast over mammalian cells is provided by the versatile genetic malleability of this organism. This characteristic of yeast, as well as the long scientific experience in yeast genetics and molecular biology, has allowed the development of a wealth of experimental tools and genetic selection systems that can now be readily converted to HTS formats for drug discovery. These molecular and cellular tools include advanced plasmid systems, homologous recombination techniques and the easy application of conditional growth selection systems. Despite its numerous advantages, yeast assays are not without limitations for the purposes of drug discovery. Principal among these, is the high concentration of compound often required to produce a biological response, likely due to the barrier presented by the cell wall, and the presence of numerous active efflux pumps and detoxification mechanisms (Smith et al., 2010). In addition, although many core processes are conserved between yeast and human, several “metazoan-specific” processes are not.

Technology	*In vitro* HTS	Mammalian cellular HTS	Yeast cellular HTS
Pros	• A well-optimized assay has less data scatter than a cellular assay	• Target protein is presented in its native conformation in a physiological environment • Selection for membrane permeability and against cytotoxicity • Eukaryotic environment • Self-renewal system	• Genetic malleability and established wealth of genetic tools for analysis of biological functions • Target protein is presented in its native conformation in a physiological environment • Selection for membrane permeability and against cytotoxicity • Clean read-out in a heterologous, yet eukaryotic environment • Self-renewal system • Simple handling • Fast discrimination of real hits from false positives
Cons	• Target protein has to be purified and biochemically characterized • No self-renewal system • Suitable substrate must be identified and synthesized	• Function of the target protein is influenced by redundant cellular processes • Difficulty to discriminate real hits from false positives • Difficult and time-consuming genetic manipulations	• Reduced sensitivity to defined compound classes owing to efficient drug efflux pumps
Costs	• Expensive: protein purification, synthesis of substrate	• Expensive culture conditions	• Inexpensive culture conditions

Figure 5.2. Comparison summary between *in vitro* HTS, mammalian cellular HTS and yeast cellular HTS. From Barberis et al., 2005.

The published literature contains dozens of examples of yeast-based, target-oriented screening systems, whose aim is to find one or more compound able to modulate the activity of a specific target. An alternative mode of drug screening is to identify compounds that cause a desired physiological change, rather than inhibition of a specific protein. Chemical screenings based on phenotype, named phenotype-based screenings, can be used to find new potential therapeutic compounds and ultimately to identify new proteins in a pathway or to dissect cellular processes (Mayer et al., 1999; Mundy et al., 1999; Haggarty et al., 2000). Recently Couplan and colleagues developed a two-step yeast phenotype-based assay, called “Drug drop test”, to identify active drugs against human mitochondrial diseases affecting ATP synthase, in particular NARP (neuropathy, ataxia, and retinitis pigmentosa) syndrome. An appropriate yeast model of such disorders is the deletion mutant for the nuclear gene *FMC1* that encodes a protein required at high temperatures (35-37°C) for the assembly of the F1 sector of ATP synthase. Indeed when the *fmc1Δ* mutant is grown at high temperatures, its mitochondria contain fewer assembled ATP synthase complexes than a wild-type strain.

The Drug drop test was performed in solid medium and it was composed of a primary screening in which ~12.000 compounds from various chemical libraries were tested for their ability to suppress the respiratory growth defect of the *fmc1Δ* mutant. Some of the tested compounds were from the Prestwick Chemical Library, a collection of drugs for which bioavailability and toxicity studies have already been carried out in humans; therefore, active compounds from this library can directly enter drug optimization programs. Experimentally, *fmc1Δ* cells were spread on solid glycerol medium and exposed to filters spotted with the compounds. After incubation at 35°C, active compounds were then identified by a halo of enhanced growth around a filter (example in Fig.5.3).

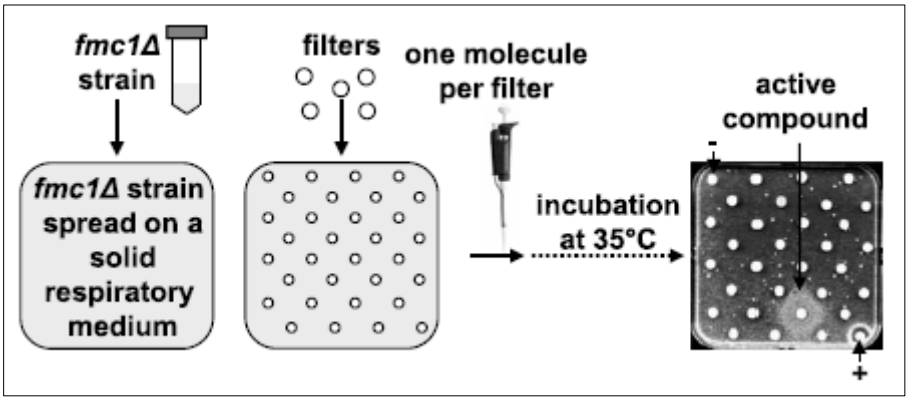

Figure 5.3. Schematic representation of the "Drug drop test" technique. From Couplan et al., 2011.

Active compounds, isolated from primary screening, were tested in a secondary screening, on the five yeast *atp6*-NARP mutants which are the yeast models of the five most common mutations in *ATP6* related to NARP syndrome, using the same experimental procedure. The advantage of this method is that, in one simple experiment, it allows numerous compounds to be tested across a large range of concentrations, due to diffusion of the drugs in the growth medium. Two compounds were identified as active. Further studies demonstrated that both these molecules were active also on human cells (Couplan et al., 2011). A similar approach has recently been used in our laboratory for the search of active molecules against mitochondrial disorders caused by mutations in *POLG*, which encodes for the catalytic subunit of the

DNA polymerase γ. In this study, *mip1* mutated yeast strains carrying different thermo-sensitive mutations, which led to a high frequency of *petite* mutants at 37°C, were used. Using the "Drug drop test" method previously described, six molecules, named MRS1-6, proved able to rescue the mutant phenotypes of the *mip1* yeast strains. Interestingly one of these molecules, MRS3, was active also on *C. elegans* and human fibroblasts. This finding can lead the way, for MRS3, for a clinical trial in the search of treatments for human mitochondrial diseases related to POLG (Pitayou et al., in press). Altogether these results demonstrate that *S. cerevisiae* is a useful model for drug discovery approaches. Furthermore, as yeast models of inherited mitochondrial disorders continue to be developed, the high-throughput screening approach described here will continue to yield both promising chemical therapeutics and insights into disease mechanisms.

Aim of the research

The work described in this thesis is part of FIRB 2013 project entitled “From yeast to human: how OPA1 isoforms and pathogenic mutations cause neurodegenerations characterized by mtDNA instability” that involves the close partnership between the Laboratory of Genetics (University of Parma), where all yeast experiments have been performed, and the Department of Pharmacy and Biotechnology (University of Bologna), in particular Dr. Claudia Zanna group, specialized in studying OPA1 isoforms and mutations in MEF and patients fibroblasts.

The present study has two main aims.

The first aim is to generate a *Saccharomyces cerevisiae* model to study OPA1 mutations associated with Autosomal Dominant Optic Atrophy (ADOA). Because of the very weak sequence identity between *OPA1* and the yeast orthologue *MGM1*, only few pathological mutations involving conserved residues can be introduced and studied in *MGM1* for the analysis in yeast (Section 1). So, a novel yeast model has been constructed, by generating a *MGM1*/*OPA1* chimeric gene able to complement the OXPHOS defect of the *mgm1Δ* mutant. This fusion gene contains a large part of *OPA1* in which a set of new ADOA and ADOA plus associated mutations, found in patients by the researchers of Dr. Zanna group, have been introduced. The pathogenicity of these mutations has been validated, both by characterizing the phenotypic defects associated with the mutant alleles, and investigating their dominance/recessivity in the yeast model (Section 2). The *S. cerevisiae* model thus created will contribute to validate new mutations found in patients, to elucidate the results obtained in humans and to gain new insight into the pathological mechanisms underlying this neurodegenerative disease.

The second aim of this thesis is to exploit the *S. cerevisiae* model to search for an ADOA treatment. A yeast-based phenotypic screening of chemical libraries, designed to search for molecules acting as chemical suppressors able to rescue the mitochondrial defective phenotypes induced by pathogenic mutations in the *OPA1* gene, has been set up (Section 3). This drug discovery approach, through which several potential active compounds have been found, has a double goal: on one hand it will allow to further understand the role of OPA1 protein and, on the other, it will pave the

way for new pharmacological therapies aimed at recovering specific OPA1 dysfunctions, thus improving the conditions of ADOA/ADOA-plus patients.

Results and Discussion

1. Validation of mutations in conserved residues of Mgm1/OPA1

1. Validation of mutations in conserved residues of Mgm1/OPA1

1.1. Construction of *mgm1Δ* host strain

The yeast *Saccharomyces cerevisiae* is a suitable model organism to test the pathogenicity of human mutations associated with many different diseases (Jones and Fangman, 1992). Different strategies are used to validate pathological mutations in yeast, depending on the conservation of the residues involved and/or on the ability of the human wild-type cDNA to complement the absence of the gene (reviewed in Barrientos, 2003; Rinaldi et al., 2010; Baile and Claypool, 2013; Lodi et al., 2015; Lasserre et al., 2015). In order to introduce and study the equivalent pathological mutations found to be associated with DOA and DOA plus in the *MGM1* gene of *Saccharomyces cerevisiae*, at first we created a *mgm1Δ* haploid mutant. As previously said, the deletion of *MGM1* gene causes loss of mitochondrial DNA, thus making the *mgm1Δ* strain rho^0. A rho^0 strain is not useful to this study, making impossible to investigate the effects of pathological mutations on mitochondrial respiration, oxidative growth and mtDNA maintenance. In order to avoid loss of mitochondrial DNA the *MGM1* gene was disrupted in presence of the wild-type allele. In this condition, mitochondrial DNA is maintained thanks to the functional copy of plasmid-borne *MGM1*. Primarily we cloned *MGM1* gene in pFL38 plasmid (centromeric, *URA3* marker). *MGM1* gene and its upstream and downstream regions were PCR amplified using genomic DNA of W303-1B strain as template and MGM1CSalIFw and MGM1CSacIRv as primers. The amplicon was then digested with *Sac*I and *Sal*I and cloned in pFL38, digested with the same enzymes. pFL38*MGM1* was used to transform both W303-1A and W303-1B strains. The *MGM1* gene was then disrupted in W303-1A and W303-1B strains transformed with pFL38*MGM1* by “one step gene disruption” (Rothstein et al, 1983) modified according to Wach et al. (Wach et al., 1994) as described in Materials and Methods. By this technique, the gene of interest is disrupted at the chromosomal locus by the KanMX4 cassette conferring geneticin resistance to the transformed yeast strain. The mgm1::KanMX4 cassette was amplified from the genomic DNA of BY4742 *mgm1Δ* strain and inserted into both strains through

high efficiency yeast transformation protocol (Giets and Woods, 2002). The mgm1::KanMX4 cassette could recombine either at the *MGM1* gene harbored on pFL38, or at the wild-type gene in the genome. To distinguish between these two cases we performed *plasmid shuffling* on 5-FOA and then checked the phenotype of the *mgm1Δ* strains on non-fermentable carbon sources. Cells in which the genomic *MGM1* locus was disrupted were not able to grow on oxidative carbon sources, due to the loss of mtDNA after pFL38*MGM1* counter selection in 5-FOA plates. Vice versa, cells in which the mgm1::KanMX4 cassette recombined at the *MGM1* plasmid copy maintained mtDNA and were able to grow on non-fermentable carbon sources.

1.2. Study of mutations in conserved residues of Mgm1/OPA1

So far more than 300 pathogenic mutations, spread throughout the entire *OPA1* gene, have been identified (OPA1 LSDB http://opa1.mitodyn.org). About 50% of these *OPA1* mutations (frameshift and nonsense mutations, stop codons, splicing errors, or deletions/insertions) generate a haploinsufficiency situation, where the mutated transcript is degraded by nonsense mediated mRNA decay, thus reducing to 50% the amount of OPA1 protein (Schimpf et al., 2008). The remaining ones are missense mutations, mostly clustered in the GTPase domain, which cause heterozygous amino acid substitutions thought to exert a severe dominant negative effect (Amati-Bonneau et al., 2009). These latter mutations are often associated with a more severe syndromic disorder named “DOA plus” (Amati-Bonneau et al., 2008; Hudson et al., 2008; Yu-Wai-Man et al., 2010). Although Mgm1 and OPA1 own equivalent functional domains, their amino acid sequences are weakly conserved, therefore only few pathological mutations involve conserved residues that can be substituted in *MGM1* and analyzed in yeast. As shown by the alignment in Fig.1.1 all four substitutions found in patients affect conserved residues between yeast Mgm1 and human OPA1 proteins. We decided to study these equivalent Mgm1/OPA1 pathological mutations in *S. cerevisiae MGM1* gene.

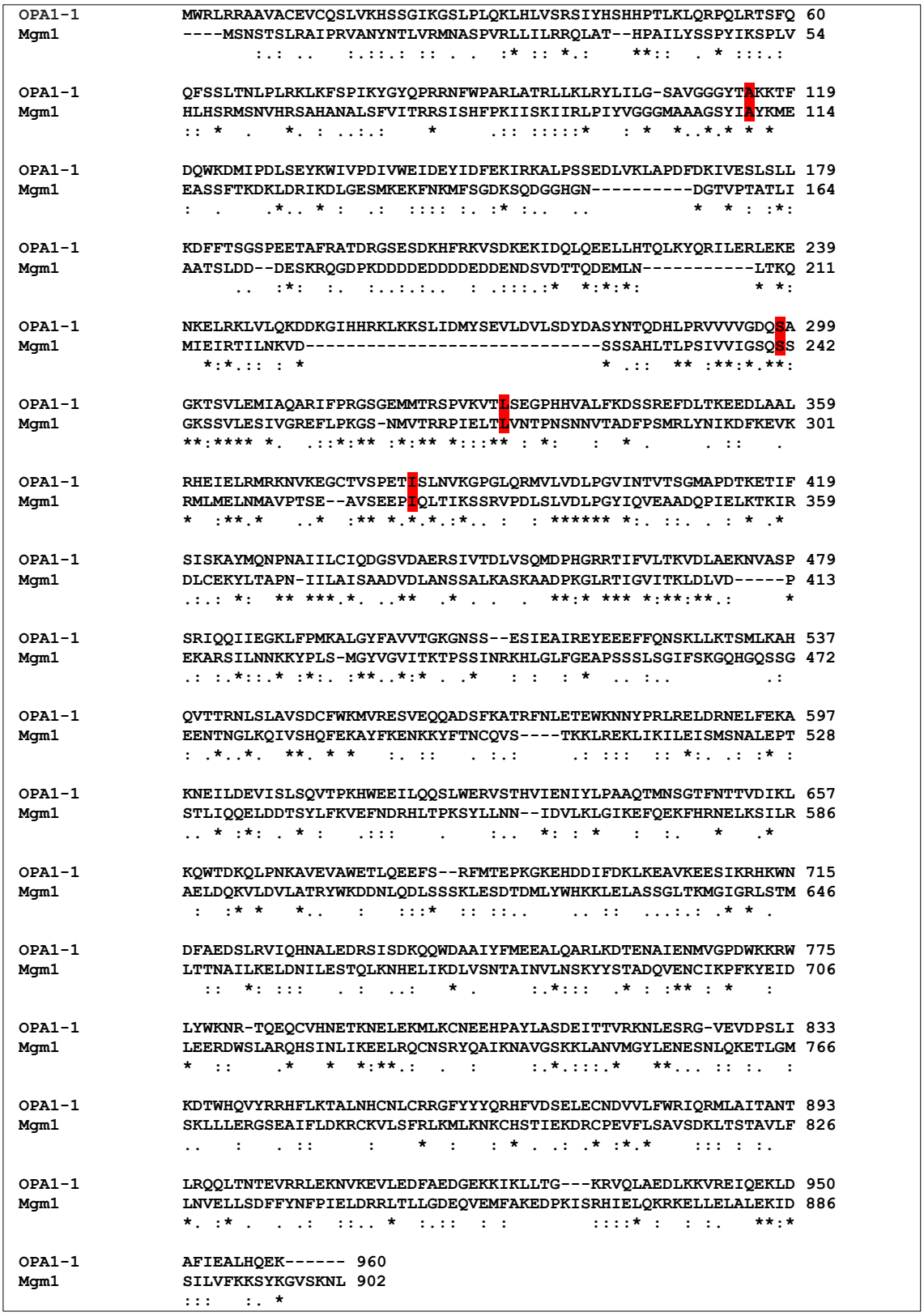

Figure 1.1. Alignment of OPA1 (isoform 1) and Mgm1 protein sequences obtained with ClustalW (http://www.ebi.ac.uk/Tools/clustalw). The four conserved amino acid residues analyzed in this study are highlighted in red.

A115V and S298N (equivalent to A110V and S241N in Mgm1) were identified in DOA plus patients, whereas L273P and I322M (equivalent to L331P and I382M in Mgm1) cause DOA (Table 1.2).

OPA1	Mgm1	Domain	Disease
A115V	A110V	TM	DOA plus
S298N	S241N	GTPase	DOA plus
L331P	L273P	GTPase	DOA
I382M	I322M	GTPase	DOA

Table 1.2. Equivalent mutations in Mgm1 and OPA1.

Three of these mutations are localized in the GTPase domain of Mgm1, whereas A110V lies in the transmembrane domain. The four substitutions were introduced in *MGM1* gene cloned in pFL38, by site directed mutagenesis using the overlap extension technique. Mutated alleles were then cloned into pFL39 vector (centromeric, *TRP1* marker) obtaining the so called plasmids: pFL39*mgm1*^{A110V}, pFL39*mgm1*^{S241N}, pFL39*mgm1*^{L273P} and pFL39*mgm1*^{I322M} by which we transformed strain W303-1A *mgm1Δ*/pFL38*MGM1.* To obtain strains containing only the mutated alleles, we then counter-selected the pFL38*MGM1* through *plasmid shuffling* on 5-FOA, as described in Materials and Methods. If the mutant allele was able to complement the loss of mtDNA of the *mgm1Δ* strain, transformant cells would be rho^{+} and they would grow on non-fermentable carbon sources. On the contrary, if the mutant allele failed the complementation, the cells would be rho^{0} and so respiratory deficient (RD). In order to discriminate between the two situations, the phenotype of the mutant strains was analyzed by spot assay on oxidative carbon source at both 28°C and 37°C, as shown in Fig. 1.3.

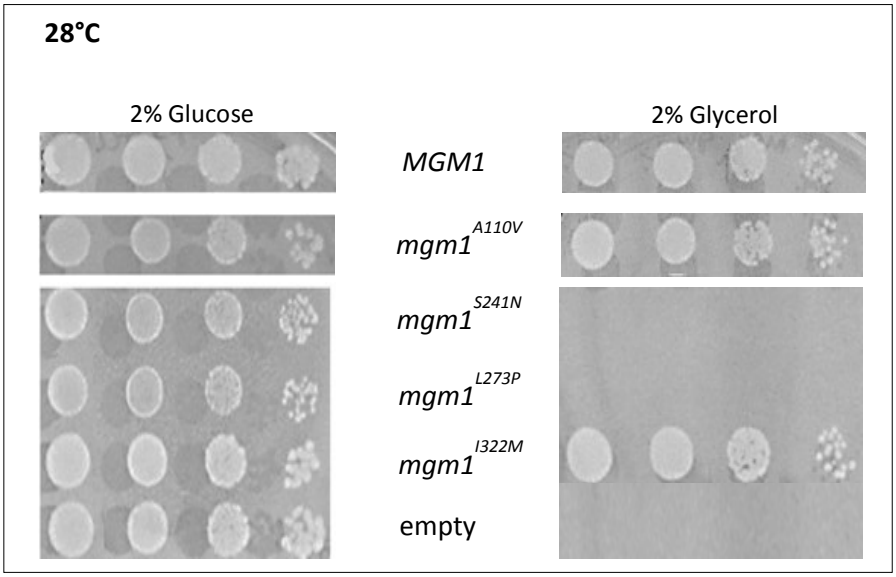

Figure 1.3. Spot assay at 28°C of W303-1A *mgm1Δ* strain transformed with pFL39*MGM1*, pFL39*mgm1*^{A110V}, pFL39*mgm1*^{S241N}, pFL39*mgm1*^{L273P}, pFL39*mgm1*^{I322M} and pFL39 empty vector on YNB DO-TRP medium supplemented with 2% glucose (left) or 2% glycerol (right).

Strains carrying *mgm1*^{S241N} and *mgm1*^{L273P} mutant alleles were unable to grow on both glycerol and ethanol as non-fermentable carbon sources at 28°C, suggesting that these mutations failed to complement the deletion of *MGM1* gene, thus showing their severe pathological effect in yeast. Cells harboring *mgm1*^{A110V} and *mgm1*^{I322M} alleles were respiratory sufficient at 28°C indicating that these mutations were able to complement the growth defect of *mgm1Δ* mutant. Interestingly *mgm1*^{I322M} mutant, when grown on oxidative carbon sources at 37°C, a less permissive temperature for yeast, showed a respiratory deficient phenotype. This phenotype is known as thermo-sensitive: the mutant is able to grow as the wild-type strain at 28°C on non-fermentable carbon sources, but loses this ability when forced to grow at 37°C on the same sources (Fig.1.4). *mgm1*^{A110V} mutant strain growth was comparable to that of *MGM1* wild-type strain at 37°C on oxidative carbon sources (data not shown).

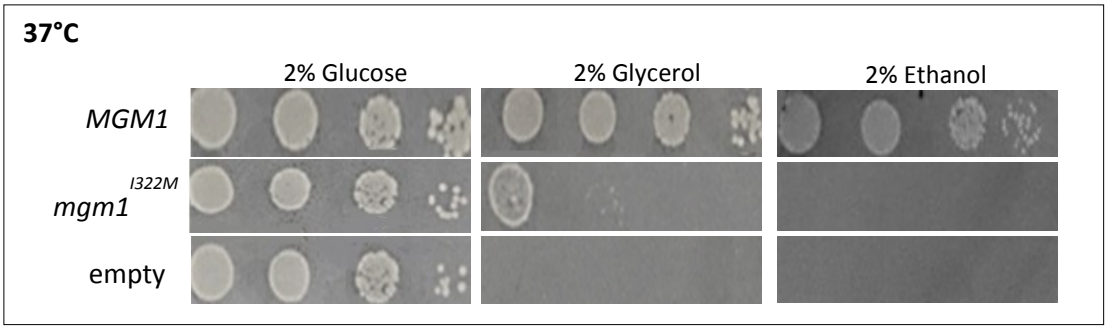

Figure 1.4. Spot assay at 37°C of W303-1A *mgm1Δ* strain transformed with pFL39*MGM1*, pFL39*mgm1*^{I322M} and pFL39 empty vector on YNB DO-TRP medium supplemented with 2% glucose (left), 2% glycerol (central) and 2% ethanol (right).

1.2.1. Analysis of OXPHOS metabolism

Mgm1 is known to be involved in formation and maintenance of mitochondrial *cristae* structures. *Cristae* are the sites where respiratory complexes are located. A *mgm1Δ* mutant is characterized by aberrant *cristae* morphology and by loss of both structural integrity and functionality of respiratory complexes (Olichon et al., 2003; Griparic et al., 2004; Sesaki et al., 2003). In order to assess if the four mutations had an effect on the mitochondrial respiratory complexes, we analyzed the cytochromes spectra profile, which is an index of the structural integrity of the respiratory chain complexes. As shown in Fig.1.5 *mgm1*^{S241N} and *mgm1*^{L273P} mutants showed a pronounced reduction of the absorption peaks corresponding to cytochrome b and aa3, component of complex IV, indicating loss of the structural integrity of complex IV. This behavior was similar to that displayed by the *mgm1Δ* strain transformed with pFL39 empty vector. *mgm1*^{A110V} and *mgm1*^{I322M} mutants showed a cytochromes spectra profile comparable to that of wild-type strain, indicating that these mutations do not affect the structure of the respiratory chain complexes.

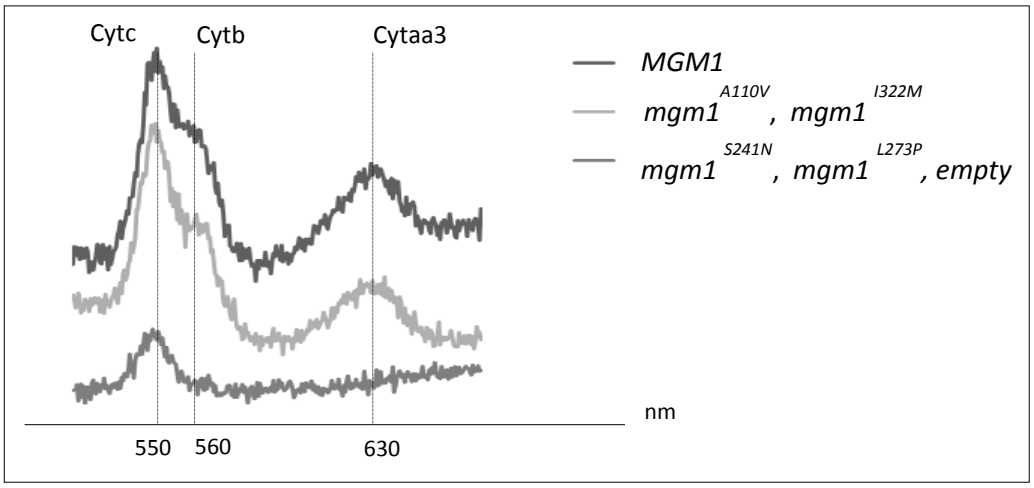

Figure 1.5. Cytochrome profiles of W303-1A *mgm1Δ* strain transformed with pFL39*MGM1*, pFL39*mgm1*^{A110V}, pFL39*mgm1*^{S241N}, pFL39*mgm1*^{L273P}, pFL39*mgm1*^{I322M} and pFL39 empty vector grown in YNB DO-TRP medium supplemented with 0.6% glucose at 28°C. Cells were grown until glucose was exhausted to de-repress the expression of respiratory chain components. The peak at 550nm corresponds to the cytochrome c-type, that at 560nm to cytochrome b and 603nm peak corresponds to cytochromes aa3.

We then recorded oxygen consumption on whole cells, as described in Materials and Methods. The measurement of respiration rate is a convenient method to evaluate the real functionality of mitochondrial respiratory complexes. As shown in Fig.1.6 both *mgm1*^{S241N} and *mgm1*^{L273P} mutants showed a decreased respiratory ability compared to wild-type at 28°C, according to their respiratory deficient phenotype previously observed in the spot assay analysis. This result also parallelizes with the loss of structural integrity of respiratory chain complexes observed in these mutants and described above. *mgm1*^{A110V} and *mgm1*^{I322M} mutants showed a respiratory rate comparable to that of wild-type strain at 28°C. When the same analysis was performed at 37°C, *mgm1*^{I322M} mutant lost its respiratory ability, in accordance with its thermo-sensitive phenotype, instead *mgm1*^{A110V} still behaved as wild-type strain.

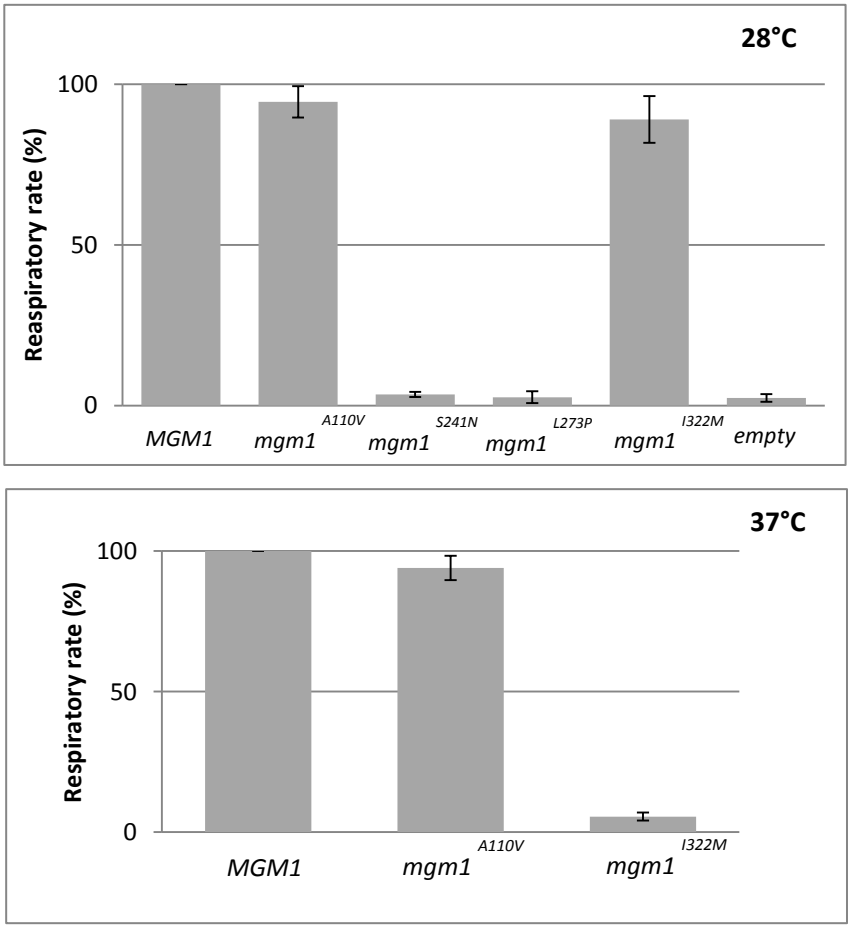

Figure 1.6. Oxygen consumption of W303-1A *mgm1Δ* strain transformed with pFL39*MGM1*, pFL39*mgm1*^{A110V}, pFL39*mgm1*^{S241N}, pFL39*mgm1*^{L273P}, pFL39*mgm1*^{I322M} and pFL39 empty vector at 28°C (upper figure) and W303-1A *mgm1Δ* strain transformed with pFL39*MGM1*, pFL39*mgm1*^{A110V} and pFL39*mgm1*^{I322M} at 37°C (lower figure) grown in YNB DO-TRP medium supplemented with 0.6% glucose. Cells were grown until glucose was exhausted to promote the expression of respiratory chain components.

1.2.2. Analysis of mtDNA mutability

S. cerevisiae has the unique property to produce cells with homoplasmic deleted mtDNA molecules, referred as *petite* mutants. Yeast *petite* colonies are compromised at different extent in their mtDNA, which in turn results in loss of respiratory activity and complete dependence on fermentative metabolism. Analysis of mtDNA mutability was performed at 28°C and 37°C only in the case of respiratory sufficient strains, as described in Materials and Methods.

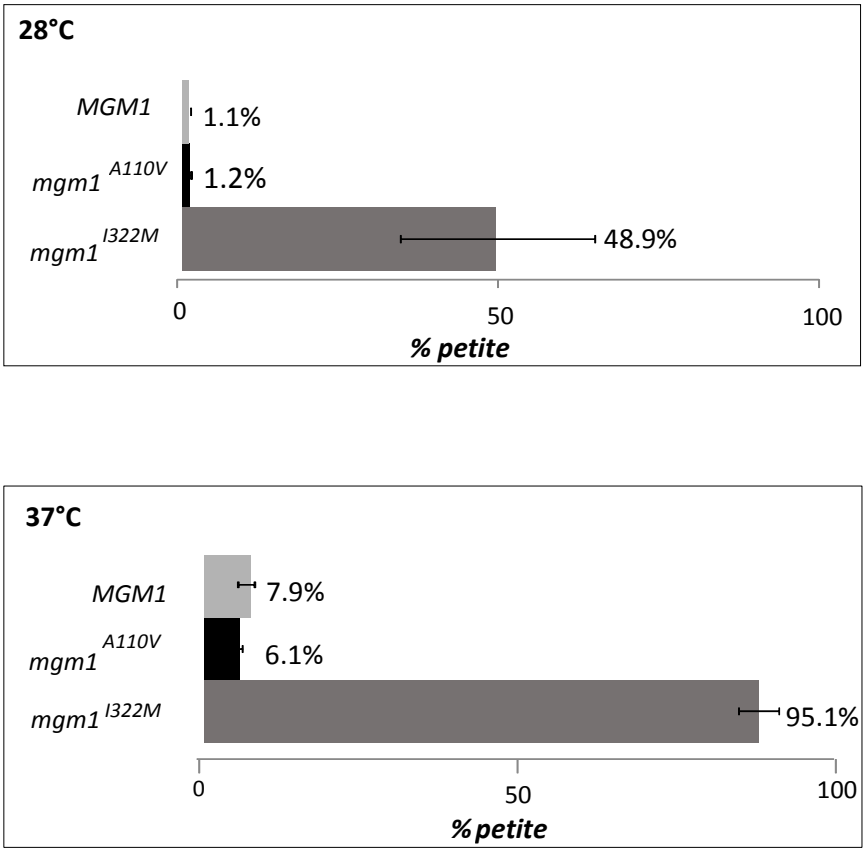

Figure 1.7. Analysis of mtDNA mutability was performed on respiratory sufficient W303-1A *mgm1Δ* strain transformed with pFL39*MGM1*, pFL39*mgm1*^{A110V} and pFL39*mgm1*^{I322M} at 28°C (upper panel) and 37°C (lower panel) in YNB DO-TRP supplemented with ethanol 2% and then shifted in 2% glucose.

As shown in Fig.1.7, *mgm1*^{A110V} mutant displayed a *petite* frequency comparable to that of the wild-type strain at both temperatures tested. This result suggests that A110V substitution has no effect on mtDNA stability. *mgm1*^{I322M} mutant at 28°C displayed a *petite* frequency almost 50 fold higher than that of wild-type. At 37°C, 95% of the cells were *petite*, according to the thermo-sensitive phenotype of this mutant. This evidence indicates that I322M mutation affects mtDNA stability. We can hypothesize that the compromised respiratory rate, observed for *mgm1*^{I322M} mutant, could be a consequence of the high level of mtDNA instability that characterizes this thermo-sensitive mutant strain.

Summary of the first section

In this section, four *OPA1* mutations were introduced in the equivalent position of *MGM1* gene and their effects on OXPHOS metabolism were analyzed.

A110V mutation in yeast is equivalent to A115 mutation in human that causes DOA plus. When introduced in *S. cerevisiae* this mutation did not affect the growth on non-fermentable carbon sources neither at 28°C nor at 37°C, as demonstrated by spot analysis assay. A110V mutation did not have any effect on both the structure and the activity of the respiratory chain complexes. Accordingly, the strain carrying $mgm1^{A110V}$ allele displayed a respiratory rate comparable to that of wild-type strain. Moreover, the *petite* frequency measured in this mutant was similar to that of *MGM1* wild-type strain, indicating that the A110V mutation did not affect the stability of mtDNA at both temperatures tested. Taken together these results do not allow us to validate the A110V mutation as pathological in our model. This substitution is localized in the transmembrane domain (TM) of both Mgm1 and Opa1, where the level of amino acids conservation is very low. It is possible to hypothesize that this alanine plays different roles in yeast and in human, so that mutations involving this residue could have differential effects in the two organisms.

S241N and L273P mutations in yeast are equivalent to S298N and L331P in human and are associated to DOA plus and DOA respectively. When introduced in yeast, both these substitutions showed very severe effects. $mgm1^{S241N}$ and $mgm1^{L273P}$ alleles did not restore the oxidative growth defect of *mgm1Δ* strain, indicating that they were unable to complement *MGM1* deletion. Moreover mutant strains showed loss of cytochrome structural integrity and consequently a very low respiratory rate, comparable to that of *mgm1Δ* strain. Then, from our results S241N and L273P mutations can be validated as pathological.

I322M in yeast is equivalent to I382M in human and is associated with DOA. Spot assay analysis showed that *mgm1* allele, carrying this mutation, complemented the growth defect of *mgm1Δ* strain only at 28°C. In fact the mutant was able to grow on non-fermentable carbon sources at the permissive temperature of 28°C, but not at 37°C.

This thermo-sensitive behavior affected also the respiratory activity that, at the restrictive temperature, was comparable to that of *mgm1Δ* strain. I322M mutation had also effects on mtDNA stability: *petite* frequency was almost 50 fold higher than wild-type at 28°C and it enormously increased at 37°C according to the thermo-sensitivity of this mutant strain.

Results and Discussion

2. *MGM1/OPA1* chimeric genes

2. *MGM1/OPA1* chimeric genes

2.1. *OPA1* cDNA did not rescue the *mgm1Δ* mutation in *Saccharomyces cerevisiae*

One of the strategies often applied to study non-conserved human pathological mutations in *S. cerevisiae* is to introduce them in human cDNA expressed in deletant yeast. However, this strategy works only in the case of human cDNA able to complement the absence of the yeast gene. At first, we tried to express the human *OPA1* cDNA in the *S. cerevisiae mgm1Δ* mutant. The *OPA1* cDNA was cloned both in single or multicopy plasmid, under the control of either the *MGM1* endogenous promoter or the strong constitutive promoter *PGK*, and the recombinant constructs were then introduced into the *mgm1Δ* mutant containing *MGM1* gene cloned in pFL38 vector. After *plasmid shuffling* on 5-FOA, to counter select the *MGM1* gene, the phenotypical analysis of the strain transformed with *OPA1* cDNA was carried out by spot analysis assay, using ethanol and glycerol as non-fermentable carbon sources. Transformant cells were not able to grow in these conditions, indicating that *OPA1* cDNA fails to complement the oxidative growth defect of the *mgm1Δ* mutant (data not shown). In addition, cells were devoid of mtDNA, as demonstrated by the crossing with a rho^0 strain of the opposite mating type. The lack of complementation of the *mgm1Δ* OXPHOS defect by *OPA1* cDNA can be the consequence of i) incorrect import of the OPA1 protein in the heterologous mitochondria; ii) incorrect processing of OPA1 to short and long form by the yeast Pcp1 protease; iii) inability of OPA1 to interact with yeast proteins involved in the fusion process, such as Fzo1 and Ugo1 (Sesaki and Jensen, 2004); iv) incorrect folding of the human protein in yeast. To overcome some of these problems, we decided to construct chimeric proteins composed of the N-terminal part of Mgm1, including the mitochondrial peptide signal (MPS), and the C-terminal region of OPA1, in particular the whole GTPase region in which the majority of pathological mutations are located. In Fig.2.1, the alignment of Mgm1 and OPA1 amino acid sequences is shown and the different functional domains (i.e. the mitochondrial peptide signal (MPS), the transmembrane (TM), the rhomboid cleavage

region (RCR), the coiled-coil (CC), the GTPase, the middle and the GED domains) are highlighted.

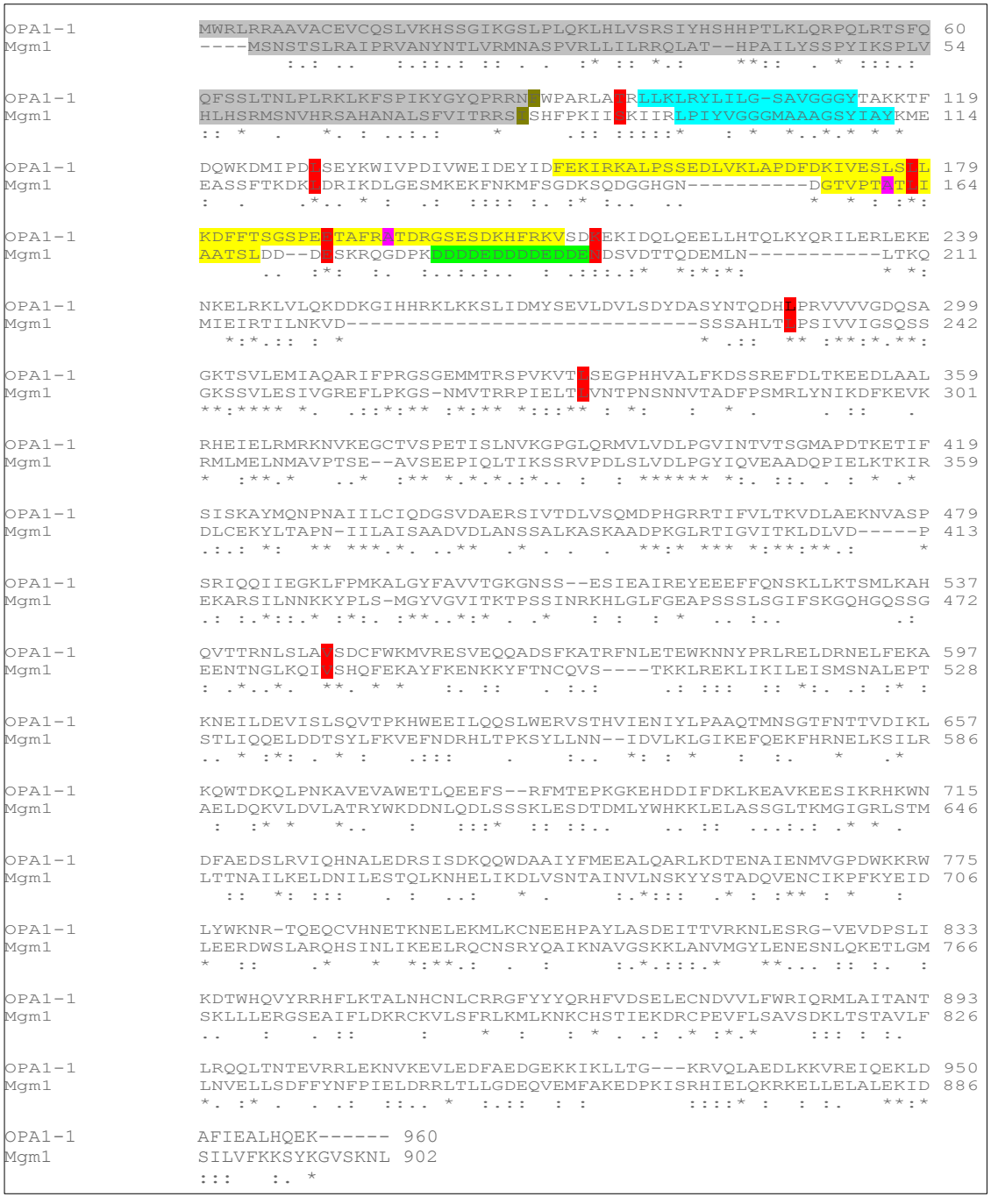

Figure 2.1. Alignment of Mgm1 and OPA1 isoform 1. Highlighted in grey the mitochondrial peptide signal (MPS), in brown the long-form cleavage site, in light blue the transmembrane domain (TM), in violet the short-form cleavage site, in yellow the rhomboid cleavage region (RCR) and in green the Mgm1 ED-rich region. In red the sites used for the construction of the chimeric genes are highlighted.

2.2. Construction of chimeric genes *MGM1/OPA1*

As depicted in Fig.2.2, using the "two step overlap extension technique" (described in Materials and Methods) six chimeras were constructed, where the Mgm1 region was gradually longer and the OPA1 region gradually shorter. The six chimeras also included the following Mgm1 features respectively: Chim1, the Mgm1 MPS and additional 8 amino acids, in order to maintain the cleavage site of the yeast matrix metalloprotease (MPP) necessary to produce the long-isoform; Chim2, the Mgm1 transmembrane region also; Chim3, the RCR and the D/E-stretch region of Mgm1; Chim4, the Mgm1 coiled coil domain; Chim5, a part of, and Chim6, the whole Mgm1 GTPase domain. Chim1 and Chim2 have the cleavage S site of OPA1, whereas the other chimeras have the S cleavage site of Mgm1, which is cut by the rhomboid protease Pcp1.

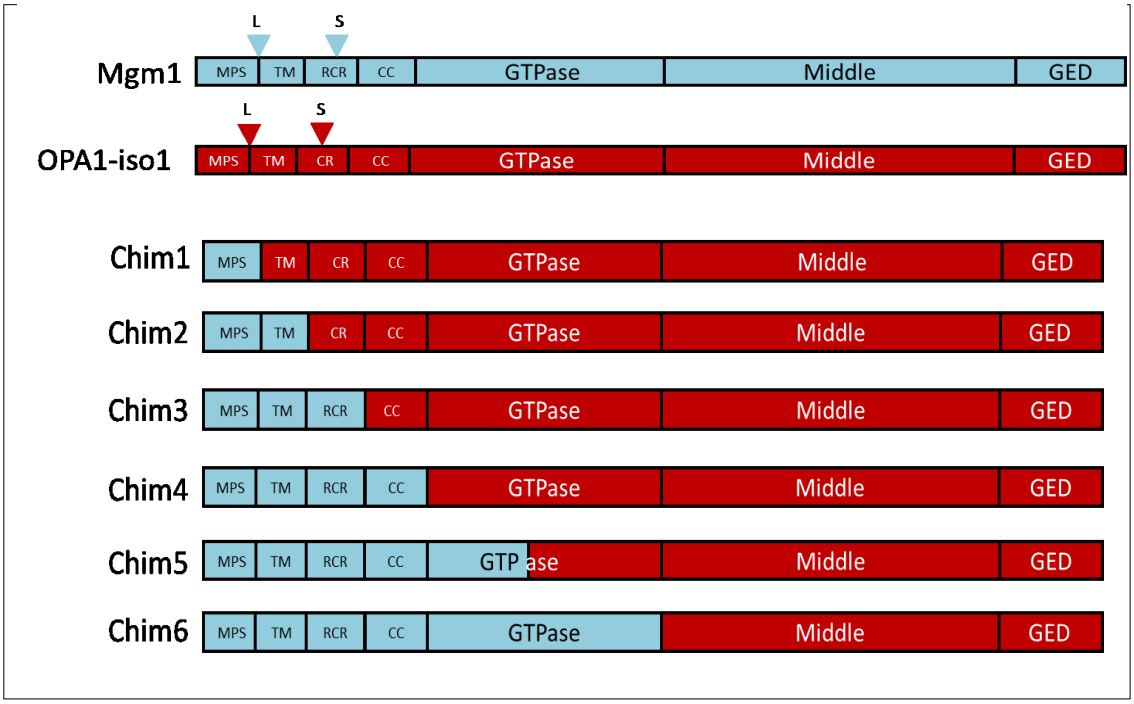

Figure 2.2. Schematic representation of the 6 constructed chimeric proteins.

The six chimeras (*CHIM1-6*), cloned either in pFL39 (centromeric, *TRP1* marker) or in YEplac112 (multicopy, *TRP1* marker) vectors under the endogenous promoter *MGM1*, were introduced into the *mgm1Δ* mutant, and transformant strains were tested for their ability to grow on non-fermentable carbon sources. As shown in Fig.2.3 only *CHIM3* cloned in multicopy was able to recover, albeit not completely, the growth defect of the mutant strain.

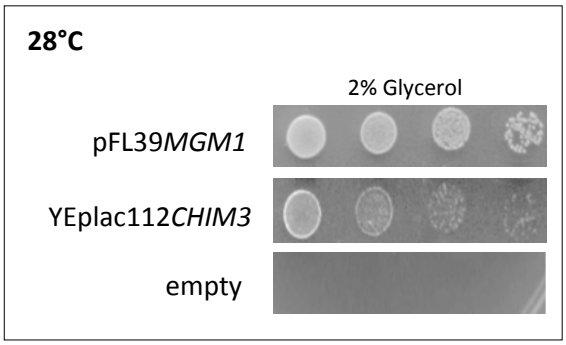

Figure 2.3. Spot analysis on W303-1A *mgm1Δ* mutant transformed with pFL39*MGM1*, YEplac112*CHIM3* and YEplac112 empty vector at 28°C on YNB DO-TRP medium supplemented with glycerol 2%.

This result indicates that the presence of Mgm1 RCR is necessary for the activity of the chimeric protein. *CHIM3* contains the OPA1 coiled coil domain whose presence appears to be essential to complement the *mgm1Δ* respiratory deficiency. We also observed that *CHIM4*, *CHIM5*, *CHIM6* were not able to complement the growth defect of the mutant strain, suggesting that probably a larger portion of Mgm1 is deleterious for the chimera activity. Since *CHIM3* is able to complement the *mgm1Δ* OXPHOS defect but *CHIM2* does not, we decided to create two chimeric genes with an intermediate structure between *CHIM2* and *CHIM3*, in the attempt to better identify the minimal *MGM1* region essential for complementation. So we constructed two new chimeric genes called *CHIM2B* and *CHIM2C* respectively, with the fusion point *MGM1-OPA1* within the Mgm1 RCR domain. *CHIM2B* contained a part of Mgm1 RCR including the S cleavage site of Mgm1, recognized by the rhomboid protease Pcp1. *CHIM2C*, included some extra amino acids downstream the Mgm1/OPA1 fusion point of *CHIM2B*. In Fig. 2.4 a scheme of the *MGM1/OPA1* junction is reported.

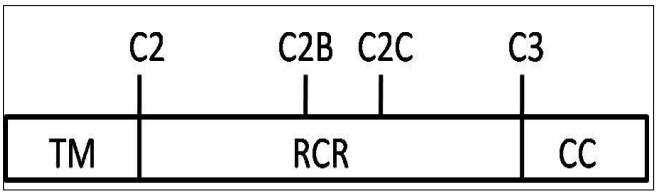

Figure 2.4. A scheme of the Mgm1-OPA1 junction sites in Chim2 (indicated as C2), Chim2B (C2B), Chim2C (C2C) and Chim3 (C3) is shown.

Both these new chimeric genes were cloned in YEplac112 vector under *MGM1* endogenous promoter and were used to transform m*gm1Δ* strain. Only *CHIM2C* could partially restore the growth defects of the *mgm1Δ* strain as showed in Fig.2.5.

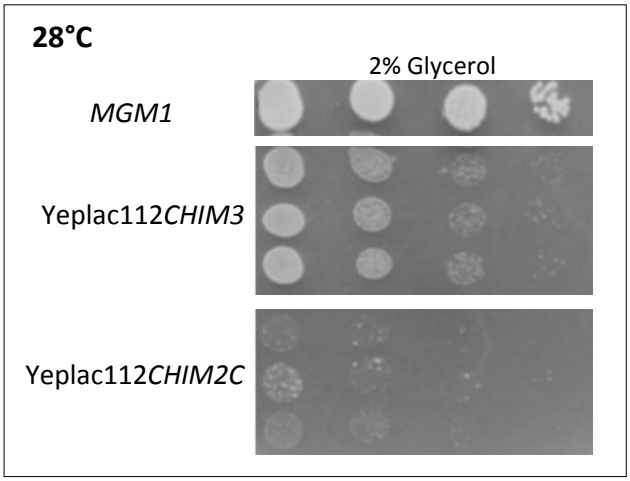

Figure 2.5. Spot assay on W303-1A *mgm1Δ* mutant transformed with pFL39MGM1, YEplac112CHIM3 and YEplac112CHIM2 at 28°C on YNB DO-TRP medium supplemented with 2% glycerol.

2.2.1. Chim1-4 proteins processing

Mgm1 native protein, as well as OPA1, is processed in two mitochondrial isoforms: a long one (l-Mgm1), which is an integral inner membrane protein that spans the inner membrane thanks to an N-terminal transmembrane segment (TM), and a short soluble isoform (s-Mgm1), which lacks the inner-transmembrane domain and is therefore located in the intermembrane space (Herlan et al., 2003). The two isoforms are present in equal amounts and have different roles in mitochondrial membrane fusion (Zick et al., 2009; Devay et al., 2009). The formation of s-Mgm1 is dependent on the rhomboid protease Pcp1 (Herlan et al., 2003; McQuibban et al., 2003; Sesaki et al., 2003), but the insertion of Mgm1 into the inner membrane, through its transmembrane fragment, or its processing by Pcp1 at the rhomboid cleavage region (RCR) are competing processes, which are known as “alternative topogenesis” (Herlan et al., 2004). Correct processing in both long and short forms is crucial for mitochondrial fusion, which indicates that the long and short forms function together in this pathway, albeit with distinct roles (Meeusen et al., 2006). We next addressed by Western blot analysis whether the failed complementation observed in strains transformed with *CHIM1*, *CHIM2*, *CHIM2B* and *CHIM4* was due to an incorrect processing of these chimeric proteins. According to this hypothesis, we instead expected a correct processing for Chim2C and Chim3 that proved able to rescue the *mgm1Δ* growth defects. The size of the expected native form and l-form of each chimera is reported in Fig. 2.6.

CHIMERIC PROTEIN	M. W. NATIVE FORM	M.W. LONG ISOFORM (L-FORM)
1	108 kD	101 kD
2	108 kD	100 kD
2B	106 kD	98 kD
2C	106 kD	96 kD
3	106 kD	99 kD
4	101 kD	94 kD

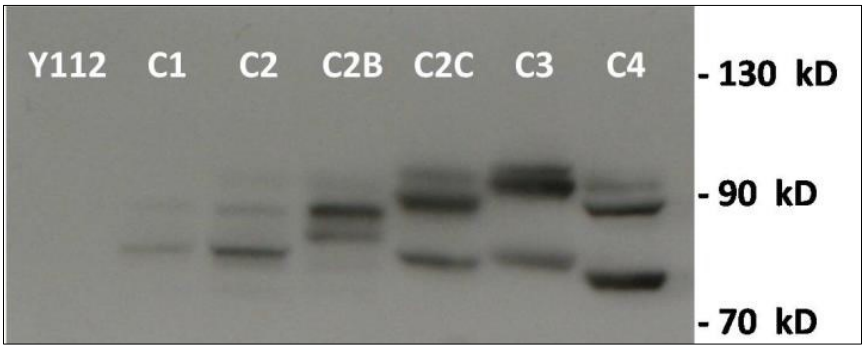

Figure 2.6. In the upper panel the sizes of the native forms and long forms of the Chim1-4 proteins. In the lower panel Western Blot on whole cell protein extracts from W303-1A *mgm1Δ* strain transformed with CHIM1-4 cloned in YEplac112 vector.

We found that Chim2 and Chim2B were not correctly processed. This result can explain the lack of complementation by these chimeric proteins. Chim1 was correctly processed but its expression level appeared very low, suggesting that this chimera could not complement *MGM1* deletion due to the low expression rate. Otherwise Chim2C, Chim3 and Chim4 seemed to be correctly processed in l-form and s-form. However, Chim4 was not able to restore *mgm1Δ* OXPHOS phenotype. This observation suggests that Mgm1 coiled-coiled domain is essential for the function of the chimeric protein. Although being correctly processed, both Chim2C and Chim3 showed an imbalance between the two isoforms; this could explain the partial ability of these chimeric proteins to complement the deletion of *MGM1.* In any case, the better complementation was reached by Chim3, and for this reason the following experiments were performed with this construct.

2.2.2. Improvement of Chim3 expression

In order to improve the complementation ability of Chim3, we decided to clone it under different promoters, to differentially modulate its expression. We chose firstly *CYC1*TETOFF promoter, a tetracycline/doxycycline-repressible promoter. It is composed by 7 repeats of the 19bp bacterial TetO operator sequence located upstream the *CYC1* promoter. This region is called "tetracycline response element" (TRE). In absence of doxycycline, the TetO operator sequence is recognized and bound by the transcriptional factor tTA protein (tetracycline transactivator). Addition of tetracycline determines a conformational change of tTA, which is not so longer able to bind to TRE (tetracycline response element) sequences, thereby preventing transactivation of TRE-controlled genes. This doxycycline-repressible promoter has two advantages: it is a strong promoter, able to express the controlled gene at high level and it can be easily modulated if necessary. We created the pFL39*CYC1*TETOFF vector, subcloning the *CYC1*TETOFF cassette from pCM189 plasmid (as described in Materials and Methods), in which we cloned *CHIM3*. In addition, *CHIM*3 was expressed under the control of the strong *PGK* promoter, which is constitutive, both in pFL39 plasmid (centromeric) and in YEplac112 (multicopy) vector (Materials and Methods). All the constructs were introduced in the *mgm1Δ* strain. *CHIM3* cloned in pFL39*CYC1*TEToff was able to complement the respiratory deficient phenotype of the mutant, as shown in Fig.2.7, whereas *CHIM3* cloned under the control of PGK promoter was unable. The complementation by pFL39*CYC1*TETOff*CHIM3* was also improved, compared to that of YEplac112*CHIM3* under *MGM1* promoter.

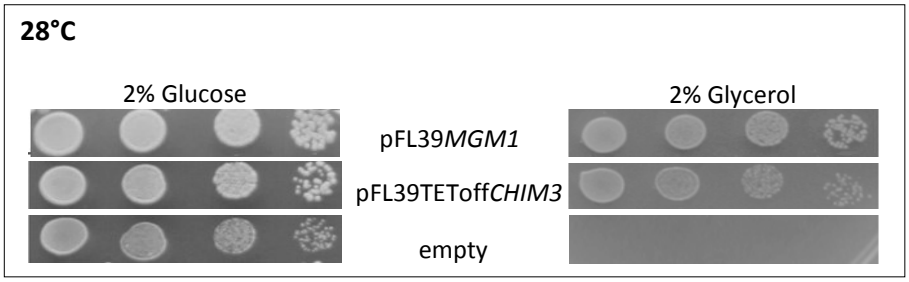

Figure 2.7. Spot assay on W303-1A *mgm1Δ* strain transformed with pFL39*MGM1*, pFL39TETOff*CHIM3* and pFL39TETOff empty vector at 28°C on YNB DO-TRP medium supplemented with 2% glucose (left) and 2% glycerol (right).

pFL39*CYC1*TEToff*CHIM3* will be called from now pFL39TETOff*CHIM3* implying *CYC1* promoter. In order to test the expression level of CHIM3 in the different constructs, we performed RT-qPCR analysis, as described in Materials and Methods. The mRNA levels of *CHIM3* cloned under the *MGM1* promoter in pFL39 were the same as those of *MGM1* cloned in the pFL38 plasmid and they were considered as basal levels. The mRNA levels of *CHIM3* cloned either in YEplac112 under the *MGM1* promoter or in pFL39 under the TETOff promoter were about 16–18-fold higher compared to the level of the *MGM1* transcript. Instead *CHIM3* mRNA was strongly increased in the presence of the *PGK* promoter (Fig. 2.8).

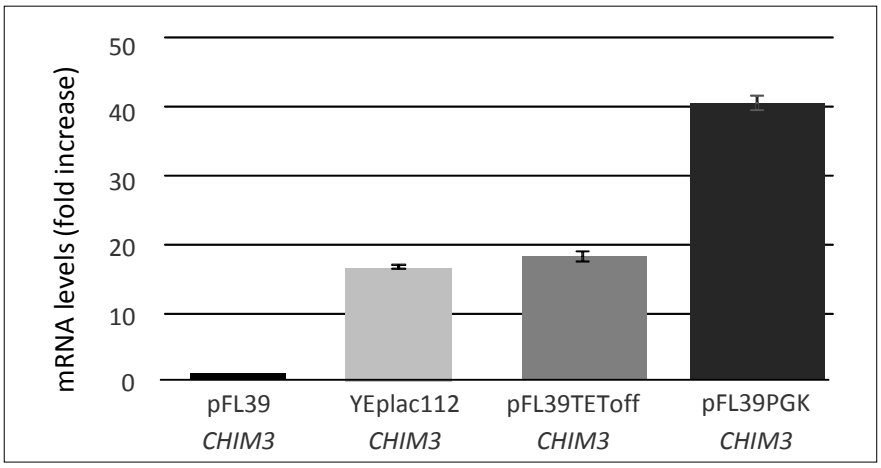

Figure 2.8. Chim3 mRNA levels in W303-1A *mgm1Δ* strain transformed with pFL39*CHIM3*, YEplac112*CHIM3*, pFL39TETOff*CHIM3* and pFL39PGK*CHIM3* vectors determined by RT-PCR.

Together these results indicate that a precise expression level of the chimeric construct is crucial for right complementation. We hypothesized that the failed complementation observed when *CHIM3* was cloned under the strong constitutive *PGK* promoter could be ascribed to toxicity, due to excessive expression of the chimeric construct. Based on these results, the experimental work was continued by using *CHIM3*, cloned in the centromeric pFL39 vector under the TETOff promoter. As said before TETOff promoter is doxycycline repressible.

We performed doxycycline modulation experiments which indicated that addition of this compound, at concentrations up to 1 µg/ml, did not improve the oxidative growth of *CHIM3* strain, whereas addition of higher concentration of doxycycline partially or totally inhibited its growth (Fig.2.9). In no case we observed an improvement of the growth, and for this reason the following experiments were performed without doxycycline.

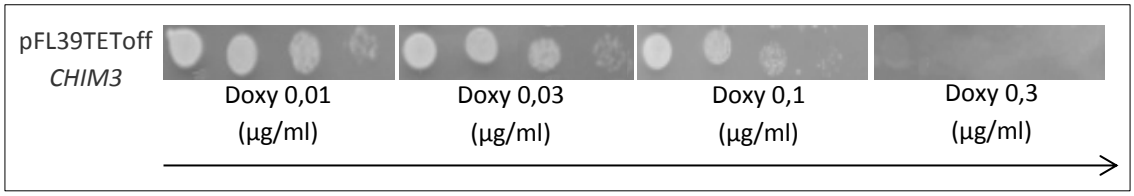

Figure 2.9. Spot assay of W303-1A *mgm1Δ* strain transformed with pFL39TEToffCHIM3 on YNB DO-TRP medium supplemented with ethanol at different doxycycline concentrations at 28°C.

2.3. *CHIM3* complements the *mgm1Δ* OXPHOS negative phenotypes

2.3.1. mtDNA stability

As said before, the *mgm1Δ* mutant is respiratory deficiency due to loss of mtDNA. To gain a better insight into the ability of *CHIM3* to rescue this peculiar *mgm1Δ* mutant phenotype we analyzed the mtDNA mutability in the mutant strain transformed with the chimeric gene. The mtDNA mutability was evaluated by measuring the frequency of *petite* mutants in the *mgm1Δ* mutant, transformed with *CHIM3*, compared with wild-type *MGM1*. The analysis was performed both at 28°C and 37°C. As reported in Table 2.10 the strain containing *CHIM3* displayed higher *petite* frequency compared to the strain transformed with pFL39*MGM1* at both temperatures tested. However, this result indicates that in the presence of *CHIM3* most cells maintain a full mitochondrial genome.

STRAIN	*% petite* **28°C**	*% petite* **37°C**
pFL39*MGM1*	2.4%	10.2%
pFL39TEToff*CHIM3*	30.9%	54.1%

Table 2.10. Petite frequency in W303-1A *mgm1Δ* strain transformed with pFL39*MGM1* and pFL39TETOff*CHIM3* vectors at 28°C and 37°C on YNB DO-TRP medium supplemented with 2% ethanol and then shifted in 2% glucose.

These data parallelize with the results obtained by measuring mtDNA levels by qPCR. mtDNA copy number was calculated as the ratio of the mitochondrial target gene *COX1* relative to the nuclear target gene *ACT1*. As shown in Fig.2.11, in presence of *CHIM3* approximately 62% of mtDNA, compared to the level of wild-type strain, was maintained. This evidence underlines the ability of *CHIM3* to avoid mitochondrial genome loss and to rescue this typical *mgm1Δ* phenotype.

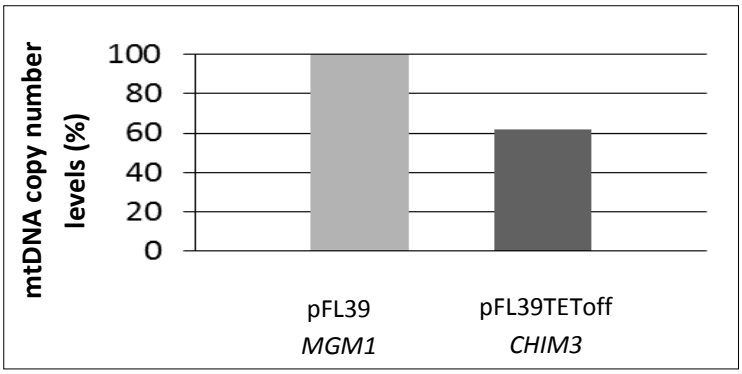

Figure 2.11. Mitochondrial DNA copy number in W303-1A *mgm1Δ* strain transformed with pFL39*MGM1* and pFL39TETOff*CHIM3* vectors determined by qRT-PCR.

2.3.2. Respiratory rate and respiratory complex activity

In order to investigate if Chim3 was able to rescue the respiratory activity of a *mgm1Δ* strain we measured the respiratory rate of the mutant strain transformed with pFL39TEToff*CHIM3*. The analysis was performed in ethanol to counter-select *petite* cells present in the cell population. As shown in Fig.2.12, Chim3 was able to restore the respiratory activity in an *mgm1Δ* strain even though, a slight reduction in the oxygen consumption rate, in respect to the wild-type strain, was recorded. To assess whether Chim3 had a rescuing effect also on the activity of NADH-cytochrome c reductase (NCCR, NADH reductase + CIII), succinate coenzyme Q DCPIP reductase (SQDR, CII) and the cytochrome c oxidase (COX, CIV) we measured the enzymatic activities of these complexes on isolated mitochondria. All the enzyme activities were lower compared to that of *MGM1* wild-type strain, though to different extents, ranging from 45% for COX activity to 65% for NCCR activity, as shown in Fig.2.12. Altogether these results indicate that *CHIM3* partially complements the OXPHOS negative phenotype of the *mgm1Δ* mutant.

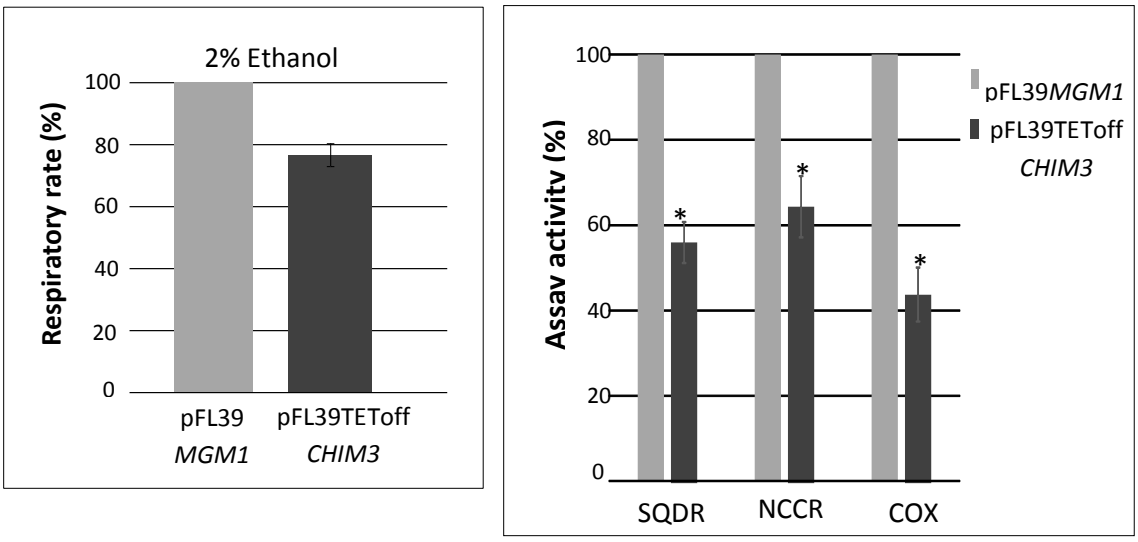

Figure 2.12. Left panel: respiratory activity of W303-1A *mgm1Δ* strain transformed with pFL39*MGM1* or pFL39TETOff*CHIM3* after growth on YP + 2% ethanol medium. Respiratory activity was normalized to 100% for strain transformed with pFL39*MGM1*. Right panel: SQDR, NCCR and COX activity in the same strains. Each activity was normalized to 100% for strain transformed with pFL39*MGM1*. **: p<0.01; ***: p<0.001 on at least three different experiments.

2.3.3. Mitochondrial network morphology

A second phenotype associated to *MGM1* deletion is related to mitochondrial morphology. In a wild-type cell mitochondrial morphology is regulated by two dynamic opposite processes called fusion and fission. Wild-type mitochondria appear to be linked one another, forming a tubular structure called mitochondrial network. As previously described, Mgm1 acts in the fusion pathway, interacting with Ugo1 and Fzo1 proteins. In the absence of Mgm1, mitochondria lose their ability to fuse and undergo ongoing fission. This determines a switch in the mitochondrial network morphology from the tubular to the fragmented shape in the mutant cells (Okamoto and Shaw, 2005). In order to investigate whether Chim3 was able to restore the tubular mitochondrial network in a *mgm1Δ* mutant we analyzed mitochondrial network shape by fluorescence microscopy. To do that, we transformed *mgm1Δ* strain containing either *CHIM3* or *MGM1* or the empty pFL39 vector with a plasmid harboring a mt-GFP, i.e. the GFP gene fused with the mitochondrial peptide signal, required for import into mitochondria. Import and expression of GFP in mitochondria allow the visualization of the mitochondrial network by fluorescence microscopy. In Fig.2.13 representative examples for each morphotype (tubular, fragmented and giant mitochondria) are shown.

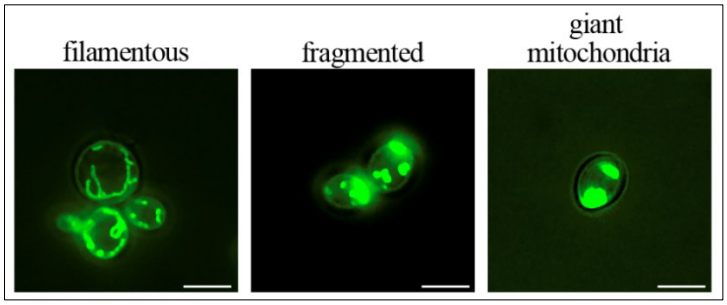

Figure 2.13. Mitochondrial morphotypes in the W303-1A *mgm1Δ* strain transformed with pFL39TEToff*CHIM3*. The strain was transformed with mitochondrial localized GFP (pYEF1/mtGFP). Representative examples for each morphotype are shown. Scale bars represent 5 µm of length. The proportion of the different morphotypes was determined by counting approximately 2000 cells of each transformant strain. The predominant morphotype in the analyzed strains were: pFL39*MGM1*, >95% filamentous; *mgm1Δ*, 100% fragmented or giant mitochondria; pFL39*CHIM3*, 30% filamentous and 70% fragmented or giant mitochondria.

The highly fragmented mitochondrial network of the *mgm1Δ* mutant completely resumed a tubular structure when the strain was transformed with wild-type *MGM1*, and was partially rescued by Chim3. This partial complementation could be due to incorrect interaction between Chim3 and the Mgm1 fusion interactors Fzo1 and Ugo1. In human Opa1 interacts with the mitofusins MFN1 and MFN2 which are orthologous to yeast Fzo1. No Ugo1 orthologous exist in human (Okamoto and Shawn, 2005). It will be interesting to evaluate whether the proportion of cells presenting tubular mitochondrial network could increase by expressing MFN1 and MFN2 in yeast.

2.4. *CHIM3* as a model for the study of DOA and DOA plus associated mutations

In order to validate if S. *cerevisiae* containing *CHIM3* gene could be a suitable model for the study of dominant optic atrophy we introduced and studied four non-conserved mutations in *CHIM3*. The pathogenic features of these substitutions were already known in human patients as described in Figure 2.14.

OPA1 protein mutation[a]	Domain	Pathology	Dominance/recessivity in human	References
I382M (I437M)	GTPase	Non pathological or DOA DOA+ or Berh syndrome in heterozygosis with a second pathological mutation	Phenotypic modifier	Ferré et al. (2009) Bonifert et al. (2014) Schaaf et al. (2011)
R445H (R500H)	GTPase	DOA+	Dominant negative	Shimizu et al. (2003) Amati-Bonneau et al. (2003)
K468E (K523E)	GTPase	DOA	Dominant by haploinsufficiency	Pesch et al. (2001)
V903Gfs*3 (V958Gfs*3)	GED	DOA	Dominant by haploinsufficiency	Delettre et al. (2000)

[a] The nomenclature of the mutations used in this work is relative to OPA1 isoform 1. In parentheses, the first nomenclature relative to isoform 8 and used at the "MITOchondrial DYNamics variation pages: optic atrophy 1 (autosomal dominant) (OPA1)" (http://mitodyn.org/home.php?select_db=OPA1).

Figure 2.14. Non-conserved mutations introduced in Chim3 (from Nolli et al., 2015).

I382M, R445H, K468E and V903Gfs*3 substitutions were introduced in *CHIM3* by site-directed mutagenesis. The mutated alleles were later cloned in the pFL39TEToff vector and introduced in the W303-1A *mgm1Δ*/pFL38*MGM1* strain. The pFL38*MGM1* vector was then counter-selected by *plasmid shuffling* on 5-FOA plates. At first we tested the effects of the mutations on the oxidative growth of *mgm1Δ* haploid yeast strains. Spot assay analysis was performed both at 28°C, that is the optimal growth temperature, and 37°C, a less permissive temperature for *S. cerevisiae.* By this double analysis it is possible to check whether a thermo-sensitive phenotype is associated to a mutation. As shown in Fig. 2.15 only *chim3*^{I382M} allele could rescue the growth defect of the *mgm1Δ* strain on non-fermentable carbon sources at both temperatures tested. None of the remaining mutated alleles was able to complement *MGM1* depletion, indicating the severe pathological role of the inserted mutations. In addition, qPCR analysis revealed that these mutations led to complete loss of mtDNA, making the mutant strains rho^0 (data not shown).

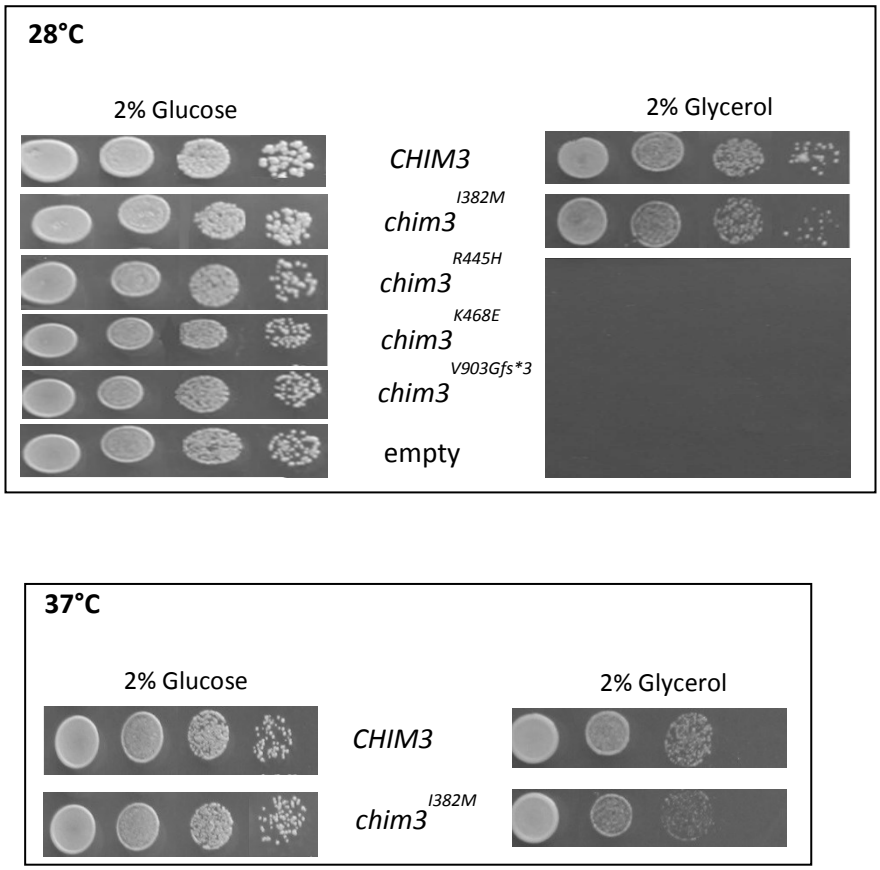

Figure 2.15. Spot assay of W303-1A *mgm1Δ* strain transformed with *CHIM3* wild-type and mutant alleles on YP medium supplemented with 2% glucose and 2% glycerol at 28°C (upper panel) and at 37°C (lower panel).

2.4.1. Processing of mutated chimeric proteins

In order to assess whether the failed complementation observed was due to incorrect processing of the chimeric proteins in l-form and s-form, a Western Blot with Anti-Opa1 was performed. Immunoblot for the mitochondrial outer membrane protein porin was used as a control of protein loads per lane (Fig.2.16).

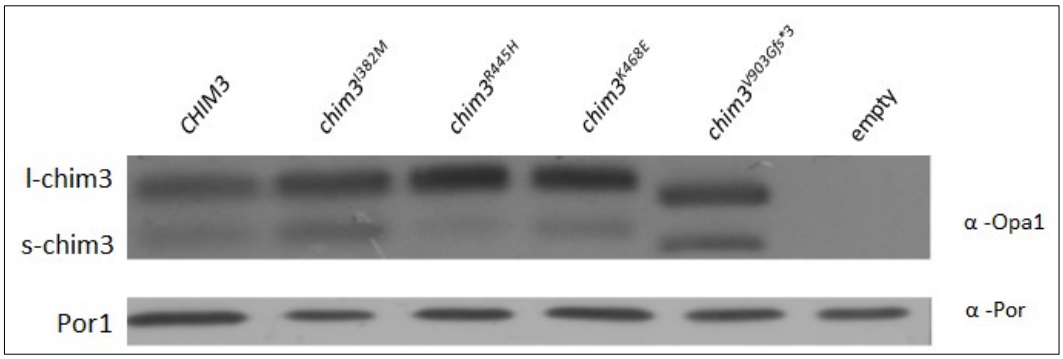

Figure 2.16. Western blot on W303-1A *mgm1Δ* strain transformed with *CHIM3* wild-type and mutant alleles.

As shown in Fig.2.16, in the case of *chim3*^{R445H}, *chim3*^{K468E} the ratio between l-form and s-form was altered compared to that of Chim3 wild-type. This could be due to impairment in the process of alternative topology. This imbalance could also partially explain the severe respiratory deficient phenotype observed in the yeast strains carrying these alleles. In the case of *chim3*^{I382M} we observed an l-form/s-form ratio comparable to that of wild-type strain, in agreement with the observed oxidative growth complementation by this chimeric allele. Also *chim3*^{V903Gfs*3} protein appeared to be correctly processed in l-form and s-form. However, it failed to complement the growth defect of *mgm1Δ* strain, probably because the inserted stop codon led to a loss of function, thus impairing the corresponding chimeric protein to restore a wild-type phenotype in *MGM1* depleted cells.

2.4.2. Mitochondrial network morphology

It has been reported that impairment of mitochondrial fusion process leads to loss of tubular mitochondrial structure and, because of ongoing fission, mitochondria appear to be fragmented. This fragmentation causes, in turn, loss of mtDNA and oxidative growth defects (Okamoto and Shawn, 2005). In order to assess whether the mutated chimeric proteins were able to restore tubular mitochondrial structure of *mgm1Δ* mutant, fluorescence microscopy analysis was performed on yeast strains transformed with *chim3*^{I382M}, *chim3*^{R445H}, *chim3*^{K468E} *chim3*^{V903Gfs*3} alleles, as previously described for Chim3. In Fig.2.17 the types and proportions of mitochondrial morphology found by this analysis are described.

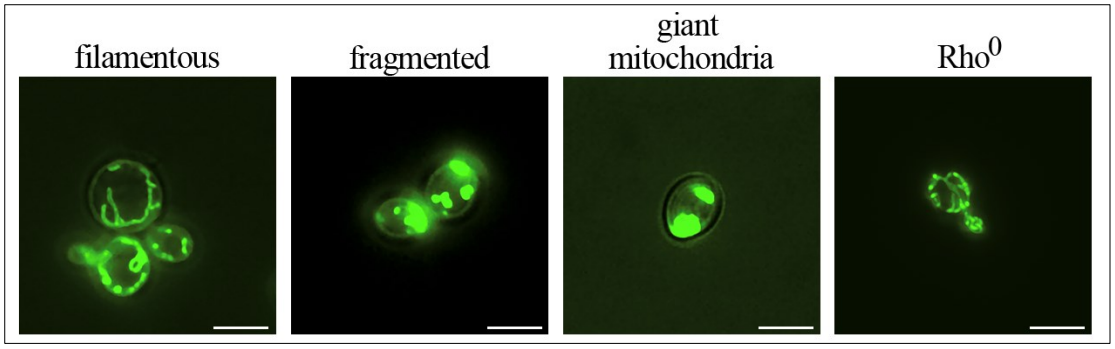

Figure 2.17. Mitochondrial morphotypes in the W303-1A *mgm1Δ* strain transformed with pFL39TEToff vector containing *CHIM3* wild-type and mutant alleles. The strains were transformed with mitochondrial localized GFP (pYEF1/mtGFP). Representative examples for each morphotype are shown. Scale bars represent 5 µm of length. The proportion of the different morphotypes was determined by counting approximately 2000 cells of each strain. The predominant morphotype in the analyzed strains were: pFL39TEToff*chim3*^{R445H}, pFL39TEToff*chim3*^{K468E} and pFL39TEToff*chim3*^{V903Gfs*3}, 100% fragmented or giant mitochondria; pFL39TEToff*CHIM3*, 30% filamentous and 70% fragmented or giant mitochondria; pFL39TEToff*chim3*^{I382M} 18% filamentous and 82% fragmented or giant mitochondria.

Strains carrying the mutated chimeric proteins, except for *chim3*^{I382M}, showed aberrant mitochondrial network morphology, with 100% fragmented or giant mitochondria. As previously reported, all these strains are not only respiratory deficient (RD), but also devoid of mtDNA (rho^0). It is noteworthy to mention that the observed mitochondria fragmentation was not the consequence of the rho^0 condition, since rho^0 strains display tubular mitochondrial network (Fig.2.17). In contrast, the mitochondria

fragmentation is the consequence of the fusion process impairment caused by *MGM1* depletion. In *chim3*^{I382M} mutant strain the percentage of cells presenting tubular mitochondria was approximately 18%, i.e. 40% less than that of the strain harboring wild-type *CHIM3*. Therefore *chim3*^{I382M} mutant allele weakly complements the lack of tubular mitochondria in a *mgm1Δ* strain, indicating that the I382M mutation affects OPA1 activity, even in the absence of a phenotypic effect on the oxidative growth,.

2.4.3. I382M: not a neutral polymorphism

As described in the previous paragraphs, among the mutated chimeric proteins chim3^{I382M} was the only one that proved able to complement the growth defect of *mgm1Δ* strain. Western blot analysis showed that chim3^{I382M} was correctly processed in l-form and s-form. However, fluorescence microscopy analysis revealed that in *chim3*^{I382M} mutant strain mitochondrial fusion was impaired, indicating a pathological role for I382M mutation. To gain more insight into the pathological mechanism of I382M mutation we performed several analyses. At first we evaluated the mtDNA stability in the *chim3*^{I382M} mutant strain by measuring the *petite* frequency, both at 28°C and 37°C. As shown in Table 2.18 in *chim3*^{I382M} mutant strain the percentage of *petite* cells was slightly higher than that observed in a wild-type *CHIM3* strain at both temperatures tested. This indicates a mild negative effect of I382M mutation on mitochondrial genome stability.

STRAIN	*% petite* 28°C	*% petite* 37°C
CHIM3	30.9%	54.1%
chim3^{I382M}	46.7%	63.6%

Figure 2.18. *petite* frequency of W303-1A *mgm1Δ* strain transformed with pFL39TEToff*CHIM3* or pFL39TEToff*chim3*^{I382M} at 28°C and 37°C.

We then measured the mtDNA copy number in the *chim3*^{I382M} mutant strain, by qPCR. As reported in Fig.2.19 mtDNA levels stood at 82% compared to that of wild-type strain, suggesting that I382M, similarly to other pathological mutations in OPA1, led to mtDNA loss, even if with a weaker effect.

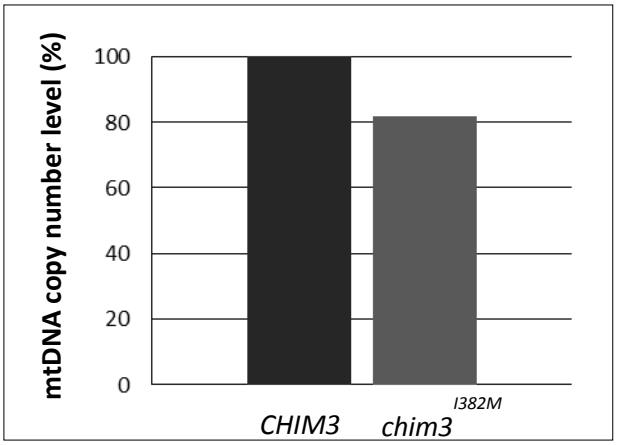

Figure 2.19. Mitochondrial DNA copy number in W303-1A *mgm1Δ* strain transformed with pFL39TEToff*CHIM3* or pFL39TEToff*chim3*^{I382M} determined by qRT-PCR.

In addition, we tested *chim3*^{I382M} ability to complement the impairment of respiratory activity which is one of the major phenotypes associated with *MGM1* depletion (Olichon et al., 2003; Griparic et al., 2004; Sesaki et al., 2003).

In *chim3*^{I382M} mutant the oxygen consumption rate was about 30% less than in wild-type strain. Respiratory complex activities were also decreased, ranging from 75% activity for the SQDR to approximately 80% for COX as shown in Fig.2.20.

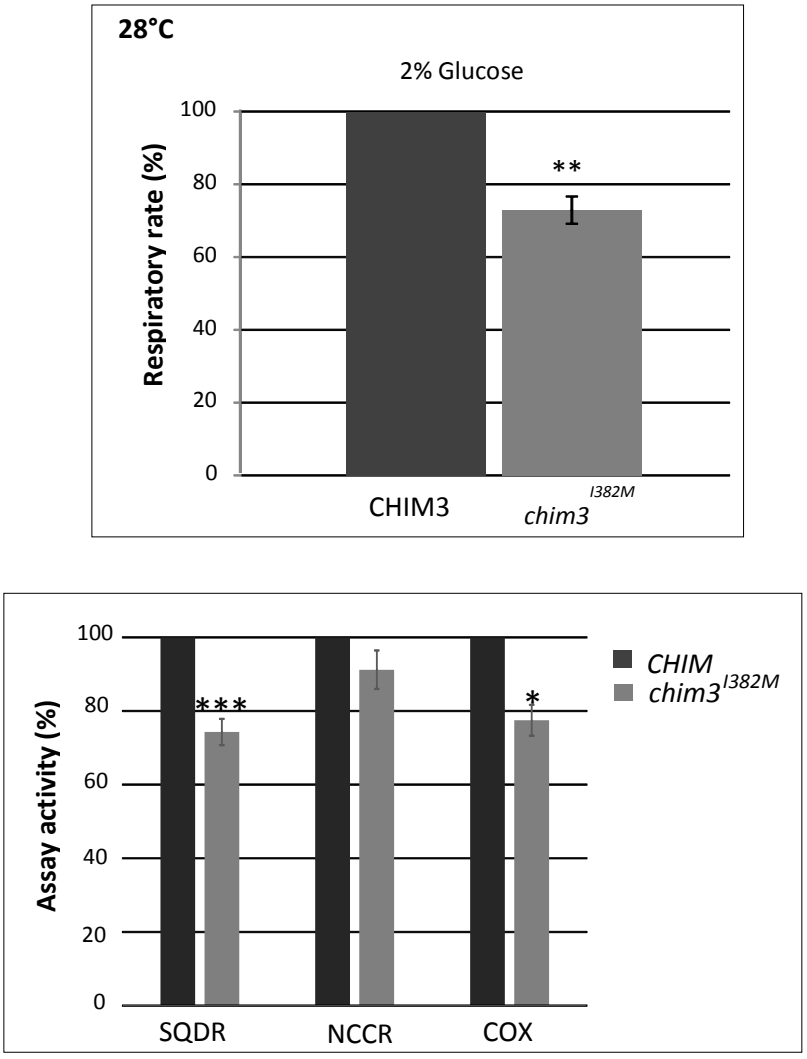

Figure 2.20. Upper panel: respiratory activity in W303-1A *mgm1Δ* strain transformed with pFL39TEToff*CHIM3* or pFL39TEToff*chim3*^{I382M} measured at 28°C. Respiratory activity was normalized to 100% for strain transformed with wild-type *CHIM3*. Lower panel: Respiratory complex activities on the same strains at 28°C. Each activity was normalized to 100% for strain transformed with wt *CHIM3*. *: p<0.05; **: p<0.01; ***: p<0.001 on at least three replicates.

Altogether these results indicate that in yeast the I382M mutation does not behave as a neutral polymorphism, but has a pathological role, even though less severe than the other studied mutations. This mutation was initially identified as a cause of DOA, but it is also present in healthy subjects (Schaaf et al., 2011; Bonifert et al., 2014; Carelli et al., 2015). In addition, it has recently been reported that the I382M is not pathogenic *per se*, either in heterozygous or in homozygous state (Bonifert et al., 2014). However, OPA1 bi-allelic cases have been described, in which patients, who carry the I382M mutation in compound with the V903Gfs*3 mutation, (which alone results in optic atrophy) are affected by a more severe form of this disease, with additional symptoms such as hypotonia, gastrointestinal dysmotility and dysphagia (Schaaf et al., 2011). Further case have been reported in which a subject with severe DOA plus, whose parents were unaffected, was carrying the I382M mutation combined *in trans* with other OPA1 nonsense mutations (Bonifert et al., 2014). Finally, mutation I382M in compound heterozygosis with the OPA1 nonsense mutation c.1705+ 1G>T, which is associated with DOA, led to Behr syndrome, a neurological syndrome characterized by congenital and severe optic atrophy, spastic paraplegia, peripheral neuropathy with axonal loss, cerebellar signs and mild 3- metylglutaconic aciduria (Carelli et al., 2015; Behr, 1909; Costeff et al., 1989). This indicates that the I382M mutation alone is not able to lead to clinical symptoms, but acts as a phenotypic modifier that contributes to the worsening of the compound heterozygote phenotype.

2.4.4. Dominance/recessivity of OPA1 mutations

In order to gain more insight into the ability of the yeast model to give information on dominance/recessivity of I382M, R445H, K468E and V903Gfs*3 mutations, we created diploids strains containing either two copies of *CHIM3* wild-type (homoallelic diploid) or a *CHIM3* wild-type copy and a mutated *chim3* copy (heteroallelic diploids). To generate these strains we first crossed W303-1A *mgm1Δ/*pFL38*MGM1* with W303-1B *mgm1Δ*/pFL36TEToff*CHIM3* strain, obtaining a diploid that we called W303 1.1. This strain was transformed with the wild-type *CHIM3* (to obtain homoallelic diploid) or with all the four mutated *chim3* alleles (to obtain heteroallelic diploids) cloned in pFL39TETOff vector. pFL38*MGM1* was then lost through *plasmid shuffling* on 5-FOA, as described in Materials and Methods. The growth phenotype of diploid strains was evaluated by spot assay analysis on both fermentable and oxidative carbon sources at 28°C. In the event that a mutation behaves as recessive (loss-of-function) we expected the corresponding heteroallelic strain to grow like the homoallelic one. This was the case of I382M mutation as showed in Fig.2.21.

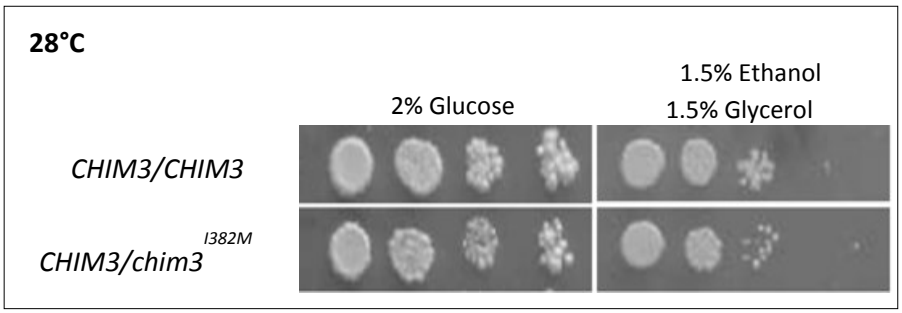

Figure 2.21. Spot assay of W303 1.1 heteroallelic and homoallelic diploid strain containing *mgm1*^{I382M} allele on YNB DO-TRP and -LEU supplemented with 2% glucose (left) and 1.5% ethanol - 1.5% glycerol (right) at 28°C.

A partial dominant mutation, instead, is expected to partially compromise the oxidative growth of the corresponding heteroallelic strain, leading to a worse oxidative growth phenotype compared to that of homoallelic strain. R445H, K468E mutations behaved like partial dominant Fig.2.22.

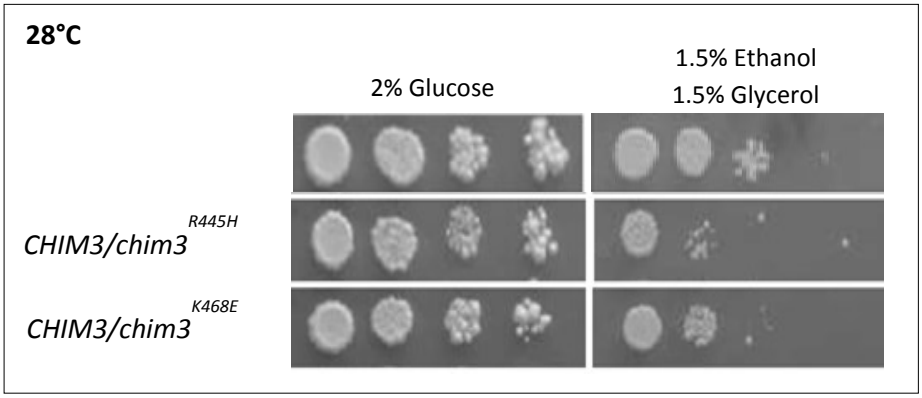

Figure 2.22. Spot assay of W303 1.1 heteroallelic and homoallelic diploid strain containing *mgm1*^{R445H} and *mgm1*^{K468E} alleles on YNB DO-TRP and -LEU supplemented with 2% glucose and 1.5% ethanol - 1.5% glycerol at 28°C.

If the mutation behaves as dominant negative, leading to a complete gain-of-function, the heteroallelic diploid loses its ability to grow on non-fermentable carbon sources Surprisingly V903Gfs*3 mutation behaved like dominant (Fig.2.23).

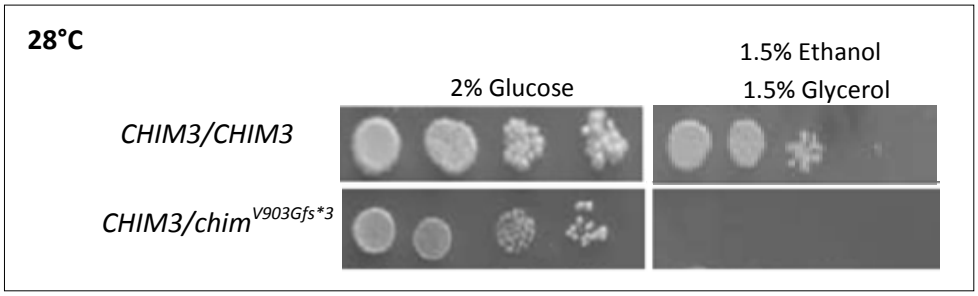

Figure 2.23. Spot assay of W303 1.1 heteroallelic and homoallelic diploid strain containing *mgm1*^{V903Gfs*3} allele on YNB DO-TRP and -LEU supplemented with 2% glucose and 1.5% ethanol - 1.5% glycerol at 28°C.

We wondered whether this dominant effect could be due to an interference of the mutated protein with the processing of the wild-type one. To answer this question we performed a Western Blot analysis on diploid strains, as shown in Fig.2.24.

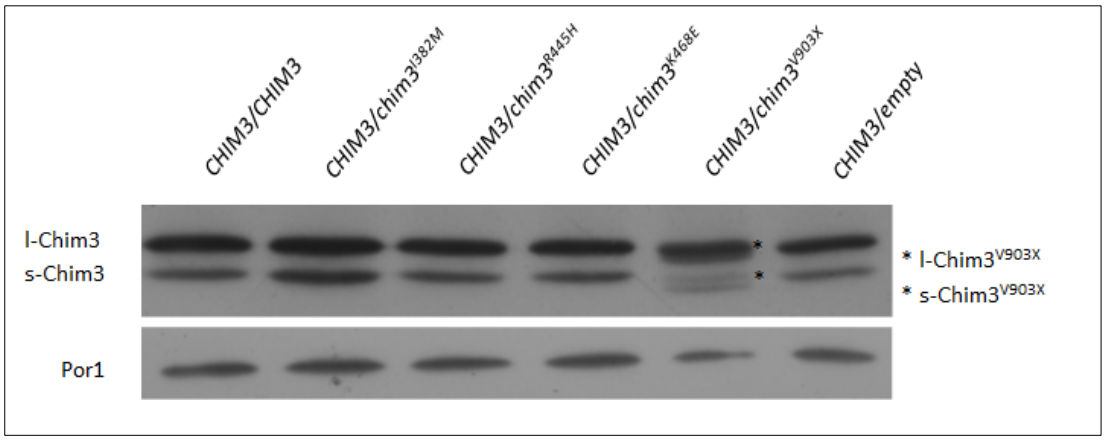

Figure 2.24. Western blot on whole cell extracts from DW1.1 *mgm1Δ/mgm1Δ* heteroallelic and homoallelic diploid strains containing *chim3*^{I382M}, *chim3*^{R445H}, *chim3*^{K468E} and *chim3*^{V903Gfs*3} mutant alleles.

All chimeric proteins were correctly processed. In particular, in the lanes corresponding to *chim3*^{I382M}, *chim3*^{R445H}, *chim3*^{K468E} we observed 2 bands, corresponding to the l-form and s-form: we cannot distinguish between the mutated l-form and s-form and the wild-type ones having both the same molecular weight. Interestingly in the lane corresponding to *chim3*^{V903Gfs*3} we found, as expected in the case of a correct processing, four bands. Two of them were the l-form and s-form corresponding to the wild-type Chim3; the others, of lower molecular weight and marked with the asterisks, were the two isoforms corresponding to *chim3*^{V903Gfs*3}. Since the processing in the yeast diploid strain containing *chim3*^{V903Gfs*3} was not affected, to explain the dominant effect observed we hypothesized that the mutated protein could interfere functionally with the activity of the wild-type protein, for example in the fusion process. In human patients V903Gfs*3 mutation is known to give haploinsufficiency. Schimpf et al. demonstrated that mRNA codifying for this mutated protein undergoes nonsense mediated mRNA decay, leading to 50% decrease in the OPA1 content, thus explaining the haploinsufficiency (Schimpf et al., 2008). In contrast to what happens in human, in yeast *chim3*^{V903Gfs*3} protein is correctly translated and processed. This observation demonstrates that, in this particular case, nonsense mediated mRNA decay is not active in yeast. The difference observed between human and yeast model indicates that *S. cerevisiae* diploid strains are not useful models for the study of nonsense mutation.

2.5. Validation of new identified DOA and DOA plus pathological mutations

Up to now more than 300 mutations, spread all along OPA1, are known to be associated with DOA and DOA plus (OPA1 LSDB http://opa1.mitodyn.org). 11 new OPA1 associated mutations have been recently identified in DOA and DOA plus patients by Professor Carelli group at the University of Bologna (Zanna and Carelli, personal communication) (Table 2.25).

OPA1	DOMAIN	DISEASE	MUTATION TYPE
S298N	GTPase	DOA+	Missense
G300E	GTPase	DOA	Missense
L331P	GTPase	DOA	Missense
G439V	GTPase	DOA+	Missense
T449P	GTPase	DOA+	Missense
T449fsX	GTPase	DOA	Nonsense
S545R	Middle	DOA	Missense
L593P	Middle	DOA	Missense
D603H	Middle	DOA	Missense
Q785R	Middle	DOA	Missense
V910D	GED	DOA	Missense

Table 2.25. New mutations analyzed.

We introduced and studied these 11 mutations in *CHIM3* fusion gene, in order to validate them as pathological. The mutated chimeric alleles were constructed as previously described in Section 2.4 and introduced in the haploid *mgm1Δ* strain.

To evaluate the ability of the mutant alleles to complement the oxidative growth defect of *mgm1Δ* strain a spot assay analysis was performed.

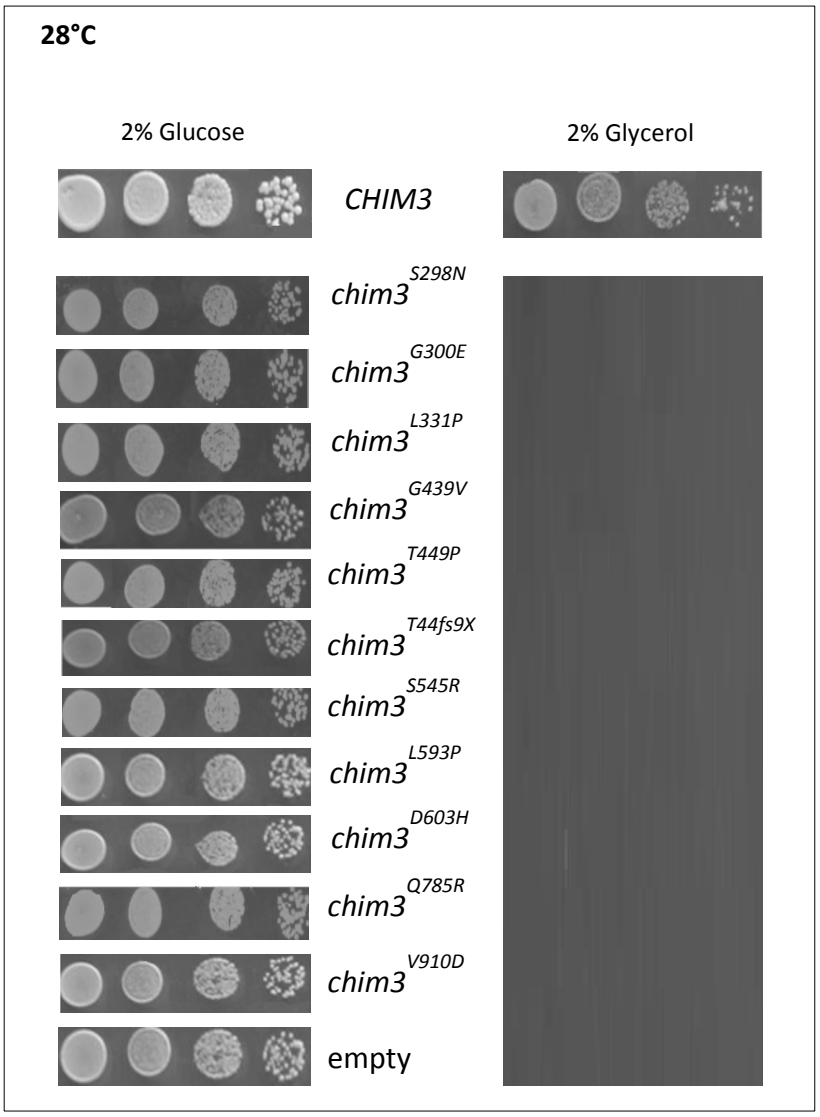

Figure 2.26. Spot assay of W303-1A *mgm1Δ* strain transformed with *CHIM3* wild-type and mutant alleles on YP medium supplemented with 2% glucose (left) and 2% glycerol (right).

As shown in Fig. 2.26, all mutant strains showed a respiratory deficient phenotype (RD). This observation indicates that no one of the mutant alleles was able to complement *MGM1* deletion, confirming the severe pathological role of the mutations.

2.5.1. Dominance/recessivity of OPA1 mutations

In order to gain more insight into the dominance/recessivity of these mutations, we created 11 heteroallelic diploid strains using the same technique described in Section 2.4.4. The growth phenotype of diploid strains was evaluated by spot assay analysis on both fermentable and oxidative carbon sources at 28°C. As observed in Section 2.4.4, the mutations could be classified in three main categories: recessive mutations (loss-of-function), partial dominant mutation (partial gain-of-function) and dominant mutations (total gain-of-function). G300E, L331P, T449fsX, T449P, S545R, Q785R and V910D mutations showed a recessive phenotype. In fact, the growth of the corresponding mutant strains was comparable to that of homoallelic strain on non-fermentable carbon sources.

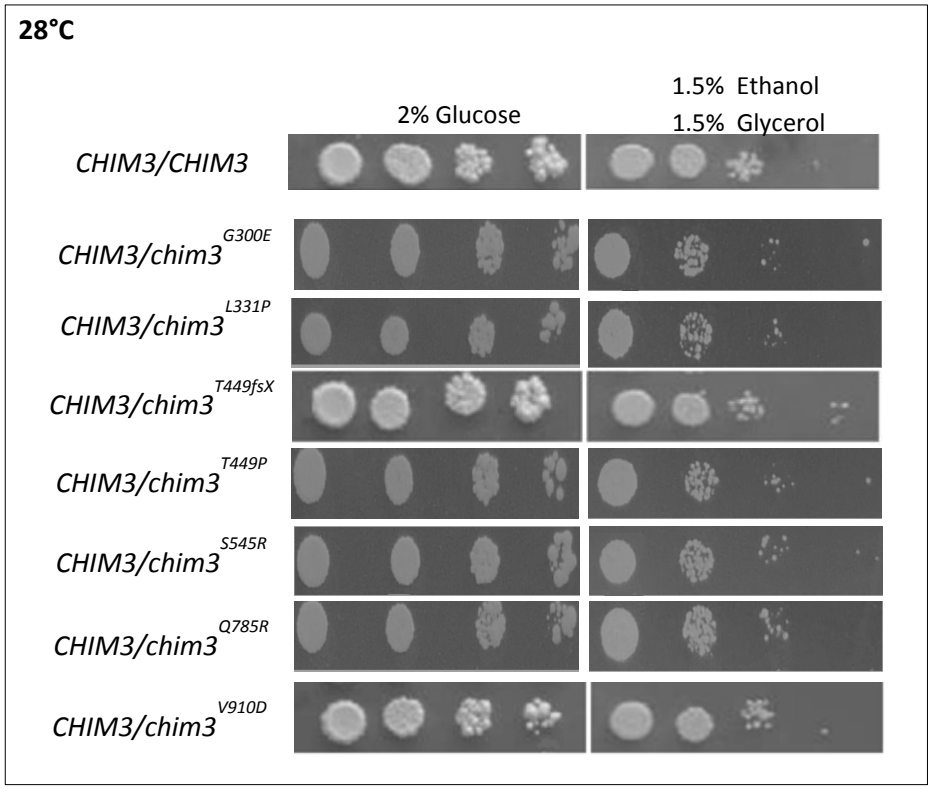

Figure 2.27. Spot assay of W303 1.1 homoallelic and heteroallelic diploid strain containing *mgm1*^{G300E}, *mgm1*^{L331P}, *mgm1*^{T449fsX}, *mgm1*^{T449P}, *mgm1*^{S545R}, *mgm1*^{Q785R} and *mgm1*^{V910D} alleles on YNB DO-TRP and -LEU supplemented with 2% glucose and 1.5% ethanol - 1.5% glycerol at 28°C.

S298N, G439V and D603H behaved as partial dominant mutations as shown in Fig.2.28. In fact, the growth of the corresponding mutants on oxidative carbon sources was affected, compared to that of homoallelic diploid strain.

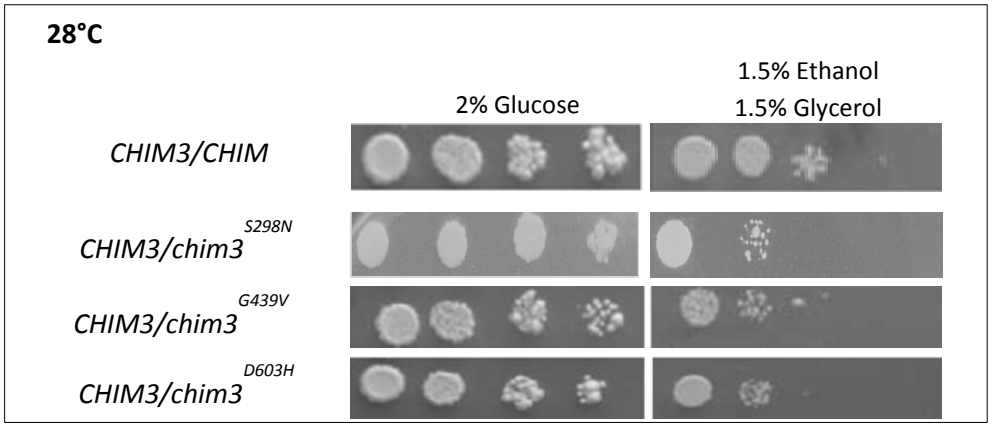

Figure 2.28. Spot assay of W303 1.1 heteroallelic and homoallelic diploid strain containing *mgm1*^{G439V} and *mgm1*^{D603H} alleles on YNB DO-TRP and -LEU supplemented with 2% glucose and 1.5% ethanol - 1.5% glycerol at 28°C.

L593P mutation behaved as a dominant mutation, totally impairing the growth of the heteroallelic *chim3*^{L593P} strain on oxidative carbon sources, as shown in Fig. 2.29.

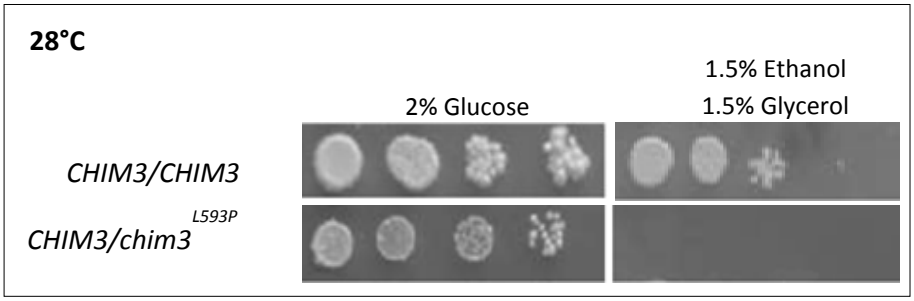

Figure 2.29. Spot assay of W303 1.1 heteroallelic and homoallelic diploid strain containing *mgm1*^{L593P} allele on YNB DO-TRP and -LEU supplemented with 2% glucose and 1.5% ethanol - 1.5% glycerol at 28°C.

We hypothesize that *chim3*^{L593P} protein interferes with the activity of the wild-type protein, for example in the fusion process resulting, in yeast, in a dominant negative effect.

Summary of the second section

In order to study non conserved pathological mutations associated with DOA and DOA plus in yeast, we first tried to express the human *OPA1* cDNA in *S. cerevisiae* under a yeast promoter. Differently to what was found in *S. pombe*, where most *OPA1* isoforms are able to complement the deletion of the yeast orthologous gene (Olichon et al., 2007), the experiment in *S. cerevisiae* was unsuccessful, which indicates that *OPA1* cannot substitute the *MGM1* gene. Next several chimeric genes bearing the 5' region of *MGM1*, which was gradually longer, and the 3' region of *OPA1,* included the whole GTPase region, where the majority of pathological mutations are located, have been constructed. Chimeras have been cloned under the control of different promoters in single copy or multicopy plasmids. One *MGM1/OPA1* chimera, *CHIM3*, when placed under TETоff promoter in a centromeric plasmid (pFL39), proved capable to complement the oxidative growth defect of *MGM1* deletion. This chimera contained the mitochondrial processing signal (MPS), the transmembrane domain (TM) and the rhomboid cleavage region (RCR) of Mgm1 and the GTPase domain, the middle domain and the GTPase effector domain (GED) of OPA1. By Western Blot analysis we found that this construct was correctly processed in the two isoforms, long and short, whose ratio was about 2:1. In the presence of *CHIM3* most cells maintained a full mitochondrial genome, as demonstrated by q-PCR. Moreover, *CHIM3* partially restored the mitochondrial respiratory activity and contributed in maintaining the tubular structure of mitochondrial network. To validate *S. cerevisiae* carrying *CHIM3* as a yeast model for the study of non-conserved mutations, associated with DOA and DOA plus, we introduced and studied four substitutions in Chim3. Mutant alleles carrying three of them, R445H, K468E and V903Gfs*3, proved unable to complement *MGM1* deletion. Haploid strains harboring $chim3^{R445H}$, $chim3^{K468E}$, $chim3^{V903Gfs*3}$ were respiratory deficient due to complete loss of mtDNA and displayed aberrant mitochondrial morphology. I382M mutation did not affect oxidative growth in the *mgm1Δ* strain, but it showed mild pathological effects on both respiratory activity and mitochondrial network morphology.

Our results parallelize with recent studies that indicate I382M as phenotypic modifier rather than a pathological polymorphism (Carelli et al., 2015). The proposed model also provides a useful approach for detecting loss-of-function or gain-of-function mutations. If a mutation causes loss of function, it is expected that the oxidative growth of the heteroallelic diploid will be similar to that of the strain containing one or two copies of the *CHIM3* wild-type allele. On the other hand, in the case of a gain-of-function mutation, it is expected that the mutant protein will interfere with the activity of wild-type Chim3, with consequent impairment of the growth of the heteroallelic strain. The heteroallelic strain expressing the I382M mutation grew like the homoallelic strain, indicating a recessive behavior, like in human. K468E and R445H mutations behaved like partial dominant, indicating that these mutations could be responsible for a partial gain-of-function. In the latter case this observation is in agreement with R445H character of dominant negative mutation in human. Intriguingly, mutation V903Gfs*3 is completely dominant in yeast, making the heteroallelic strain unable to grow on oxidative carbon sources. Since the truncated protein is present and correctly processed, and it does not affect the processing of the wild-type chimera, the dominance could be due to inhibition of the wild-type protein activity carried out by the truncated one. It is possible to hypothesize that the truncated protein competes with the wild-type chimera over binding to one or more Mgm1 interactors, and that at the same time is unable to stimulate the fusion, due to the lack of part of the GED domain. In human the V903Gfs*3 mutation is dominant by haploinsuficiency. The difference between humans and yeast may be due to nonsense mediated mRNA decay, which in humans is responsible of decreased levels of V903Gfs*3 truncated protein, whereas in yeast seems to be inactive, since the levels of the mutant protein are similar to those of the wild-type one.

By the results obtained we validated *S. cerevisiae* carrying *CHIM3* as a suitable yeast model to evaluate the pathogenicity of OPA1 mutations and to define whether a mutation is dominant by haploinsufficiency or is dominant negative. The model allows us to study the effects of missense mutations but appears to be less effective for the

analysis of nonsense mutations due to the interference in yeast of the truncated protein with the wild-type one.

Results described in this section have been recently published in:

Nolli C., Goffrini P., Lazzaretti M., Zanna C., Vitale R., Lodi T., Baruffini E., 2015. Validation of a *MGM1/OPA1* chimeric gene for functional analysis in yeast of mutations associated with dominant optic atrophy. *Mitochondrion*, 25, 38-48.

Results and Discussion

3. Search of potential therapeutic drugs for DOA and DOA plus treatment

3. Search of potential therapeutic drugs for DOA and DOA plus treatment

In the last years, yeast has proved to be a good model for high-throughput screening (HTS) in drug discovery. HTS has been defined as "the process of assaying a large number of potential effectors of biological activity against targets (a biological event)" (Armstrong J.W, 1999) and its goal is to accelerate drug discovery by screening large libraries often composed of thousands of compounds. In 2011 Couplan and collaborators set up one yeast-based screening, called Drug drop test, to search active compounds for NARP syndrome which is a hereditary mitochondrial disease that affects ATP synthase activity (Couplan et al., 2011). They employed *fmc1Δ,* a thermo-sensitive mutant involved in the assembly of the F1 sector of ATP synthase, which was unable to grow on oxidative carbon sources at high temperatures (35°-37°C). Mutant cells were spread on a plate containing a non-fermentable carbon source and then small filters spotted with the different compounds to be tested were placed on the agar surface. Plates were then incubated at 35°C and the mutant growth was monitored for 7 days. A halo of growth around a filter indicated that the spotted molecule was able to restore the growth on oxidative carbon source, with a rescuing effect of the pathological phenotype. In this way, Couplan and collaborators found 2 molecules able to rescue the RD phenotype of the *fmc1Δ* mutant. A similar approach has been recently applied in our laboratory to find potential therapeutic drugs for mitochondrial diseases, caused by mutations in *POLG* gene, coding for a catalytic subunit of DNA polymerase γ. A *S. cerevisiae* thermo-sensitive strain, carrying a mutation in Mip1 (orthologous of Polγ in yeast), was used. 1200 compounds from Prestwick Chemical library were tested through HTS and 6 molecules were found able to rescue the RD phenotype of the *mip1* yeast strain. (Pitayou et al., in press). We decided to apply this technique for the detection of drugs for DOA treatment. As previously said, this type of screening is usually performed using thermo-sensitive (*ts*) mutants. In fact, in the case of pathological mutations affecting the mtDNA stability, as in the case of POLG but also OPA1, mutations associated to a severe phenotype often cause loss of mtDNA (rho^0), an irreversible condition that cannot be rescued by any

pharmacological treatment. In these cases it is useful to use mutants with milder phenotypes, such as conditional mutants, i.e. *ts* mutant, in which mtDNA is maintained at the permissive temperature and lost at high temperature. Unfortunately, no one of the 11 created *chim3* mutants had a *ts* phenotype useful for this HTS. However, as described in Section 1, during the study of mutations affecting conserved amino acid residues between Mgm1 and OPA1 proteins, we created the *mgm1*^{I322M} mutant, which is thermo-sensitive. So we decided to use this mutant for the screening of drug libraries by the "Drug drop test" technique (Couplan et al., 2011) described in Materials and Methods. A schematic overview of the Drug Drop Test is reported in Fig.3.1.

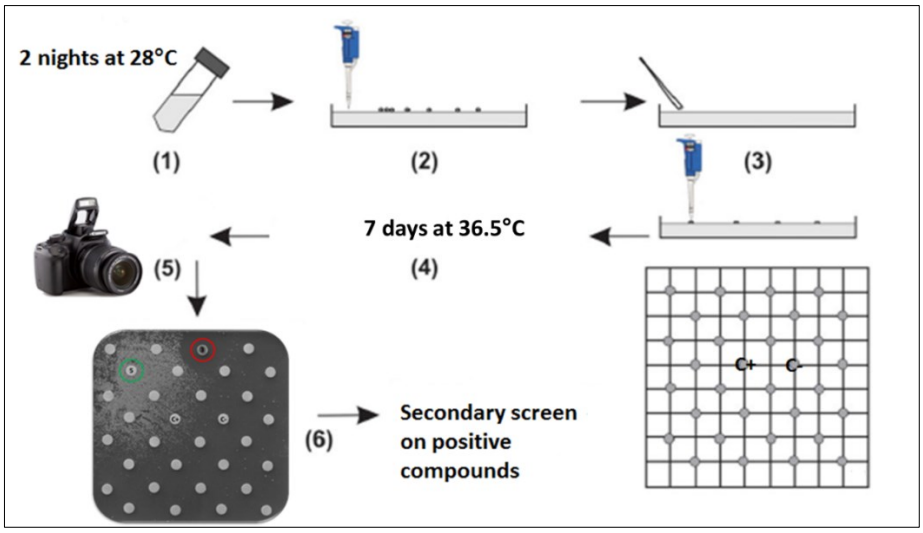

Figure 3.1. Schematic representation of primary screening using Drug drop test method (modified from Bach *et al.*, 2003). (1) Cells growth in liquid media, (2) Cells seeding on plates (3) Filters disposition on agar surface (4) Plates incubation at 36.5°C for 7 days (5) Photos of plates after different days of growth (6) Identification of active compounds that will be re-tested in secondary screening.

Mutant cells, spread on 12x12 plates containing media supplemented with a non-fermentable carbon source, are exposed to filters spotted with the compounds to test. Plates are then incubated at 36/37°C and the growth of mutant cells is monitored for some days. Depending on the presence/absence of a halo of growth around the filters, compounds are classified into four groups: i) compounds that led to formation of an enhanced halo of growth near the filter, (indicated in green in the example of Fig.3.2).

These molecules have a rescuing effect; ii) compounds that led to formation of a halo of no growth near the filter and an external crown of growth (indicated in yellow in Fig.3.2). These molecules are toxic at high concentrations (near the filter) and active at lower concentration (far from the filter). iii) molecules that inhibited the growth of the mutant strain as the one in red in Fig.3.2). iv) compounds without any effect (the majority of the screened molecules).

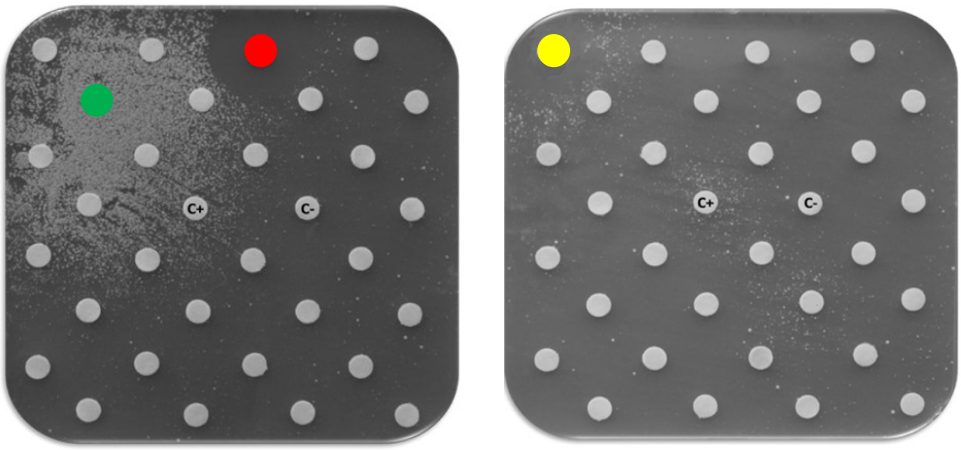

Figure 3.2. Examples of halo of enhanced growth indicated in green, internal halo of no growth and external halo of enhanced growth indicated in yellow, growth inhibitor compound indicated in red.

The screening is performed in two steps. The compounds of the first and second classes were considered as active, and subsequently re-tested in a second screening to re-confirm their rescuing effect. This two-step approach allows to minimize the number of false-positive molecules.

3.1. Definition of optimal screening conditions

In order to evaluate the ability of the molecules to rescue the impaired growth of the mutant strain, and at the same time to avoid a great number of false-positives, it is fundamental to define the optimal conditions by which the screening has to be performed. We focused on three different parameters: the non-fermentable carbon source to be used, the number of cells to be spread on plates and the optimal temperature at which plates had to be incubated. We decided to perform the screening on YP medium. In fact, in previous experiments, we observed that in synthetic medium molecules appear to be less bio-available, maybe due to the interaction with the saline components of the medium. We tested ethanol or glycerol as oxidative carbon sources. We spread different cell concentration (1-2-4-8x10^5 cell/plate) and we tested two temperatures, 36°C and 37°C. In this preliminary phase we also tested the effect of three different compounds, named MRS2, MRS3 and MRS4 that had been previously identified in a similar screening performed in our laboratory (Pitayou et al., in press). These molecules were able to rescue both the RD phenotype and the high level of mtDNA instability of a mutant in the mitochondrial DNA polymerase (Mip1) in *S. cerevisiae*. Since these two phenotypes are shared between *mip1* and *mgm1*^{I322M} mutants, we wondered whether these compounds were able to exert their rescuing effects also on *mgm1*^{I322M} mutant. After several tests (data not shown) we decided to employ ethanol as a non-fermentable carbon source, and to discard glycerol because of the elevated background growth observed using this carbon source. In addition we chose to spread 6x10^5cell/plate, an intermediate concentration between 4x10^5cell/plate (low cell number for rescue visualization) and 8x10^5cell/plate (elevated background growth). Optimal temperature was fixed at 36.5°C. Interestingly, we found that in these conditions MRS4, at the final concentration of 15mM, was able to rescue the growth defect of *mgm1*^{I322M} mutant, as shown in Fig.3.3.

Figure 3.3. Growth test on YP medium supplemented with 2% ethanol. MRS4 15mM is used as positive control and it is indicated as C+. All the remaining filters were spotted with DMSO used as negative control. Photo taken after 5 days of growth.

For this reason, MRS4 has been chosen as a positive control. In Table 3.4 the final conditions chosen for the screening are reported.

Cells/plate	$6x10^5$
Temperature	36.5°C
Carbon source	Ethanol
Positive control	MRS4 15 mM

Table 3.4. Scheme of the conditions chosen for the screening.

3.2. Chemical libraries

Two different chemical libraries were screened:

- *Fisher Bioservices Diversity Set IV* containing 1596 different compounds (http://www.fisherbioservices.com/). This chemical library is distributed by NCI (National Cancer Institute) which collects and organizes chemical molecules from different laboratories.

- *Selleck FDA-approved Drug Library* containing 1018 FDA-approved compounds and bought from Selleck Chemicals (http://www.selleckchem.com/).

All the compounds of both chemical libraries are solubilized in DMSO at a final concentration of 10mM and organized in 96-well plates. The compounds were stored at -80°C.

3.3. Screening of *Fisher Bioservices Diversity Set IV* chemical library

In every plate set up for the screening (seeded with $6x10^5$ cells of *mgm1*^{I322M} mutant) 32 filters were placed, one was used for the positive control (MRS4) and one for the negative control (DMSO). 2.5 µl of every molecule of the chemical library (at a final concentration of 10mM in DMSO) were spotted onto the remaining 30 filters. In this way we could test 30 different molecules each plate. The plates were incubated at 36.5°C and the growth of the *mgm1*^{I322M} mutant was monitored for 7 days. In Fig 3.5 an example of primary screening is reported.

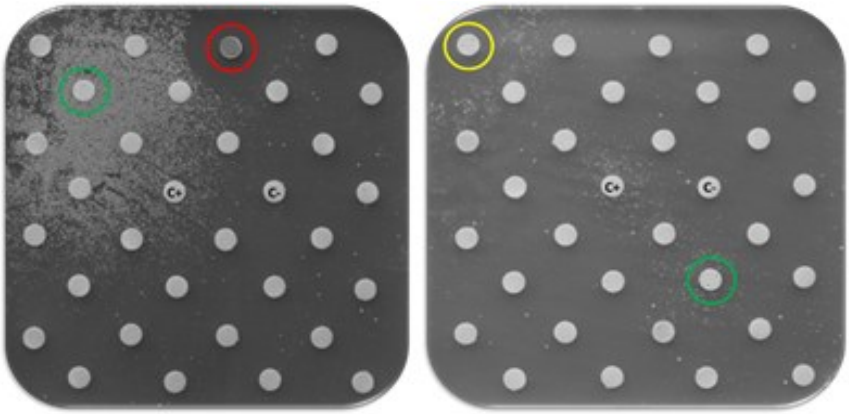

Figure 3.5. Examples of plates set up for primary screening. In the left plate an active molecule is indicated with the green circle. An inhibitor compound is indicated in red. (photo taken after 4 days of growth). In the right plate a molecule producing a halo of no growth near the filter and an external crown of growth is indicated in yellow. An active molecule is indicated in green. (photo taken after 5 days of growth). C+:MRS4 15mM. C-:DMSO.

Of 1596 tested compounds about 60 were classified as active (see page 95) and were tested in a secondary screening in order to counter-select false positive compounds. We used the same conditions described for the primary screening, except for the number of filters placed on each plate. In the secondary screening each plate contained only four equidistant filters: two of them were used for positive control and negative control respectively and the others were spotted with two different compounds to test. Molecules of class 1, leading to enhanced halo of growth, were spotted at the same concentration used in the primary screening (2.5 µl). Molecules of class 2, leading to a halo of no growth plus halo of growth, were tested at lower concentration (1-1.5 µl), depending on the size of the halo of no growth observed in primary screening. In Fig. 3.6 an example of secondary screening is reported.

Figure 3.6. Example of a plate set up for secondary screening. The molecule in the lower left corner re-confirmed its activity leading to a halo of growth bigger than the one of C+. The compound in the upper right corner did not re-confirm its activity so it was classified as a false-positive. C+:MRS4 15mM and C-:DMSO. (Photo taken after 3 days of growth).

In this secondary screening 25 molecules re-confirmed their ability to rescue the growth defect of the *mgm1*^{I322M} mutant and were classified as active. The compounds found to be inactive were classified as false-positive. In order to ascertain if the halo of growth observed was due to a true rescue, and not to activation of fermentative growth by some sugar components present in the molecule, the 25 active molecules selected from the secondary screening were subjected to a tertiary screening. In this analysis we used the W303-1B rho^0 strain, unable to grow on non-fermentable carbon sources. If some of the 25 compounds proved able to rescue the growth of the W303-1B rho^0 strain we would not consider them as active molecules but as false-positive. This analysis was performed in the same conditions described for the secondary screening. In Fig. 3.7 an example of tertiary screening is shown.

Figure 3.7. On the two filters two compounds classified as active in the secondary screening were spotted. (Photo taken after 7 days of growth) C+: MRS4 15mM. C-: DMSO.

No one of the molecules tested proved able to rescue the growth of the W303-1B rho^0 strain. Then all the 25 compounds isolated in the *Fisher Bioservices Diversity Set IV* chemical library were considered as active.

3.4. Screening of the *Selleck FDA-approved Drug Library*

Selleck FDA-approved Drug Library is a unique collection of 1018 FDA-approved drugs for high-throughput screenings. These molecules are structurally diverse, medicinally active and cell permeable. All compounds have been approved by FDA and their bioactivity and safety were confirmed by clinical trials. Every compound is also accompanied by a rich documentation concerning its structure, IC50 and customer reviews. In addition for each drug NMR and HPLC have been performed to ensure high purity. This chemical library contains drugs related to oncology, cardiology, anti-inflammatory, immunology, neuropsychiatry, analgesia etc.

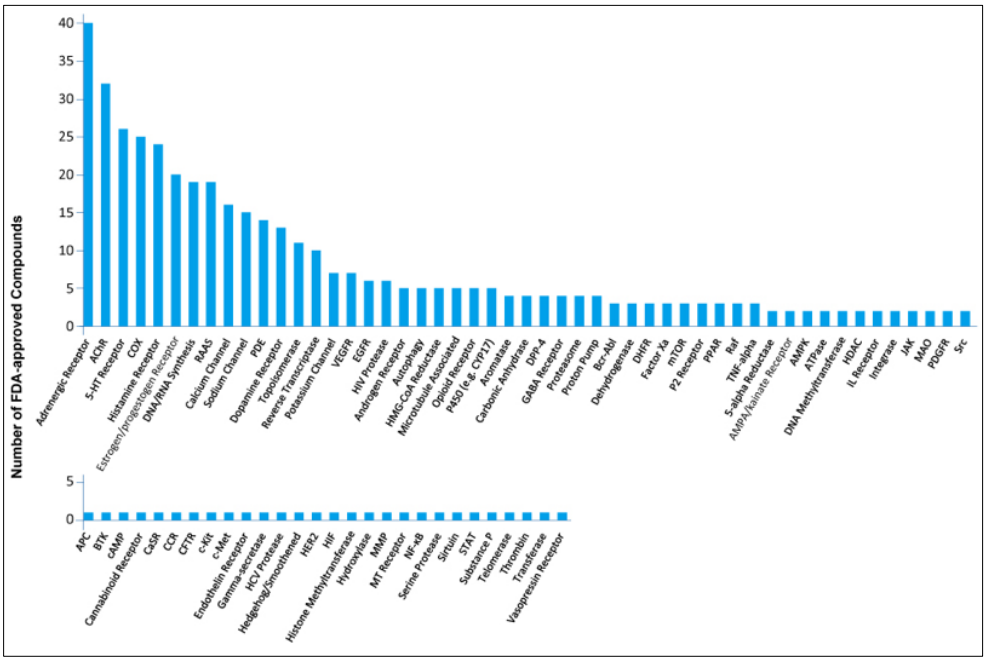

Figure 3.8. Composition of *Selleck FDA-approved Drug library*. (http://www.selleckchem.com/screening/fda-approved-drug-library.html).

Compounds are solubilized in DMSO at the final concentration of 10mM and organized in 96-well plates. Using the same conditions illustrated before for the *Fisher Bioservices Diversity Set IV* chemical library, we performed the primary screening on the 1018 molecules of the *Selleck FDA-approved Drug library*. Approximately 40 molecules were classified as active and were re-tested in a secondary screening. From the secondary screening 23 molecules proved able to rescue the growth defect of the *mgm1*^{I322M} mutant and were classified as active. Tertiary screening confirmed all 23 compounds isolated in secondary screening as active.

3.5. Search of a thermo-sensitive *chim3* mutant

S. cerevisiae containing *CHIM3* represents our model system for the study of mutations associated with DOA and DOA plus. It would be desirable to use this strain, or strains containing a *chim3* mutant allele, also in screening aimed to found potential therapeutic drugs, as the one described in Section 3.3. Unfortunately, no *ts* strains are included in our collection of *chim3* mutants. The lack of thermosensitivity and the severity of the mutations make it impossible to use these mutants in chemical library screenings. We then decided to construct a thermo-sensitive (*ts*) *chim3* mutant useful for this experimental approach. To do that, we selected missense mutations predicted to have mild effects, and we introduced them in *CHIM3*, with the aim of creating mutant alleles with a thermo-sensitive phenotype.

3.5.1. *In silico* analysis and mutations selection

The *OPA1* LSDB database (http://opa1.mitodyn.org) collects all the pathological mutations known to be localized in *OPA1* gene. We focused on missense mutations that are reported to affect the GTPase domain, the Dynamin central domain (also called Middle domain) and the GED domain (GTPase effector domain). In fact, most of the mutations associated with DOA and DOA plus are localized in these regions (Olichon et al., 2006). We selected 63 mutations: 39 localized in the GTPase domain, 17 in the Dynamin central domain and 7 in the GED domain. *In silico* prediction of pathogenicity was performed using 8 different bioinformatics tools on all 63 selected mutations. By these bioinformatics software, each of which uses a different prediction algorithm, we were able to predict the effect of each amino acid substitution on the protein function. Here a list of the 8 bioinformatic tools employed is reported.

- **SIFT** (http://sift.jcvi.org). Ranges from 0 to 1. The amino acid substitution is predicted damaging if the score is <=0.05 and tolerated if the score is >0.05.

- **PolyPhen-2** (http://genetics.bwh.harvard.edu/pph2/). Ranges from 0.00 (benign) to 1.00 (probably damaging). The amino acid substitution is predicted as benign - possibly damaging - probably damaging.

- **PANTHER** (http://www.pantherdb.org). Ranges from 0 (neutral) to 1 (pathological).

- **SNPs & GO** (http://snps-and-go.biocomp.unibo.it/snps-and-go/index.html). Ranges from 0 (unreliable) to 10 (reliable).

- **Snap** (https://www.rostlab.org/services/SNAP/). The predicted amino acid substitution is predicted to have a strong effect (score >50), a weak effect (-50<score<50) or as neutral (score <-50).

- **PON-P2** (http://structure.bmc.lu.se/PON-P2/). The substitutions are predicted as pathogenic, neutral and unknown.

- **META-SNP** (http://snps.biofold.org/meta-snp/). Ranges from 0 (neutral) to 1 (disease). If >0.5 mutation is predicted as disease.

- **Predict snp** (http://loschmidt.chemi.muni.cz/predictsnp/). The predicted effect is color-coded: neutral mutations are in green while deleterious mutations in red.

The output results are different depending on which program is used. In order to homogenize the results obtained by the 8 bioinformatic programs, to each of the 8 outputs predicted for each mutation a score and a color-code were given, according to

the following rules: score 1 and color green if the mutation was predicted as “neutral”; score 2 and color yellow if the output was “tolerated”; score 3 and color red if the mutation was predicted as “damaging” or “probably damaging”. Fig.3.9 shows an example of color-code and score for R290Q mutation analyzed using three different bioinformatics tools.

Mutation	**SIFT**[1]		**PolyPhen-2**[2]		**PANTHER**[3]	
		Score		*Score*		*Score*
R290Q	NEUTRAL	1	PROBABLY DAMAGING	3	0,61288 (TOLERATED)	2

Figure 3.9. Example of pathogenicity prediction using three of the eight bioinformatics tools employed.

[1] **http://sift.jcvi.org**
[2] **http://genetics.bwh.harvard.edu/pph2/**
[3] **http://www.pantherdb.org**
Color green and score 1 indicate a mutation predicted as “neutral”, yellow and score 2 indicated a “tolerated” mutation and red and score 3 indicated a “probably damaging” or “damaging” predicted mutation.

So for each mutation 8 scores were defined. Then, for each mutation a single “Consensus score” was obtained by summing the 8 scores and by subtracting 8 (that corresponds to the number of bioinformatics tools used) from the sum. On the basis of these “Consensus scores” we classified the mutations in three different groups:

- 0 - 7: mutations were predicted as “neutral” and colored in green
- 8 - 15: mutations were predicted as “tolerated” and colored in yellow
- 16 - 24: mutations were predicted as “damaging” or “probably damaging” and colored in red

In this way, out of the 63 mutations analyzed, 6 were classified as “neutral”, 15 as “tolerated” and 42 as “damaging”.

We were interested in mutations that could lead to a thermo-sensitive phenotype when introduced in yeast. So we discarded all the 42 mutations predicted as "damaging", in the hypothesis that these mutations could determine a complete loss of function, due to the high level of predicted pathogenicity. Among the remaining mutations we selected 4 mutations: 2 of them predicted as "neutral" and the others predicted as "tolerated". In Fig. 3.10 chosen mutations are reported.

Mutation	**Domain**	**References**	**"Consensus Score"**
Arg290Gln	GTPase (exons 10-17)	Alexander et al. (2000)	7
Ala357Thr	GTPase (exons 10-17)	Ferre et al. (2009)	5
Asp438Ala	GTPase (exons 10-17)	Almind et al. (2012)	11
Ser646Leu	Dynamin Central (exons 18-26)	Ferre et al. (2009)	9

Figure 3.10. Mutations introduced in *CHIM3*. R290Q and A357T mutations were predicted as "neutral" whereas D438A and S646L substitution were predicted as "tolerated". The "Consensus score" is reported in the last column.

The four mutations were then introduced in *CHIM3* by site-directed mutagenesis and the mutated *chim3* alleles, cloned in a pFL39TEToff vector, were used to transform a *mgm1Δ* strain. The phenotype of transformant strains was then analyzed by spot assay on non-fermentable carbon sources both at 28°C and 37°C in order to highlight the possible thermo-sensitive phenotype. As showed in Fig.3.11 one of the mutant alleles, *chim3*^{S646L}, proved able to confer a *ts* phenotype when introduced in a *mgm1Δ* strain.

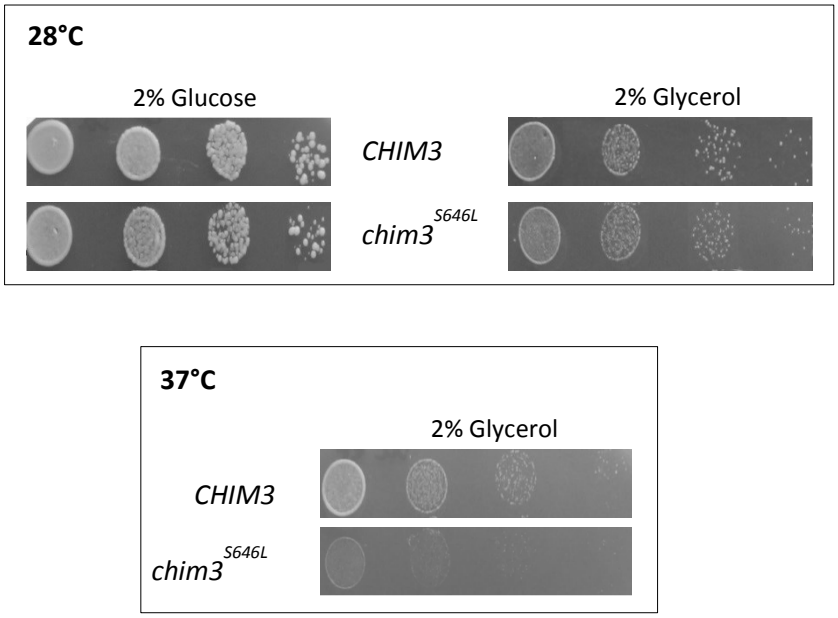

Figure 3.11. Upper panel: spot assay of W303-1A *mgm1Δ* strain transformed with pFL39TEToff*CHIM3* and pFL39TEToff*chim3*^{S646L} vectors on YP medium supplemented with 2% glucose (left) and 2% glycerol (right) at 28°C. Lower panel: spot analysis assay on the same strains on YP medium supplemented with 2% glycerol at 37°C.

3.5.2. *chim3*^{S646L} as a model to search potential therapeutic molecules for DOA and DOA plus treatment

Due to its thermo-sensitive phenotype *S. cerevisiae chim3*^{S646L} mutant represents a suitable model for screenings of potential therapeutic drugs for DOA and DOA plus treatment. At first we looked for the optimal growth conditions for this analysis. As previously done for *mgm1*^{I322M} mutant, we tested different non fermentative carbon sources (ethanol and glycerol), two different temperatures (36.5°C and 37°C) and several cell concentrations to seed on the plates (1-2-4-6x10^5 cells/plate). We performed the screening on YP medium, as for *mgm1*^{I322M} mutant, using MRS4 at the final concentration of 15mM as positive control. After several tests (data not shown) the optimal conditions for the screening were identified (Fig. 3.12).

Temperature	36.5°C	37°C
Carbon source	2% glycerol	0.5% glycerol + 2% ethanol
Cells/plate	$2x10^5$	$2x10^5$
Positive control	MRS4 15mM	MRS4 15mM

Figure 3.12. Scheme of the conditions used for the screening.

Differently from the screening performed with *mgm1*^{I322M} mutant, in the case of *chim3*^{S646L} mutant it was necessary to use different combinations of temperature and carbon source in order to highlight the *ts* phenotype. So the molecules were analyzed for their ability to rescue the growth of the *chim3*^{S646L} mutant both on YP supplemented with 2% glycerol at 36.5°C and on YP supplemented with 0.5% glycerol and 2% ethanol at 37°C. The screening was performed using Drug drop test technique as for *mgm1*^{I322M} mutant. In these experimental conditions, we checked whether the molecules, isolated as active using *mgm1*^{I322M} mutant, were also active in rescuing the *ts* growth of *chim3*^{S646L} mutant using the same experimental procedure described in Section 3. By the two-step screening of the *Fisher Bioservices Diversity set IV* chemical library we identified 25 molecules able to rescue the growth defect of the *mgm1*^{I322M} mutant among which 10 were strongly active. 7 out of these 10 molecules were isolated as active using *chim3*^{S646L} mutant. These molecules were named with the conventional name: *Fisher* ORM (**O**PA1 **R**eactive **M**olecules) 1-7. From the screening of the *Selleck FDA-approved Drug library* on *mgm1*^{I322M} mutant strain we identified 23 molecules able to rescue the growth defect. 5 of them were excluded since they were classified by FDA as anti-cancer drugs, not suitable for non-cancer disease treatments in human patients. Of the remaining 18 compounds, 16 proved able to rescue the growth defect of *chim3*^{S646L} mutant both in primary and secondary screening. To differentiate these molecules from both the ones identified in the *Fisher Bioservices Diversity set IV* chemical library and the ones classified as active on *mgm1* mutant, we called them *Selleck* ORM (**O**PA1 **R**eactive **M**olecules) 1-16.

In addition, we found that the molecule called MRS5, identified in a screening previously performed in our laboratory (Pitayou et al., in press), had a strong positive effect on the growth of *chim3*^{S646L} mutant at very low concentration (2mM).

Figure 3.13. Example of a plate set up with different MRS5 concentration. Clockwise C-:DMSO, MRS5 5mM, MRS5 2.5mM and MRS5 1mM. (Photo taken after 3 days of growth).

Summary of the third section and conclusions

One of the aims of this work was to search for potential therapeutic drugs for DOA and DOA plus treatment using *S. cerevisiae* as a model system. Yeast has been widely used for these types of high throughput screening during the last few years. For this purpose, we used a phenotypic screening based on thermo-sensitive yeast mutants. A molecule was selected as active if it was able to restore the growth impairment of the mutant at the restrictive temperature. The screening was first performed using the *mgm1*^{I322M}, the only *ts* mutant available. Using Drug drop test method we screened two different chemical libraries and we found 47 active molecules able to rescue the respiratory deficient phenotype of the *mgm1*^{I322M} mutant. Interestingly, one of these compounds was found both in the *Fisher Bioservices Diversity Set IV* library and in the *Selleck FDA-approved Drug library*. This finding supports the reliability and the reproducibility of this screening technique. *S. cerevisiae* containing *CHIM3* is our model system to study mutations associated with DOA and DOA plus in yeast. So it would be desirable to perform the above mentioned screenings using a *chim3* mutant with a thermo-sensitive phenotype. In order to obtain such a *chim3* mutant we used a computational approach. We analyzed 63 missense mutations found in literature, predicting their pathogenicity by means of 8 different bioinformatic programs. We selected 4 mutations, predicted as neutral or tolerated, one of which, S646L, when introduced in *CHIM3* was able to give a *ts* phenotype to transformant *mgm1Δ* strain. *chim3*^{S646L} mutant was then used to confirm the potential therapeutic activity of the 10 molecules from the *Fisher Bioservices Diversity set IV* chemical library, previously selected as the most active in the HTS performed on *mgm1*^{I322M} mutant. Seven of these proved able to be active also on the *chim3*^{S646L} mutant. Using the same procedure we tested the 18 molecules selected from the *Selleck FDA-approved Drug library*. 16 of them rescued the *ts* phenotype of *chim3*^{S646L} mutant. All the 23 molecules identified were called ORM (**O**PA1 **R**eactive **M**olecule) and were differentiated into two groups: 7 *Fisher* ORM and 16 *Selleck* ORM. Further analysis will be pursued to gain insight into the rescuing mechanisms of these 23 molecules. All the molecules classified as active will be examined by an expert in pharmacology and pharmaceutical

chemistry in order to have information about their structure and reactivity. The compounds will be also tested for their ability to rescue other phenotypes associated with mutations in *MGM1* gene such as: mtDNA instability, reduced mitochondrial respiratory activity and mitochondrial network aberrant morphology. If one of these compound will exhibit a rescuing effect on some of these phenotypes it will be used in drug validation tests on higher eukaryotic models, such as MEF cells (Mouse Embryonic Fibroblasts) and fibroblasts of DOA and DOA plus affected patients, in collaboration with Dr. Claudia Zanna (Dept. of Pharmacy and Biotechnology, University of Bologna). Active compounds eventually found and characterized in these models could be employed as a starting point for future researches for ADOA and ADOA plus treatment.

To summarize the work described in this thesis, we can conclude that the *S. cerevisiae* model constructed and characterized has proved to be suitable both for the validation and the study of mutations associated with DOA and DOA plus and also for a drug discovery approach, used to search for potential therapeutic drugs for the treatment of dominant optic atrophy.

Material and Methods

1.1. Strains used

All *S. cerevisiae* strains used in this work are listed below:

STRAIN	GENOTYPE	REFERENCES
W303-1A	*Mata, ade2-1, leu2-3, ura3-1, trp1-1, his3-11, can1-100, rho^0*	Thomas and Rothstein, 1989
W303-1B	*Matα, ade2-1, leu2-3, ura3-1, trp1-1, his3-11, can1-100, rho^0*	Thomas and Rothstein, 1989
BY4742 *mgm1Δ*	*Matα his3Δ1, leu2Δ0, lys2Δ0, ura3Δ0*	Euroscarf collection; Brachmann et al., 1998
W303-1A *mgm1Δ*	*Mata, ade2-1, leu2-3, ura3-1, trp1-1, his3-11, can1-100*, *mgm1*::KanMX4	This work
W303-1B *mgm1Δ*	*Matα, ade2-1, leu2-3, ura3-1, trp1-1, his3-11, can1-100* *mgm1*::KanMX4	This work
W303 1.1 *mgm1Δ/mgm1Δ*	*Mata/Matα*, *ade2-1/ade2-1, leu2-3/leu2-3, ura3-1/ura3-1, trp1-1/trp1-1, his3-11/his3-11,can1-100/can1-100* *mgm1*::KanMX4/*mgm1*::KanMX4	This work

The bacteria strain used in this work is listed below:

STRAIN	GENOTYPE
DH10B	*F-mcrA Δ(mrr-hsdRMS-mcrBC) φ80d DlacZ ΔM15 ΔlacX74 deoR recA1 endA1 araD139 Δ(ara, leu)7697 galU galKλ-rpsL hupG*

1.2. Media and growth conditions

For yeast the following media were used:

- YP (1% peptone, 0.5% yeast extract)
- YPA (2% peptone, 1% yeast extract, 75mg/ml adenine)
- YNB (YNB ForMedium™ w/o aminoacids w/o NH_4SO_4 1,9 g/L, NH_4SO_4 5 g/L). Minimum media was enriched with drop-out powder (Kaiser et al. 1994).
- SD (YNB ForMedium™ w/o aminoacids w/o NH_4SO_4 6,7 g/L).
- 5-FOA YNB: YNB ForMedium™ with 1 g/l 5-Fluoroorotic Acid (Melford), 50 mg/l uracile with aminoacids necessary to complement the auxotrophies (Boeke et al., 1984).

If necessary singles amino acids could be excluded from complete drop-out to maintain selective pressure. As solidifying agent agar ForMedium™ 2% was added. Carbon sources were added at final concentration of 2% if not specified differently. The following sources were used: Glucose (D), Ethanol (E), Glycerol (G), Galactose (Gal), Lactate (L). *S. cerevisiae* was cultured at 28˚C, in constant shaking 120 rpm if liquid media was used. To induce heat stress, cultures were incubated at 37˚C in thermostat or water bath.

For *E. coli* LB media was used (1% bacto tryptone Difco™, 0.5% yeast extract Difco™, 0.5% NaCl, pH 7.2-7.5). Agar 2% and ampicillin (Sigma-Aldrich®) 100mg/ml were added if needed. For α-complementation selection 80µl of 5-bromo-4-chloro-3-indolyl-b-D-galactopyranoside (Xgal) 2% (dissolved in dimethilformamide) and 40µl isopropyl-beta-D-thiogalactopyranoside (IPTG) 23.8 mg/ml were added. Cultures were incubated at 37˚C in constant shaking if necessary.

1.3. Plasmids

PLASMIDS	MARKERS IN *S. cerevisiae*	TYPE	REFERENCES	FIGURE
pFL36	*LEU2*	Centromeric	Bonneaud et al., 1991	1.1
pFL36TEToff	*LEU2*	Centromeric	This work	1.5B
pFL38	*URA3*	Centromeric	Bonneaud et al., 1991	1.2
pFL39	*TRP1*	Centromeric	Bonneaud et al., 1991	1.3
pFL39TEToff	*TRP1*	Centromeric	This work	1.5C
pFL39PGK	*TRP1*	Centromeric	This work	1.6B
Yeplac112	*TRP1*	Multicopy	Gietz and Sugino, 1988	1.4
Yeplac112PGK	*TRP1*	Multicopy	This work	1.6C
pCM189	*URA3*	Centromeric	Garì et al., 1997	1.5A
pFL61	*URA3*	Multicopy	Minet et al., 1992	1.6A
pYEF1mtGFP	*URA3*	Multicopy	Rinaldi et al., 2008	-

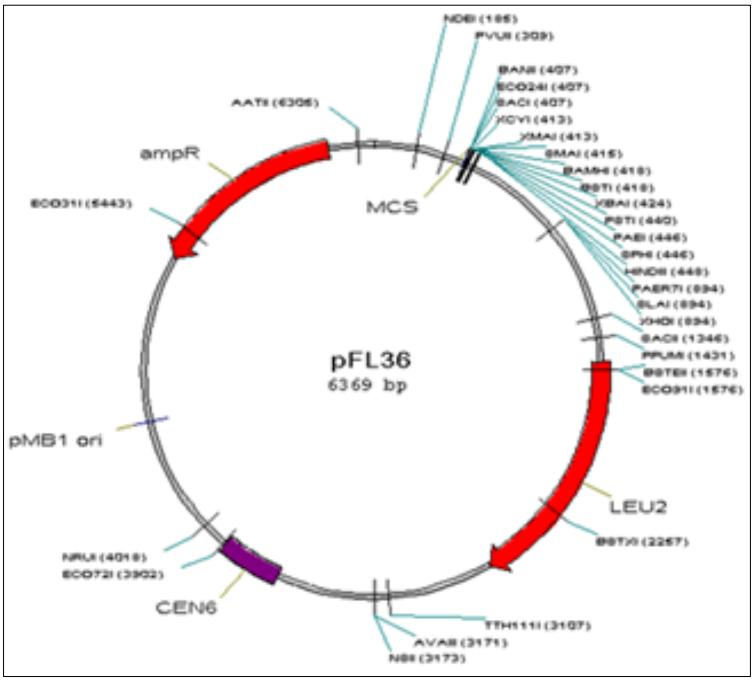

Figure 1.1. pFL36 plasmid.

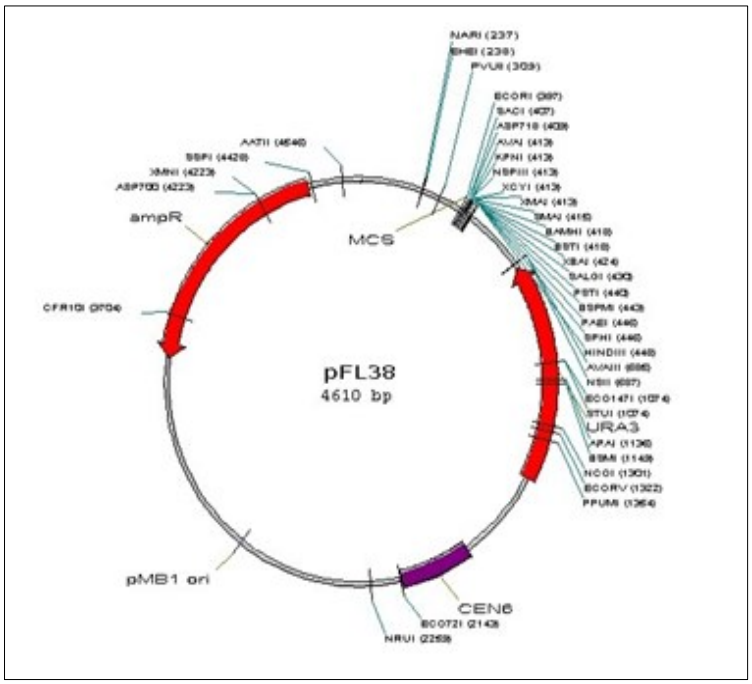

Figure 1.2. pFL38 plasmid.

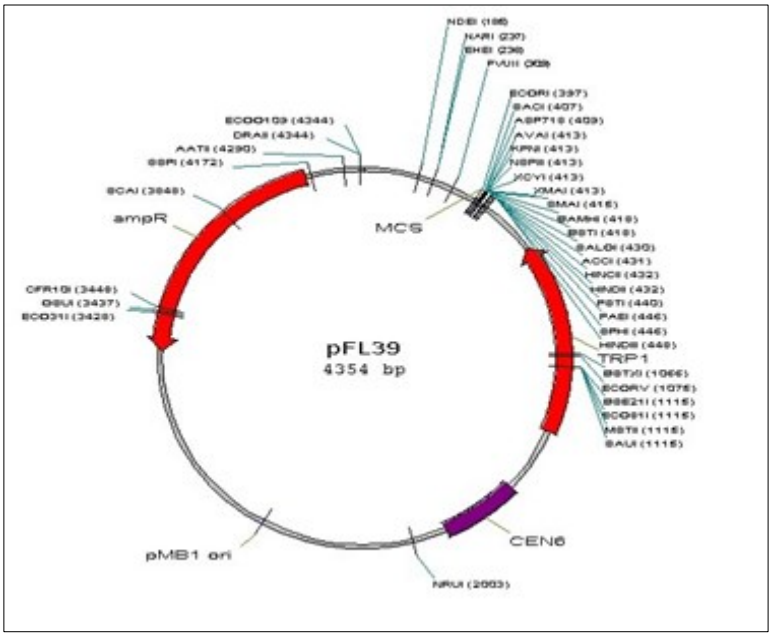

Figure 1.3. pFL39 plasmid.

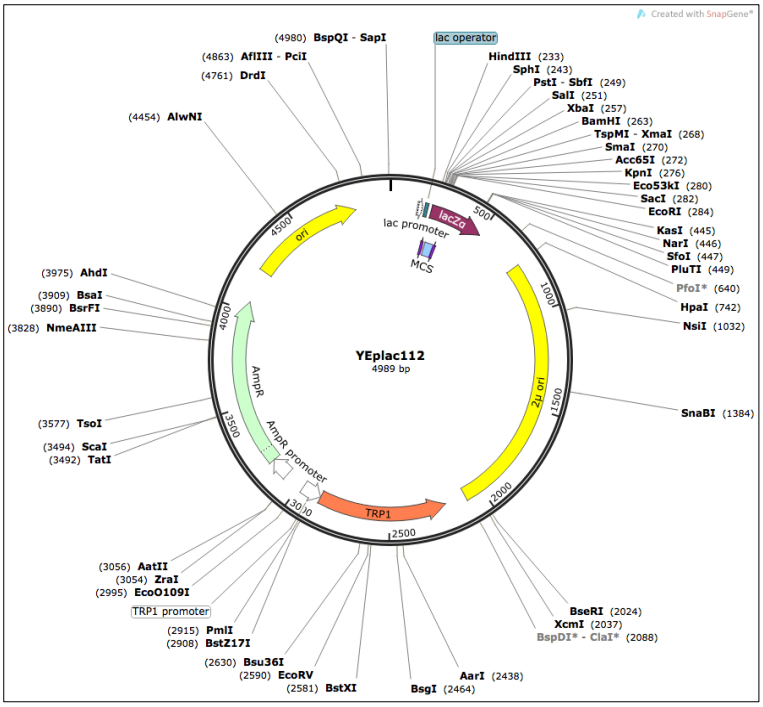

Figure 1.4. YEplac112 plasmid.

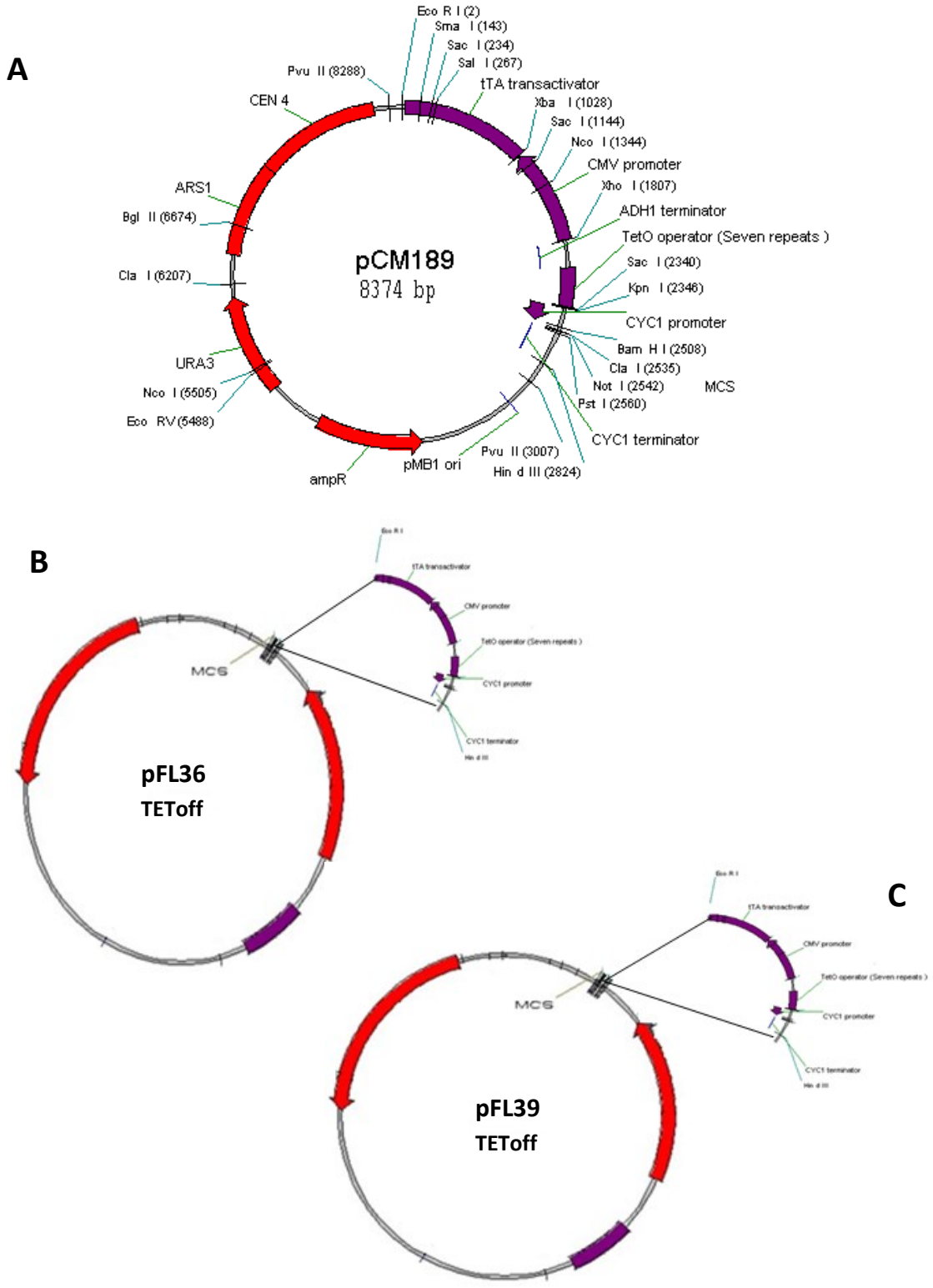

Figure 1.5. A) pCM189 plasmid. B) pFL36TETOff plasmid obtained by cloning *CYC1*TETOff between EcoRI-HindIII sites from pCM189 plasmid. C) pFL39TETOff plasmid obtained by cloning *CYC1*TETOff between EcoRI-HindIII sites from pCM189 plasmid.

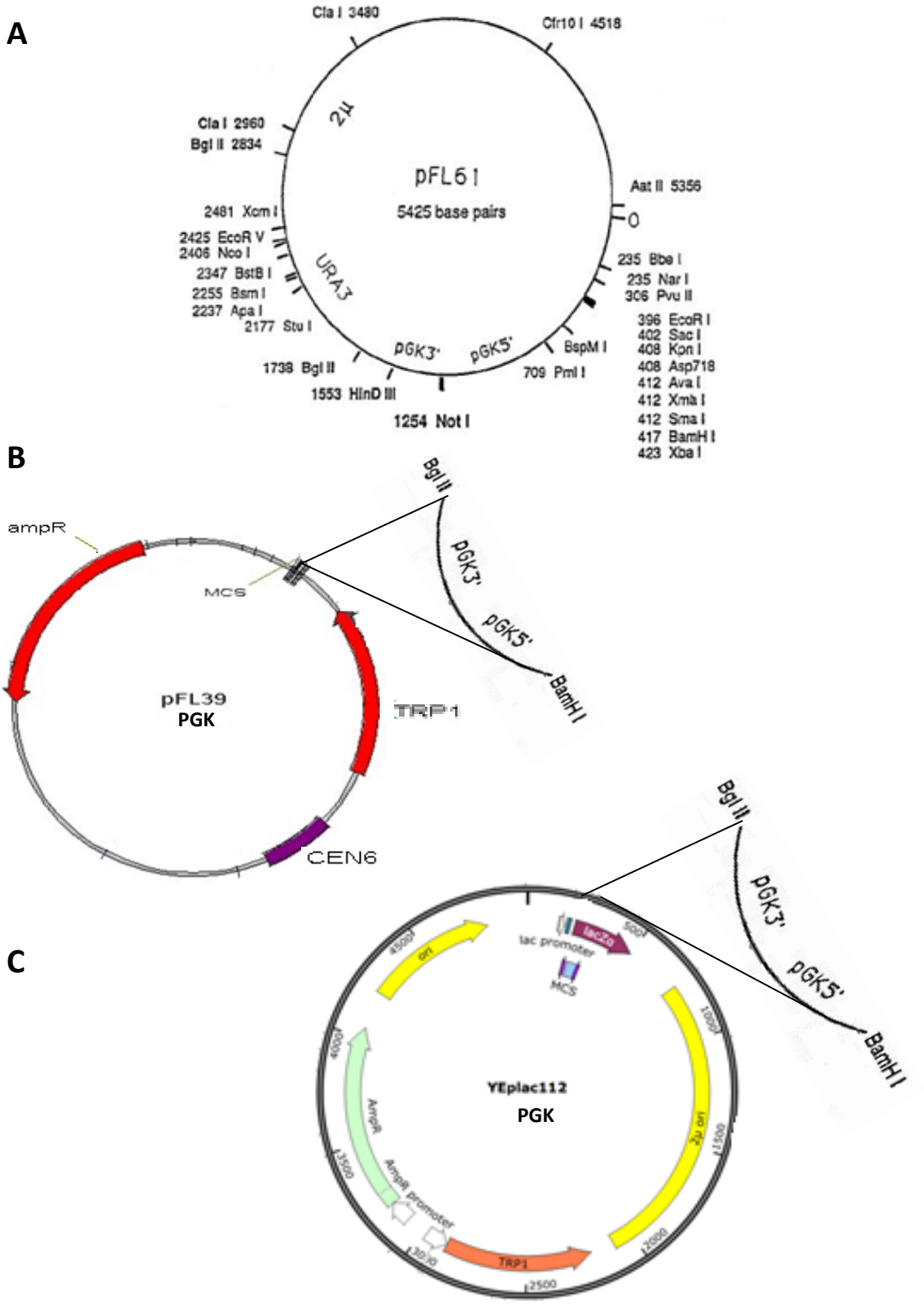

Figure 1.6. A) pFL61 plasmid. B) pFL39*PGK* plasmid obtained by cloning *PGK* promoter between BglII-BamHI sites from pFL61 plasmid. C) YEplac112PGK plasmid obtained by cloning *PGK* promoter between BglII-BamHI sites from pFL61 plasmid.

1.4. Polymerase Chain Reactions

All the reactions were performed following manufacturer indications. For analytical purpose GoTaq® DNA polymerase (©Promega) was used. Preparative reactions for gene cloning and site specific mutagenesis were performed with a high fidelity (HiFi) polymerase. KOD Hot Start HiFi DNA polymerase was used (Novagen®). All the reactions were performed using "Applied Biosystem 2720 Thermal Cycler".

1.4.1. *MGM1* amplification

MGM1 amplification was performed using KOD Hot Start HiFi DNA polymerase (Novagen®) and MGM1CSalFw and MGM1SacIRv as primers (see Table 1.7.). The reaction was performed following manufacturer indications. 10 ng of genomic DNA from W303-1B strain and 1U of KOD HiFi DNA polymerase were used in a final volume of 50 µl. The amplification was performed using the following conditions:

- 2' at 95°C

30 cycles:

- 20'' at 95°C
- 18'' at 52°C
- 20''/Kb at 70°C
- 3' at 70°C
- ∞ at 10°C

MGM1 was then cloned in a pFL38 vector between *Sal*I and *Sac*I restriction sites.

1.4.2. *MGM1* disruption

MGM1 disruption in W303-1A and W303-1B strains with KAN^R was performed using KOD HiFi DNA polymerase (Novagen®) and MGM1CSalFw and MGM1RvSacI as primers (see Table 1.7). The reaction was performed following manufacturer indications. 10 ng of genomic DNA from BY4742 *mgm1Δ* (containing KanMX4 cassette) strain and 1U of KOD HiFi DNA polymerase were used in a final volume of 50 µl.

The amplification was performed using the following conditions:

- 2’ at 95°C

30 cycles:

- 20’’ at 95°C
- 18’’ at 52°C
- 20’’/Kb at 70°C
- 3’ at 70°C
- ∞ at 10°C

1.4.3. *CHIM1-6* amplification

All the chimeric genes *CHIM1-6* were constructed using the two step overlap extension technique, a modification of the protocol used for site directed mutagenesis (Ho et al., 1989). For each chimera, the first PCR reaction was performed using the external forward primer MGM1CSalFw and the external reverse primer OPA1XhoRv, each in combination with reverse or forward internal primers respectively, designed in order to amplify different portions of *MGM1* (gradually longer) and *OPA1* (gradually shorter), see Table 1.7. The PCR reaction was performed using as templates respectively: pFL38*MGM1* to amplify different portions of *MGM1* and *OPA1* cDNA to amplify different portions of *OPA1*. The reaction was performed following manufacturer indications and KOD HiFi DNA polymerase (Novagen®) was used. 1 ng of template and 1U of KOD HiFi DNA polymerase were used in a final volume of 50 µl. The amplification was performed using the following conditions:

- 2’ at 95°C
- 30 cycles:
- 20’’ at 95°C
- 18’’ at 54°C
- 20’’/Kb at 70°C
- 3’ at 70°C
- ∞ at 10°C

Final chimeric constructs were obtained by using the different overlapping PCR fragments in equimolar ratio as templates and MGM1CSalFw and OPA1XhoRv as primers. The reaction was performed following manufacturer indications and KOD HiFi DNA polymerase (Novagen®) was used. About 70 ng of template and 1U of KOD HiFi DNA polymerase were used in a final volume of 50 µl. The first amplification was performed using the following conditions:

- 2’ at 95°C

10 cycles:

- 20’’ at 95°C
- 30’’ at 60°C
- 1’10’’/Kb at 70°C

After 10 cycles MGM1CSalFw and OPA1XhoRv primers, at a final concentration of 10 µM, were added and the second amplification was performed using the following conditions:

25 cycles:

- 20’’ at 95°C
- 18’’ at 54°C
- 1’10’’/Kb at 70°C
- 3’ at 70°C
- ∞ at 10°C

The products, together with the whole OPA1 coding region amplified with OPA1CFw and OPA1XhoRv, were then digested with *Sal*I and *Xho*I and cloned in a *Sal*I-*Xho*I-digested pFL39*MGM1* centromeric plasmid and in a *Sal*I-*Xho*I digested YEplac112*MGM1* multicopy plasmid, in each of which a *Xho*I site was introduced by site specific mutagenesis just after the stop codon of *MGM1* ORF. The *CHIM3* construct was also cloned in pFL39*PGK*, pFL39TEToff and pFL36TEToff. pFL39PGK*CHIM3*, pFL39TEToff*CHIM3* and pFL36TEToff*CHIM3* were obtained by PCR-amplification using pFL39*CHIM3* as template and MGMOPACNotFw and MGMOPACNotRv as primers. After digestion with *Not*I, the PCR fragments were cloned in the different plasmids.

1.4.4. Site directed mutagenesis

A110V, S241N, L273P and I322M mutations were introduced in *MGM1* using pFL38*MGM1* as template. For each mutation, the first PCR reaction was performed using the external forward primer MGM1SalIFw and the external reverse primer MGM1PostBamRv, each in combination with reverse or forward internal primers for each mutation (see Table 1.7). R290Q, S298N, G300E, L331P, A357T, I382M, D438A G439V, R445H, T449P, T449X, K468E, S545R, L593P, D603H, S646L, Q785R, V903Gfs*3, V910D mutations were introduced in *CHIM3* using pFL39TETOff*CHIM3* as template. For each mutation, the first PCR reaction was performed using the external forward primer CYC1TATAFw and the external reverse primer MGM1OPACNotRv, each in combination with reverse or forward internal primers for each mutation (see Table 1.7). The reaction was performed following manufacturer indications and KOD HiFi DNA polymerase (Novagen®) was used. 1 ng of template and 1U of KOD HiFi DNA polymerase were used in a final volume of 50 µl. The amplification was performed using the following conditions:

- 2’ at 95°C

30 cycles:

- 20’’ at 95°C
- 18’’ at 54°C
- 20’’/Kb at 70°C
- 3’ at 70°C
- ∞ at 10°C

Final mutated genes (*MGM1* and *CHIM3*) were obtained by using the different overlapping PCR fragments in equimolar ratio as templates and MGM1CSalFw and MGM1PostBamRv as primers for *MGM1* site directed mutagenesis and CYC1TATAFw and MGM1OPACNotRv as primers for *CHIM3* site directed mutagenesis. The reaction was performed following manufacturer indications and KOD HiFi DNA polymerase (Novagen®) was used. About 70 ng of template and 1U of KOD HiFi DNA polymerase were used in a final volume of 50 µl. The first amplification was performed using the following conditions:

- 2’ at 95°C

10 cycles:

- 20’’ at 95°C
- 30’’ at 60°C
- 1’10’’/Kb at 70°C

After 10 cycles MGM1CSalFw and MGM1PostBamRv as primers (*MGM1* site directed mutagenesis) and CYC1TATAFw and MGM1OPACNotRv as primers (*CHIM3* site directed mutagenesis), at a final concentration of 10 µM, were added and the second amplification was performed using the following conditions:

25 cycles:

- 20’’ at 95°C
- 18’’ at 54°C
- 1’10’’/Kb at 70°C
- 3’ at 70°C
- ∞ at 10°C

Mutated *mgm1* PCR products, digested with *Sal*I-*Bam*HI, were cloned in *Sal*I-*Bam*HI digested pFL39*MGM1* vector. Mutated chimeric alleles, digested with *Not*I, were cloned in *Not*I- digested pFL39TEToff vector.

1.4.5. RT-PCR and qPCR

For RT-qPCR, cells were grown in SC supplemented with 2% glucose until 0.9-1.2 OD was reached. Total RNA was extracted from 10 OD with hot acidic phenol (Ausubel et al., 1994), treated with DNase I (New England Biolabs), retrotranscribed with M-MuLV Reverse Transcriptase (NewEngland Biolabs) with oligo (dT) 20primer (Euroclone) and murine RNase inhibitor (NewEngland Biolabs). A RNA stock of 0.5 µg/µl was prepared.

DNAse Reaction:

RNA	2 µg
DNAse I Buffer	2 µl
DNAse I	2 µl
H_20 + DEPC 1%	16 µl

1. Incubate the samples 15’ at room T.
2. Add 2 µl EDTA 25 mM to inactivate DNAse I and incubate the samples 10’ at 65 °C.
3. Precipitate the reactions with 1/10 vol NaAc 3M pH 5.2 and 2.5 vol of EtOH 96%. Freezing with N_2 before storing at -80 °C overnight.

Reverse Transcriptase Reaction:

RNA+oligodT	4,5 µl
RT-Buffer (10X)	1 µl
5mM dNTPs	1 µl
RNAse-OUT	0,25 µl
Reverse Transcriptase	0,5 µl
H_20 + DEPC 1%	2,75 µl

1. After precipitation, resuspend RNA pellets in 10.5 µl H_20+DEPC 1%. The samples are split in two eppendorf tubes: one will be for the control without Reverse Transcriptase.
2. Add 1 µl oligo-dT and incubate the samples 10’ at 70°C.

Transcriptase is added to all samples except for the control.

3. Incubate the samples at 42°C for 2h and stop reactions with heat inactivation (70°C for 15’).
4. Process the samples with PCR or stock them at -20°C.

qPCR on retro-transcribed *CHIM3* and, as reference, *ACT1* mRNA was performed by using Power Sybr Green mix with ROX (Life Technologies), supplemented with the primers reported in Table 1.7 and ACT1qFw and ACT1qRv (Baruffini et al., 2015) at a final concentration of 120 nM in the AB 7300 instrument (Life Technologies) at default settings:

- 2’ at 50°C
- 10‘ at 95°C

41 cycles

- 15’’ at 95°C
- 1’at 60°C

1 cycle

- 15’’ at 95°C
- 15’’ at 60°C

Statistical analysis was performed through an unpaired two-tailed t-test.

For qPCR, cells that were pre-grown in YP supplemented with 2% ethanol were grown in 10 ml of SC supplemented with 0.5% glucose until exhaustion. Total (genomic and mitochondrial) DNA was extracted as previously reported (Hoffman and Winston, 1987). The nucleic acid pellet was dissolved in 50 µl of TE buffer containing DNase-free RNaseA (20 µg/ml) and incubated at 37°C for 30’. This DNA was quantified by absorbance at 260 nm. Nuclear DNA and mtDNA PCR were done in individual wells for each sample dilution in the following standard 20-µl SYBR Green reaction: 10 µl of Bio-Rad iQ SYBR Green Supermix, 4 µl of diluted template at 12 ng/µl, 4.4 µl of H2O, and 0.8 µl of each nuclear primer (*ACT1* forward and reverse primers) or each mtDNA primer (*COX1* forward and reverse primers). Each primer was stored separately as a working stock of 3 µM. qPCR was performed on mtDNA gene *COX1* and, as reference, on nDNA gene *ACT1* as previously reported (Baruffini et al., 2015) with the primers reported in Table 1.7. For each analyzed strain, the copy number of the mtDNA and the nuclear DNA was calculated using the threshold cycle number (C_T). This is done in triplicate to obtain an average value for C_T for *COX1* and *ACT1*, C_T (*COX1*) and C_T

(*ACT1*), respectively. The difference (ΔC_T) between these averages C_T (*COX1*) - C_T (*ACT1*) is determined and used to arrive at a value of the relative mtDNA copy number (RCN) of each strain, which is equal to $2^{-\Delta\Delta CT}$. The fold change in the RCN of each mutant strain is calculated by dividing its RCN by the wild-type RCN value, which yields the fold change compared with wild type, which now has a value of 1.

1.5. Primers

OLIGONUCLEOTIDE	SEQUENCE 5'-3'	USE
MGM1CSalFw	gggccgtcgaccgtaatgtgtacctgattgagc	*MGM1* cloning and disruption
MGM1RvSacI	ggggggagctcgagattaagtgttcctcaatatgg	*MGM1* cloning and disruption
MGM1S1Fw	caggtgtcagtaaataacagag	*MGM1* sequencing
MGM1S2Fw	catggaaacgatggaacggtg	*MGM1*/chimeras sequencing
MGM1S3Fw	ccttcttcgtcattaagtgg	*MGM1* sequencing
OPA1S1Fw	gggaaattgatgagtatatcg	*OPA1/*chimeras sequencing
OPA1S2Fw	catactgtgtattcaagatgg	*OPA1/*chimeras sequencing
OPA1S3Fw	gagggttattcaacacaatgc	*OPA1/*chimeras sequencing
MGM1XhoTerFw	ggcgtctccaaaaatttatgactcgagataaatagtgtcattagag	Introduction of *Xho*I site downstream *MGM1* ORF
MGM1XhoTerRv	ctctaatgacactatttatctcgagtcataaatttttggagacgcc	Introduction of *Xho*I site downstream *MGM1* ORF

OPA1XhoRv	gggggctcgagttatttctcctgatgaagagc	Chimeras construction
MGMOPAC1overFw	cacattttcctaaaattatatctagactcttaaaacttcgctatc	*CHIM1* construction
MGMOPAC1overRv	gatagcgaagttttaagagtctagatataattttaggaaaatgtg	*CHIM1* construction
MGMOPAC2overFw	gctcttttactaaggacaaactaagtgaatataaatggattgtgcc	*CHIM2* construction
MGMOPAC2overRv	ggcacaatccatttatattcacttagtttgtccttagtaaaagagc	*CHIM2* construction
MGMOPAC3overFw	tgatgacgaggatgatgaaaacgagaaaattgaccaacttcagg	*CHIM3* construction
MGMOPAC3overRv	cctgaagttggtcaattttctcgttttcatcatcctcgtcatca	*CHIM3* construction
MGMOPAC4overFw	cttcttctgcacatttaactttaccacgggttgttgtggttggag	*CHIM4* construction
MGMOPAC4overRv	ctccaaccacaacaacccgtggtaaagttaaatgtgcagaagaag	*CHIM4* construction
MGMOPAC5overFw	cagatttatcattggtggatctaccaggtgtgattaatactgtg	*CHIM5* construction
MGMOPAC5overRv	cacagtattaatcacacctggtagatccaccaatgataaatctg	*CHIM5* construction
MGMOPAC6overFw	caatggtttaaaacaaattgtgtcagactgcttttggaaaatgg	*CHIM6* construction
MGMOPAC6overRv	ccattttccaaaagcagtctgacacaatttgttttaaaccattg	*CHIM6* construction

MGMOPACNotFw	gacgagcggccgcgtaaggatgaatgcgagcccag	*CHIM3* subcloning
MGMOPACNotRv	gacgtgcggccgcttatttctcctgatgaagagc	*CHIM3* subcloning and mutagenesis
MGM1PostBamRv	gctggccttttgaaaatatcc	*MGM1* mutagenesis
MGM1A110VFw	ggctgctgcagggagttatatagtctacaagatggaagaagc	*MGM1* mutagenesis
MGM1A110VRv	gcttcttccatcttgtagactatataactccctgcagcagcc	*MGM1* mutagenesis
MGM1S241NFw	cgtgataggttcacaaaactccggtaaatcctcagtactagaatcc	*MGM1* mutagenesis
MGM1S241NRv	ggattctagtactgaggatttaccggagttttgtgaacctatcacg	*MGM1* mutagenesis
MGM1L273PFw	cacaagaagactaactcgcccattgaattgactccggtcaatacac	*MGM1* mutagenesis
MGM1L273PRv	gtgtattgaccggagtcaattcaatgggcgagttagtcttctgtg	*MGM1* mutagenesis
MGM1I322MFw	ggctgtttcagaggagcccatgcaattgacaatcaaatcgttcc	*MGM1* mutagenesis
MGM1I322MRv	ggaacgatttgattgtcaattgcatgggctcctctgaaacagcc	*MGM1* mutagenesis
CYC1TATAFw	ctgtatgtatataaaactcttgtt	*CHIM3* mutagenesis
OPA1R290QFw	cgcaagatcatctgccacaggttgttggttggagatcagag	*CHIM3* mutagenesis
OPA1R290QRv	ctctgatctccaaccacaacaacctgtggcagatgatcttgcg	*CHIM3* mutagenesis
OPA1S298NFw	gttgtggttggagatcagaatgctggaaagactagtgtgttg	*CHIM3* mutagenesis

OPA1S298NRv	caacacactagtctttccagcattctgatctccaaccacaac	*CHIM3* mutagenesis
OPA1G300EFw	ggttggagatcagagtgctgaaaagactagtgtgttggaaatg	*CHIM3* mutagenesis
OPA1L331PFw	cgttctccagttaaggtgactccgagtgaaggtcctcaccatg	*CHIM3* mutagenesis
OPA1L331PRv	catggtgaggaccttcactcggagtcaccttaactggagaacg	*CHIM3* mutagenesis
OPA1A357TPFw	cttaccaaagaagaagatttgacagcattaagacatgaaatagaac	*CHIM3* mutagenesis
OPA1A357TPRv	gttctatttcatgtcttaatgctgtcaaatcttcttctttggtaag	*CHIM3* mutagenesis
OPA1I382MFw	ccgttagccctgagaccatgtccttaaatgtaaaaggccctg	*CHIM3* mutagenesis
OPA1I382MRv	cagggccttttacatttaaggacatggtctcagggctaacgg	*CHIM3* mutagenesis
OPA1D438APFw	ccatcatactgtgtattcaagctggttctgtggatgctgaacg	*CHIM3* mutagenesis
OPA1D438APRv	cgttcagcatccacagaaccagcttgaatacacagtatgatgg	*CHIM3* mutagenesis
OPA1R445HFw	gatggatctgtggatgctgaacactcgattgttacagacttggtc	*CHIM3* mutagenesis
OPA1R445HRv	gaccaagtctgtaacaatcgagtgttcagcatccacagatccatc	*CHIM3* mutagenesis
OPA1T449PFw	gctgaacgcagtattgttccagacttggtcagtcaaatggacc	*CHIM3* mutagenesis
OPA1T449PRv	ggtccatttgactgaccaagtctggaacaatactgcgttcagc	*CHIM3* mutagenesis

OPA1T449XFw	gctgaacgcagtattgttatagtgatggtcagtcaaatggacc	*CHIM3* mutagenesis
OPA1T449XRv	ggtccatttgactgaccatcactataacaatactgcgttcagc	*CHIM3* mutagenesis
OPA1K468EFw	gaaccatattcgttttgaccgaagtcgacctggcagagaaaaatg	*CHIM3* mutagenesis
OPA1K468ERv	cattttttctctgccaggtcgacttcggtcaaaacgaatatggttc	*CHIM3* mutagenesis
OPA1S545RFw	cacaccaagtgactacaagaaatttaaggcttgcagtatcagac	*CHIM3* mutagenesis
OPA1S545RRv	gtctgatactgcaagccttaaatttcttgtagtcacttggtgtg	*CHIM3* mutagenesis
OPA1L593PFw	gaacttgaccggaatgaaccattcgaaaaagctaaaaatg	*CHIM3* mutagenesis
OPA1L593PRv	cattttttagctttttcgaatggttcattccggtcaagttc	*CHIM3* mutagenesis
OPA1D603Hw	gaaaaagctaaaaatgaaatcttgcatgaagttatcagtctgagcc	*CHIM3* mutagenesis
OPA1D603HRv	ggctcagactgataacttcatgcaagatttcatttttagctttttc	*CHIM3* mutagenesis
OPA1S646LFw	ccagctgcgcagaccatgaatttaggaacttttaacaccacag	*CHIM3* mutagenesis
OPA1S646LRv	ctgtggtgttaaaagttcctaaattcatggtctgcgcagctgg	*CHIM3* mutagenesis
OPA1Q785RFw	ggaagaatcggacccaagaaaggtgtgttcacaatgaaacc	*CHIM3* mutagenesis

OPA1Q785RRv	ggtttcattgtgaacacacctttcttgggtccgattcttcc	*CHIM3* mutagenesis
OPA1V903XFw	gcaacaacttacaaatactgaatgatagcgattagagaaaaatgtt	*CHIM3* mutagenesis
OPA1V903XRv	aacatttttctctaatcgctatcattcagtatttgtaagttgttgc	*CHIM3* mutagenesis
OPA1V910DFw	ggcgattagagaaaaatgataaagaggtattggaagattttgc	*CHIM3* mutagenesis
qMGM1Fw	tttaggtgaatcgatgaaggaa	RT-qPCR on *MGM1* and *CHIM3*
qMGM1Rv	gtagcagttggcaccgttc	RT-qPCR on *MGM1* and *CHIM3*
q1OPA1Fw	ggaggacagcttgagggtta	RT-qPCR on *CHIM3*
q1OPA1Rv	tgcagagcctcttccataaa	RT-qPCR on *CHIM3*
q2OPA1Fw	ggaatgcaatgatgtggtct	RT-qPCR on *CHIM3*
q2OPA1Rv	ttcagtatttgtaagttgttgcctt	RT-qPCR on *CHIM3*
ACT1qFw	gtatgtgtaaagccggttttg	qPCR on *ACT1*
ACT1qRv	catgataccttggtgtcttgg	qPCR on *ACT1*
COX1qFw	ctacagatacagcatttccaaga	qPCR on *COX1*
COX1qRv	gtgcctgaatagatgataatggt	qPCR on *COX1*

1.6. Sequencing

Sequencing of all genes was performed with external services (©Eurofins-MWG). The primers used for the sequencing are reported in Table 1.7.

1.7. Nucleid Acid Manipulation

All the manipulations were carried out with standard techniques (Maniatis et al., 1982). Genomic DNA from *S. cerevisiae* was extracted as previously described (Hoffman and Winston, 1987; Lõoke et al. 2011). Plasmid DNA was extracted from *E. coli* with Wizard® Plus SV Minipreps, Wizard® Plus Minipreps (Promega©) or following standard procedures (Sambrook and Russel, 2001). DNA recovery from agarose gel and purification of PCR products were carried out with GenElute™ PCR-Clean Up kit (Sigma-Aldrich®) commercial kit. Enzymatic manipulations (restriction, ligation, dephosphorylation) were carried out following manufacturer indications (New England Biolabs® Inc. NEB, Invitrogen™).

1.8. Transformation procedures

1.8.1. *S. cerevisiae* transformation

Yeast transformation was carried out with Lithium Acetate (LiAc) as described by Gietz et al. If a greater efficiency was desired, the long protocol was applied (Gietz and Woods. 2002).

1.8.2. *E. coli* transformation

E. coli transformation was achieved with electroporation. Competent cells were prepared as previously described (Dower et al. 1988). Transformation was carried out with 1-3 µl of plasmid DNA or ligation product. 2 mm cuvettes were used, applying respectively a current of 2KV, 25 µF 200 Ω. Alternatively, $CaCl_2$ competent cells were prepared and transformed with standard techniques (Maniatis et al., 1982).

1.9. Analyses in whole cell

1.9.1. Spot assay

Spot assay is a classical phenotypic analysis used to test growth of single strains in different conditions. The principle is a 10-fold serial dilution of a starting culture at $1x10^7$ cells/ml, performed four times to a final $1x10^4$ cells/ml. After an o/n culture at 28 °C in SC or YNB medium (enriched with drop out powder), the OD 600 was measured for each strain. A first dilution was made to dilute each strain to a concentration of 1 OD ($1x10^7$) except for diploid strains that were diluted to an initial concentration of 5OD ($5x10^7$). Then three 10-fold serial dilutions were made. From these suspensions 5µl were spotted in ordered rows on agar plates and then incubated for several days.

1.9.2. Cytochrome spectra absorption

(Ferrero et al., 1981)

Mitochondrial respiratory chain intactness can be assessed easily recording the cytochromes absorption profile on whole cells. All the experiments were carried out with a Cary 300Scan UV-vis spectrophotometer (Varian Inc.), recording continuously from 630 to 540nm. Strains were pre-grown in YP supplemented with 2% ethanol to counter select *petite* cells. The following general protocol was used:

1. 2. Inoculate 2.5ml in 100ml of YPD 0.6% or YNBD+DO-Trp and incubate 24hrs at 28°C or 37°C.
2. After checking that glucose is finished (to be sure that any repression is affecting the cells) harvest cells centrifuging 5000rpm 10 minutes, 4˚C.
3. Resuspend the cells in water proportionally to their humid wet (to normalize concentration among different strains).
4. Register the spectra oxidized versus reduced.

Raw data were processed using Excel functions (Microsoft® Office). Wild-type strain was included in each analysis.

1.9.3. Oxygen consumption

(Ferrero et al., 1981)

To measure the respiratory activity, strains were pre-grown in YP supplemented with 2% ethanol to counter select *petite* cells. Cells were inoculated at a final concentration of 0.08 OD/ml in SC supplemented with 0.5% glucose and grown until glucose was exhausted for approximately 16–18 h. The oxygen consumption rate was measured on whole cells at 30°C using a Clark-type oxygen electrode (Oxygraph System Hansatech Instruments England) with 1 ml of air-saturated respiration buffer (0.1 M phthalate–KOH, pH 5.0), 10 mM glucose. The reaction started by addition of 20 mg of wet-weight cells, as described previously (Goffrini et al., 2009: Panizza et al., 2013). Statistical analysis was performed through a paired two-tailed t-test. Oxygen consumption rate was expressed as nmol O_2 for minute for mg of cells (nmolO_2/min mg).

1.9.4. Plasmid shuffling

Haploid and diploid strains which contained pFL38*MGM1* plasmid and pFL39 plasmid carrying a mutant allele, and in which the chromosomal copy of the *MGM1* gene has been disrupted, underwent *plasmid shuffling* on 5-FOA medium to counter-select pFL38*MGM1* plasmid. Haploid cells were grown in YNBD+DO-Trp solid medium for 24h in order to counter-select pFL38*MGM1* plasmid. Then the plate was replica-plated twice on 5-FOA medium and finally on YNBD+DO-Trp. Since 5-FOA is toxic in the presence of the genic product of *URA3* gene, if the mutated allele on pFL39 plasmid was completely functional the pFL38*MGM1* plasmid could be lost without preventing growth of the strain, which would appear to be 5-FOA resistant. On the other hand, if the mutated allele on pFL39 plasmid was completely non-functional the strain would not grow on 5-FOA medium. The same procedure was followed for diploid strain which were grown on YNBD+DO-Trp-Leu.

1.9.5. Crude total protein extraction

Cells were pre-grown for 24h on SC medium supplemented with 0.6% glucose and then were inoculated in SC medium supplemented with 0.2% glucose and 2% galactose until an OD/ml = 1.5-2 was reached. Galactose was chosen as carbon source since it does not inhibit mitochondrial function and minimizes the presence of *petite* cells (galactose does not allow the growth on SC medium of *petite* cells, whose frequency was lower than 3%). The following protocol was used:

1. Grow cells overnight to 0.6-2 OD
2. Harvest the equivalent of 3.6 OD (for haploid strains) and 4.8 OD (for diploid strains) of cells by centrifugation 1 min 6000-8000 rpm.
3. Wash once with water and resuspend the pellet in 75 µl of Rodel mix (see below)
4. Add 500 µl of water
5. Add 575 µl of TCA50%
6. Incubate on ice for 30 minutes. Centrifuge 15000 rpm 10min at 4°C.
7. Wash pellet once with 0.5M Tris-base without resuspending (about 1 ml)
8. Wash pellet once with water without resuspending (about 1 ml)
9. Resuspend in 1X Laemmli Buffer (15-20 µl every 1.2 OD) and add 3 µl of Tris-base 0.5M if the color is yellowish

Rodel Mix: NaOH 1.85 M, β-mercaptoethanol 7.5%, PMSF 0.1 M

Laemmli Buffer: Tris-HCl pH 6.8 33.5 mM, 5% glycerol, 5% β-mercaptoethanol, 2% SDS, Bromophenol blue.

1.9.6. Protein separation with SDS-page

Protein separation with SDS-page was performed with classical Laemmli system (Laemmli, 1970). Separating gels were prepared at 8% polyacrylamide, stacking gels at 4%.

SOLUTION	Separating gel 8% (7.5ml)	Stacking gel 4% (3ml)
Tris HCL 1M pH 8.8	2.81 ml	-
Tris HCL 1M pH 6.8	-	0.75 ml
Polyacrylamide-bis (37.5-1)	1.5 ml	300 µl
SDS 20%	37.5 µl	15 µl
APS 10%	37.5 µl	15 µl
TEMED	3.75 µl	3 µl
H_2O	3.11 ml	1.92 ml

Running Buffer 5X for 1 liter: 15 g Tris-Base, 72 g glycine, H_2O to final volume. Diluite to 1X and add 0.5% SDS 20%. Running was performed for 1h 30'-2h at 100-120 Volts.

1.9.7. Western Blotting and Ig-detection

Separated proteins were transferred to nitrocellulose membranes by electro-blot for 1hr 40' at 2.5-3mA/cm^2 in PerfectBlue™ Semi-Dry ElectroBlotter (PeqLab). Transfer buffer (see below) was used.

Transfer Buffer: 200mM glycine, 25 mM Tris, 20% methanol

After semi-dry blotting membranes were blocked 1hr at RT with 5% non-fat dry milk prepared in washing buffer (see below) and then incubated o/n with appropriate primary antibody (mono or polyclonal, 5% non-fat dry milk prepared in washing buffer) at 4°C.

Washing Buffer: TBS 1%, tween 0.1%

Blocked membranes were washed 3 times 10 min with washing buffer prior incubation with suitable secondary antibodies (Anti-mouse), conjugated with horseradish peroxidase (1:5000 in 5% milk if anti-mouse Ig).

After 2hr incubation membranes were washed as above and developed with Clarity^{TM} Western ECL Substrate (BIO-RAD) commercial kit.

Primary antibodies	Secondary antibodies
anti-Opa1 1:2500 (BD Biosciences)	anti-mouse 1:5000 (Millipore)
anti α-porin 1:5000 (Abcam Mitoscience)	α-mouse 1:5000 (Millipore)

1.9.8. Mitochondrial morphology and fluorescence microscopy

Strains carrying wild-type *MGM1*, *CHIM3* or *chim3* mutant alleles were transformed with pYEF1mtGFP (Rinaldi et al., 2008, a kind gift from Agnes Delahodde). Cells were pre-grown in SC medium supplemented with 0.5% glucose. After 24 h, the cells were transferred to SC medium supplemented with 0.15% glucose and 2% galactose in order to induce the expression of mtGFP, until the mid-log phase was reached. Once adjusted to 0.4 OD/ml, the cells were observed with a Zeiss Observer 2.1 microscope using a 630X magnification and captured using an AxioVision Rel 4.8 software.

1.10. Mutational rate analysis: *petite* frequency determination

mtDNA stability was evaluated by the frequency of spontaneous cytoplasmic *petite*. They grow as small colonies on medium supplemented with respiratory carbon sources such as ethanol and glycerol. The protocol is the following:

1. The pre-existing petite were counter-selected on YNB+DO-Trp medium supplemented with 2% ethanol.

2. Replicate the YNB+DO-Trp 2% ethanol plates on selectable medium supplemented with 2% glucose. The strains were grown for 24h at 28°C or at 37°C.

3. Replicate on a new plate of the same medium and incubate again for 24h.

4. Resuspend a part of cells in H_2O and evaluate the cellular concentration.

5. Plate about 250 cells on YNB+DO-Trp medium supplemented with 0.4% glucose and 2% ethanol. Incubate at 28°C for 5-6 days and count the cells.

0.4% glucose is added in order to allow the growth of *petite* mutants which are respiratory deficient and are unable to use ethanol like the "wild-type" cells. When glucose is exhausted the wild-type cells uses ethanol to grow, while the *petite* mutants arrest their growth. Indeed the *petite* mutants will form small colonies unlike the big colonies formed by wild-type cells.

1.11. Analysis in mitochondria

1.11.1. Preparation of a mitochondrial enriched fraction

(Soto et al., 2009)

Cells were pre-grown on SC medium supplemented with 2% glucose were inoculated in SC medium supplemented with 0.15% glucose and 2% galactose until an OD/ml = 1.5-2 was reached. Galactose was chosen as carbon source since it does not inhibit mitochondrial function and minimizes the presence of petite cells (galactose does not allow the growth on SC medium of petite cells, whose frequency was lower than 3%).

The following protocol was used:

1. Harvest 20-40 ml of cells at about 2 OD
2. Spin at 4000-5000 rpm for 5 min
3. Resuspend pellet in 25 ml of H_20 and spin at 4000-5000 rpm for 3 min
4. Resuspend pellet in 1 ml of H_20 and transfer cells to eppendorf tubes. Centrifuge at 7000 rpm for 30 sec and get rid of the supernatant.
5. Resuspend pellet in 400 µl of sorbitol 0.6M and DTT 5mM and store at RT for 10 min
6. Centrifuge at 7000 rpm for 30 sec and get rid of the supernatant

7. Resuspend pellet in 400 µl of sorbitol 1.2M and Tris-HCl 10mM pH 7.5 and zymolyase 5mg/ml
8. Incubate at RT for 10-40 min until 80-90% of the cells have been converted to spheroplasts
9. Work on ice. Centrifuge at 5400 g for 8 min at 4°C and get rid of the supernatant
10. Wash pellet twice with 1 ml of STE solution (sorbitol 0.6M, Tris-HCl 20mM pH 7.5, EDTA 1mM). Centrifuge at 5400 g for 5 min at 4°C.
11. Suspend pellet in 100-200 µl STE solution accordingly to the pellet
12. Freeze at -80°C and defrost at RT three times (10 min freeze + 10 min defrost)
13. Determine protein concentration

1.11.2. Quantification of proteins with Bradford method

Protein concentration was determined with Bradford method (Bradford, 1976). The "BioRad Protein Assay" commercial kit was utilized according to the manufacturer's instructions.

1.11.3. Succinate Dehydrogenase (SQDR) enzymatic activity

This assay measures the rate of reduction of an artificial electron acceptor as dichlorophenolindophenol (DCPIP) by complex II as modified by Kim and Beattie, 1973. Mitochondria were prepared as described in section 1.11.1.

Solutions needed:

- 10 mM K-phosphate pH 7.8 + EDTA 2mM
- 80mM KCN
- 10mM succinate pH 7.4
- 20mM DCPIP
- 100mM NaN_3

- 50mM ATP
- 1% Na-DOC
- 20mM dUQ_2

The SDH activity was recorded at 600nm on 4 mg/ml mitochondrial aliquots. Specific activity: SQDR activity was calculated with ε of 22 and the following formula (ΔOD*ε/min mg).

1.11.4. Cytochrome c oxidase (COX) enzymatic activity

This assay measures the rate of cytochrome c oxidation by complex IV in yeast as described by Warthon and Tzagaloff, 1967. Mitochondria were prepared as described in section 1.11.1.

Solutions needed:

- 20mM K-phosphate pH 7.5
- 1% cytochrome c in 20mM K-phosphate pH 7.5
- 1% Na-DOC
- $KFeCN_3$

COX activity was recorded at 550 nm on 2 mg/ml mitochondrial aliquots. Specific Activity: COX activity was calculated with ε of 18.5 and the following formula [2.3log (A_1/A_2)/ (ε*min*mg)]*ΔOD.

1.11.5. NADH Cytochrome c Reductase (NCCR) enzymatic activity

This assay measures the combined activity of NADH dehydrogenase and complex III in yeast. Electron flux is from NADH-DH to complex III *via* ubiquinol to the final acceptor cytochrome c. Mitochondria were prepared as described in section 1.11.1.

Solution needed:

- 10mM K-phosphate pH 7.5
- 80mM KCN
- 1% cytochrome c (bovine or horse heart, in K-phosphate pH 7.5 buffer)
- 0.1M NADH in K-phosphate pH 7.5

- 1% Na-DOC

NCCR activity is registered at 550nm on 2mg/ml mitochondrial aliquots. Specific activity is calculated with cytochrome c ε of 18.5 and the following formula (ΔOD*ε/min mg).

1.12. High throughput screening: Drug drop test (Couplan et al., 2011)

Cells were inoculated in YP medium + 2% ethanol and incubated at 28°C in constant shaking. 12x12 plates were filled with 90 ml of YP solid medium supplemented with i) 2% ethanol and 0.5X streptomycin-ampicillin in the case of *mgm1*^{I322M} mutant; ii) with 2% glycerol and 0.5X streptomycin-ampicillin or iii) 2% ethanol + 0.5% glycerol and 0.5X streptomycin-ampicillin for *chim3*^{S646L} mutant. After 2 days of growth 6x10^5 (*mgm1*^{I322M}) or 2x10^5 (*chim3*^{S646L}) cells are seeded onto the plates. After the seed, filters of 6 mm of diameter were put on the agar surface and spotted with the compound to test, varying the quantity both of the filters and the molecule depending on primary or secondary screening. As positive control MRS4 15mM (*mgm1*^{I322M}, *chim3*^{S646L}) and MRS5 2mM (*chim3*^{S646L}) were used. DMSO was used as negative control. Plates were incubated at 36.5°C (*mgm1*^{I322M}, *chim3*^{S646L}) or 37°C (*chim3*^{S646L}) for 7 days and the growth of the mutant strain was monitored. For tertiary screening the procedure was the same, except for the W303-1B rho^0 strain, which was inoculated in YP medium supplemented with 2% glucose at 28°C in constant shaking the day before the test.

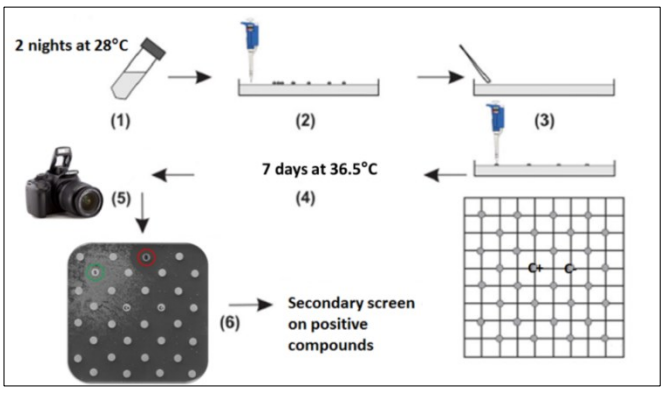

Figure 1.8. Schematic representation of Drug drop test. From Couplan et al., 2011.

References

Abou-Sleiman P.M., Muqit M.M., Wood N.W., 2006. Expanding insights of mitochondrial dysfunction in Parkinson's disease. *Nat. Rev. Neurosci.*, 7, 207-19.

Ackerman S.H. and Tzagoloff A., 2005. Function, structure, and biogenesis of mitochondrial ATP synthase. *Progress in nucleic acid research and molecular biology*, 80, 95–133.

Alexander C., Votruba M., Pesch U.E., Thiselton D.L., Mayer S., Moore A., Rodriguez M., Kellner U., Leo-Kottler B., Auburger G., Bhattacharya S.S., Wissinger B., 2000. OPA1, encoding a dynamin-related GTPase, is mutated in autosomal dominant optic atrophy linked to chromosome 3q28. *Nat. Genet.*, 26, 211-215.

Almind G.J., Ek J., Rosenberg T., Eiberg H., Larsen M., Lucamp L., Brøndum-Nielsen K., Grønskov K., 2012. Dominant optic atrophy in Denmark - report of 15 novel mutations in OPA1, using a strategy with a detection rate of 90%. *BMC Med. Genet.*, 13-65.

Amati-Bonneau P., Guichet A., Olichon A., Chevrollier A., Viala F., Miot S., Ayuso C., Odent S., Arrouet C., Verny C., Calmels M.N., Simard G., Belenguer P., Wang J., Puel J.L., Hamel C., Malthiery Y., Bonneau D., Lenaers G., Reynier P., 2005. OPA1 R445H mutation in optic atrophy associated with sensorineural deafness. *Ann. Neurol.*, 58, 958-63.

Amati-Bonneau P., Milea D., Bonneau D., Chevrollier A., Ferré M., Guillet V., Gueguen N., Loiseau D., de Crescenzo M.A., Verny C., Procaccio V., Lenaers G., Reynier P., 2009. OPA1-associated disorders: phenotypes and pathophysiology. *Int. J. Biochem. Cell Biol.*, 41, 1855-65.

Amati-Bonneau P., Odent S., Derrien C., Pasquier L., Malthiery Y., Reynier P., Bonneau D., 2003. The association of autosomal dominant optic atrophy and moderate deafness may be due to the R445H mutation in the OPA1 gene. *Am. J. Ophthalmol.*, 136, 1170-71.

Amati-Bonneau P., Valentino M.L., Reynier P., Gallardo M.E., Bornstein B., Boissière A., Campos Y., Rivera H., de la Aleja J.G., Carroccia R., Iommarini L., Labauge P., Figarella-Branger D., Marcorelles P., Furby A., Beauvais K., Letournel F., Liguori R., La Morgia C., Montagna P., Liguori M., Zanna C., Rugolo M., Cossarizza A., Wissinger B., Verny C., Schwarzenbacher R., Martín M.A., Arenas J., Ayuso C., Garesse R., Lenaers G., Bonneau D., Carelli V., 2008. OPA1 mutations induce mitochondrial DNA instability and optic atrophy 'plus' phenotypes. *Brain*, 131, 338-51.

Amiott E. A., Lott P., Soto J. et al., 2008. Mitochondrial fusion and function in Charcot-Marie-Tooth type 2A patient fibroblasts with mitofusin 2 mutations. *Experimental Neurology*, 211, 115-27.

Anderson S., Bankier A.T., Barrell B.G., de Bruijn M.H., Coulson A.R., Drouin J., Eperon I.C., Nierlich D.P., Roe B.A., Sanger F., Schreier P.H., Smith A.J., Staden R., Young I.G., 1981. Sequence and organization of the human mitochondrial genome. *Nature*, 290(5806), 457–65.

Andrews R.M., Griffiths P.G., Johnson M.A., Turnbull D.M., 1999. Histochemical localisation of mitochondrial enzyme activity in human optic nerve and retina. *Br. J. Ophthalmol.*, 83, 231-35.

Armstrong J.W., 1999. A review of high-throughput screening approaches for drug discovery. *Thousand Oaks, CA: HTS Consulting Ltd.,* 19-33.

Ausubel F.M., Brent R., Kingston R.E., Moore D.D., Seidman J.G., Smith J.A., Struhl K., 1994. *Current Protocols in Molecular Biology*. Wiley, New York.

Bach S., Talarek N., Andrieu T., Vierfond J-M., Mettey Y., Galons H., Dormont D., Meijer L., Cullin C., Blondel M., 2003. Isolation of drugs active against mammalian prions using a yeast-based screening assay. *Nature biotechnology*, 21, 1075-81.

Baile M.G. and Claypool S.M., 2013. The power of yeast to model diseases of the powerhouse of the cell. *Front. Biosci.*, 18, 241-78.

Barberis A., Gunde T., Berset C., Audetat S., Luthi U., 2005. Yeast as a screening tool. *Drug Discovery Today: Technologies.*, 2, 2187-92.

Barrientos A., 2003. Yeast models of human mitochondrial diseases. *Life*, 55, 83-95.

Baruffini E., Ferrari J., Dallabona C., Donnini C., Lodi T., 2015. Polymorphisms in DNA polymerase γ affect the mtDNA stability and the NRTI-induced mitochondrial toxicity in Saccharomyces cerevisiae. *Mitochondrion*, 20, 52-63.

Bassett D.E. Jr, Boguski M.S., Hieter P., 1996. Yeast genes and human disease. *Nature*, 379 589-90.

Beal M.F., 2005. Mitochondria take center stage in aging and neurodegeneration. *Ann. Neurol.*, 58, 495–505.

Behr C., 1909. Die komplizierte, hereditar-familiare optikusatrophie des kindesalters – ein bisher nicht beschriebener symptomkomplex. *Klin. Monatsbl. Augenheilkd.*, 47, 138-60.

Bendich A.J., 1996. Structural analysis of mitochondrial DNA molecules from fungi and plants using moving pictures and pulsed-field gel electrophoresis. *Journal of molecular biology*, 255(4), 564–88.

Bereiter-Hahn J. and Vöth M., 1994. Dynamics of mitochondria in living cells: shape changes, dislocations, fusion, and fission of mitochondria. *Microscopy research and technique*, 27(3), 198–219.

Bleazard W., McCaffery J.M., King E.J., Bale S., Mozdy A., Tieu Q., Nunnari J., Shaw J.M., 1999. The dynamin-related GTPase Dnm1 regulates mitochondrial fission in yeast. *Nat. Cell Biol.*, 1, 298-304.

Boeke J.D., LaCroute F., Fink G.R., 1984. A positive selection for mutants lacking orotidine-5'-phosphate decarboxylase activity in yeast: 5-fluoro-orotic acid resistance. *Mol. Gen. Genet.*, 197, 345-6.

Boldogh I.R., Yang H.C. and Pon L.A., 2001. Mitochondrial Inheritance in Budding Yeast. *Traffic,* 2001 2, 368-374.

Bolotin M., Coen M.D., Deutsch J., Dujon B., Netter P., Petrochilo E. Slonimski P.P., 1971. La recombinaison des mitochondries chez *Saccharomyces cerevisiae*. *Bull. Inst. Pasteur*, 69, 215-39.

Bonifert T., Karle K.N., Tonagel F., Batra M., Wilhelm C., Theurer Y., Schoenfeld C., Kluba T., Kamenisch Y., Carelli V., Wolf J., Gonzalez M.A., Speziani F., Schüle R., Züchner S., Schöls L.,Wissinger B., Synofzik M., 2014. Pure and syndromic optic atrophy explained by deep intronic OPA1 mutations and an intralocus modifier. *Brain*, 137, 164-77.

Bonneaud N., Ozier-Kalogeropoulos O., Li G.Y., Labouesse M., Minvielle-Sebastia L., Lacroute F., 1991. A family of low and high copy replicative, integrative and single-stranded *S. cerevisiae/E. coli* shuttle vectors. *Yeast*, 7, 609-15.

Brachmann C. B., Davies A., Cost G. J., Caputo E. , Li J., Hieter P. and Boeke J. D., 1998. Designer Deletion Strains derived from *Saccharomyces cerevisiae* S288C: a Useful set of Strains and Plasmids for PCR-mediated Gene Disruption and Other Applications. *Yeast*, 14, 115-132.

Bradford M.M., 1976. A rapid and sensitive method for the quantitation of microgram quantities of proteins utilizing the principle of protein dye binding. *Anal. Biochem.*, 72, 248-54.

Carelli V., Sabatelli M., Carrozzo R., Rizza T., Schimpf S.,Wissinger B., Zanna C., Rugolo M., La Morgia C., Caporali L., Carbonelli M., Barboni P., Tonon C., Lodi R., Bertini E., 2015. 'Behr syndrome' with OPA1 compound heterozygote mutations. *Brain*, 138, 1-5.

Carnero A., 2006. High Throughput Screening in drug discovery. *Clinical and Translational Oncology*, 8, 482-90.

Castellani R.J., Rolston R.K., Smith M.A., 2010. Alzheimer disease. *Dis. Mon.*, 56, 484-546.

Cerveny K.L., and Jensen R.E., 2003. The WD-repeats of Net2p interact with Dnm1p and Fis1p to regulate division of mitochondria. *Mol. Biol. Cell*, 14, 4126-39.

Chan D.C., 2012. Fusion and Fission: Interlinked Processes Critical for Mitochondrial Health. *Annu. Rev. Genet.*, 46, 265-287.

Chan N.C., Salazar A.M., Pham A.H., Sweredoski M.J., Kolawa N.J., Graham R.L., Hess S., Chan D.C., 2011. Broad activation of the ubiquitin-proteasome system by Parkin is critical for mitophagy. *Hum. Mol. Genet.*, 20, 1726-37.

Chen H., Detmer S.A., Ewald A.J., Griffin E.E., Fraser S.E., Chan D.C., 2003. Mitofusins Mfn1 and Mfn2 coordinately regulate mitochondrial fusion and are essential for embryonic development. *J. Cell Biol.*,160, 189-200.

Chen X.J. and Butow R., 2005. The organization and inheritance of the mitochondrial genome. *Nature reviews*. *Genetics*, 6(11), 815-25.

Chen H. and Chan D.C., 2009. Mitochondrial dynamics–fusion, fission, movement, and mitophagy in neurodegenerative diseases. *Hum. Mol. Genet.*, 18, 169-76.

Chen H., Chomyn A., Chan C., 2005. Disruption of fusion results in mitochondrial heterogeneity and dysfunction. *J. Biol. Chem.*, 280, 26185-92.

Chen H., Chomyn A., Chan D.C., 2005. Disruption of fusion results in mitochondrial heterogeneity and dysfunction. *J. Biol. Chem.*, 280, 26185-92.

Chen H., McCaffery J.M., Chan D.C., 2007. Mitochondrial fusion protects against neurodegeneration in the cerebellum. *Cell*, 130, 548–562.

Chen H., Vermulst M., Wang Y.E., Chomyn A., Prolla T.A., McCaffery J.M., Chan D.C., 2010. Mitochondrial fusion is required for mtDNA stability in skeletal muscle and tolerance of mtDNA mutations. *Cell*, 141, 280-9.

Chen H., Vermulst M., Wang Y.E., Chomyn A., Prolla T.A., McCaffery J.M., Chan D.C., 2010. Mitochondrial fusion is requiredfor mtDNA stability in skeletal muscle and tolerance of mtDNA mutations. *Cell*, 141, 280-89.

Chen X. J., Wang X., Kaufman B. A. and Butow R. A. 2005. Aconitase couples metabolic regulation to mitochondrial DNA maintenance. *Science,* 307, 714-717.

Cipolat S., de Brito O.M., Dal Zilio B., Scorrano L., 2004. OPA1 requires mitofusin 1 to promote mitochondrial fusion. *Proc. Natl. Acad. Sci.*, 101, 15927-32.

Costeff H., Gadoth N., Apter N., Prialnic M., Savir H., 1989. A familial syndrome of infantile optic atrophy,movement disorder, and spastic paraplegia. *Neurology*, 39, 595-97.

Couplan E., Aiyar R.S., Kucharczyk R., Kabala A., Ezkurdia N., Gagneur J., St. Onge R.P., Sali B., Soubigou F., Le Cann M., Steinmetz L.M., di Rago J-P., Blondel M., 2011. A yeast-based assay identifies drugs active against human mitochondrial disorders. *Proceedings of the National Academy of Sciences of the United States of America*, 108, 11989-94.

de Brito O.M. and Scorrano L., 2008. Mitofusin 2 tethers endoplasmic reticulum to mitochondria. *Nature*., 456, 605-610.

Delettre C., Griffoin J.M., Kaplan J., Dollfus H., Lorenz B., Faivre L., Lenaers G., Belenguer P., Hamel C.P., 2001. Mutation spectrum and splicing variants in the OPA1 gene. *Hum. Genet.*, 109, 584-591.

Deng H., Dodson M.W., Huang H., Guo M., 2008. The Parkinson's disease genes *pink1* and *parkin* promotemitochondrial fission and/or inhibit fusion in *Drosophila*. *Proc. Natl. Acad. Sci.*, 105, 14503-8.

Detmer S. A. and D. C. Chan, 2007. Complementation between mouse Mfn1 and Mfn2 protects mitochondrial fusion defects caused by CMT2A disease mutations. *Journal of Cell Biology*, 176, 405-14.

Detmer S.A. and Chan D.C., 2007. Functions and dysfunctions of mitochondrial dynamics. *Nat. Rev. Mol. Cell Biol.*, 8, 870-79.

DeVay R.M., Dominguez-Ramirez L., Lackner L.L., Hoppins S., Stahlberg H., Nunnari J., 2009. Coassembly of Mgm1 isoforms requires cardiolipin and mediates mitochondrial inner membrane fusion. *J. Cell Biol.*,186, 793-803.

DiMauro S. and Schon E.A., 2003. Mitochondrial respiratory-chain diseases. *The New England journal of medicine*, 348(26), 2656-68.

Dimmer K.S., Fritz S., Fuchs F., Messerschmitt M.,Weinbach N., et al. 2002. Genetic basis of mitochondrial function and morphology in Saccharomyces cerevisiae. *Mol. Biol. Cell* 13, 847-53.

Dower W. J., Miller J. F., Ragsdale C. W., 1988. High efficiency transformation of *E. coli* by high voltage electroporation. *Nucleic Acids Res.*, 16, 6127-45

Dujon B., 1981. Molecular biology of the yeast Saccharomyces: life cycle and inheritance. *In C S. Harbor, ed. Mitochondrial genetics and functions*, 505-635.

Duvezin-Caubet S., Koppen M., Wagener J., Zick M., Israel L., Bernacchia A., Jagasia R., Rugarli E.I., Imhof A., Neupert W., Langer T., Reichert A.S., 2007. OPA1 processing reconstituted in yeast depends on the subunit composition of the m-AAA protease in mitochondria. *Mol. Biol. Cell*, 18, 3582-90.

Elachouri G., Vidoni S., Zanna C., Pattyn A., Boukhaddaoui H., Gaget K., Yu-Wai-Man P., Gasparre G., Sarzi E., Delettre C., Olichon A., Loiseau D., Reynier P., Chinnery P.F., Rotig A., Carelli V., Hamel C.P., Rugolo M., Lenaers G., 2011. OPA1 links human mitochondrial genome maintenance to mtDNA replication and distribution, *Genome Res.*, 21, 12–20.

Elgass K., Pakay J., Ryan M.T., Palmer C.S., 2013. Recent advances into the understanding of mitochondrial fission. *Biochimica et Biophysica Acta*, 1833, 150-61.

Eura Y., Ishihara N., Yokota S., Mihara K., 2003. Two mitofusin proteins, mammalian homologues of FZO, with distinct functions are both required for mitochondrial fusion. *J. Biochem.*, 134, 333-44.

Ferré M., Bonneau D., Milea D., Chevrollier A., Verny C., Dollfus H., Ayuso C., Defoort S., Vignal C., Zanlonghi X., Charlin J.F., Kaplan J., Odent S., Hamel C.P., Vincent Procaccio V., Reynier P., Amati-Bonneau P., 2009. Molecular screening of 980 cases of suspected hereditary optic neuropathy with a report on 77 Novel OPA1 Mutations. *Human Mutation*, 30, 692-705.

Ferrero I., Viola A.M., Goffeau A., 1981. Induction by glucose of an antimycin-insensitive, azide-sensitive respiration in the yeast Kluyveromyces lactis. *Antonie Van Leeuwenhoek*, 47, 11-24.

Foury F., Roganti T., Lecrenier N. and Purnelle B., 1998. The complete sequence of the mitochondrial genome of *Saccharomyces cerevisiae*. *FEBS Lett.* 440, 325-331.

Fox T.D., Sanford J.C., McMullin T.W., 1988. Plasmids can stably transform yeast mitochondria lacking endogenous mtDNA. *P. Natl. Acad. Sci. USA*, 85, 7288-92.

Frezza C., Cipolat S., de Brito O.M., Micaroni M., Beznoussenko G.V., Rudka T., Bartoli D., Polishuck R.S., Danial N.N., De Strooper, Scorrano L., 2006. OPA1 controls apoptotic cristae remodeling independently from mitochondrial fusion. *B. Cell*, 126, 177-189.

Friddle R.W., Klare J.E., Martin S.S., Corzett M., Balhorn R., Baldwin E.P., Baskin R.J., Noy A., 2004. Mechanism of DNA compaction by yeast mitochondrial protein Abf2p. *Biophysical journal*, 86, 1632-9.

Fritz S., Rapaport D., Klanner E., Neupert W., Westermann B., 2001. Connection of the mitochondrial outer and inner membranes by Fzo1 is critical for organellar fusion. *J. Cell Biol.*, 152, 683-92.

Futai M., Noumi T., Maeda M., 1989. ATP synthase (H+-ATPase): results by combined biochemical and molecular biological approaches. *Annu. Rev. Biochem*. 58, 111-136.

Garí E., Piedrafita L., Aldea M., Herrero E., 1997. A set of vectors with a tetracycline-regulatable promoter system for modulated gene expression in Saccharomyces cerevisiae. *Yeast*, 13, 837-48.

Gegg M.E., Cooper J.M., Chau K.Y., Rojo M., Schapira A.H., Taanman J.W., 2010. Mitofusin 1 and mitofusin 2 are ubiquitinated in a PINK1/Parkin-dependent manner upon induction of mitophagy. *Hum. Mol. Genet.*, 19, 4861-70.

Gietz R. D. and Sugino A., 1988. New yeast-Escherichia coli shuttle vectors constructed with in vitro mutagenized yeast genes lacking six-base pair restriction sites. *Gene*, 74, 527-34.

Gietz R.D. and Wood R.A., 2002. Transformation of yeast by the LiAc/SS carrier DNA/peg method. *Methods Enzymol*., 350, 87-96.

Glater E. E., Megeath L. J., Stowers R. S., Schwarz T. L., 2006. Axonal transport of mitochondria requires Milton to recruit kinesin heavy chain and is light chain independent. *J. Cell Biol.*, 173, 545-57.

Goffeau A., Barrell B.G., Bussey H., Davis R.W., Dujon B., Feldman H., Galiber F., Hoheise J.D., Jacq C., Johnston M., Louis E.J., Mewes H.W., Murakami Y., Philippsen P., Tetteli H., Oliver S.G., 1996. Life with 6000 genes. *Science*, 546, 563-7.

Goffrini P., Ercolino T., Panizza E., Giachè V., Cavone L., Chiarugi A., Dima V., Ferrero I., Mannelli M., 2009. Functional study in a yeast model of a novel succinate dehydrogenase subunit B gene germline missense mutation (C191Y) diagnosed in a patient affected by a glomus tumor. *Hum. Mol. Genet.*, 18, 1860-68.

Griffin E.E., Graumann J., Chan D.C., 2005. TheWD40 protein Caf4p is a component of the mitochondrial fission machinery and recruits Dnm1p to mitochondria. *J. Cell Biol.*, 170, 237-48.

Griparic L., Kanazawa T., van der Bliek A.M., 2007. Regulation of the mitochondrial dynamin-like protein Opa1 by proteolytic cleavage. *J. Cell Biol.*, 178, 757-64.

Griparic L., van der Wel N.N., Orozco I.J., Peters P.J., van der Bliek A.M., 2004. Loss of the intermembrane space protein Mgm1/OPA1 induces swelling and localized constrictions along the lengths of mitochondria. *J. Biol. Chem.*, 279, 18792-98.

Guérin B., 1991. Mitochondria. *In the yeasts* Vol.4, 2nd edition, 541-600.

Guillery O., Malka F., Landes T., Guillou E., Blackstone C., Lombes A., Belenguer P., Arnoult D., Rojo M., 2008. Metalloprotease-mediated OPA1 processing is modulated by the mitochondrial membrane potential. *Biol. Cell*, 100, 315-25.

Guo X., Macleod G. T., Wellington A., Hu F., Panchumarthi S., Schoenfield M., Marin L., Charlton M.P., Atwood H.L., Zinsmaier K.E.,.2005. The GTPase dMiro is required for axonal transport of mitochondria to Drosophila synapses. *Neuron*, 47, 379-93.

Haggarty S.J., Mayer T.U., Miyamoto D.T., Fathi R., King R.W., Mitchison T.J., Schreiber S.L.,2000. Dissecting cellular processes using small molecules: identification of colchicine-like, taxol-like and other small molecules that perturb mitosis. *Chem. Biol.*, 7, 275-86.

Hales K.G. and Fuller M.T., 1997. Developmentally regulated mitochondrial fusion mediated by a conserved, novel, predicted GTPase. *Cell*, 90, 121-29.

Herlan M., Bornhövd C., Hell K., Neupert W., Reichert A.S., 2004. Alternative topogenesis of Mgm1 and mitochondrial morphology depend on ATP and a functional import motor. *J. Cell Bio.*, 165, 167-173.

Herlan M., Vogel F., Bornhovd C., Neupert W., Reichert A.S., 2003. Processing of Mgm1 by the rhomboid-type protease Pcp1 is required for maintenance of mitochondrial morphology and of mitochondrial DNA. *J. Biol. Chem.*, 278, 27781-88.

Herrmann J. M. and Neupert W., 2000. Protein transport into mitochondria. *Current opinion in microbiology*, 3, 210-4.

Herrmann J.M., 2011. MINOS is plus: a Mitofilin complex for mitochondrial membrane contacts. *Developmental cell*, 21, 599-600.

Hirai K., Aliev G., Nunomura A., Fujioka H., Russell R.L., Atwood C.S., Johnson A.B., Kress Y., Vinters H.V., Tabaton M., Shimohama S., Cash A.D., Siedlak S.L., Harris P.L., Jones P.K., Petersen R.B., Perry G., Smith M.A., 2001. Mitochondrial abnormalities in Alzheimer's disease. *J. Neurosci.*, 21, 3017-23.

Ho S.N., Hunt H.D., Horton R.M., Pullen J.K., Pease L.R., 1989. Site-directed mutagenesis by overlap extension using the polymerase chain reaction. *Gene*, 77, 51-9.

Hoffman C. S. and Winston F., 1987. A ten-minute DNA preparation from yeast efficiently releases autonomous plasmids for transformation of Escherichia coli. *Gene*, 57, 267-72.

Hudson G., Amati-Bonneau P., Blakely E.L., Stewart J.D., He L., Schaefer A.M., Griffiths P.G., Ahlqvist K., Suomalainen A., Reynier P., McFarland R., Turnbull D.M., Chinnery P.F., Taylor R.W., 2008. Mutation of OPA1 causes dominant optic atrophy with external ophthalmoplegia, ataxia, deafness and multiple mitochondrial DNA deletions: a novel disorder of mtDNA maintenance. *Brain*, 131, 329-37.

Hughes A.J., Daniel S.E., Kilford L., Lees A.J., 1992. Accuracy of clinical diagnosis of idiopathic Parkinson's disease: a clinico-pathological study of 100 cases. *J. Neurol. Neurosurg. Psychiatry*, 55, 181-84.

Hughes T.R., 2002. Yeast and drug discovery. *Funct. Integr. Genomics*, 2, 199-211.

Ishihara N., Eura Y., Mihara K., 2004. Mitofusin 1 and 2 play distinct roles in mitochondrial fusion reactions via GTPase activity. *J.Cell Sci.*, 117, 6535-46.

Ishihara N., Fujita Y., Oka T., Mihara,K. 2006. Regulation of mitochondrial morphology through proteolytic cleavage of OPA1. *EMBO J.*, 25, 2966-77.

Jacobs H T, Lehtinen S.K., Spelbrink J.N., 2000. No sex please: we're mitochondria : an hypothesis on the somatic unit of inheritance of mammalian mtDNA. *BioEssay news and reviews in molecular, cellular and developmental biology*, 22(6), 564-72.

Johnston S.A., Anziano P.Q., Shark K., Sanford J.C., Butow R.A., 1988. Mitochondrial transformation in yeast by bombardment with microprojectiles. *Science*, 240, 1538-41.

Jones B.A. and Fangman W.L., 1992. Mitochondrial DNA maintenance in yeast requires a protein containing a region related to the GTP-binding domain of dynamin. *Genes. Dev.*, 6, 380-9.

Kaiser C., Michaelis S. and Mitchell A., 1994. Methods in Yeast Genetics: a Laboratory Course Manual. *Cold Spring Harbor Laboratory Press*, Cold Spring Harbor, NY.

Kim I., Rodriguez-Enriquez S., Lemasters J.J. 2007. Selective degradation of mitochondria by mitophagy. *Arch. Biochem. Biophys.,* 462, 245-53.

Kim I.C, Beattie D.S., 1973. Formation of the yeast mitochondrial membrane. 1. Effects of inhibitors of protein synthesis on the kinetics of enzyme appearance during glucose derepression. *Eur. J. Biochem.*, 36, 509-18.

Kim J., Moody J.P., Edgerly C.K., Bordiuk O.L., Cormier K., Smith K., Beal M.F., Ferrante R.J., 2010. Mitochondrial loss, dysfunction and altered dynamics in Huntington's disease. *Hum. Mol. Genet.*, 19, 3919-35.

Kjer P., 1959. Infantile optic atrophy with dominant mode of inheritance: a clinical and genetic study of 19 Danish families. *Acta Ophthalmol. Suppl.*, 164, 1-147.

Kucej M. Kucejova B., Subramanian R., Chen X.J., Butow R.A., 2008. Mitochondrial nucleoids undergo remodeling in response to metabolic cues. *Journal of cell science*, 121, 1861-8.

Kucej, M. and Butow R., 2007. Evolutionary tinkering with mitochondrial nucleoids. *Trends in cell biology*, 17, 586-92.

Laemmli U.K., 1970. Cleavage of structural proteins during the assembly of the head of bacteriophage T4. *Nature*, 227, 680-5.

Landes T., Emorine L.J., Courilleau D., Rojo M., Belenguer P., Arnaune-Pelloquin L., 2010. The BH3-only Bnip3 binds to the dynamin Opa1 to promote mitochondrial fragmentation and apoptosis by distinct mechanisms. *EMBO*, Rep. 11, 459–465.

Lasserre J.P., Dautant A., Aiyar R.S., Kucharczyk R., Glatigny A., Tribouillard-Tanvier D., Rytka J., Blondel M., Skoczen N., Reynier P., Pitayu L., Rötig A., Delahodde A., Steinmetz L.M., Dujardin G., Procaccio V., di Rago J.P., 2015. Yeast as a system for modeling mitochondrial disease mechanisms and discovering therapies. *Dis. Model Mech.*, 8, 509-26.

Lee Y.J., Jeong S.Y., Karbowski M., Smith C.L., Youle R.J., 2004. Roles of the Mammalian mitochondrial fission and fusion mediators fis1, drp1, and opa1 in apoptosis. *Mol. Biol. Cell*, 15, 5001-11.

Legros F., Lombes A., Frachon P., Rojo M., 2002. Mitochondrial fusion in human cells is efficient, requires the inner membrane potential, and is mediated by mitofusins. *Mol. Biol. Cell*, 13, 4343-54.

Lodi T., Bove C., Fontanesi F., Viola A.M., Ferrero I., 2015. Mutation D104G in ANT1 gene: complementation study in *Saccharomyces cerevisiae* as a model system. *Biochem. Biophys. Res. Commun.*, 341, 810-15.

Lõoke M., Kristjuhan K., Kristjuhan A., 2011. Extraction of genomic DNA from yeasts for PCR-based applications. *Biotechniques*, 50, 325-8.

MacAlpine D.M., Perlman P.S., Butow R., 2000. The numbers of individual mitochondrial DNA molecules and mitochondrial DNA nucleoids in yeast are co-regulated by the general amino acid control pathway. *The EMBO journal*, 19, 767-75.

Mafalda Escobar-Henriques M., Anton F., 2013. Mechanistic perspective of mitochondrial fusion: Tubulation vs. fragmentation. *Biochimica et Biophysica Acta*, 1833, 162-175.

Malka F., Lombès A., Rojo M., 2006. Organization, dynamics and transmission of mitochondrial DNA: focus on vertebrate nucleoids. *Biochimica et biophysica acta*, 1763, 463-72.

Manczak M. and Reddy P.H., 2012. Abnormal interaction between the mitochondrial fission protein Drp1 and hyperphosphorylated tau in Alzheimer's disease neurons: implications for mitochondrial dysfunction and neuronal damage. *Hum. Mol. Genet.*, 21, 2538-47.

Manczak M., Calkins M.J., Reddy P.H., 2011. Impaired mitochondrial dynamics and abnormal interaction of amyloid beta with mitochondrial protein Drp1 in neurons from patients with Alzheimer's disease: implications for neuronal damage. *Hum. Mol. Genet.*, 20, 2495-2509.

Maniatis T., Fritsch E., Sambrook J., 1982. Molecular cloning. A laboratory manual. *Cold Spring Harbor Laboratory Press*, Cold Spring Harbor, NY.

Margulis L. and Bermudes D., 1985. Symbiosis as a mechanism of evolution: status of cell symbiosis theory. *Symbiosis (Philadelphia, Pa.)*, 1, 101-24.

Margulis L., 1975. Symbiotic theory of the origin of eukaryotic organelles; criteria for proof. *Symposia of the Society for Experimental Biology*, 29, 21-38.

Marks B., Stowell M.H., Vallis Y., Mills I.G., Gibson A., Hopkins C.R., McMahon H.T., 2001. GTPase activity of dynamin and resulting conformation change are essential for endocytosis. *Nature*, 410, 231-5.

Mayer T.U., Kapoor T.M., Haggarty S.J., King R.W., Schreiber S.L., Mitchison T.J., 1999. Small molecule inhibitor of mitotic spindle bipolarity identified in a phenotype-based screen. *Science*, 286, 971-4.

McBride H.M., Neuspiel M., Wasiak S., 2006. Mitochondria: more than just a powerhouse. *Current biology*, 16, 551-60.

Mckenzie M. and Ryan M.T., 2010. Assembly factors of human mitochondrial complex I and their defects in disease. *IUBMB life*, 62, 497-502.

McQuibban G.A., Saurya S., Freeman M., 2003. Mitochondrial membrane remodeling regulated by a conserved rhomboid protease. *Nature*, 423, 537-41.

Meeusen S., DeVay R., Block J., Cassidy-Stone A., Wayson S., McCaffery J.M., Nunnari J., 2006. Mitochondrial innermembrane fusion and crista maintenance requires the dynamin related GTPase Mgm1. *Cell*, 127, 383-95.

Merkwirth C., Dargazanli S., Tatsuta T., Geimer S., Lower B., Wunderlich F.T., von Kleist-Retzow J.C., Waisman A., Westermann B., Langer T., 2008. Prohibitins control cell proliferation and apoptosis by regulating OPA1-dependent cristae morphogenesis in mitochondria. *Genes Dev.*, 22, 476-88.

Minet M., Dufour M.E., Lacroute F., 1992. Complementation of Saccharomyces cerevisiae auxotrophic mutants by Arabidopsis thaliana cDNAs. *Plant J.*, 2, 417-22.

Miyakawa I., Sando N., Kawano S., Nakamura S., Kuroiwa T., 1987. Isolation of morfologically intact mitochondrial nucleoids from the yeast *Saccharomyces cerevisiae*. *J. Cell Sci.*, 88, 431-9.

Mundy G., Garrett R., Harris S., Chan J., Chen D., Rossini G., Boyce B., Zhao M., Gutierrez G., 1999. Stimulation of bone formation in vitro and in rodents by statins. *Science*, 286, 1946-49.

Nakada K., Inoue K., Ono T., Isobe K., Ogura A., Goto Y.I., Nonaka I., Hayashi J.I., 2001. Inter-mitochondrial complementation: Mitochondria-specific system preventing mice from expression of disease phenotypes by mutant mtDNA. *Nat. Med.*, 7, 934-40.

Newman S.M., Zelenaya-Troitskaya O., Perlman P.S., Butow R.A., 1996. Analysis of mitochondrial DNA nucleoids in wild-type and a mutant strain of *Saccharomyces cerevisiae* that lacks the mitochondrial HMG box protein Abf2p. *Nucleic acids research*, 24, 386-93.

Nolli C., Goffrini P., Lazzaretti M., Zanna C., Vitale R., Lodi T., Baruffini E., 2015. Validation of a MGM1/OPA1 chimeric gene for functional analysis in yeast of mutations associated with dominant optic atrophy. *Mitochondrion*, 25, 38-48.

Nosek J. and Tomáska L., 2003. Mitochondrial genome diversity: evolution of the molecular architecture and replication strategy. *Current genetics*, 44(2), 73-84.

Nunnari J., Marshall W.F., Straight A., Murray A., Sedat J.W.,Walter P., 1997. Mitochondrial transmission during mating in Saccharomyces cerevisiae is determined by mitochondrial fusion and fission and the intramitochondrial segregation of mitochondrial DNA. *Mol.Biol. Cell* 8, 1233-42.

Okamoto K., and Shaw J.M., 2005. Mitochondrial morphology and dynamics in yeast and multicellular eukaryotes. *Annu. Rev. Genet.*, 39, 503-536.

Olichon A., Baricault L., Gas N., Guillou E., Valette A., Belenguer P., Lenaers G., 2003. Loss of OPA1 perturbates the mitochondrial inner membrane structure and integrity, leading to cytochrome c release and apoptosis. *J. Biol. Chem.*, 278, 7743-6.

Olichon A., Emorine L.J., Descoins E., Pelloquin L., Brichese L., Gas N., Guillou E., Delettre C., Valette A., Hamel C.P., Ducommun B., Lenaers G., Belenguer P.,2002. The human dynamin-related protein OPA1 is anchored to the mitochondrial inner membrane facing the inter-membrane space. *FEBS Lett.*, 523, 171-6.

Olichon A., Guillou E. , Delettre C., Landes T. ,Arnauné-Pelloquin L., Emorine L.J., Mils V., Daloyau M.,Hamel C., Amati-Bonneau P., Bonneau D., Reynier P. Lenaers G., Belenguer P., 2006. Mitochondrial dynamics and disease, OPA1. *Biochimica et Biophysica Acta*, 1763, 500-9.

Olichon A., Landes T., Arnaune-Pelloquin L., Emorine L.J., Mils V., Guichet A., Delettre C., Hamel C., Amati-Bonneau P., Bonneau D., Reynier P., Lenaers G., Belenguer P., 2007. Effects of OPA1 mutations on mitochondrial morphology and apoptosis: relevance to ADOA pathogenesis. *J. Cell Physiol.* 211, 423-30.

OPA1 LSDB http://opa1.mitodyn.org.

Osborne N.N., Li G.Y., Ji D., Mortiboys H.J., Jackson S., 2008. Light affects mitochondria to cause apoptosis to cultured cells: possible relevance to ganglion cell death in certain optic neuropathies. *J. Neurochem.*, 105, 2013-28.

Otera H. and Mihara K., 2011. Discovery of membrane receptor for mitochondrial fission GTPase Drp1. *Small GTPases*, 3, 167-72.

Otera H. and Mihara K., 2011. Molecular mechanisms and physiologic functions of mitochondrial dynamics. *J. Biochem.*, 149, 241-51.

Otera H., Ishihara N., Mihara K., 2013. New insights into the function and regulation of mitochondrial fission. *Biochimica et Biophysica Acta*, 1833, 1256-68.

Otera H., Wang C., Cleland M.M., Setoguchi K., Yokota S., Youle R.J., Mihara K., 2010. Mff is an essential factor for mitochondrial recruitment of Drp1 during mitochondrial fission in mammalian cells, *J. Cell Biol.*, 191, 1141-58.

Panizza E., Ercolino T., Mori L., Rapizzi E., Castellano M., Opocher G., Ferrero I., Neumann H.P., Mannelli M., Goffrini P., 2013. Yeast model for evaluating the pathogenic significance of SDHB, SDHC and SDHD mutations in PHEO-PGL syndrome. *Hum. Mol. Genet.*, 22, 804-15.

Perham R.N., 2000. Swinging arms and swinging domains in multifunctional enzymes: catalytic machines for multistep reactions. *Annual review of biochemistry*, 69, 961-1004.

Pesch U.E., Leo-Kottler B., Mayer S., Jurklies B., Kellner U., Apfelstedt-Sylla E., Zrenner E., Alexander C., Wissinger B., 2001. OPA1 mutations in patients with autosomal dominant optic atrophy and evidence for semi-dominant inheritance. *Hum. Mol. Genet.*, 10, 1359-68.

Pilling A. D., Horiuchi D., Lively C. M., Saxton W. M., 2006. Kinesin-1 and Dynein are the primary motors for fast transport of mitochondria in Drosophila motor axons. *Mol. Biol. Cell*, 17, 2057-68.

Pitayu L., Baruffini E., Rotig A., Lodi T., Delahodde A., 2015. Yeast model for drug discovery: Identification of molecules acting as potential therapeutics for POLG-related diseases (IN PRESS).

Poole A.C., Thomas R.E., Yu S., Vincow E.S., Pallanck L., 2010. The mitochondrial fusion-promoting factor mitofusin is a substrate of the PINK1/Parkin pathway. *PLoS ONE*, 5, 10054.

Rapaport D., Brunner M., Neupert W., Westermann B., 1998. Fzo1p is a mitochondrial outer membrane protein essential for the biogenesis of functional mitochondria in *Saccharomyces cerevisiae*. *J. Biol. Chem.*, 273, 20150-55.

Resnick M.A. and Cox B.S., 2000. Yeast as an honorary mammal. *Mutat. Res. Jun.*, 45, 1-11.

Rinaldi T., Dallabona C., Ferrero I., Frontali F., Bolotin-Fukuhara M., 2010. Mitochondrial diseases and the role of the yeast models. *FEMS Yeast Res.*, 10, 1006-22.

Rinaldi T., Hofmann L., Gambadoro A., Cossard R., Livnat-Levanon N., Glickman M.H., Frontali L., Delahodde A., 2008. Dissection of the carboxyl-terminal domain of the proteasomal subunit Rpn11 in maintenance of mitochondrial structure and function. *Mol. Biol. Cell.*, 19, 1022-31.

Rojo M., Legros F., Chateau D., Lombes A., 2002. Membrane topology and mitochondrial targeting of mitofusins, ubiquitous mammalian homologs of the transmembrane GTPase Fzo. *J. Cell Sci.*, 115, 1663-74.

Rothstein R.J., 1983. One step gene disruption in yeast. *Methods in Enzymology*. 101, 202-11.

Sambrook J. and Russel D. W., 2001. Molecular Cloning: a Laboratory Manual. *Cold Spring Harbor Laboratory Press*, Cold Spring Harbor, NY.

Santel A. and Fuller M.T., 2001. Control of mitochondrial morphology by a human mitofusin. *J. Cell Sci.*, 114, 867-74.

Santel A., Frank S., Gaume B., Herrler M., Youle R.J., Fuller M.T., 2003. Mitofusin-1 protein is a generally expressed mediator of mitochondrial fusion in mammalian cells. *J. Cell Sci.*, 116, 2763-74.

Satoh M., Hamamoto T., Seo N., Kagawa Y., Endo H., 2003. Differential sublocalization of the dynamin-related protein OPA1 isoforms in mitochondria. *Biochem. Biophys. Res. Commun.*, 300, 482-493.

Schaaf C.P., Blazo M., Lewis R.A., Tonini R.E., Takei H., Wang J., Wong L.J., Scaglia F., 2011. Early-onset severe neuromuscular phenotype associated with compound heterozygosity for OPA1 mutations. *Mol. Genet. Metab.*, 103, 383-87.

Scheffler I. , 2008. *Mitochondria*.

Schimpf S., Fuhrmann N., Schaich S., Wissinger B., 2008. Comprehensive cDNA Study and Quantitative Transcript Analysis of Mutant OPA1 Transcripts Containing Premature Termination Codons. *Human Mutation*, 29, 106-112.

Sesaki H. and Jensen R.E., 1999. Division versus fusion: Dnm1p and Fzo1p antagonistically regulate mitochondrial shape. *J. Cell Biol.*, 147, 699-706.

Sesaki H. and Jensen R.E., 2001. UGO1 encodes an outer membrane protein required for mitochondrial fusion. *J. Cell Biol.*, 152, 1123-34.

Sesaki H. and Jensen R.E., 2004. Ugo1p links the Fzo1p and Mgm1p GTPases for mitochondrial fusion. *J. Biol. Chem.*, 279, 28298-303.

Sesaki H., Southard S.M., Hobbs A.E., Jensen R.E., 2003. Cells lacking Pcp1p/Ugo2p, a rhomboid-like protease required for Mgm1p processing, lose mtDNA and mitochondrial structure in a Dnm1p-dependent manner, but remain competent for mitochondrial fusion. *Biochem. Biophys. Res. Commun.*, 308, 276-83.

Shirendeb U., Reddy A.P., Manczak M., Calkins M.J., Mao P., Tagle D.A., Reddy P.H., 2011. Abnormal mitochondrial dynamics, mitochondrial loss and mutant huntingtin oligomers in Huntington's disease: implications for selective neuronal damage. *Hum. Mol. Genet.* 20, 1438-55.

Smith A.M., Ron Ammar R., Corey Nislow C., Giaever G., 2010. A survey of yeast genomic assays for drug and target discovery. *Pharmacology & Therapeutics*, 127, 156-64.

Song W., Chen J., Petrilli A., Liot G., Klinglmayr E., Zhou Y., Poquiz P., Tjong J., Pouladi M.A., Hayden M.R., Masliah E., Ellisman M., Rouiller I., Schwarzenbacher R., Bossy B., Perkins G., Bossy-Wetzel E., 2011. Mutant huntingtin binds the mitochondrial fission GTPase dynamin-related protein-1 and increases its enzymatic activity. *Nat. Med.*, 17, 377-82.

Song Z., Chen H., Fiket M., Alexander C., Chan D.C., 2007. OPA1 processing controls mitochondrial fusion and is regulated by mRNA splicing, membrane potential, and Yme1L. *J. Cell Biol.*, 178, 749-755.

Soto I.C., Fontanesi F., Valledor M., Horn D., Singh R., Barrientos A., 2009. Synthesis of cytochrome c oxidase subunit 1 is translationally downregulated in the absence of functional F1F0-ATP synthase. *Biochim. Biophys. Acta.*, 1793, 1776-86.

Stock D., Leslie A.G., and Walker J.E., 1999. Molecular architecture of the rotary motor in ATP synthase. *Science*, 286, 1700-5.

Stojanovski D., Koutsopoulos O.S., Okamoto K., Ryan M.T., 2004. Levels of human Fis1 at the mitochondrial outer membrane regulate mitochondrial morphology. *J. Cell Sci.*, 117, 1201-10.

Suen D.F., Kristi L. Norris K.L., Youle R.J., 2008. Mitochondrial dynamics and apoptosis. *Genes Dev.*, 22, 1577-90.

Sugioka R., Shimizu S., Tsujimoto Y., 2004. Fzo1, a protein involved in mitochondrial fusion, inhibits apoptosis. *J. Biol. Chem.*, 279, 52726-34.

Tanaka A., Cleland M.M., Xu S., Narendra D.P., Suen D.F., Karbowski M., Youle R.J., 2010. Proteasome and p97 mediate mitophagy and degradation of mitofusins induced by Parkin. *J. Cell Biol.*, 191, 1367-80.

Tardiff D.F and Lindquist S., 2013. Phenotypic screens for compounds that target the cellular pathologies underlying Parkinson's disease. Drug Discovery Today: Technologies, 10, 121-8.

Thiselton D.L., Alexander C., Taanman J.W., Brooks S., Rosenberg T., Eiberg H., Andreasson S., Van Regemorter N., Munier F.L., Moore A.T., Bhattacharya S.S., Votruba M.,2002. A comprehensive survey of mutations in the OPA1 gene in patients with autosomal dominant optic atrophy. *Invest .Ophthalmol. Vis. Sci.*, 43, 1715-24.

Thomas B. J. and Rothstein R., 1989. Elevated recombination rates in transcriptionally active DNA. *Cell*, 56, 619-30.

Turner N. and Heilbronn L.K., 2008. Is mitochondrial dysfunction a cause of insulin resistance? *Trends Endocrinol. Metab.*, 9, 324-30.

Tzagoloff A. and Dieckmann C.L., 1990. PET genes of *Saccharomyces cerevisiae*. *Microbiological Review*, 54, 211-25.

Vance J. M., 2000. The many faces of Charcot-Marie-Tooth disease. *Archives of Neurology*, 57, 638-40.

Venter J.C., Adams M.D., Myers E.W., Li P.W., Mural R.J., Sutton G.G., Smith H.O., Yandell M., Evans C.A., Holt R.A., Gocayne J. D., Amanatides P., Ballew R. M., Huson D. H., Wortman J. R., Zhang Q., Kodira C. D., Zheng X. H., Chen L., Skupski M., Subramanian G., Thomas P. D., Zhang J., Gabor Miklos G. L., Nelson C., Broder S., Clark A. G., Nadeau J., McKusick V. A., Zinder N., Levine A. J., Roberts R. J., Simon M., Slayman C., Hunkapiller M., Bolanos R., Delcher A., Dew I., Fasulo D., Flanigan M., Florea L., Halpern A., Hannenhalli S., Kravitz S., Levy S., Mobarry C., Reinert K., Remington K., Abu-Threideh J., Beasley E., Biddick K., Bonazzi V., Brandon R., Cargill M., Chandramouliswaran I., Charlab R., Chaturvedi K., Deng Z., Di Francesco V., Dunn P., Eilbeck K., Evangelista C., Gabrielian A. E., Gan W., Ge W., Gong F., Gu Z., Guan P., Heiman T. J., Higgins M. E., Ji R. R., Ke Z., Ketchum K. A., Lai Z., Lei Y., Li Z., Li J., Liang Y., Lin X., Lu F., Merkulov G. V., Milshina N., Moore H. M., Naik A. K., Narayan V. A., Neelam B., Nusskern D., Rusch D. B., Salzberg S., Shao W., Shue B., Sun J., Wang Z., Wang A., Wang X., Wang J., Wei M., Wides R., Xiao C., Yan C., Yao A., Ye J., Zhan M., Zhang W., Zhang H., Zhao Q., Zheng L., Zhong F., Zhong W., Zhu S., Zhao S., Gilbert D., Baumhueter S., Spier G., Carter C., Cravchik A., Woodage T., Ali F., An H., Awe A., Baldwin D., Baden H., Barnstead M., Barrow I., Beeson K., Busam D., Carver A., Center A., Cheng M. L., Curry L., Danaher S., Davenport L., Desilets R., Dietz S., Dodson K., Doup L., Ferriera S., Garg N., Gluecksmann A., Hart B., Haynes J., Haynes C., Heiner C., Hladun S., Hostin D., Houck J., Howland T., Ibegwam C., Johnson J., Kalush F., Kline L., Koduru S., Love A., Mann F., May D., McCawley S., McIntosh T., McMullen I., Moy M., Moy L., Murphy B., Nelson K., Pfannkoch C., Pratts E., Puri V., Qureshi H., Reardon M., Rodriguez R., Rogers Y. H., Romblad D., Ruhfel B., Scott R., Sitter C., Smallwood M., Stewart E., Strong R., Suh E., Thomas R., Tint N. N., Tse S., Vech C., Wang G., Wetter J., Williams S., Williams M., Windsor S., Winn-Deen E., Wolfe K., Zaveri J., Zaveri K., Abril J. F., Guigó R., Campbell M. J., Sjolander K. V., Karlak B., Kejariwal A., Mi H., Lazareva B., Hatton T., Narechania A., Diemer K., Muruganujan A., Guo N., Sato S., Bafna V., Istrail S., Lippert R., Schwartz R., Walenz B., Yooseph S., Allen D., Basu A., Baxendale J., Blick L., Caminha M., Carnes-Stine J., Caulk P., Chiang Y. H., Coyne M., Dahlke C., Mays A., Dombroski M., Donnelly M., Ely D., Esparham S., Fosler C., Gire H.,

Glanowski S., Glasser K., Glodek A., Gorokhov M., Graham K., Gropman B., Harris M., Heil J., Henderson S., Hoover J., Jennings D., Jordan C., Jordan J., Kasha J., Kagan L., Kraft C., Levitsky A., Lewis M., Liu X., Lopez J., Ma D., Majoros W., McDaniel J., Murphy S., Newman M., Nguyen T., Nguyen N., Nodell M., Pan S., Peck J., Peterson M., Rowe W., Sanders R., Scott J., Simpson M., Smith T., Sprague A., Stockwell T., Turner R., Venter E., Wang M., Wen M., Wu D., Wu M., Xia A., Zandieh A., Zhu X., 2001. The sequence of the human genome**.** *Science.*, 201, 1304-51.

Votruba M., Fitzke F.W., Holder G.E., Carter A., Bhattacharya S.S., Moore A.T., 1998. Clinical features in affected individuals from 21 pedigrees with dominant optic atrophy. *Arch. Ophthalmol.*, 116, 351-58.

Wach A., Brachat A., Pohlmann R. Philippsen P.,1994. New heterologous modules for classical or PCR-based gene disruptions in *Saccharomyces cerevisiae*. *Yeast*, 10, 1793–1808.

Wallace D.C., 2001. Mitochondrial defects in neurodegenerative disease. *Mental retardation and developmental disabilities research reviews*, 7(3), 158-66.

Wang H., Lim P.J., Karbowski M., Monteiro M.J., 2009. Effects of overexpression of huntingtin proteins on mitochondrial integrity. *Hum. Mol. Genet.*, 18, 737-52.

Wang X., Su B., Lee H.G., Li X., Perry G., Smith M.A., Zhu X., 2009. Impaired balance of mitochondrial fission and fusion in Alzheimer's disease. J. Neurosci., 29, 9090-103.

Wang X., Winter D., Ashrafi G., Schlehe J., Wong Y.L., Selkoe D., Rice S., Steen J., LaVoie M.J., Schwarz T.L.,2011. PINK1 and Parkin target Miro for phosphorylation and degradation to arrest mitochondrial motility. *Cell*, 147, 893-906.

Warren G. and Wickner W., 1996. Organelle inheritance. *Cell*, 84(3), 395-400.

Westermann B., 2010. Mitochondrial dynamics in model organisms: What yeasts, worms and flies have taught us about fusion and fission of mitochondria. *Nat. Rev. Mol. Cell Biol.*, 11(12), 872-884.

Wharton D.C. and Tzagoloff A., 1967. Cytochrome oxidase from beef heart mitochondria. *Methods Enzymol.*, 10, 245-50.

Williamson D.H. and Fennell D.J., 1979. Visualization of yeast mitochondrial DNA with the fluorescent stain “DAPI” *Methods in enzymology*, 56, 728-33.

Wong E.D., Wagner J.A., Gorsich S.W., McCaffery J.M., Shaw J.M., Nunnari J., 2000. The dynamin-related GTPase, Mgm1p, is an intermembrane space protein required for maintenance of fusion competent mitochondria. *J. Cell Biol.*, 151, 341-352.

Wong E.D., Wagner J.A., Scott S.V., Okreglak V., Holewinske T.J., Cassidy-Stone A., Nunnari J., 2003. The intramitochondrial dynamin-related GTPase, Mgm1p, is a component of a protein complex that mediates mitochondrial fusion. *J. Cell Biol.*, 160, 303-11.

Yaffe M.P., 1999. The machinery of mitochondrial inheritance and behavior. *Science,* 283, 1493-97.

Yoneda M., Miyatake T., Attardi G., 1994. Complementation of mutant and wild-type human mitochondrial DNAs coexisting since the mutation event and lack of complementation of DNAs introduced separately into a cell within distinct organelles. *Mol. Cell. Biol.*, 4,2699-712.

Yoon Y., Krueger E.W., Oswald B.J., McNiven M.A., 2003. The mitochondrial protein hFis1 regulates mitochondrial fission in mammalian cells through an interaction with the dynamin-like protein DLP1. *Mol. Cell Biol.*, 23, 5409-20.

Youle R.J. and van der Bliek A. M., 2012. Mitochondrial Fission, Fusion, and Stress. *Science*, 337, 1062.

Yu-Wai-Man P., Griffiths P.G., Burke A., Sellar P.W., Clarke M.P., Gnanaraj L., Ah-Kine D., Hudson G., Czermin B., Taylor R.W., et al., 2010. The prevalence and natural history of dominant optic atrophy due to OPA1 mutations. *Ophthalmology*, 117, 1531-46.

Zanna C., Ghelli A., Porcelli A.M., Karbowski M., Youle R.J., Schimpf S., Wissinger B., Pinti M., Cossarizza A., Vidoni S., Valentino M.L., Rugolo M., Carelli V., 2008. OPA1 mutations associated with dominant optic atrophy impair oxidative phosphorylation and mitochondrial fusion. *Brain*, 131, 352-67.

Zeviani M. and Di Donato S., 2004. Mitochondrial disorders. *Brain: a journal of neurology*, 127, 2153–72.

Zhao J., Lendahl U., Nister M., 2012. Regulation of mitochondrial dynamics: convergences an divergences between yeast and vertebrates, *Cell Mol. Life Sci*., 70, 951-76.

Zick M., Duvezin-Caubet S., Schäfer A., Vogel F., Neupert W., Reichert A.S., 2009. Distinct roles of the two isoforms of the dynamin-like GTPase Mgm1 in mitochondrial fusion. *FEBS Letters*, 583 , 2237-43.

Zuchner S., Mersiyanova I.V., Muglia M., Bissar-Tadmouri N., Rochelle J., Dadali E.L., Zappia M., Nelis E., Patitucci A., Senderek J., Parman Y., Evgrafov O., Jonghe P.D., Takahashi Y., Tsuji S., Pericak-Vance M.A., Quattrone A., Battaloglu E., Polyakov A.V., Timmerman V., Schroder J.M., Vance J.M., 2004. Mutations in the mitochondrial GTPase mitofusin 2 cause Charcot-Marie-Tooth neuropathy type 2A. *Nat. Genet.*, 36, 449-51.

Appendix

Mitochondrion 25 (2015) 38–48

Contents lists available at ScienceDirect

Mitochondrion

journal homepage: www.elsevier.com/locate/mito

Validation of a *MGM1/OPA1* chimeric gene for functional analysis in yeast of mutations associated with dominant optic atrophy

Cecilia Nolli [a,1], Paola Goffrini [a,1], Mirca Lazzaretti [a], Claudia Zanna [b,c], Rita Vitale [d], Tiziana Lodi [a,2], Enrico Baruffini [a,*,2]

[a] Department of Life Sciences, University of Parma, Viale delle Scienze 11/A, 43124 Parma, Italy
[b] Department of Pharmacy and Biotechnology (FABIT), University of Bologna, Via Irnerio 48, 40126 Bologna, Italy
[c] IRCCS Institute of Neurological Sciences of Bologna, Bellaria Hospital, Via Altura 3, 40139 Bologna, Italy
[d] Department of Basic Medical Sciences, Neurosciences and Sensory Organs, University of Bari "Aldo Moro", Piazza Giulio Cesare 11, 70124 Bari, Italy

ARTICLE INFO

Article history:
Received 3 August 2015
Received in revised form 24 September 2015
Accepted 1 October 2015
Available online xxxx

Keywords:
MGM1/OPA1 chimeric constructs
Yeast model
DOA
DOA plus
Modeling human mutations

ABSTRACT

Mutations in *OPA1* are associated with DOA or DOA plus. Novel mutations in *OPA1* are periodically identified, but often the causative effect of the mutation is not demonstrated. A chimeric protein containing the N-terminal region of Mgm1, the yeast orthologue of OPA1, and the C-terminal region of OPA1 was constructed. This chimeric construct can be exploited to evaluate the pathogenicity of most of the missense mutations in *OPA1* as well as to determine whether the dominance of the mutation is due to haploinsufficiency or to gain of function.

1. Introduction

Dominant optic atrophy (DOA) is a mitochondrial disease characterized by mild to severe decrease in visual acuity, color vision deficiency and visual field defects, due to selective degeneration of retinal ganglion cells and optic nerve atrophy (Kjer, 1959; Lenaers et al., 2012). DOA is a genetically inherited disorder associated, in most cases, with mutations in the *OPA1* gene (Delettre et al., 2000; Alexander et al., 2000), which encodes the mitochondrial GTPase of the dynamin family OPA1, a highly conserved protein primarily involved in mitochondrial fusion events and in mtDNA maintenance. This protein is inserted in the inner mitochondrial membrane (IMM) and displays three highly conserved regions: a GTPase domain, a middle domain and a GTPase effector domain, involved in oligomerization and activation of dynamins. Eight OPA1 isoforms resulting from alternative splicing of exon 4, 4b and 5b are present in humans. These isoforms exhibit tissue-specific patterns whose specific function is still unknown (Landes et al., 2010). Each isoform can also undergo proteolytic cleavage generating long and short isoforms both of which are required for the IMM fusion and are involved in membrane tethering and GTPase activity respectively (Escobar-Henriques and Anton, 2013).

More than 200 pathogenic mutations spread throughout the entire *OPA1* gene have been identified so far (*OPA1* LSDB http://opa1.mitodyn.org). About 50% of these *OPA1* mutations (frame-shift and non-sense mutations, stop codons, splicing errors, or deletions/insertions) generate a haploinsufficiency situation where the mutated transcript is degraded by mRNA decay, thus reducing to 50% the amount of OPA1 protein (Schimpf et al., 2008). The remaining ones are missense mutations, which are mostly clustered in the GTPase domain and cause heterozygous amino acid substitutions thought to exert a severe dominant negative effect, because the mutated protein might interfere with and inhibit the wild-type protein (Amati-Bonneau et al., 2009). These latter mutations are often associated with a more severe syndromic disorder named "DOA-plus", which includes optic atrophy appearing in childhood, followed by chronic progressive external ophthalmoplegia (PEO), ataxia, sensorineural deafness, sensory-motor neuropathy, myopathy and mtDNA multiple deletions in adult life (Amati-Bonneau et al., 2008; Hudson et al., 2008; Yu-Wai-Man et al., 2010).

Abbreviations: CC, coiled coil; CMV, cytomegalovirus; COX, cytochrome c oxidoreductase; DOA, Dominant Optic Atrophy; DOA plus, Dominant Optic Atrophy plus phenotype; GED, GTPase effector domain; MPS, mitochondrial peptide signal; NCCR, NADH-cytochrome c oxidoreductase; PGK, phosphoglycerate kinase; RCR, rhomboid cleavage region; SQDR, succinate-coenzyme Q-2,6-Dichlorophenol Indophenol reductase; TETOff, tetracycline off promoter; TM, transmembrane region; wt, wild type.

* Corresponding author at: Department of Life Sciences, University of Parma, Viale delle Scienze 11/A, 43124 Parma, Italy.
E-mail address: enrico.baruffini@unipr.it (E. Baruffini).

[1] These authors contributed equally to this work.
[2] These authors contributed equally to this work and must be considered both as senior authors.

http://dx.doi.org/10.1016/j.mito.2015.10.002
1567-7249/

Studies carried out in fibroblasts and in lymphoblasts as well as in skeletal muscle from DOA patients have demonstrated that OPA1 has other crucial functions besides its role in mtDNA maintenance and mitochondrial fusion, i.e. *cristae* ultrastructure integrity and apoptosis regulation (Frezza et al., 2006), respiratory supercomplexes stability and energetic efficiency (Cogliati et al., 2013). However, even though skin fibroblasts are important in vitro cellular models for the study of DOA pathophysiology, using other in vivo models which are genetically easier to manipulate and are characterized by a strikingly different mutant phenotype from the wild-type one can be desirable.

To this purpose, the yeast *Saccharomyces cerevisiae*, whose *OPA1* orthologous gene is *MGM1* (Mitochondrial Genome Maintenance), can be considered a suitable model organism (Jones and Fangman, 1992) to test for pathogenicity of new *OPA1* variants identified in patients, as done previously for several mutations causing mitochondrial diseases. A number of cases are reported in which allegedly pathological human substitutions have been validated in yeast by using different strategies depending on the conservation of the residues involved and/or on the ability of the human wt gene to complement the function of the yeast gene (reviewed in Barrientos, 2003; Rinaldi et al., 2010; Baile and Claypool, 2013; Lodi et al., 2015; Lasserre et al., 2015). Although Mgm1 and OPA1 own equivalent functional domains, their amino acid sequences are weakly conserved, therefore only few pathological mutations can be introduced in *MGM1* and analyzed in yeast. Moreover in *S. cerevisiae OPA1* cannot substitute the *MGM1* gene. To overcome these problems chimeric proteins composed of the N-terminal region of Mgm1 fused with the catalytic region of OPA1 were constructed. One *MGM1*/*OPA1* chimera was able to complement the oxidative growth defect of the *S. cerevisiae mgm1* null mutant, thus validating this recombinant construct as a model for the study of the *OPA1* pathological mutations.

2. Materials and methods

2.1. Yeast strains and media

The yeast strains used in this work were W303-1A (*MATa leu2-3, trp1-1, can1-100, ura3-1, ade 2–1, his3-11*), W303-1B (*MATα leu2-3, trp1-1, can1-100, ura3-1, ade 2–1, his3-11*) and their isogenic strains *mgm1*::*KanR* harboring plasmid pFl38*MGM1* (see below). The diploid DW1.1 was obtained by crossing W303-1A *Δmgm1* and W303-1B *Δmgm1*.

Synthetic complete medium (SC) contained 6.9 g/l yeast nitrogen base without amino acids (Formedium), 1 g/l drop-out mix according to Kaiser et al. (1994). YP medium contained 0.5% yeast extract (Formedium) and 1% peptone (Formedium); YPA medium was YP 2X supplemented with 40 mg/ml adenine base (Formedium). Carbon sources were added as indicated in the text.

2.2. Plasmid construction

Constructs produced in this work were cloned in plasmids pFL38 (centromeric, *URA3* marker), pFL39 (centromeric, *TRP1* marker), pFL36 (centromeric, *LEU2 marker*) (Bonneaud et al., 1991) and YEplac112 (multicopy, *TRP1* marker) (Gietz and Sugino, 1988). All the primers employed in this study are reported in Supplementary Table 1.

The yeast *MGM1* gene and its upstream and downstream regions were first PCR amplified using genomic DNA of strain W303-1B as template and MGM1CFw and MGM1CRv as primers, then digested with *Sac*I and *Sal*I and cloned in pFL38, digested with the same enzymes (pFL38*MGM1*). *MGM1* was then subcloned in pFL39 and YEplac112 to obtain pFL39*MGM1* and YEPlac112*MGM1*.

MGM1/*OPA1* constructs, hereafter called *CHIM1-6*, each containing different portions of *MGM1* and *OPA1*, were obtained using the two-step overlap extension technique, a modification of the protocol used for site directed mutagenesis (Ho et al., 1989). For each chimera, the first PCR reaction was performed using the external forward primer MGM1CFw and the external reverse primer OPA1XhoRv, each in combination with reverse or forward internal primers respectively, designed in order to amplify different portions of *MGM1* (gradually longer) and *OPA1* (gradually shorter), as reported in Supplementary Table 1. Final chimeric constructs were obtained by using the different overlapping PCR fragments as templates and MGM1CFw and OPA1XhoRv as primers. The products, together with the whole *OPA1* coding region amplified with OPA1CFw and OPA1XhoRv, were then digested with *Sal*I and *Xho*I and cloned in a *Sal*I-*Xho*I-digested pFL39*MGM1* centromeric plasmid and in a *Sal*I-*Xho*I digested YEplac112*MGM1* multicopy plasmid, in each of which a *Xho*I site was introduced by site specific mutagenesis just after the stop codon of *MGM1* ORF.

The *CHIM3* construct was also cloned in pFL39PGK, pFL39TEToff and pFL36TEToff. pFL39PGK was obtained by subcloning the PGK promoter and the PGK terminator from plasmid pFL61 (Minet et al., 1992) digested with *Bam*HI and *Bgl*II in *Bam*HI-digested pFL39. pFL39TEToff and pFL36TEToff were obtained by subcloning the tTA transactivator under the CMV promoter, seven repeats of the tetO promoter upstream of the *CYC1* promoter and the *CYC1* terminator from plasmid pCM189 (Garì et al., 1997) digested with *Eco*RI and *Hind*III in *Eco*RI-*Hind*III-digested pFL39 and pFL36, respectively.

pFL39PGKCHIM3, pFL39TEToffCHIM3 and pFL36TEToffCHIM3 were obtained by PCR-amplification using pFL39*CHIM3* as template and MGMOPACNotFw and MGMOPACNotRv as primers. After digestion with *Not*I, the PCR fragments were cloned in the different plasmids and sequenced.

2.3. Construction of mutant alleles

chim3 mutant alleles were obtained by site-directed mutagenesis of a *CHIM3* gene fragment, using the overlap extension technique (Ho et al., 1989). In the first PCR, the forward primer TATACYC1Fw and specific reverse mutagenic primers were used. In the second PCR, specific forward mutagenic primers and the reverse primer MGMOPACNotRv were employed. The final mutagenized products were obtained by using the overlapping PCR fragments (obtained in the first and second PCR) as templates, with TATACYC1Fw and MGMOPACNotRv as external primers.

Each final product was then digested with *Not*I and cloned in *Not*I-digested pFL39TEToff, obtaining pFL39TEToff plasmid-borne $CHIM3^{I382M}$, $CHIM3^{R445H}$, $CHIM3^{K468E}$ and $CHIM3^{V903Gfs*3}$ mutant alleles.

2.4. Construction of strains harboring CHIM3 wt and mutant alleles

MGM1 was disrupted in W303-1A and W303-1B by one step gene disruption. At first both strains were transformed with pFL38*MGM1*. Then, the cassette *mgm1*::KanMX4 was amplified from the genomic DNA of BY4742 *Δmgm1* and inserted into both strains through high efficiency yeast transformation protocol (Gietz and Woods, 2002). Clones resistant to geneticin were PCR-amplified to verify the correctness of disruption. The W303-1A *Δmgm1*/pFL38*MGM1* strain was transformed with plasmids harboring the *TRP1* marker, and pFL38*MGM1* was lost through plasmid shuffling as previously reported (Boeke et al., 1987; Baruffini et al., 2010). To obtain diploid strains, W303-1A *Δmgm1*/pFL38*MGM1* was crossed with W303-1B *Δmgm1*, which had been transformed with pFL36TEToff. This diploid strain, selected on medium without leucine and uracil, was then transformed with *CHIM3* wt and mutant alleles on pFL39TEToff and subjected to plasmid shuffling to remove pFL38*MGM1*.

2.5. Complementation studies and measurement of extended mtDNA mutability

Oxidative growth was evaluated by spotting serial cell dilutions ($5x10^4$, $5x10^3$, $5x10^2$ and $5x10^2$ cell/spot), in a total volume of 5 μl, on

solid SC or YP medium, supplemented with 2% glucose, 2% glycerol or 2% ethanol. *Petite* frequency was measured in solid SC medium supplemented with 2% glucose as previously reported (Baruffini et al., 2010). *Petite* frequency was defined as the percentage of colonies that showed the *petite* phenotype after a 5 day-incubation at 28°C. Statistical analysis was performed through an unpaired two-tailed t-test.

2.6. Respiration measurement and respiratory chain complex activities

To measure the respiratory activity, strains were pre-grown in YP supplemented with 2% ethanol to counter select *petite* cells. Cells were inoculated at a final concentration of 0.08 OD/ml in SC supplemented with 0.5% glucose and grown until glucose was exhausted for approximately 16–18 h. *Petite* frequency was lower than 5% in each case. The oxygen consumption rate was measured on whole cells at 30°C using a Clark-type oxygen electrode (Oxygraph System Hansatech Instruments England) with 1 ml of air-saturated respiration buffer (0.1 M phthalate–KOH, pH 5.0), 10 mM glucose. The reaction started by addition of 20 mg of wet-weight cells, as described previously (Goffrini et al., 2009: Panizza et al., 2013). Statistical analysis was performed through a paired two-tailed t-test.

To evaluate the respiratory chain complex activities, cells which were pre-grown on SC medium supplemented with 2% glucose were inoculated in SC medium supplemented with 0.15% glucose and 2% galactose until an OD/ml = 1.5–2 was reached. Galactose was chosen as carbon source since it does not inhibit mitochondrial function and minimizes the presence of *petite* cells (galactose does not allow the growth on SC medium of *petite* cells, whose frequency was lower than 3%). Succinate-coenzyme Q-DCPIP reductase (SQDR), NADH-cytochrome *c* oxidoreductase (NCCR) and cytochrome c oxidoreductase (COX, complex IV) specific activities were measured spectrophotometrically as previously described (Fontanesi et al., 2009, Barrientos et al., 2001 Jarreta et al., 2000) on a mitochondrial-enriched fraction prepared according to Soto et al. (2009). Protein concentration was determined with Bradford's method, using the BioRad protein assay following the manufacturer's instructions (Bradford, 1976). Statistical analysis was performed through a paired two-tailed t-test.

2.7. RT-qPCR and qPCR

For RT-qPCR, cells were grown in SC supplemented with 2% glucose until 0.9–1.2 OD was reached. Total RNA was extracted from 10 OD with hot acidic phenol (Ausubel et al., 1994), treated with DNase I (New England Biolabs), retrotranscribed with M-MuLV Reverse Transcriptase (NewEngland Biolabs) with oligo (dT) 20primer (Euroclone) and murine RNase inhibitor (NewEngland Biolabs). qPCR on retro-transcribed *CHIM3* and, as reference, *ACT1* mRNA was performed by using Power Sybr Green mix with ROX (Life Technologies), supplemented with the primers reported in Supplementary Table 1 and ACT1qFw and ACT1qRv (Baruffini et al., 2015) at a final concentration of 120 nM in the AB 7300 instrument (Life Technologies) at default settings: 50°C 2 min, 95°C 10 min, 41 cycles at 95°C for 15 s and 60°C for 1 min, and one cycle at 95°C for 15 s and at 60°C for 15 s. Statistical analysis was performed through an unpaired two-tailed t-test.

For qPCR, cells that were pre-grown in YP supplemented with ethanol 2% were grown in 10 ml of SC supplemented with 0.5% glucose until exhaustion. Total (genomic and mitochondrial) DNA was extracted as previously reported (Hoffman and Winston, 1987). qPCR was performed on mtDNA gene *COX1* and, as reference, on nDNA gene *ACT1* as previously reported (Baruffini et al., 2015).

2.8. Western blot analysis

Total proteins from 4.8 OD of cells grown in SC supplemented with 0.5% glucose until exhaustion were extracted with the trichloroacetic acid (TCA) method by chilling the cells supplemented with 120 mM NaOH, 0.5% β-meracaptoethanol, 650 μM PMSF and 25% TCA on ice, then re-suspending the proteins in 60 μl of Laemmli Isample buffer at pH 6.8. 10 μl of such suspension were separated by 8% SDS-PAGE, and electro-blotted onto nitrocellulose filters which were then incubated with anti-OPA1 (BD Biosciences) and anti-Porin (Abcam Mitoscience) antibodies. After incubation with anti-mouse secondary antibodies, ECL Western blotting Substrate (Thermo Scientific Pierce) was used for final detection. Signals were quantified through Quantity One Software (Bio-Rad).

2.9. Mitochondrial morphology and fluorescence microscopy

Strains carrying wt *MGM1*, *CHIM3* or *chim3* mutant alleles were transformed with pYEF1mtGFP (Rinaldi et al., 2008, a kind gift from Agnes Delahodde). Cells were pregrown in SC medium supplemented with 0.5% glucose. After 24 h, the cells were transferred to SC medium supplemented with 0.15% glucose and 2% galactose in order to induce the expression of mtGFP, until the mid-log phase was reached. Once adjusted to 0.4 OD/ml, the cells were observed with a Zeiss Observer 2.1 microscope using a 630X magnification and captured using an AxioVision Rel 4.8 software.

3. Results

3.1. OPA1 cDNA did not rescue the Δmgm1 mutation in Saccharomyces cerevisiae

As OPA1, yeast Mgm1 is crucial for the fusion of the inner membrane and is involved in the maintenance of the *cristae* in *S. cerevisiae* (Wong et al., 2000; Meeusen et al., 2006). However, although Mgm1 and OPA1 own equivalent functional domains, their amino acid sequences are weakly conserved (approximately 20%, Supplementary Fig. 1), hence only few pathological mutations involve conserved residues. To validate pathological mutations in yeast, we express the human *OPA1* cDNA in a *S. cerevisiae* mutant devoid of *MGM1*. At first we constructed a *Δmgm1* mutant, in the W303-1B strain, by deleting the *MGM1* gene at chromosomal locus. Since loss of *MGM1* irreversibly depletes cells of mtDNA (*rho*^{0}), *MGM1* was disrupted in the presence of the wt allele cloned in the centromeric vector pFL38. In this condition, mitochondrial DNA can be maintained, thanks to the functional copy of plasmid-borne *MGM1*. The *OPA1* cDNA was cloned in either single or multicopy plasmid, under the control of either the *MGM1* endogenous promoter or of the strong constitutive promoter *PGK*, and the recombinant constructs were then introduced into the *Δmgm1* mutant. The pFL38*MGM1* vector was then counter-selected by plasmid shuffling on 5-FOA plates. The phenotypic analysis of the strain transformed by *OPA1* cDNA was carried out by spotting cells on plates containing ethanol and glycerol as non-fermenting carbon sources. Transformant cells were not able to grow in these conditions, which indicates that the *OPA1* cDNA fails to complement the oxidative growth defect of the *Δmgm1* mutant (data not shown). In addition, cells were devoid of mtDNA, as demonstrated by crossing with a *rho*^{0} strain of the opposite mating type.

3.2. Production of MGM1/OPA1 chimeric constructs

The lack of complementation of the *Δmgm1* OXPHOS defect by *OPA1* cDNA can be the consequence of: i) incorrect import of the OPA1 protein in the heterologous mitochondria; ii) incorrect processing of OPA1 to short and long form by the yeast Pcp1 protease; iii) inability of OPA1 to interact with the yeast protein involved in the fusion process, such as Fzo1 and Ugo1 (Sesaki and Jensen, 2004); iv) incorrect folding of the human protein in yeast. To overcome some of these problems, we decided to construct chimeric proteins composed of the N terminal part of Mgm1, including the mitochondrial peptide signal (MPS), and the C terminal region of OPA1, in particular the whole GTPase region in which the majority of pathological mutations are located. In

Supplementary Fig. 1, the alignment of Mgm1 and OPA1 amino acid sequences is shown and the different functional domains (i.e. the mitochondrial peptide signal (MPS), the transmembrane (TM), the rhomboid cleavage region (RCR), the coiled-coil (CC), the GTPase, the middle and the GED domains) are highlighted.

As depicted in Fig. 1, six chimeras were constructed where the Mgm1 region was gradually longer and the OPA1 region gradually shorter. The six chimeras also included the following Mgm1 features respectively: Chim1, the Mgm1 MPS and additional 8 amino acids, in order to maintain the cleavage site of the yeast matrix metalloprotease (MPP) necessary to produce the long-isoform; Chim2, the Mgm1 transmembrane region also; Chim3, the RCR and the D/E-stretch region of Mgm1; Chim4, the Mgm1 coiled coil domain; Chim5, a part of, and Chim6 the whole of the Mgm1 GTPase domain. Chim1 and Chim2 have the cleavage S1 site of OPA1, whereas the other chimeras have the S cleavage site of Mgm1, which is cut by the rhomboid protease Pcp1.

The six chimeras, cloned either in centromeric or in multicopy vectors under the endogenous promoter *MGM1*, were introduced into the *Δmgm1* mutant, and transformant strains were tested for growth on non-fermentable carbon sources. Only *CHIM3* cloned in multicopy was able to recover, albeit not completely, the growth defect of the mutant strain (Fig. 2A). This result indicates that: i) the presence of Mgm1 RCR is necessary for the activity of the chimeric protein; ii) the presence of the OPA1 coiled coil is necessary for the activity of the chimeric protein; ii) larger portion of Mgm1 is deleterious for the chimera activity.

Two isoforms are encoded by *MGM1*: a long one (l-Mgm1), which is an integral inner membrane protein that spans the inner membrane thanks to an N-terminal transmembrane segment; and a short soluble isoform (s-Mgm1), which lacks the inner-transmembrane domain and is therefore present in the intermembrane space (Herlan et al., 2003). The two isoforms are present in equal amounts and have different roles in mitochondrial membrane fusion (Zick et al., 2009; Devay et al., 2009). The formation of s-Mgm1 is dependent on the rhomboid protease Pcp1 (Herlan et al., 2003; McQuibban et al., 2003; Sesaki et al., 2003), but the insertion of Mgm1 into the inner membrane through its transmembrane fragment or its processing by Pcp1 at the rhomboid cleavage region are competing processes, which are known as "alternative topogenesis" (Herlan et al., 2004). Correct processing in both long and short forms is crucial for the mitochondrial fusion, which indicates that the long and short forms function together in this pathway, albeit with distinct roles (Meeusen et al., 2006). In order to check whether chimeric constructs were correctly processed, leading to the production of long and short mature forms in equivalent ratio, a Western analysis was performed. We found that Chim3, but not Chim1 and Chim2, were correctly processed, leading to the production of both a long and a short isoform (plus an unprocessed band corresponding to the full length chimera harboring the MPS) (Fig. 2B). This finding can explain the lack of complementation by these two latter constructs. Chim4 was also processed correctly, which further supports the hypothesis that chimeras harboring large portions of both proteins are not functional. In Chim3, the ratio between the short and the long isoform is approximately 50%.

In order to improve its complementation ability, we cloned *CHIM3* under the control of either the constitutive strong PGK promoter or the doxycycline repressible TETtoff promoter in centromeric vectors. Whereas the former construct was unable to complement the respiratory deficient phenotype of the mutant, the latter was effective, even more than *CHIM3* cloned in YEplac112 (Fig. 3A).

The expression level of chimeric constructs, cloned under the control of the different promoters, was analyzed by RT-qPCR. The mRNA levels of *CHIM3* cloned under the *MGM1* promoter in pFL39 were the same as those of *MGM1* cloned in the same plasmid. The mRNA levels of *CHIM3* cloned either in YEplac112 under the *MGM1* promoter or in pFL39 under the TETtoff promoter were about 16–18-fold higher compared to the level of the *MGM1* transcript. *CHIM3* mRNA was strongly increased in the presence of the *PGK* promoter (Fig. 3B). This result indicates that i) a precise expression level of the chimeric construct is crucial for right complementation; ii) the absence of complementation by *PGK-CHIM3* could be ascribed to toxicity due to an excessive expression of the chimeric construct.

Based on these results, the experimental work was continued by using *CHIM3*, cloned in the centromeric pFL39 vector under the TETtoff promoter. Doxycycline modulation experiments indicated that addition of this compound at concentrations up to 1 μg/ml did not ameliorate the oxidative growth of *CHIM3* strains, whereas addition of higher concentration of doxycycline partially or totally inhibited its growth (Supplementary Fig. 2). In no case we observed an improvement of the growth, and for this reason following experiments were performed without doxycycline.

3.3. CHIM3 complementation of Δmgm1 mutant OXPHOS phenotypes

The *Δmgm1* mutant is respiratory deficient due to loss of mtDNA. We analyzed the rescue of this phenotype in the *Δmgm1* mutant transformed by *CHIM3* by measuring i) mtDNA mutability; ii) oxygen consumption; iii) respiratory complex activity. For all these experiments, cells were pregrown in ethanol-supplemented medium, to counter select *petite* mutants eventually accumulated in the cell population, before being cultured in the experimental conditions required for the specific analysis.

The mtDNA instability was evaluated by measuring the frequency of *petite* mutants in the *Δmgm1* mutant transformed with *CHIM3* compared with wt *MGM1*, which in the presence of *CHIM3* was higher

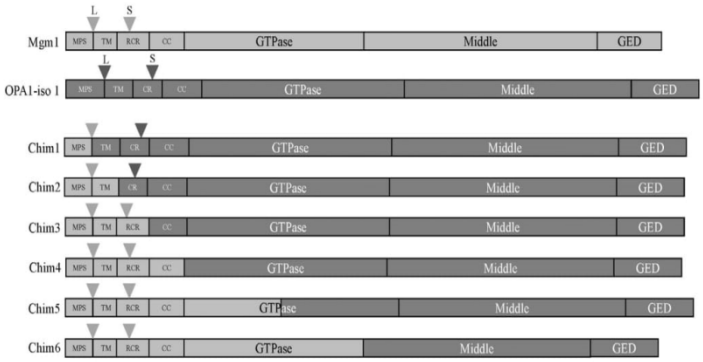

Fig. 1. Schematic representation of the motif/domain organization of Mgm1 (light gray), the OPA1 isoform 1ong (dark gray) and the six chimeric constructs. The "L" and "S" arrows indicate the site where Mgm1 and OPA1 are processed to produce the long and the short isoform, respectively.

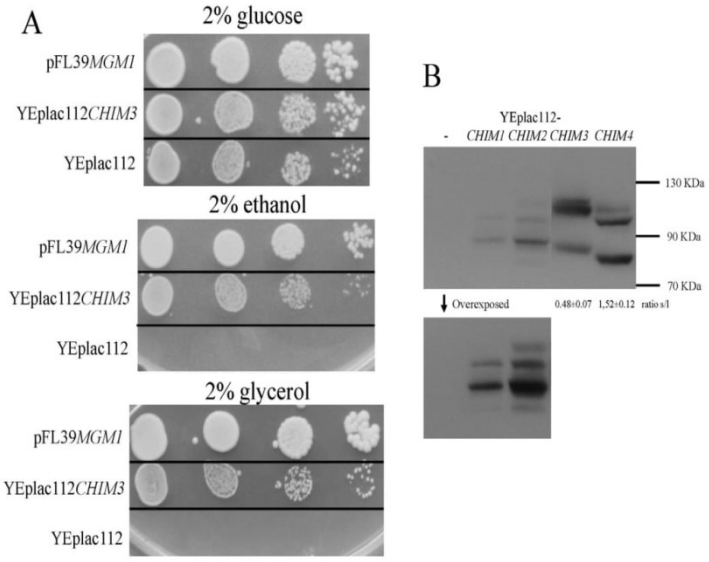

Fig. 2. (A) Spot assay of W303-1A *Δmgm1* strain transformed with pFL39*MGM1*, YEplac112*CHIM3* and YEplac112 on YP medium supplemented with different carbon sources. (B) Western blot of W303-1A *Δmgm1* strain transformed with *CHIM1-4* cloned in YEplac112.

(30.9%) compared to the strain transformed with pFL39*MGM1* (2.4%). This indicates that in the presence of *CHIM3* most cells maintain a full mitochondrial genome. mtDNA levels were also measured, through qPCR. They were found to be approximately 62% compared to the levels of the strain harboring wt *MGM1*.

The respiratory activity of the *CHIM3* strain was measured either in glucose, where it was reduced by approximately 50%, or in ethanol, where it was reduced by 30% (Fig. 4A). Finally, we measured the respiratory complex activity, in particular the NADH-cytochrome c reductase (NCCR, NADH reductase + CIII), the succinate coenzyme Q DCPIP

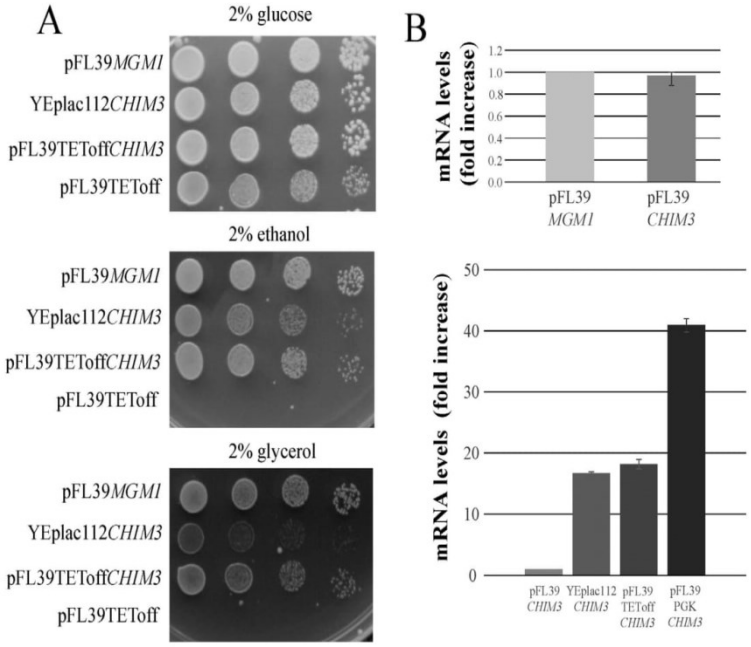

Fig. 3. (A) Spot assay of W303-1A *Δmgm1* strain transformed with pFL39*MGM1*, YEplac112*CHIM3*, pFL39TETOff*CHIM3* and pFL39TETOff on YP supplemented with different carbon sources. (B) Upper panel: RT-qPCR on W303-1A *Δmgm1* strain transformed with pFL39*MGM1* and pFL39*CHIM3*. Primers amplifying a region present in both *MGM1* and *CHIM3* were used. The ratio *MGM1*/*ACT1* was normalized to 1 for the strain transformed with pFL39*MGM1*. Lower panel: RT-qPCR on W303-1A *Δmgm1* strain transformed with different constructs containing *CHIM3*. Two pairs of primers amplifying two different *OPA1* fragments present in *CHIM3* were used. The ratio *OPA1*/*ACT1* was normalized to 1 for strain transformed with pFL39*CHIM3*.

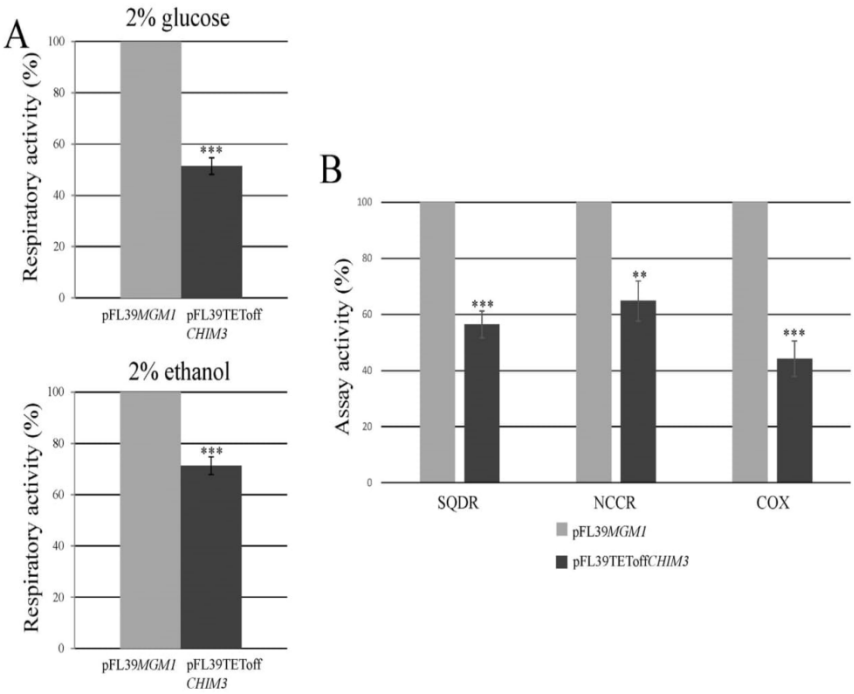

Fig. 4. Respiratory activity of W303-1A *Δmgm1* strain transformed with pFL39*MGM1* or pFL39TETOff*CHIM3* after growth on SC + 2% glucose or YP + 2% ethanol. Respiratory activity was normalized to 100% for the strain transformed with pFL39*MGM1*. (B) SQDR, NCCR and COX activity on the same strains. Each activity was measured on mitochondria-enriched fraction extracted from cells in which the *petite* frequency was lower than 3% and was normalized to 100% for the strain transformed with pFL39*MGM1*. **: $p < 0.01$; ***: $p < 0.001$ on at least three different experiments.

reductase (SQDR, CII) and the cytochrome c oxidase (COX, CIV) in mitochondria. All the enzyme activities were lower, though to different extents, ranging from 45% for COX activity to 65% for NCCR activity (Fig. 4B). Altogether these results indicate that *CHIM3* partially complements the OXPHOS negative phenotype of the *Δmgm1* mutant.

A second phenotype of the *Δmgm1* mutant is related to mitochondrial morphology. In the absence of the Mgm1 protein, cells are deficient in mitochondrial fusion and display fragmented or giant mitochondria. The aberrant mitochondrial morphology is not the result of the rho^0 condition of the *Δmgm1* mutant, but is in fact due to the absence of Mgm1: more than 95% of *MGM1* cells, either rho^+ or rho^0, display normal tubular mitochondrial network (Fig. 5). In order to study this phenotype and to quantify the *CHIM3* complementation, we created a *Δmgm1* mutant strain which carries both a plasmid-encoding GFP targeted at the mitochondria, to allow visualization of the mitochondrial network, and either *MGM1* or *CHIM3* constructs. Transformant cells, grown until the exponential phase is reached in galactose in order to induce mtGFP, were analyzed by fluorescence microscopy. The highly fragmented mitochondrial network of the *Δmgm1* mutant completely resumed a tubular structure when transformed with *MGM1* wt. In the presence of *CHIM3*, approximately 30% of mitochondria displayed a tubular or linear morphology. In the remaining cells, mitochondria were fragmented or giant, which indicates that aberrant mitochondrial morphology was partially rescued.

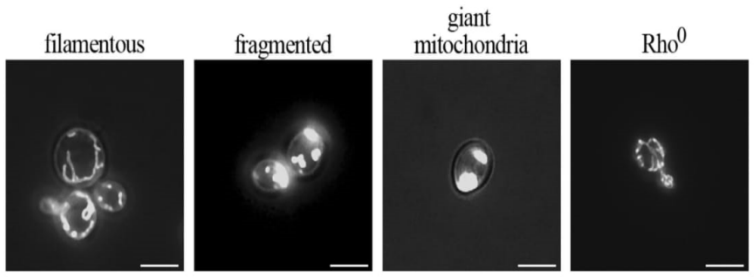

Fig. 5. Mitochondrial morphotypes in the investigated yeast strains. The strains were transformed with mitochondria localized GFP (pYEF1/mtGFP). Representative examples for each morphotype are shown. Scale bars represent 5 μm of length. The proportion of the different morphotypes was determined by counting approximately 2000 cells of each strain. The predominant morphotype in the analyzed strains were: pFL39*MGM1*, >95% filamentous; *Δmgm1*, 100% fragmented or giant mitochondria; pFL39*MGM1* rho^0, >95% filamentous; pFL39*CHIM3*, 30% filamentous and 70% fragmented or giant mitochondria.

Table 1
Mutations analyzed in this study.

OPA1 protein mutation[a]	Domain	Pathology	Dominance/recessivity in human	References
I382M (I437M)	GTPase	Non pathological or DOA DOA+ or Berh syndrome in heterozygosis with a second pathological mutation	Phenotypic modifier	Ferré et al. (2009) Bonifert et al. (2014) Schaaf et al. (2011)
R445H (R500H)	GTPase	DOA+	Dominant negative	Shimizu et al. (2003) Amati-Bonneau et al. (2003)
K468E (K523E)	GTPase	DOA	Dominant by haploinsufficiency	Pesch et al. (2001)
V903Gfs*3 (V958Gfs*3)	GED	DOA	Dominant by haploinsufficiency	Delettre et al. (2000)

[a] The nomenclature of the mutations used in this work is relative to OPA1 isoform 1. In parentheses, the first nomenclature relative to isoform 8 and used at the "MITOchondrial DYNamics variation pages: optic atrophy 1 (autosomal dominant) (OPA1)" (http://mitodyn.org/home.php?select_db=OPA1).

3.4. Construction of chim3 mutant alleles

In order to validate *CHIM3* as a suitable model to study non conserved pathological mutations in yeast, three missense mutations (I382M, R445H, K468E) and the nonsense mutation V903Gfs*3, known to be associated with DOA or DOA plus pathologies (Table 1), were introduced by site-directed mutagenesis in *CHIM3*.

At first, we tested the effect of the mutations on the oxidative growth of haploid yeast strains (Fig. 6A). Mutant chimeric alleles carrying R445H, V903Gfs*3 and K468E were not able to rescue the respiratory deficient phenotype of the *Δmgm1* mutant strain, in agreement with the severe pathological role of these mutations, and strains harboring these mutations lacked tubular mitochondria, behaving like strains without Mgm1 (data not shown). Diploids obtained by crossing a wt *rho*^{0} with strains carrying R445H, V903Gfs*3 and K468E mutant alleles were respiratory deficient, which demonstrates that these strains are devoid of mtDNA, as confirmed by qPCR on mtDNA.

In agreement with the very low potential pathogenic characteristics of the I382M mutation (Schaaf et al., 2011; Bonifert et al., 2014; Carelli et al., 2015), a strain carrying *chim3*^{I382M} displayed wt growth on non-fermentable carbon sources. The *chim3*^{I382M} strain was further analyzed in order to estimate the mtDNA stability. The analysis was carried out at 21°C, 28°C and 37°C (Fig. 6B). In all conditions, the *petite* frequency was increased compared to the strain carrying *CHIM3*. In addition, mtDNA levels, measured by qPCR, stood at 82% compared to those of the strain containing wt *CHIM3*. Moreover, the respiratory activity as well as the respiratory complex activities were decreased (Fig. 6C and 6D). Finally, we measured the percentage of cells presenting tubular mitochondria, which stood at approximately 18% ($p < 0.05$), 40% less than those of the strain harboring wt *CHIM3*. Altogether, these results indicate that, even in the absence of a phenotypic effect on the oxidative growth, the I382M mutation affects OPA1 activity.

By Western blot, we observed that in the case of Chim3^{R445H}, and, to a lesser extent, in the case of Chim3^{K468E}, the ratio between the s-

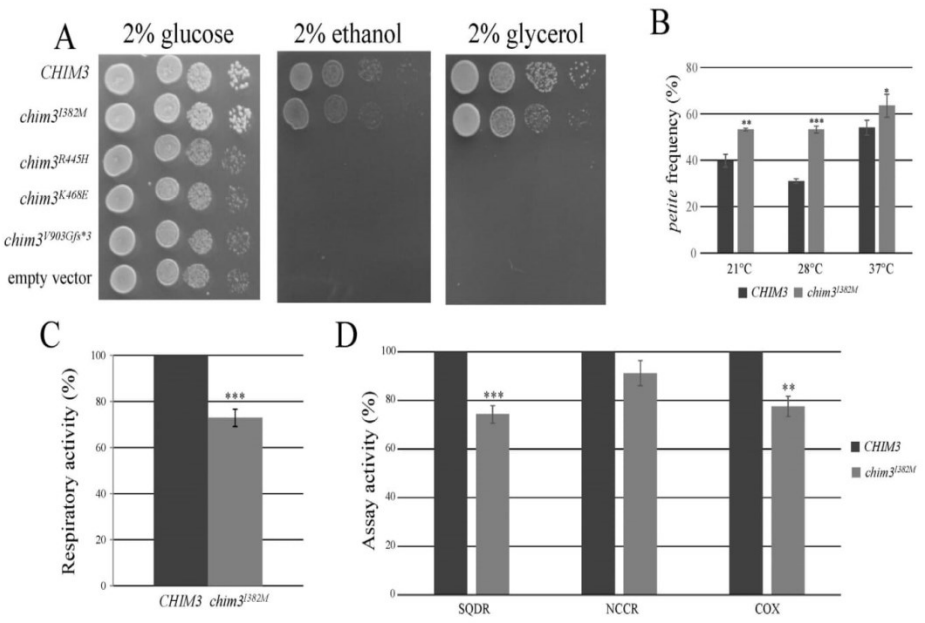

Fig. 6. (A) Spot assay of W303-1A strain transformed with *CHIM3* wt and mutant alleles on YP medium supplemented with different carbon sources. (B) *petite* frequency of *CHIM3* and *chim3*^{I382M} strain at different temperatures. (C) Respiratory activity of the same strains. Respiratory activity was measured on cells in which the *petite* frequency was lower than 5%, as described in Materials and Methods, and was normalized to 100% for the strain transformed with wt *CHIM3*. (D) Respiratory complex activities on the same strains. Each activity was measured on mitochondria-enriched fraction extracted from cells in which the *petite* frequency was lower than 3% and was normalized to 100% for the strains transformed with wt *CHIM3*. *: $p < 0.05$; **: $p < 0.01$; ***: $p < 0.001$ on at least three replicates.

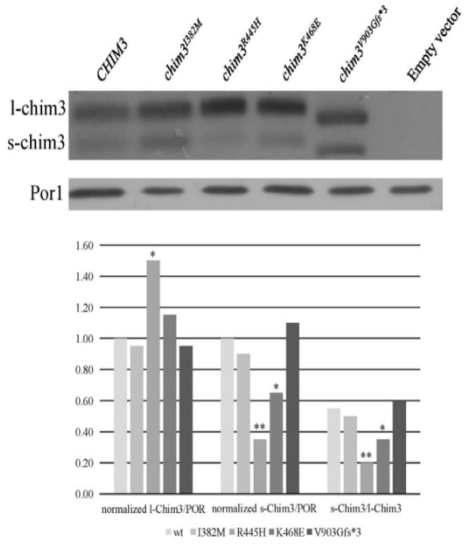

Fig. 7. Western blot on W303-1A strain transformed with *CHIM3* wt and mutant alleles. For each mutant allele, the long isoform/Por, the short isoform/Por and the short isoform/long isoform ratios were calculated. *: $p < 0.05$; **: $p < 0.01$ on three Western blot replicates.

isoform and the l-isoform is lower compared to that of the wt Chim3 (Fig. 7). This change is due both to a decrease of the s-form and to an increase of the l-isoform, which suggests that the process of the alternative topogenesis is altered.

3.5. Dominance/recessivity of OPA1 mutations

Dominance/recessivity of each *OPA1* mutation was determined in diploid strains in which both chromosomal *MGM1* genes were deleted and replaced by either two copies of wt *CHIM3* (homoallelic strain) or one copy of wt *CHIM3* and one copy of mutant *CHIM3* (heteroallelic strains). The growth phenotype of such strains was analyzed by spot assay in media supplemented with glucose or oxidative carbon sources (Fig. 8A). Heteroallelic strains containing either the I382M or the K468E mutation were able to grow on ethanol at the same level as the homoallelic strain (Fig. 8A). Diploid strains containing the R445H mutation displayed a decreased growth rate, which indicates that this mutation, associated with a DOA plus phenotype, behaves as partial dominant. Surprisingly, mutation V903Gfs*3 behaved as dominant, since the corresponding heteroallelic strain was unable to grow on a non-fermentable carbon source. This dominance is not due to the interference of the mutant Chim3 with the processing of the wt Chim3, since both of them are processed correctly (Fig. 8B).

4. Discussion

Functional studies using *S. cerevisiae* have been successfully used to validate the pathological significance of new mutations in disease-associated genes or in a newly identified gene (Rinaldi et al., 2010; Baile and Claypool, 2013).

Regarding Dominant Optic Atrophy (DOA) and DOA-plus, more than 200 pathogenic mutations spread throughout the entire *OPA1* gene have been identified so far, and periodically novel mutations in *OPA1* are found. Whereas heterozygous nonsense mutations, which produce a truncated protein, cause DOA through dominance by haploinsufficiency, missense mutations can be responsible either for a lack of function, causing haploinsufficiency, or for a gain of function, causing

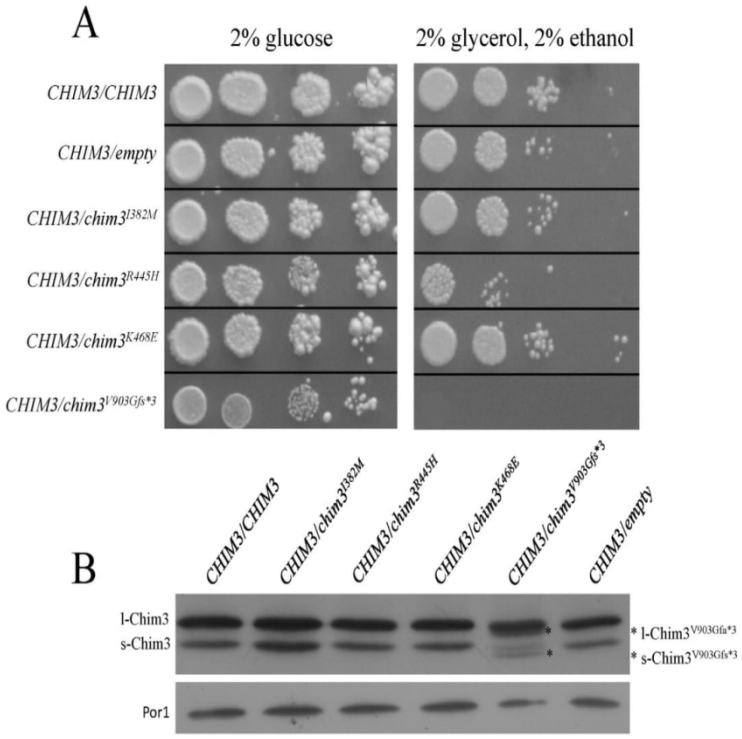

Fig. 8. (A) Spot assay of DW1.1 Δ*mgm1*/Δ*mgm1* heteroallelic and homoallelic diploid strains on SC supplemented with different carbon sources. (B) Western blot on the same strains.

negative dominance, which is responsible for the DOA plus phenotype. It is not always possible to establish the type of dominance by studying the patients and their family, nor is it to determine whether the mutation is pathological or is a neutral polymorphism.

Due to the low conservation between OPA1 protein and its yeast orthologue Mgm1, only few mutations can be validated in the yeast model. To overcome these problems, we first tried to express the human *OPA1* in *S. cerevisiae* under a yeast promoter. Differently to what was found in *Schizosaccharomyces pombe*, where most *OPA1* isoforms can complement the deletion of the yeast orthologous gene (Olichon et al., 2007), the experiment in *S. cerevisiae* was unsuccessful, which indicates that *OPA1* cannot substitute the *MGM1* gene. Next several chimeric genes bearing the 5′ region of *MGM1*, which was gradually longer, and the 3′ region of *OPA1* included the whole GTPase region, where the majority of pathological mutations are located, have been constructed. A similar experimental approach has been previously used in order to create models in which non-conserved pathological mutations of human genes encoding mitochondrial proteins could be validated in yeast (Paret et al., 1999; Lodi et al., 2015; Fontanesi et al., 2008; Stewart et al., 2010; Qian et al., 2014).

Chimeras have been cloned under the control of different promoters in single copy or multicopy plasmids. One *MGM1*/*OPA1* chimera, *CHIM3*, when placed under the promoter TETOff in a single copy plasmid, proved capable of complementing, although partially, the growth defect of *MGM1* deletion. This chimera contains the mitochondrial processing signal, the transmembrane domain and the rhomboid cleavage region of Mgm1 and the GTPase domain, the middle domain and the GTPase effector domain of OPA1. We found that this construct is correctly processed in the two isoforms, long and short, whose ratio is about 2:1, and partially allows the maintenance of the mtDNA and of the tubular structure of mitochondria.

In order to assess whether a yeast strain harboring this chimera was a good model to validate *OPA1* mutations, three missense mutations were selected and introduced in *CHIM3*: I382M, a phenotypic modifier (Bonifert et al., 2014); R445H, known to be associated with DOA plus (Amati-Bonneau et al., 2003); and K468E, one of the first mutations associated with DOA to be identified (Pesch et al., 2001). The frameshift mutation of V903Gfs*3, one of the most common nonsense mutations and one of the first to be identified (Delettre et al., 2000), was also studied. With the exception of the I382M mutation, all haploid strains expressing the mutant alleles showed a complete loss of mtDNA due to the inability of the mutant protein to induce mitochondrial fusion, as shown by the lack of tubular mitochondria and by the presence of fragmented or giant mitochondria in all the cells observed. This finding is consistent with the known pathological role of these mutations. In contrast, the chimera bearing mutation I382M was able to complement the deletion of *MGM1*, though to a lesser extent compared to the *CHIM3* wt, as demonstrated by the higher frequency of *petite*, by lower levels of mtDNA, and by decreased respiratory rate and respiratory complex activities.

These defects are consistent with a role of I382M as phenotypic modifier rather than as a pathological variant or a neutral polymorphism. In fact, the I382M substitution was initially identified as a cause of DOA, but it is also present in healthy subjects (Schaaf et al., 2011; Bonifert et al., 2014; Carelli et al., 2015). In addition, it has recently been reported that the I382M is not pathogenic per se, either in heterozygous or in homozygous state (Bonifert et al., 2014). However, *OPA1* bi-allelic cases have been described, in which patients who carry the I382M mutation in compound with the V903Gfs*3 mutation (which alone results in optic atrophy) are affected by a more severe form of this disease, which also includes additional symptoms such as hypotonia, gastrointestinal dysmotility and dysphagia. (Schaaf et al., 2011). Further cases have been reported in which a subject with severe DOA plus, whose parents were unaffected, was carrying the I382M mutation combined in trans with other OPA1 nonsense mutations (Bonifert et al., 2014). Finally, mutation I382M in compound heterozygosis with the OPA1 nonsense mutation c.1705 + 1G > T, which is associated with DOA, led to Behr syndrome, a neurological syndrome characterized by congenital and severe optic atrophy, spastic paraplegia, peripheral neuropathy with axonal loss, cerebellar signs and mild 3-metylglutaconic aciduria (Carelli et al., 2015; Behr, 1909; Costeff et al., 1989). This indicates that the I382M mutation is not able to lead to clinical symptoms, but acts as a phenotypic modifier that contributes to the worsening of the compound heterozygote phenotype.

Western analysis showed that in Chim3^{I382M} the protein levels of the two isoforms, long and short, are overall similar. In contrast, in the case of chimeras harboring R445H and K468E, the processing through alternative topogenesis is impaired, which leads to a decrease of the short form and to an increase of the long form. This result suggests that the cause of the disease may also reside in an alteration of the quantitative ratio between the long-OPA1 and the short-OPA1. Further experiments in mammal models are required to test this hypothesis. It was also shown by Western analysis that the levels of the truncated protein harboring the V903Gfs*3 mutation are normal, as well as the s-form/l-form ratio.

The proposed model also provides a useful approach for detecting loss-of-function or gain-of-function mutations. Since in the diploid yeast strain there is no haploinsufficiency, i.e. the presence of one or two copies of the chimera determines the same growth rate, it is expected that if the mutation causes a loss of function, the oxidative growth of the heteroallelic strain will be similar to that of the strain containing one or two copies of the *CHIM3* wt. On the other hand, a gain-of-function mutation will be expected to interfere with the activity of wt Chim3, and the growth of the heteroallelic strain will be impaired. As expected, the heteroallelic strains expressing the I382M and K468E mutations grew like the homoallelic strain. On the contrary, the heteroallelic strain carrying the R445H mutation showed a decreased growth rate, in agreement with its character of dominant negative mutation.

Intriguingly, mutation V903Gfs*3 is completely dominant, making the heteroallelic strain unable to grow on oxidative carbon sources. Since the truncated protein is present and correctly processed, and does not affect the processing of the wt chimera, the dominance could be due to inhibition of the wt protein activity carried out by the truncated one. It is possible to hypothesize that the truncated protein competes with the wt chimera over binding to one or more Mgm1 interactors, and that at the same time is unable to stimulate the fusion due to the lack of part of the GED domain. In humans, all nonsense mutations are associated with DOA and thus determine loss of function. The difference between humans and yeast may be due to nonsense-mediated mRNA decay, which in humans can decrease levels of OPA1 truncated proteins up to 2.5-fold (Schimpf et al., 2008), whereas in yeast the levels of the mutant protein are similar to those of the wt one.

5. Conclusion

In this study we validated a yeast model to evaluate the pathogenicity of OPA1 mutations and to define whether a mutation is dominant by haploinsufficiency or is dominant negative. The model allows us to study the effects of missense mutations but cannot be used for the analysis of nonsense mutations due to the interference in yeast of the truncated protein with the wt one.

Since most of the *OPA1* mutations are located in the GTPase domain, in the middle domain or in the GED domain, and Chim3 contains all these OPA1 domains, it is possible to estimate that 80 to 90% of the *OPA1* missense mutations found in patients can be introduced and studied in this chimeric gene.

Supplementary data to this article can be found online at http://dx.doi.org/10.1016/j.mito.2015.10.002.

Acknowledgements

We thank Beatrice Martinelli (kelimatranslations.com, UK) for proofreading the manuscript and Antonietta Cirasolo (Department of

Life Sciences, University of Parma, Italy) for the helpful technical assistance. This work was supported by MIUR grant FIR2013 (RBFR13IWDS).

References

Alexander, C., Votruba, M., Pesch, U.E., Thiselton, D.L., Mayer, S., Moore, A., Rodriguez, M., Kellner, U., Leo-Kottler, B., Auburger, G., Bhattacharya, S.S., Wissinger, B., 2000. OPA1, encoding a dynamin- related GTPase, is mutated in autosomal dominant optic atrophy linked to chromosome 3q28. Nat. Genet. 26, 211–215.

Amati-Bonneau, P., Milea, D., Bonneau, D., Chevrollier, A., Ferré, M., Guillet, V., Gueguen, N., Loiseau, D., de Crescenzo, M.A., Verny, C., Procaccio, V., Lenaers, G., Reynier, P., 2009. OPA1-associated disorders: phenotypes and pathophysiology. Int. J. Biochem. Cell Biol. 41, 1855–1865.

Amati-Bonneau, P., Odent, S., Derrien, C., Pasquier, L., Malthiéry, Y., Reynier, P., Bonneau, D., 2003. The association of autosomal dominant optic atrophy and moderate deafness may be due to the R445H mutation in the OPA1 gene. Am J. Ophthalmol. 136, 1170–1171.

Amati-Bonneau, P., Valentino, M.L., Reynier, P., Gallardo, M.E., Bornstein, B., Boissière, A., Campos, Y., Rivera, H., de la Aleja, J.G., Carroccia, R., Iommarini, L., Labauge, P., Figarella-Branger, D., Marcorelles, P., Furby, A., Beauvais, K., Letournel, F., Liguori, R., La Morgia, C., Montagna, P., Liguori, M., Zanna, C., Rugolo, M., Cossarizza, A., Wissinger, B., Verny, C., Schwarzenbacher, R., Martín, M.A., Arenas, J., Ayuso, C., Garesse, R., Lenaers, G., Bonneau, D., Carelli, V., 2008. OPA1 mutations induce mitochondrial DNA instability and optic atrophy 'plus' phenotypes. Brain 131, 338–351.

Ausubel, F.M., Brent, R., Kingston, R.E., Moore, D.D., Seidman, J.G., Smith, J.A., Struhi, K., 1994. Saccharomyces cerevisiae. Curr. Protoc. Mol. Biol. 2.

Baile, M.G., Claypool, S.M., 2013. The power of yeast to model diseases of the powerhouse of the cell. Front. Biosci. 18, 241–278 (Landmark Ed).

Barrientos, A., 2003. Yeast models of human mitochondrial diseases. Life 55, 83–95.

Barrientos, A., Fontanesi, F., Diaz, F., 2001. Evaluation of the Mitochondrial Respiratory Chain and Oxidative Phosphorylation System Using Polarography and Spectrophotometric Enzyme Assays. Current Protocols in Human Genetics.

Baruffini, E., Ferrero, I., Foury, F., 2010. In vivo analysis of mtDNA replication defects in yeast. Methods 51, 426–436.

Baruffini, E., Ferrari, J., Dallabona, C., Donnini, C., Lodi, T., 2015. Polymorphisms in DNA polymerase γ affect the mtDNA stability and the NRTI-induced mitochondrial toxicity in Saccharomyces cerevisiae. Mitochondrion 20, 52–63.

Behr, C., 1909. Die komplizierte, hereditar-familiare optikusatrophie des kindesalters – ein bisher nicht beschriebener symptomkomplex. Klin. Monatsbl. Augenheilkd. 47, 138–160.

Boeke, J.D., Trueheart, J., Natsoulis, G., Fink, G.R., 1987. 5-fluoroorotic acid as a selective agent in yeast molecular genetics. Methods Enzymol. 154, 164–175.

Bonifert, T., Karle, K.N., Tonagel, F., Batra, M., Wilhelm, C., Theurer, Y., Schoenfeld, C., Kluba, T., Kamenisch, Y., Carelli, V., Wolf, J., Gonzalez, M.A., Speziani, F., Schüle, R., Züchner, S., Schöls, L., Wissinger, B., Synofzik, M., 2014. Pure and syndromic optic atrophy explained by deep intronic OPA1 mutations and an intralocus modifier. Brain 137, 164–177.

Bonneaud, N., Ozier-Kalogeropoulos, O., Li, G.Y., Labouesse, M., Minvielle-Sebastia, L., Lacroute, F., 1991. A family of low and high copy replicative, integrative and single-stranded S. cerevisiae/E. coli shuttle vectors. Yeast 7, 609–615.

Bradford, M.M., 1976. A rapid and sensitive method for the quantitation of microgram quantities of proteins utilizing the principle of protein dye binding. Anal. Biochem. 72, 248–254.

Carelli, V., Sabatelli, M., Carrozzo, R., Rizza, T., Schimpf, S., Wissinger, B., Zanna, C., Rugolo, M., La Morgia, C., Caporali, L., Carbonelli, M., Barboni, P., Tonon, C., Lodi, R., Bertini, E., 2015. 'Behr syndrome' with OPA1 compound heterozygote mutations. Brain 138, 1–5.

Cogliati, S., Frezza, C., Soriano, M.E., Varanita, T., Quintana-Cabrera, R., Corrado, M., Cipolat, S., Costa, V., Casarin, A., Gomes, L.C., Perales-Clemente, E., Salviati, L., Fernandez-Silva, P., Enriquez, J.A., Scorrano, L., 2013. Mitochondrial cristae shape determines respiratory chain supercomplexes assembly and respiratory efficiency. Cell 155, 160–171.

Costeff, H., Gadoth, N., Apter, N., Prialnic, M., Savir., H., 1989. A familial syndrome of infantile optic atrophy, movement disorder, and spastic paraplegia. Neurology 39, 595–597.

Delettre, C., Lenaers, G., Griffoin, J.M., Gigarel, N., Lorenzo, C., Belenguer, P., Pelloquin, L., Grosgeorge, J., Turc-Carel, C., Perret, E., Astarie-Dequeker, C., Lasquellec, L., Arnaud, B., Ducommun, B., Kaplan, J., Hamel, C.P., 2000. Nuclear gene OPA1, encoding a mitochondrial dynamin-related protein, is mutated in dominant optic atrophy. Nat. Genet. 26, 207–210.

DeVay, R.M., Dominguez-Ramirez, L., Lackner, L.L., Hoppins, S., Stahlberg, H., Nunnari, J., 2009. Coassembly of opa1 isoforms requires cardiolipin and mediates mitochondrial inner membrane fusion. J. Cell Biol. 186, 793–803.

Escobar-Henriques, M., Anton, F., 2013. Mechanistic perspective of mitochondrial fusion: tubulation vs. fragmentation. Biochim. Biophys. Acta 1833, 162–175.

Ferré, M., Bonneau, D., Milea, D., Chevrollier, A., Verny, C., Dollfus, H., Ayuso, C., Defoort, S., Vignal, C., Zanlonghi, X., Charlin, J.F., Kaplan, J., Odent, S., Hamel, C.P., Procaccio, V., Reynier, P., Amati-Bonneau, P., 2009. Molecular screening of 980 cases of suspected hereditary optic neuropathy with a report on 77 novel OPA1 mutations. Hum. Mutat. 30, E692–E705.

Fontanesi, F., Diaz, F., Barrientos, A., 2009. Evaluation of the mitochondrial respiratory chain and oxidative phosphorylation system using yeast models of OXPHOS deficiencies. Curr. Protoc. Hum. Genet. (Chapter 19: Unit 19.5).

Fontanesi, F., Soto, I.C., Barrientos, A., 2008. Cytochrome c oxidase biogenesis: new levels of regulation. IUBMB Life 60, 557–568.

Frezza, C., Cipolat, S., Martins de Brito, O., Micaroni, M., Beznoussenko, G.V., Rudka, T., Bartoli, D., Polishuck, R.S., Danial, N.N., De Strooper, B., Scorrano, L., 2006. OPA1 controls apoptotic cristae remodeling independently from mitochondrial fusion. Cell 126, 177–189.

Garì, E., Piedrafita, L., Aldea, M., Herrero, E., 1997. A set of vectors with a tetracycline-regulable promoter system for modulated gene expression in Saccharomyces cerevisiae. Yeast 13, 837–848.

Gietz, R.D., Sugino, A., 1988. New yeast Escherichia coli shuttle vectors constructed with in vitro mutagenized yeast genes lacking six-base pair restriction sites. Gene 74, 527–534.

Gietz, R.D., Woods, R.A., 2002. Transformation of yeast by the LiAc/SS carrier DNA/peg method. Methods Enzymol. 350, 87–96.

Goffrini, P., Ercolino, T., Panizza, E., Giachè, V., Cavone, L., Chiarugi, A., Dima, V., Ferrero, I., Mannelli, M., 2009. Functional study in a yeast model of a novel succinate dehydrogenase subunit B gene germline missense mutation (C191Y) diagnosed in a patient affected by a glomus tumor. Hum. Mol. Genet. 18, 1860–1868.

Herlan, M., Bornhövd, C., Hell, K., Neupert, W., Reichert, A.S., 2004. Alternative topogenesis of Mgm1 and mitochondrial morphology depend on ATP and a functional import motor. J. Cell Biol. 165, 167–173.

Herlan, M., Vogel, F., Bornhövd, C., Neupert, W., Reichert, A.S., 2003. Processing of Mgm1 by the rhomboid-type protease Pcp1 is required for maintenance of mitochondrial morphology and of mitochondrial DNA. J. Biol. Chem. 278, 27781–27788.

Ho, S.N., Hunt, H.D., Horton, R.M., Pullen, J.K., Pease, L.R., 1989. Site-directed mutagenesis by overlap extension using the polymerase chain reaction. Gene 77, 51–59.

Hoffman, C.S., Winston, F., 1987. A ten-minute DNA preparation from yeast efficiently releases autonomous plasmids for transformation of Escherichia coli. Gene 51 267–212.

Hudson, G., Amati-Bonneau, P., Blakely, E.L., Stewart, J.D., He, L., Schaefer, A.M., Griffiths, P.G., Ahlqvist, K., Suomalainen, A., Reynier, P., McFarland, R., Turnbull, D.M., Chinnery, P.F., Taylor, R.W., 2008. Mutation of OPA1 causes dominant optic atrophy with external ophthalmoplegia, ataxia, deafness and multiple mitochondrial DNA deletions: a novel disorder of mtDNA maintenance. Brain 131, 329–337.

Jarreta, D., Orús, J., Barrientos, A., Miró, O., Roig, E., Heras, M., Moraes, C.T., Cardellach, F., Casademont, J., 2000. Mitochondrial function in heart muscle from patients with idiopathic dilated cardiomyopathy. Cardiovasc. Res. 45, 860–865.

Jones, B.A., Fangman, W.L., 1992. Mitochondrial DNA maintenance in yeast requires a protein containing a region related to the GTP-binding domain of dynamin. Genes Dev. 6, 380–389.

Kaiser, C., Michaelis, S., Mitchell, A., 1994. Methods in Yeast Genetics: A Laboratory Course Manual, Cold Spring Harbor Laboratory Press. Cold Spring Harbor, NY.

Kjer, P., 1959. Infantile optic atrophy with dominant mode of inheritance: a clinical and genetic study of 19 Danish families. Acta Ophthalmol. (Copenh) 164, 1–147.

Landes, T., Leroy, I., Bertholet, A., Diot, A., Khosrobakhsh, F., Daloyau, M., Davezac, N., Miquel, M.C., Courilleau, D., Guillou, E., Olichon, A., Lenaers, G., Arnauné-Pelloquin, L., Emorine, L.J., Belenguer, P., 2010. OPA1 (dys) functions. Semin. Cell Dev. Biol. 21, 593–598.

Lasserre, J.P., Dautant, A., Aiyar, R.S., Kucharczyk, R., Glatigny, A., Tribouillard-Tanvier, D., Rytka, J., Blondel, M., Skoczen, N., Reynier, P., Pitayu, L., Rötig, A., Delahodde, A., Steinmetz, L.M., Dujardin, G., Procaccio, V., di Rago, J.P., 2015. Yeast as a system for modeling mitochondrial disease mechanisms and discovering therapies. Dis. Model Mech. 8, 509–526.

Lenaers, G., Hamel, C., Delettre, C., Amati-Bonneau, P., Procaccio, V., Bonneau, D., Reynier, P., Milea, D., 2012. Dominant optic atrophy. Orphanet. J. Rare Dis. 7, 46.

Lodi, T., Bove, C., Fontanesi, F., Viola, A.M., Ferrero, I., 2015. Mutation D104G in ANT1 gene: complementation study in Saccharomyces cerevisiae as a model system. Biochem. Biophys. Res. Commun. 341, 810–815.

McQuibban, G.A., Saurya, S., Freeman, M., 2003. Mitochondrial membrane remodelling regulated by a conserved rhomboid protease. Nature 423, 537–541.

Meeusen, S., DeVay, R., Block, J., Cassidy-Stone, A., Wayson, S., McCaffery, J.M., Nunnari, J., 2006. Mitochondrial inner-membrane fusion and crista maintenance requires the dynamin-related GTPase Mgm1. Cell 127, 383–395.

Minet, M., Dufour, M.E., Lacroute, F., 1992. Complementation of Saccharomyces cerevisiae auxotrophic mutants by Arabidopsis thaliana cDNA. Plant J. 2, 417–422.

Olichon, A., Landes, T., Arnauné-Pelloquin, L., Emorine, L.J., Mils, V., Guichet, A., Delettre, C., Hamel, C., Amati-Bonneau, P., Bonneau, D., Reynier, P., Lenaers, G., Belenguer, P., 2007. Effects of OPA1 mutations on mitochondrial morphology and apoptosis: relevance to ADOA pathogenesis. J. Cell. Physiol. 211, 423–430.

Panizza, E., Ercolino, T., Mori, L., Rapizzi, E., Castellano, M., Opocher, G., Ferrero, I., Neumann, H.P., Mannelli, M., Goffrini, P., 2013. Yeast model for evaluating the pathogenic significance of SDHB, SDHC and SDHD mutations in PHEO-PGL syndrome. Hum. Mol. Genet. 22, 804–815.

Paret, C., Ostermann, K., Krause-Buchholz, U., Rentzsch, A., Rödel, G., 1999. Human members of the SCO1 gene family: complementation analysis in yeast and intracellular localization. FEBS Lett. 447, 65–70.

Pesch, U.E., Leo-Kottler, B., Mayer, S., Jurklies, B., Kellner, U., Apfelstedt-Sylla, E., Zrenner, E., Alexander, C., Wissinger, B., 2001. OPA1 mutations in patients with autosomal dominant optic atrophy and evidence for semi-dominant inheritance. Hum. Mol. Genet. 10, 1359–1368.

Qian, Y., Kachroo, A.H., Yellman, C.M., Marcotte, E.M., Johnson, K.A., 2014. Yeast cells expressing the human mitochondrial DNA polymerase reveal correlations between polymerase fidelity and human disease progression. J. Biol. Chem. 289, 5970–5985.

Rinaldi, T., Dallabona, C., Ferrero, I., Frontali, L., Bolotin-Fukuhara, M., 2010. Mitochondrial diseases and the role of the yeast models. FEMS Yeast Res. 10, 1006–1022.

Rinaldi, T., Hofmann, L., Gambadoro, A., Cossard, R., Livnat-Levanon, N., Glickman, M.H., Frontali, L., Delahodde, A., 2008. Dissection of the carboxyl-terminal domain of the proteasomal subunit Rpn11 in maintenance of mitochondrial structure and function. Mol. Biol. Cell 19, 1022–1031.

Schaaf, C.P., Blazo, M., Lewis, R.A., Tonini, R.E., Takei, H., Wang, J., Wong, L.J., Scaglia, F., 2011. Early-onset severe neuromuscular phenotype associated with compound heterozygosity for OPA1 mutations. Mol. Genet. Metab. 103, 383–387.

Schimpf, S., Fuhrmann, N., Schaich, S., Wissinger, B., 2008. Comprehensive cDNA study and quantitative transcript analysis of mutant OPA1 transcripts containing premature termination codons. Hum. Mutat. 29, 106–112.

Sesaki, H., Jensen, R.E., 2004. Ugo1p links the Fzo1p and Mgm1p GTPases for mitochondrial fusion. J. Biol. Chem. 279, 28298–28303.

Sesaki, H., Southard, S.M., Hobbs, A.E., Jensen, R.E., 2003. Cells lacking Pcp1p/Ugo2p, a rhomboid-like protease required for Mgm1p processing, lose mtDNA and mitochondrial structure in a Dnm1p-dependent manner, but remain competent for mitochondrial fusion. Biochem. Biophys. Res. Commun. 308, 276–283.

Shimizu, S., Mori, N., Kishi, M., Sugata, H., Tsuda, A., Kubota, N., 2003. A novel mutation in the OPA1 gene in a Japanese patient with optic atrophy. Am. J. Ophthalmol. 135, 256–257.

Soto, I.C., Fontanesi, F., Valledor, M., Horn, D., Singh, R., Barrientos, A., 2009. Synthesis of cytochrome c oxidase subunit 1 is translationally downregulated in the absence of functional F1F0-ATP synthase. Biochim. Biophys. Acta, Mol. Cell. Res. 1793, 1776–1786.

Stewart, J.D., Horvath, R., Baruffini, E., Ferrero, I., Bulst, S., Watkins, P.B., Fontana, R.J., Day, C.P., Chinnery, P.F., 2010. Polymerase γ gene POLG determines the risk of sodium valproate-induced liver toxicity. Hepatology 52, 1791–1796.

Wong, D.E., Wagner, J.A., Gorsich, S.W., McCaffery, J.M., Shaw, J.M., Nunnari, J., 2000. The dynamin-related GTPase, Mgm1p, is an intermembrane space protein required for maintenance of fusion competent mitochondria. J. Cell Biol. 151, 341–352.

Yu-Wai-Man, P., Sitarz, K.S., Samuels, D.C., Griffiths, P.G., Reeve, A.K., Bindoff, L.A., Horvath, R., Chinnery, P.F., 2010. OPA1 mutations cause cytochrome c oxidase deficiency due to loss of wild-type mtDNA molecules. Hum. Mol. Genet. 19, 3043–3052.

Zick, M., Duvezin-Caubet, S., Schäfer, A., Vogel, F., Neupert, W., Reichert, A.S., 2009. Distinct roles of the two isoforms of the dynamin-like GTPase Mgm1 in mitochondrial fusion. FEBS Lett. 583, 2237–2243.